ISTANBUL TECHNICAL UNIVERSITY ★ INSTITUTE OF SCIENCE AND TECHNOLOGY

ISOLATION AND STRUCTURE ELUCIDATION OF *VINCA* ALKALOIDS FROM *VINCA* SPECIES AND INVESTIGATION OF CYTOTOXIC ACTIVITY OF VINORELBINE LOADED NANODRUG DELIVERY SYSTEMS

Ph. D. THESIS

Fatemeh BAHADORI

Department : Chemistry

Programme : Chemistry

SEPTEMBER 2011

ISTANBUL TECHNICAL UNIVERSITY ★ INSTITUTE OF SCIENCE AND TECHNOLOGY

ISOLATION AND STRUCTURE ELUCIDATION OF *VINCA* ALKALOIDS FROM *VINCA* SPECIES AND INVESTIGATION OF CYTOTOXIC ACTIVITY OF VINORELBINE LOADED NANODRUG DELIVERY SYSTEMS

Ph. D. THESIS
Fatemeh BAHADORI
(509072206)

Date of submission: 10 August 2011
Date of defence examination: 15 September 2011

Supervisor (Chairman): Prof. Dr. Gülaçtı TOPÇU (ITU)
Members of the Examining Committee: Prof. Dr. Gürkan HIZAL (ITU)
Assoc. Prof. Dr. Erem BİLENSOY (HU)
Prof. Dr. Hayat ÖNYÜKSEL (UIC)
Prof. Dr. Ümit TUNCA (ITU)

SEPTEMBER 2011

İSTANBUL TEKNİK ÜNİVERSİTESİ ★ FEN BİLİMLERİ ENSTİTÜSÜ

VİNCA ALKALOITLERININ *VİNCA* TÜRLERİNDEN İZOLASYONU VE YAPI TAYİNİ VE VINORELBINE YÜKLENMİŞ NANO-İLAÇ TAŞIMA SİSTEMLERİNİN SİTOTOKSİK AKTİVİTELERİNİN ARAŞTIRILMASI

DOKTORA TEZİ
Fatemeh BAHADORI
(509072206)

Tezin Enstitüye Verildiği Tarih : **10 Ağustos 2011**
Tezin Savunulduğu Tarih : **15 Eylül 2011**

Tez Danışmanı : **Prof. Dr. Gülaçtı TOPÇU (İTÜ)**
Diğer Jüri Üyeleri : **Prof. Dr. Gürkan HIZAL (İTÜ)**
Doç. Dr. Erem BİLENSOY (HÜ)
Prof. Dr. Hayat ÖNYÜKSEL (UIC)
Prof. Dr. Ümit TUNCA (ITU)

EYLÜL 2011

Dedicated to My Beloved Mother,
Mina BAHADORI

FOREWORD

I am deeply indebted to Professor Dr. Gülaçtı TOPÇU for her stimulating enthusiasm, skilful guidance, keen interest, science advice and inspiration during the course of my research work.

A part of this work was completed with the excellent facilities made available to me by Lipid Base Drug Delivery Systems Laboratory, Biopharmaceutical Sciences Department, Faculty of Pharmacy, Universitu of Illinois at Chicago that is considered to be one of the best laboratories in Lipid Based Drug Delivery Systems area which is due to dedications of Professor Dr. Hayat Onyuksel who also gave me the most important scientific research opportunity of my life.

I am greatly encumbered to Dr. Antonina KUZMİS for her help, expert opinion and guidance during my research work.

I also feel honoured to express my gratitude to Professor Dr. Gürkan HIZAL, Professor Dr. Ümit TUNCA, Prof. Dr. Ufuk KOLAK and Professor Dr. Mehmet EROĞLU for their valuable guidance during the course of my studies and also to Dr. Hakan DURMAZ and Dr. Aydan DAĞ for their very nice collaborations.

I would also like to thank Yıldız Technical University, Department of Bioengineering, Cell Culture and Tissue Engineering Laboratory, Professor Dr. Adil ALAHVRDIYEV for giving me permission and facilities to carry out my research work and also M.S. Serap YEŞİLKIR BAYDAR for her precious collaboration.

I am grateful to the prays and doctrines of my (late) father, Professor Dr. Hossein Pasha BAHADORI who supported me till he breathed his last. My dear brothers who very willingly agreed for my higher studies, specially to my elder brother Abolfazl BAHADORI who has been my second father in all of my life and finally my son for love, sacrifices and encouragement to carry out these studies.

I would like to convey my deep gratitude and thanks to my senior colleagues Amrita BANERJEE, Dr. Sok Bee LIM, Mehmet BOGA and Muge SENNAROĞLU BOSTAN, and my dear colleagues in Istanbul Technical University and University of Illinois at Chicago, Seda Damla HATİPOĞLU, Ufuk Saim GÜNAY, Demet DİNÇEL, Anıl YILMAZ, Burcu BÜTÜN ÇULHAOĞLU, Ece GÜLÇÜR, Fatima KHATIB, Kerem KARAKUŞ, Mentor THAQUI, Stephanie DRAKE, Tuba BAŞKAN and Tuba KUŞMAN for their help, support and moral encouragement during the course of my studies.

August 2011

Fatemeh BAHADORI

Master of Science in Chemistry

TABLE OF CONTENTS

Page

ABBREVIATIONS

DCM	**:** Dichlormethane
Ace	**:** Acetone
Si-gel	**:** Silica Gel
DSPE	**:** Distearoyl Phosphatidyl Ethanolamine
PEG	**:** Poly Ethylene Glycol
PCL	**:** Poly-ε-Caprolactone
VLB	**:** Vinorelbine
NDDS	**:** Nano-Drug Delivery System
NMR	**:** Nuclear Magnetic Resonance Spectroscopy
MS	**:** Mass Spectroscopy
DSC	**:** Differential Scanning Calorimetry
DLS	: Dynamic Light Scattering
NCLS	**:** Non Small Cell Lung Cancer
SSM	**:** Sterically Stabilized Micelles
SSMM	**:** Sterically Stabilized Mix Micelles

LIST OF TABLES

Page

LIST OF FIGURES

Page

ISOLATION AND STRUCTURE ELUCIDATION OF VINCA ALKALOIDS FROM VINCA SPECIES AND INVESTIGATION OF CYTOTOXIC ACTIVITY OF VINORELBINE LOADED NANODRUG DELIVERY SYSTEMS

SUMMARY

This thesis study mainly consists of two different parts. The first part forms isolation and structure elucidation of *Vinca* alkaloids from the three *Vinca* species (*Vinca* major, *Vinca* minor and *Vinca* soneri). The second part consists of loading of a dimeric *Vinca* alkaloid, Vinorelbine to three different types of micellar nano drug delivery systems (MNDDS) and physical characterization of MNDDS and investigation of their cytotoxic activity.

As it is known, natural products or their derivatives have an important place in cancer therapy. Among present chemotherapeutic agents natural drugs or their semi-synthetic derivatives, namely alkaloids from *Taxus*, *Catharantus* and *Vinca* species are the most common drugs. Particularly dimeric *Vinca* alkaloids which have indeed *Catharantus alkaloids* and their derivatives are used in lung, ovarian and breast cancer therapy. However, all of the anti-cancer drugs including *Vinca* alkaloids have numerous side-effects. For this purpose, both isolation and structure elucidation studies for the *Vinca* alkaloids growing in Turkey were carried out, and the three micellar drug delivery systems were prepared and investigated for their physical properties and cytotoxic activity of the MNDDS with and without Vinorelbine.

For the phytochemical research, alkaloids' extracts of the three *Vinca* species were prepared, and structure of alkaloids, isolated by chromatographic methods, were determined with modern spectroscopic techniques, namely NMR (^{1}H and ^{13}C NMR, BB, APT, DEPT, COSY, gHSQS and gHMBC) and mass spectroscopy. From the three *Vinca* species, *Vinca soneri* has just been brought to the world of science as a new endemic species to Turkey. In fact, there are four species of *Vinca* in Turkey and among them, investigations on *V. herbacea* have just now published by our group. Vallesiachotamine and Picrinine were isolated from *Vinca soneri* as well as α and β-Yohimbine. Vallesiachotamine is also isolated from *Vinca minor* besides iso-Vallesiachotamine. This is a first isolation of Vallesiachotamine, iso-Vallesiachotamine, α and β-Yohimbine from *Vinca* species as known Indole alkaloids. It is noteworthy that 11-Hydroxypolyneuridine was obtained from *V. major* as a new Indole alkaloid in this study.

The studies of the second part is the preparation of the Vinorelbine nanoformulations. Vinorelbine is uploaded to one lipid based and two polymeric nano-drug delivery systems. The aim of these formulations is to prepare drug delivery systems which target cancerous tissue by using Enhanced Permeability and Retention (EPR) effect with high efficiency and lesser side effects.

One of the MNDDS used in this study is a very well known targeting carrier, DiStearoyl PhosphatidylEthanolamine-PolyEthyleneGlycol 2000 (DSPE-PEG 2000)

which has been used in targeted cancer therapy researches, reported for several times.

We also used two different Polymeric MNDDS to produce Nano-VLB. One of them is four arm star-shaped Poly-ε-Caprolactone (PCL), PolyEthyleneGlycol (PEG) (PCL_4-PEG_4), and the other one is Y shaped PCL_2-PEG. These polymers have been synthesized by Prof. Gurkan HIZAL and Umit TUNCA polymer research group and the synthesis procedure was not involved in this study. The structure and synthesis pathway of these two polymers are new and we are reporting characterization of micelles prepared by these two co-polymers.

For the characterization of these two polymeric micelles their CMC were investigated and gave satisfactory results (CMC is 50 mg/L and 1mg/L for Star and Y-Shaped PCL-PEG micelles, respectively) and we are introducing two new drug delivery systems for hydrophobic agents by preparing two new Nano-VLB formulations.

As a result, although both polymeric nano-VLB formulations and DSPE-PEG formulation showed enhanced *in vitro* cytotoxic activity, the latter one exhibited higher activity and drug loading capacity than the former one. Thus, it can be summarized that DSPE-PEG systems can be considered as better drug delivery systems, at least based on our experimental results as well as the accumulated knowledge.

VİNCA ALKALOITLERININ VİNCA TÜRLERİNDEN İZOLASYONU VE YAPI TAYİNİ VE VINORELBINE YÜKLENMİŞ NANO-İLAÇ TAŞIMA SİSTEMLERİNİN SİTOTOKSİK AKTİVİTELERİNİN ARAŞTIRILMASI

ÖZET

Bu tez çalışması başlıca iki farklı kısımdan oluşmaktadır. İlk kısım, Türkiye'de yetişen üç *Vinca* türünden (*V. minor, V. major* ve *V. soneri*'den) alkaloitlerinin izole edilmesi ve yapılarının tayininden oluşmaktadır. İkinci kısım ise kanser tedavisinde kullanılan dimerik *Vinca* alkaloitlerinden birinin seçilerek ki bu amaçla Vinorelbin seçilmiş ve farklı üç misel ile hazırlanan nano-taşıyıcı sistemlere yüklenerek fiziksel ve sitotoksik aktivitesi yönüyle incelenmesinden ibarettir.

Bilindiği gibi kanser tedavisinde doğal ürünler veya onların yarı-sentetik türevleri oldukça önemli bir yer almaktadır. Günümüzdeki kemoterapötik ajanların en önde gelenlerini yine doğal ürünler veya türevleri ve özellikle de alkaloitler oluşturmaktadır ki başlıcaları Taxol, Catharanthus ve *Vinca* alkaloitleri veya yarı-sentetik türevlerinden ibarettir. Bunlardan biri olan dimerik *Vinca* alkaloitlerinin farklı ürünleri akciğer, yumurtalık ve meme kanseri tedavisinde kullanılmakta, fakat *Vinca* alkaloitleri de dahil tüm antikanser ilaçların pek çok yan tesiri bulunmaktadır. Bu amaçla bu tez çalışmasında hem Türkiyede yetişen *Vinca* türlerinin alkaloitleri izole edilerek yapıları belirlenmiş ve ilaç olma potansiyelleri araştırılmış, hem de *Vinca* alkaloitlerinden son yıllarda tedavide sıklıkla kullanılan Vinorelbinin vücuttaki biyoyararlanımı arttırılarak yan tesirlerinin azaltması için hazirlanan yeni ilaç taşıyıcı sistemlerinin misel formu hazırlanarak Vinorelbin yüklemeden ve yüklendikten sonraki fiziksel ve kimyasal özellikleri incelenmiş, yanı sıra sitotoksik özelliklerinde bir değişlik olup olmadığı araştırılmıştır.

Yapılan fitokimyasal araştırmada öncelikle toplanan her üç *Vinca* türünün alkaloit ekstreleri hazırlandı ve kromatografik yöntemlerle içerdikleri alkaloitler izole edilerek kimyasal yapıları modern NMR (^{1}H ve ^{13}C NMR, BB, APT, DEPT, COSY, gHSQC ve gHMBC) ve kütle spektroskopisi başta olmak üzere spektroskopik yöntemlerle tayin edildi. İncelenen üç *Vinca* türünden *Vinca soneri* bilim dünyasına henüz kazandırılmış Türkiye'ye endemik yeni bir *Vinca* türü'dür . Zaten Türkiye'de 4 *Vinca* türü vardır, bunlardan *V. herbacea* grubumuz tarafından yakın geçmişte incelenmiştir. *Vinca soneri*'den α- ve β-Yohimbin alkaloitlerinin yanı sıra Vallesiachotamine alkaloidi elde edilmiştir. Bu sonuncu alkaloit Vinca minor bitkisinden iso-Vallesiachotaminin yanı sıra Vallesiachotamine de elde edilmiştir, Vallesiachotamine'in *Vinca* türlerindeki mevcudiyeti ilk kez bu çalışma ile gösterilmiştir. Sonuç olarak, Vallesiachotamine, iso-Vallesiachotamin, α- ve β-Yohimbin *Vinca* türlerinden ilk kez elde edilen indol alkaloitleri, *Vinca major* bitkisinden izole edilerek yapısı aydınlatılan 11-Hydroxypolineuridin ise doğadan ilk kez elde edilen bir indol alkaloitidir.

Tezin ikinci kısmını oluşturan Vinorelbinin nanoformülasyonların hazırlanmasında, Vinorelbin (VLB)i lipid bazlı ve ayrıca polimerik miseller oluşturarak hazırladığımız nanoilaç taşıyıcı sistemlerine (MNDD) yükleyip kanserli bölgeyi hedef almak,

yüksek geçirgenlik ve alıkonma (EPR) özelliklerine sahip yüksek etki ve düşük yan etkili bir nanoilaç haline getirmeyi amaçladık.

Bu amaçla hazırlanılan MNDDs lerden biri hedefli kanser tedaviyi amaçlayan çalışmalarda çok iyi bilinen bir hedeflendirme reaktifi olan DiStearoylPhosphatidylEthanolamine-PolyEthyleneGlycol 2000 (DSPE-PEG 2000) dir. Polimerik Nano-VLB yi hazırlamak için ise iki farklı polimerik misel nano-drug delivery (MNDD) sistem hazırlandı.Onlardan biri dört kollu yıldız şekilli Poly-ε-Caprolactone (PCL), PolyEthyleneGlycol (PEG) den ibaret (PCL_4-PEG_4) ve diğeri iseY şekilli PCL_2-PEG dir. Bu polimerler Prof. Dr. G. Hızal ve Ü. Tunca'nın polimerik sentez araştırma grubunca sentezlendiğinden bu tez çalışmasına dahil edilmemiştir. Bu iki polimerin karakterizasyonları için kritik misel konsantrasyon (CMC) ları ölçülmüş ve dört kollu yıldız polimer için CMC 50 mg/L ve Y şekilli PCL_2-PEG miselleri için 1mg/L olarak tatmin edici sonuçlar vermiştir. Sonuçta hem Polimerik Nano-VLB formülasyonları, hem de DSPE-PEG-VLB formülasyonları *in vitro* koşullarda sitotoksik aktiviteyi arttırsalarda DSPE-PEG-VLB formülasyonlarının hem daha yüksek aktivite göstermesi hem de DSPE-PEG sisteminin polimerik sistemlerden daha yüksek miktarda VLB taşıma kapasitesi göstermesi en azından bizim sonuçlarımız ve bugüne dek yapılan çalışmalara göre lipid bazlı sistemlerin daha iyi ilaç taşıyıcı sistemler olduğunu göstermektedir.

1. INTRODUCTION

1.1 General Introduction:

Every living organism, from the very beginning of its existence, has to struggle for survival. Man has familiarized himself with plants and used them in a variety of ways throughout the ages. For search of food, he has distinguished the plants suitable for nutritional purposes from others with definite pharmacological actions. Thus the drugs of plant origin have served through the ages as the mainstay in the treatment of human ailments and preservation of health.

Plants have been the basis for some of the most effective powerful drugs known to man e.g. the Chinese have been using “Ma Huang” (*Ephedra*), for thousands of years for the treatment of nasal congestion, bronchial cough and asthma. In addition, almost a quarter of all pharmaceutical used today are of plant origin.

In the Indo-Pak subcontinent, records of the indigenous system of medicines known as “Ayurveda”, go back to 700 B.C. and its systematization is attributed to Charaka and Sushurta, who cited about 700 medicinal plants. Thus the “Ayurvedic system was developed in India, whereas Srilanka (Ceylon) established the “Bantu System”. The many advances made in medicine in the earlier period are examplified by great names of Hippocrates [(Finlayson, 1892), (Sigerist, 1934), (Theophrastus and Galen Walsh, 1937)].

Actually the history of modern medicine and pharmacy begins from Hippocrates, the “Father of Modern Medicine”. In writings early 400 samples are named as medicinal substances. Theophrastus wrote a book “on the History of Plants” in which he mentioned 500 drugs. His famous book on “Materica Medica” was first published in Greece, which serves as the pharmacological handbook for a long time. Following this period, the role of medicine was gratly extended in the Islamic age of Science and Medicine. The most famous physician and philosopher of his time, Ibni-Sina described 760 herbal drugs in his book “Canon of Medicine” which served as a

textbook of Medicine in Europe till 17th century A.D, and formed the base of the Greco-Arab System of medicine known as Tibb-e-Unani.(Sultana, 1992)

In the seventeenth and eighteenth centuries great progress was made in the fields of pharmacy and medicinal chemistry. During the nineteenth century pharmaceutical chemistry emerged as an important subclass of chemistry. The discovery of the alkaloid morphine by serturner in 1805, followed by a whole series of alkaloids from herbal drugs e.g. strychnine, papaverine, quinine nicotine and cocaine , may have led to greater attention being paid to chemical investigations of medicinal plants(Figure 1.1) .

One of the first important plants on which work was carried out was *Rauwolfia serpentina* which led to the isolation of a whole series of new alkaloids, which gained worldwide importance in the treatment of cardiovascular diseases and aental ailments e.g. reserpine (Figure 1.2). About 25% of the drugs used today in developed countries contain active principles which are extracted from plants and about 2/3 of the people in developing countries rely on plants for relief from disease. Morover, studies on the structure-function releationship have enriched mankind with a better understanding of the biological systems and disease processes. Recently there has been increasing interest in the development of bioassay procedures for the selection of plants containing novel biologically active substances.(Sultana, 1992)

Thus a great deal of interest has developed throughout the world in the investigation of medicinal plants, most of which grow in the hot and humid regions of the third world. Taking into account the facts stated above, the work undertaken for the present thesis relates to the isolation of new natural products from *Vinca minor*, *Vinca major* and *Vinca soneri*.

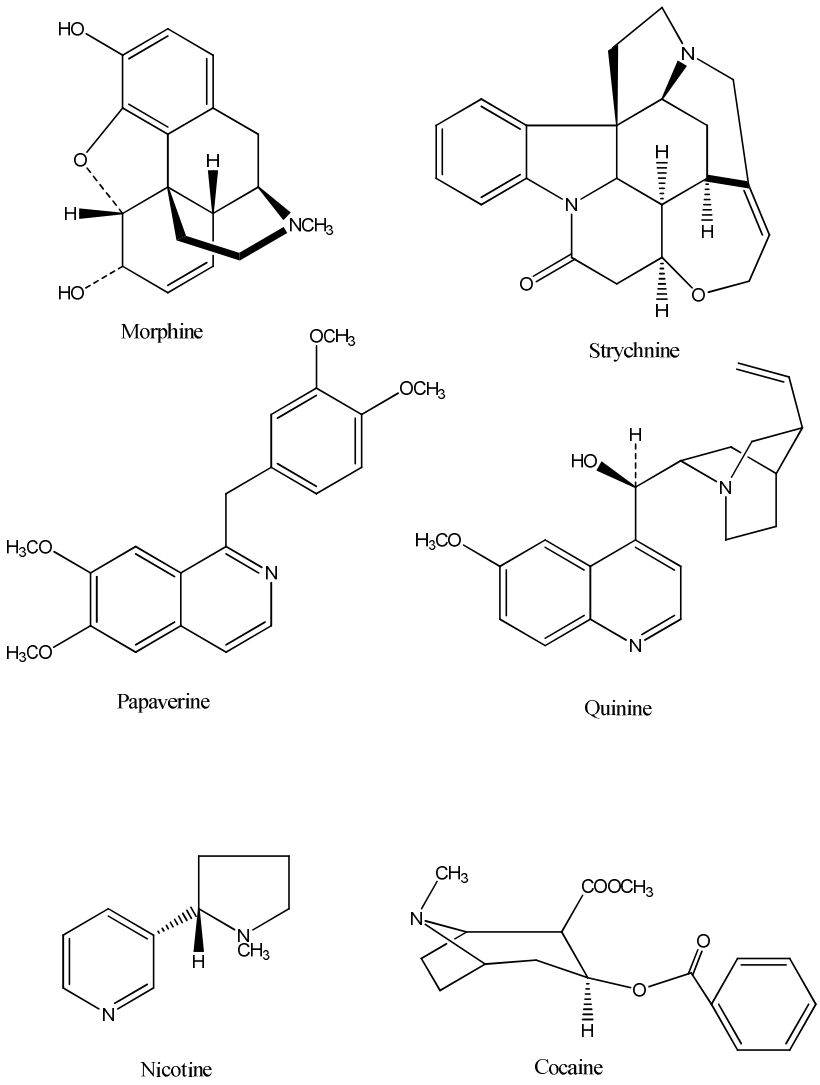

Figure 1.1: First discovered alkaloids (Sultana, 1992).

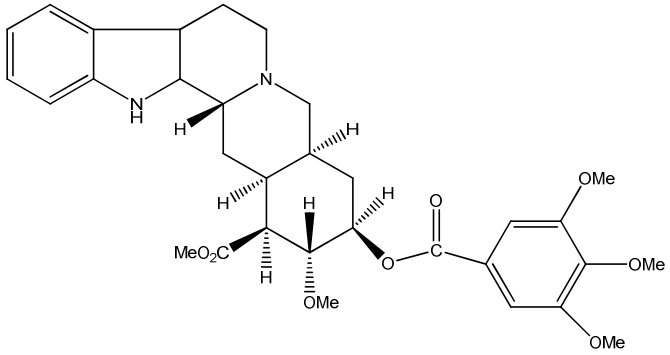

Reserpine

Figure 1.2: Chemical Structure of Reserpine (Sultana, 1992).

2. ALKALOIDS

2.1 Definition

The definition of the term alkaloid is not a simple one, and is in many cases a source of academic controversy. Difficulties with the definition of such a group of secondary and natural molecules as alkaloids stem from similarities of alkaloids with other secondary compounds. Attempts to define the term “alkaloid” originated at the time of the discovery of these compounds.

The term “alkaloid” was first mentioned in 1819 by W. Meißner, an apothecary from Halle. He observed that these compounds appeared “like alkali”, and so named them alkaloids.

From the biological point of view, the alkaloid is any biologically active and heterocyclic chemical compound which contains nitrogen and may some pharmacological activity and, in many cases, medicinal or ecological use. This definition, as a relatively wide one based on application, can be criticized as inexact. However, it presents a general picture of what kinds of compound are under consideration. The biological and chemical nature of this group of compounds leads to the conclusion that each definition of alkaloids is either too broad or too narrow. A short exact definition is not possible without a long list of exceptions.

Medicine draws attention to the fact that alkaloids create intense physiological action, and they are widely used in the medical fields as curative drugs. Some alkaloids can also be highly toxic, even in very small doses. In the database of the National Library of Medicine it is possible to find the definition of alkaloids, according to which these compounds are nitrogenous bases and occur in animal and vegetable kingdoms, while some of them have been synthesized. Another electronic database also provides a definition of alkaloids, stating that an alkaloid is a nitrogenous organic compound which has pharmacological effects on humans and other animals, and whose name is derived from the world alkaline. As can be seen, the definition of alkaloids in the field of medicine also offers parameters of “may

be", "often", "slightly" and "highly", which are not exact. This is typical of the scientific and practical fields, where alkaloids are well known and used in the bettering of human health, but where the term remains relatively difficult to define exactly and concisely.

Chemistry has provided a definition of alkaloids in purely chemical terms. Chemists stress that alkaloids are any group of complex heterocyclic nitrogen compounds, which have strong physiological activity, are often toxic, and retain their own basic chemical properties. It is also stated that there are a few exceptions to this definition. In another chemical definition, it is stated only that alkaloids are nitrogen-containing compounds derived from plants and animals.

Later, chemists stressed that alkaloids were biogenic, nitrogen-containing and mostly N-heterocyclic compounds. In this definition it is also stated that amino acids, peptides, nucleosides, amino sugars and antibiotics are not considered as to be alkaloids (Cordell, 1981).

The first modern definition by Winterstein and Trier described alkaloids as basic nitrogen containing compounds of either plant or animal origin. "True alkaloids" were defined as compounds having four additional qualifications:

(1)The nitrogen is part of a heterocyclic system

(2)The compound has a complex molecular structure

(3)The compound often manifests significant pharmacological activity.

(4)The compound is restricted to the plant kingdom.

Alkaloids frequently occur as salts of plant acids such as maleic acid, meconic acid or quinic acid some occur as glucosides e.g. solanine whereas others are found as amides e.g. piperine or as esters.

The classical definition mentioned above has been modified because there were many examples of compounds which were universally accepted as alkaloids, but which violated one or more of the cardinal requirements of a definition of the Winterstein-Trier type. For instance basicity can no longer be regarded as a necessary property of an alkaloid e.g. colchicines, piperine and amine oxides such as indicine are not basic. Moreover alkaloid-type structures have also been isolated from animal, fungal and bacterial sources.

Alkaloids are therefore better defined as cyclic organic compounds containing nitrogen in a negative oxidation state, which are of limited distribution among living organisms. The requirement of nitrogen in a negative oxidation states include amines (-3), amine oxide (-1), amides (-3) and quaternary ammonium salts (-3), but excludes nitro (+3) and nitroso (+1), compounds.

Alkaloids can be classified in the terms of their (1) biological and ecological activity; (2) chemical structures and (3) biosynthetic pathway. From the point of view of biological activity, it is possible to divide alkaloids into (1) neutral or weakly basic molecules (e.g., lactams such as ricinine, certain N-oxides (such as indicine), (2) animal-derived alkaloids (e.g., anuran, mammalian and arthropod alkaloids), (3) marine alkaloids, (4) moss alkaloids, (5) fungal and bacterial alkaloids and (6) non-natural alkaloids (structurally modified or analogues).

From a structural point of view, alkaloids are divided according to their shapes and origins. There are three main types of alkaloids: (1) true alkaloids, (2) protoalkaloids and (3) pseudoalkaloids (Cordell, 1981).

2.2 True Alkaloids

True alkaloids derive from amino acid and they share a heterocyclic ring with nitrogen. These alkaloids are highly reactive substances with biological activity even in low doses. All true alkaloids have a bitter taste and appear as a white solid, with the exception of nicotine(Figure 1.1) which has a brown liquid. True alkaloids form water-soluble salts. Moreover, most of them are well-defined crystalline substances which unite with acids to form salts. True alkaloids may occur in plants (1) in the free state (2) as salts and (3) as N-oxides. These alkaloids occur in a limited number of species and families, and are those compounds in which decarboxylated amino acids are condensed with a nonnitrogenous structural moiety. The primary precursors of true alkaloids are such amino acids as l-ornithine, l-lysine, l-phenylalanine/l-tyrosine, l-tryptophan and l-histidine. Examples of true alkaloids include such biologically active alkaloids as cocaine, quinine (Figure 1.1), dopamine, morphine and usambarensine (Figure 2.1).

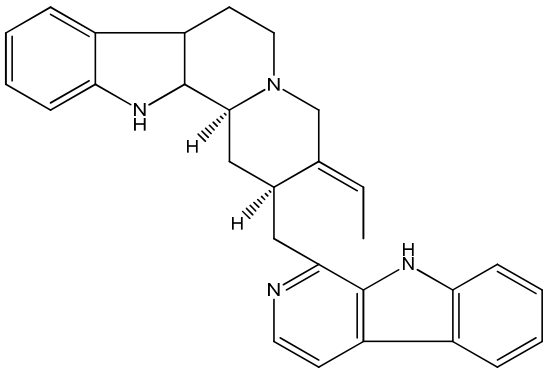

Usambarensine

Figure 2.1 Chemical structure of Usambarensine an example of true alkaloids (Cordell, 1981).

l-tyrosine-derived alkaloid usambarensine has strong anti-malarial potential. Usambarensine was extracted from the root bark of African *Strychnos usambarensis*, a small tree in East and South Africa, and a small bush in West Africa.

2.3 Protoalkaloids

Protoalkaloids are compounds, in which the N atom derived from an amino acid is not a part of the heterocyclic. Such kinds of alkaloid include compounds derived from l-Tyrosine and l-tryptophan. Protoalkaloids are those with a closed ring, being perfect but structurally simple alkaloids. They form a minority of all alkaloids. Hordenine, mescaline (Figure 2.2) and yohimbine are good examples of these kinds of alkaloid.

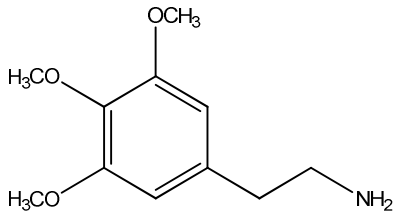

Mescaline

Figure 2.2: Chemical structure of Mescaline (an example of Protoalkaloids) (Cordell, 1981).

Mescaline is the alkaloid derived from l-tyrosine and extracted from the *Peyote cactus* (*Lophophora williamsii*) belonging to the Cactus family (Cactaceae). Mescaline has strong psychoactive and hallucinogenic properties. Peyote cactus

grows in the desert areas of northern Mexico and the southern parts of the USA. This plant was used in Pre-Columbian America in the shamanic practice of local tribes.

2.4 Pseudoalkaloids

Pseudoalkaloids are compounds, the basic carbon skeletons of which are not derived from amino acids. In reality, pseudoalkaloids are connected with amino acid pathways. They are derived from the precursors or postcursors (derivatives the indegradation process) of amino acids. They can also result from the amination and transamination reactions of the different pathways connected with precursors or postcursors of amino acids.

These alkaloids can also be derived from non-aminoacid precursors. The N atom is inserted into the molecule at a relatively late stage, for example, in the case of steroidal or terpenoid skeletons. Certainly, the N atom can also be donated by an amino acid source across a transamination reaction, if there is a suitable aldehyde or ketone. Pseudoalkaloids can be acetate and phenylalaninederived or terpenoid, as well as steroidal alkaloids. Examples of pseudoalkaloids include such compounds as coniine, capsaicin, ephedrine, solanidine, caffeine, theobromine and pinidine (Figure 2.3)(Cordell, 1981). Acetate-derived alkaloid pinidine is extracted from the Pinus species, for example, from Pinus penderosa. Pinidine has antimicrobial activity.

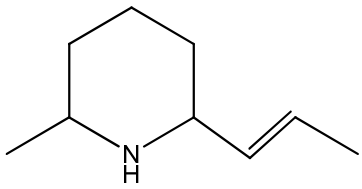

Pinidine

Figure 2.3: An example of a pseudoalkaloids (Cordell, 1981).

2.5 Alkaloid Classification According To Structure:

2.5.1 Indole alkaloids:

Indole alkaloids include many compounds which pharmacological activity is well established e.g. Morphin (Figure 1.1) derived from Opium poppy by Sertuner in 1805, is used as analgesic and narcotic, quinine (Figure 1.1) from *Cincona* bark cures or Alleviates malaria , reserpine (Figure 1.2) from *Rauwolfia serpentia* was once

used as an important hypotensive and sedative drug. Vinblastine (Figure 5.2**Hata! aşvuru kaynağı bulunamadı.**)and Vincristine (Figure 5.2) isolated from leaves of *Catanthus roseus* are used as anticancer drugs. Vincristine is highly active in the treatment of childhood leukemia. Vinblastine is used in Hodgkin's disease and choricarcinoma.

2.5.2 Taxane alkaloids:

Another class of alkaloid belongs to the taxane skeleton. These compounds have a novel diterpenoid tricycle[9.3.1.0]pentadecene skeleton. Such alkaloids exist in the family taxaceae which has five genera: (1) *Amentotaxus*, (2) *Austrotaxus*, (3) *Pseudotaxus*, (4) *Taxus* and (5) *Torrya*. Out of these the mostly studied and investigated genus is Taxus. These alkaloids show a wide range of pharmacological properties including antitumour and antileukemic.

2.5.3 Steroidal alkaloids

Another important class of alkaloids is steroidal alkaloids. These compounds possess the basic steroidal skeleton (often in modified form) with the nitrogen incorporated as an integral part of the molecule, either in the ring or in the side chain. Such alkaloids exist both in plants and animals and display a wide range of pharmacological and chemical properties and some of them can be converted into steroidal hormones by simple chemical or microbial treatment (Pelletier, 1999).

2.5.4 Classification of alkaloids according to their occurrence in nature

1.The Dogbane botanical family (Apocynaceae)

2.The Aster botanical family (Asteraceae)

3.The Logan botanical family (Loganiaceae)

4.The Poppy botanical family (Papaveraceae)

5.The Citrus botanical family (Rutaceae)

6.The Nightshade botanical family (Solanaceae)

7.The Coca botanical family (Erythroxylaceae)

8.The Borage botanical family (Boraginaceae)

9.The Legume botanical family (Fabaceae)

10.The Monseed botanical family (Menispermaceae)

11.The Berberry botanical family (Berberidaceae)

12.The Buttercup botanical family (Ranunculaceae)

13.The Lily botanical family (Liliaceae)

14.The Coffee botanical family (Rubiaceae)

15.The Amaryllis botanical family (Amaryllidaceae)

16.The Oleaster botanical family (Elaeagnaceae)

17.The Caltrop botanical family (Zygophyllaceae)

18. Mushroom Alkaloids

19. Moss Alkaloids

20.Fungus and bacter Alkaloids

21.Alkaloids that are found in the animal kingdom.

2.5.5 Monoterpenoid-derived indole alkaloids

Indole alkaloids are so-called because they incorporate an indole ring system (Figure 2.4) in their molecular structure. All indole alkaloids are biogenetically derived from tryptophan (Figure 2.4) and therefore contain two nitrogen atoms, one of which is contained within the five-membered part of the indole nucleus. In a few instances, notably the pharmaceutically important alkaloids such as quinine(Figure 1.1) from *Cinchona* species and camptothecin from *Camptotheca acuminata*, this five-membered ring is expanded by the inclusion of an extra carbon and the alkaloids chemically are classified as quinolines (Figure 2.4) rather than indoles, although their biogenetic origins are the same.

The chemistry and biological activity of indole alkaloids have received much attention over the last 50 years and several monographs1,2 and detailed reviews* have been published.

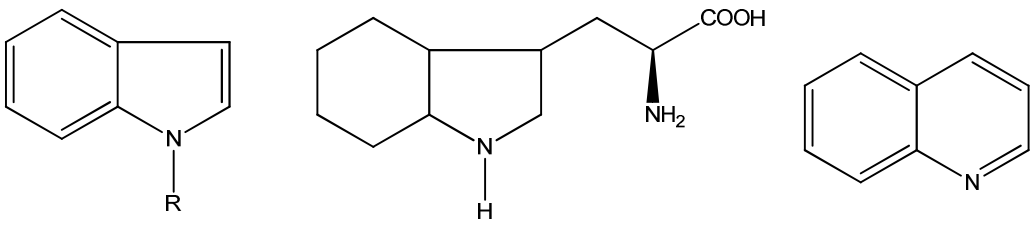

Indole Ring Tryptophan Quinolines

Figure 2.4: The mother compounds of monoterpenoid derived alkaloids (Pelletier, 1999).

The alkaloids of principal therapeutic importance are shown in the Table below, together with their sources.

Three major types of indole alkaloids are recognized by most natural product chemists although several other indole alkaloids are known which do not fit neatly into these three categories. The three major categories are the ‘‘simple’’ indoles that are formed from tryptophan without the addition of other C-skeletal moieties [e.g., harmine (Figure 2.5)], the tryptamine-amino acid congeners found particularly in fungi such as ergot (), and the largest group, numbering several thousand, where the tryptophan skeleton is linked with a monoterpene unit derived from the iridoid secologanin. Because of different rearrangements of the iridoid moiety after conjugation, three major groups of this type of indole alkaloid are generally recognized, these being the Corynanthe-type (e.g., ajmalicine, Figure 2.5), the Iboga-type (e.g., catharanthine, Figure 2.5), and the Aspidosperma-type (e.g., tabersonine, Figure 2.5). In some cases two types are linked together to form bisindoles [e.g., vincristine, (**Fig. 5.2**)], which consist of an Aspidosperma-type linked to an Iboga-type.

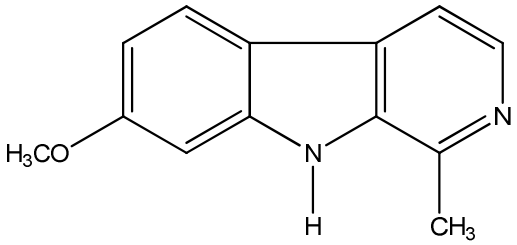

Harmine

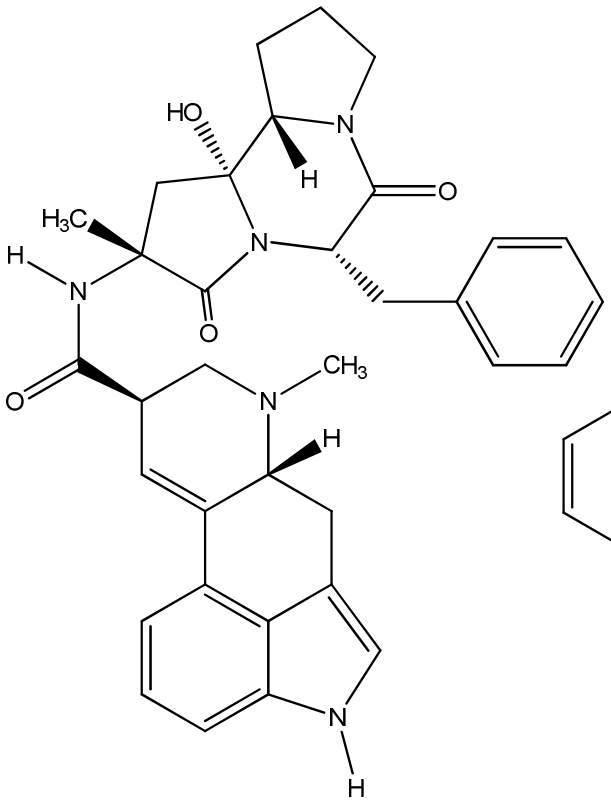

Ergotamine

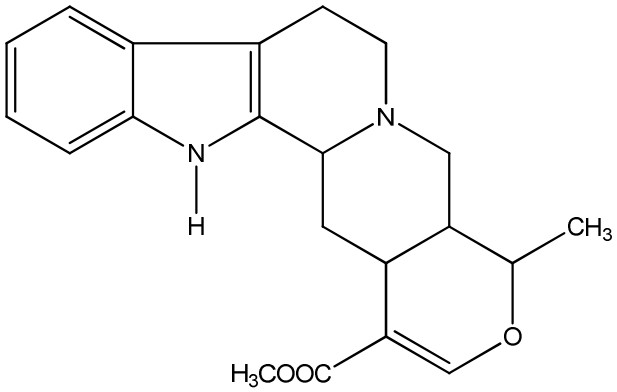

Ajmalicine

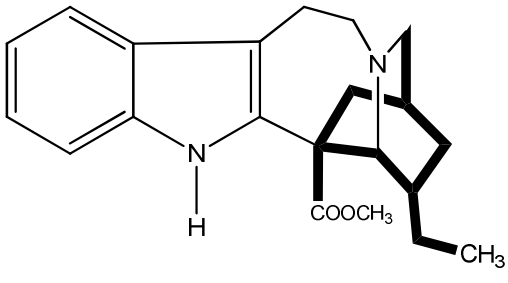

Catharanthine

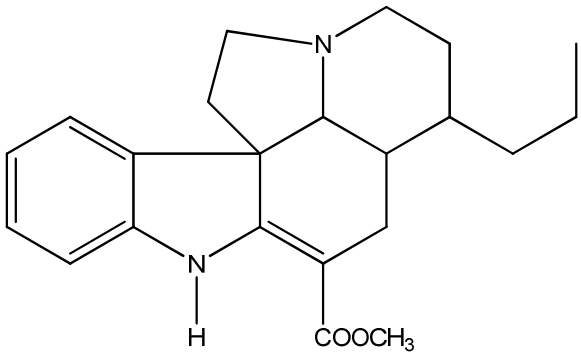

Tabersonine

Figure 2.5: Structure of some Indole alkaloids (Pelletier, 1999).

2.6 Occurrence of Indole Alkaloids in Higher Plants

The simple indoles occur sporadically in fungi and flowering plants and also in animals, since it could be argued that the mammalian neurotransmitter serotonin is also a simple indole and others are found in the skin of certain amphibians (e.g., bufotenine found in toads, Bufo spp.). The fungal genus *Psilocybe* contains alkaloids such as psilocybin, while harmane alkaloids such as harmine 4 are found in flowering plant species. Fairly simple indole alkaloids are found in the seeds of some members of the Fabaceae, physostigmine 13 probably being the bestknown compound of this type. The tryptophan–amino acid alkaloids are often called the ergot alkaloids, since many of them were first isolated from *Claviceps* spp., fungal parasites of grasses that are commonly called ergots. There was considerable surprise when, in the 1960s, they were also found in the seeds of some genera of the Convolvulaceae, considered to be one of the most evolutionary-advanced families of the dicotyledons. The large number of terpenoid–tryptamine alkaloids is largely confined to some genera of three evolutionary-advanced dicotyledonous flowering plant families (i.e., the Apocynaceae, Rubiaceae, and Loganiaceae). An amazing variety of structures belonging to this group have been determined in the last 50 years and they all arise from a Mannich-like condensation between tryptamine and the iridoid secologanin, with subsequent rearrangement of the iridoid components (Cordell, 1981; Pelletier, 1999; Sultana, 1992).

2.7 Biogenetic Classification of Indole Alkaloids

The fundamental building blocks for monoterpene indole alkaloids are tryptamine (tryptophan)(Figure 2.4) and the iridoid, secologanine. (Figure 2.6) The units combined to form (in vivo) strictosidine (Figure 2.6). The nitrogenous glycoside which is the key intermediate in biosynthetic elaboration which subsequently occurs.

Table 2.1: Some monoterpenoid Indole alkaloids of pharmacological significance.

Compound	Source	Pharmacologic Activity
Ajmalicine	*Catharanthus roseus*	Hypotensive
Ajmaline	*Rauwolfia sp.*	Antiarrythmic
Camptothecine	*Camptotheca acuminate*	Anticancer
Deserpidine	*Rauwolfia canescens*	Hypotensive
Ibogaine	*Tabernathe iboga*	Psychomimetic
Leurocristine	*Catharanthus roseus*	Anticancer
Quinidine	*Remijia sp.*	Cardiac depressant
Quinine	*Cinchona sp.*	Antimalarial
Rescinnamine	*Rauwolfia sp.*	Hypotensive
Reserpine	*Rauwolfia vomitoria*	Hypotensive
Strychnine	*Strychnos nux vomica*	CNS depressant
Vincaleukoblastine	*Catharanthus roseus*	Anticancer
Vincamine	*Vinca major*	Hypotensive

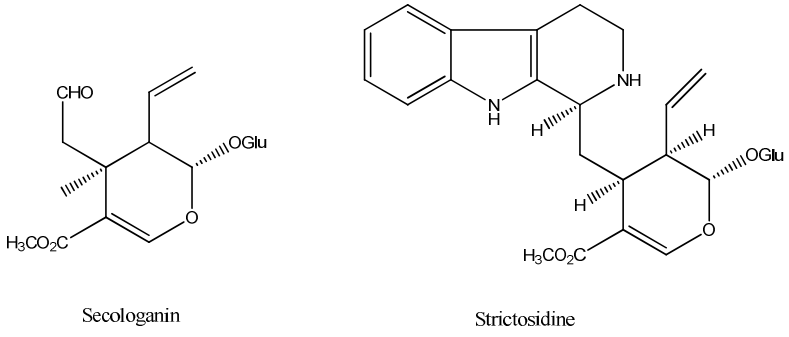

Secologanin Strictosidine

Figure 2.6: Tryptophan and Secologanine combine to form Strictosidine (Cordell, 1981).

Indole alkaloids are divided to five classes and within each class several subclasses have been developed based on their biosynthesis (Table 2.2) (Cordell, 1981).

Table 2.2: Classification of Indole alkaloids based on their biosynthesis.

Class 1 Alkaloids containing a nonrearranged secologanin skeleton			
1.1	Strictosidine group	1.11	Picraline group
1.2	Coryantheine group	1.12	Corymine group
1.3	Vallesiachotamine group	1.13	Ajmaline group
1.4	Adifoline group	1.14	Perakine group
1.5	Talbotine group	1.15	Oxindole group
1.6	Stemmadenine group	1.16	Pseudoxindole group
1.7	Mavacurine group	1.17	Condylocarpine group
1.8	Cinchonamine group	1.18	Akuammicine group
1.9	Sarpagine group	1.19	Strychnine group
1.10	Peraksine group		
Class2 Alkaloids containing an open secologanin skeleton			
2.1	Secodine group		
Class 3 Alkaloids containing a rearranged secologanin skeleton			
3.1	Quebrachamine group	3.6	Vindolinine group
3.2	Aspidospermine group	3.7	Pleiocarpine group
3.3	Schizophylline group	3.9	Oxindole group
3.5	Schizozygine group		
Class 4 Alkaloids containing a rearranged secologanin skeleton			
4.1	Fruticosine group		
Class 5 Alkaloids containing a rearranged secologanin skeleton			
5.1	Catharanthine group		
5.2	Pseudooxindole alkaloids		

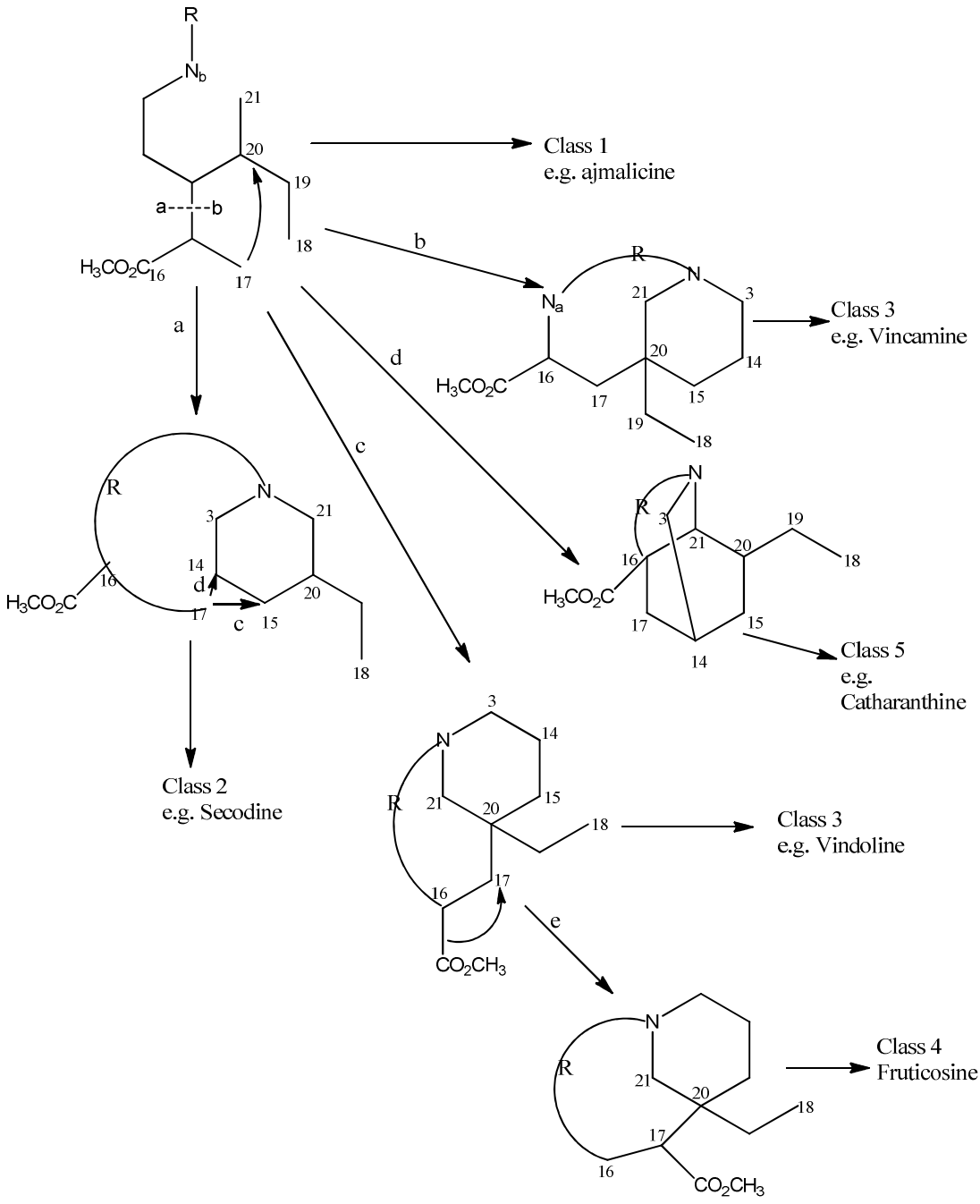

Figure 2.7: Main classes of Indole alkaloids (Cordell, 1981).

Some other sources classify Indole alkaloids according to their skeleton properties. Based on these data sources Indole alkaloids with a C9- or C10- monoterpene moiety are classified into the subgroups shown in **Fig. 2.8.** (Pelletier, 1999):

2.8 Pharmacologıcal Importance of Indole Alkaloids

The biological activity of some fungi and plants containing indole alkaloids has been known for a very long time, particularly those that have a severe effect on humans or

animals, and the elucidation of the structure of the alkaloids responsible is a comparatively recent event.

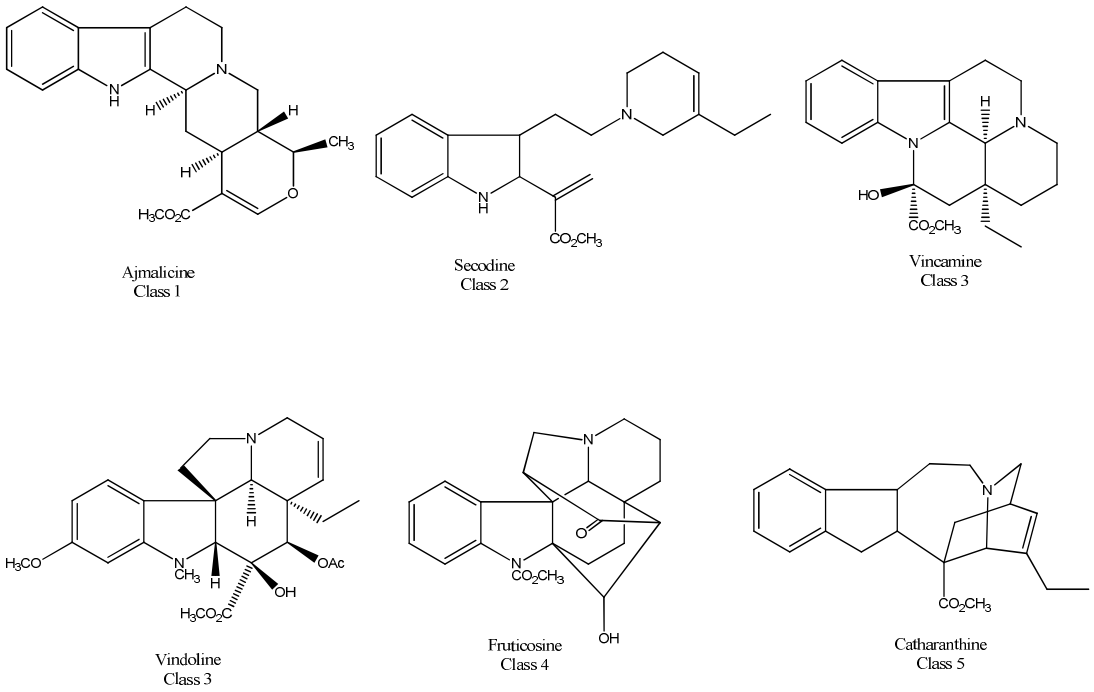

Figure 2.8: The chemical structure of some examples of main classes from Indole alkaloids (Cordell, 1981).

Ergot contamination in rye consumed by humans, and in grasses consumed by domestic grazing animals, has been known to be associated with miscarriage, gangrene, and CNS disturbances for hundreds of years and the effects of the contained alkaloids were exploited in central European traditional medicine for helping in childbirth. Ergot contains several indole alkaloids and two of them have found extensive use in pharmacy.

Ergometrine (Figure 2.10) is mainly used in childbirth because of its ability to cause contraction of the uterus and contract blood vessels, thus reducing bleeding, while ergotamine has a stronger dopaminergic effect and is mainly employed in treating migraine because it reduces vasodilation.

Several semisynthetic compounds based on ergotamine have been developed for treating Parkinsonism and related neurological disorders.

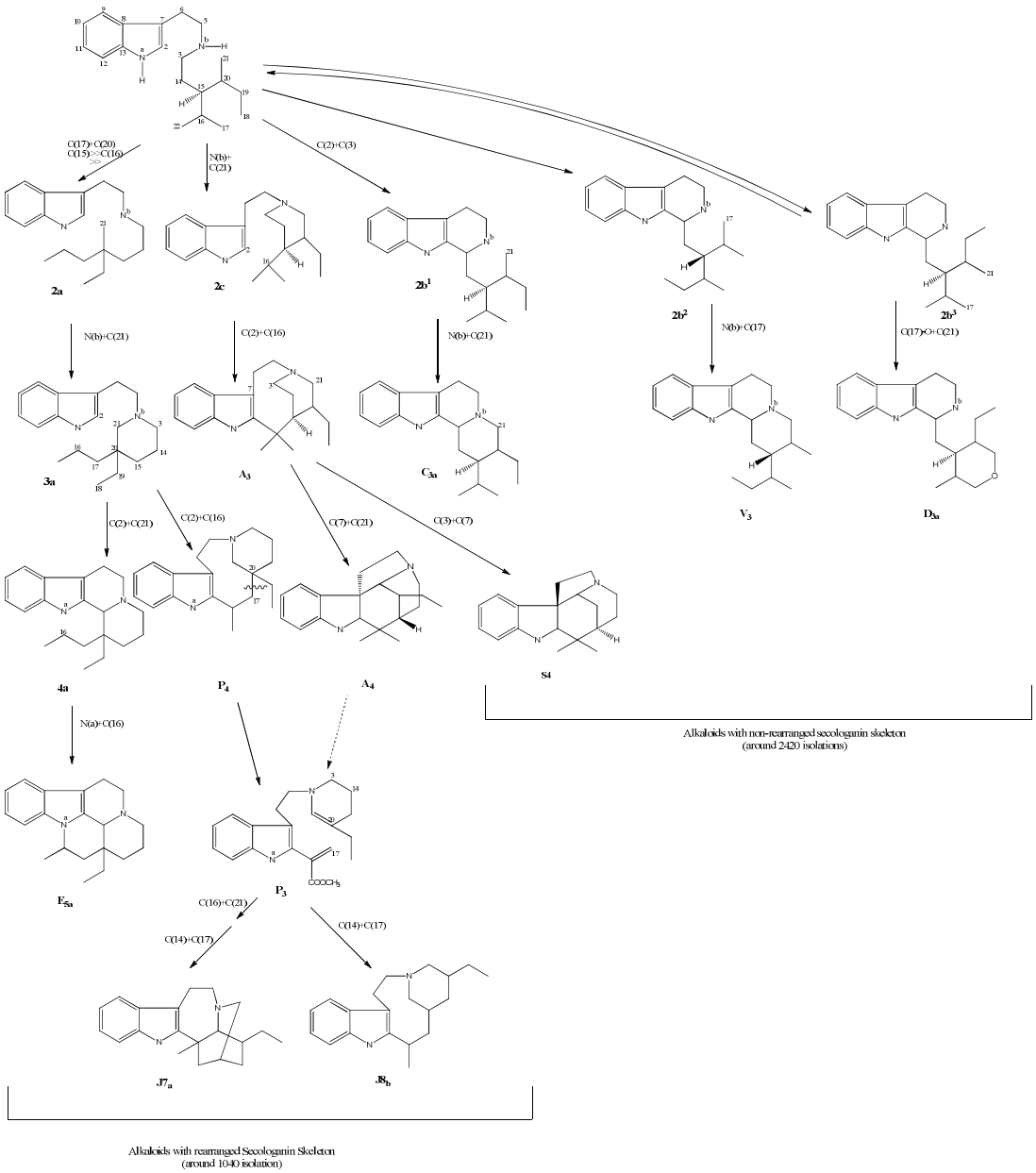

Figure 2.9: Classification of Indole alkaloids according to their structure (Cordell, 1981).

In southern Asia, the toxic nature of *Strychnos nux* vomica was well known and other species of the genus were known as a source of arrow poisons in Africa and South America. Many fungi and plants containing indole alkaloids have been used as hallucinogens or in religious rites because of their effect on consciousness and these include the Psilocybe fungi in Oaxaca (Mexico) which were known as ‘‘teonanácatl’’; the roots of Tabernanthe iboga in west central Africa known as

‘‘iboga’’; and the seeds of Ipomoea spp., known in Mexico as ‘‘ololiuqui.’’ Physostigmine (also called eserine) is an interesting example of an indole alkaloid that was discovered because of the use of the seeds of a plant *Physostigma venenosum*, in southeastern Nigeria as an ordeal poison. It was the first acetylcholinesterase inhibitor to be discovered and has been used to treat glaucoma and myasthenia gravis. Analogues have been developed as insecticides as well as drugs, the most recent being rivastigmine, which is used for symptomatic relief in Alzheimer’s disease.

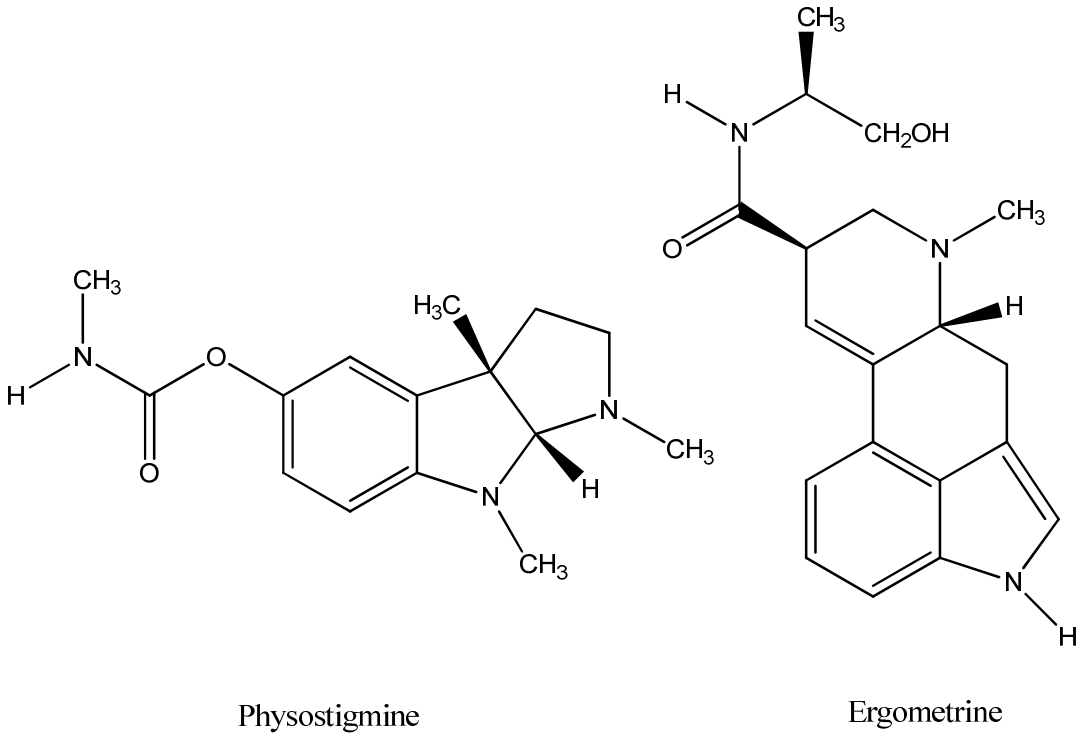

Physostigmine Ergometrine

Figure 2.10: Two alkaloids with significant pharmacological activity (Mukhopadhyay, 1981).

Other plant species containing indole alkaloids were widely used in traditional medical systems (e.g., *Rauwolfia serpentina* roots), known as ‘‘sarpagandha’’ in Ayurvedic medicine have a long tradition of use as a treatment for snakebite and some psychiatric diseases. *Rauwolfia* species contain many indole alkaloids but the one which was most widely used in the mid 20th century was reserpine (Figure 1.2), which was the first tranquilizing drug but also extensively used at one time as a hypotensive. Ajmaline 16 is another *Rauwolfia* indole alkaloid, which is used to treat cardiac arrhythmia in some countries. Yohimbine (Figure 2.11) from *Pausinystalia yohimbe*, the bark of which has a reputation as a male aphrodisiac, has been used to treat erectile dysfunction. Extracts from barks of *Cinchona* spp. were introduced in

Europe for the treatment of malaria not long after the conquest of much of South america by the Spanish in the 16th century and the major alkaloid quinine (Figure 1.1), which contains a quinoline ring system rather than indole, has been used for many years as an antimalarial drug although now used only where other antimalarials are ineffective.

Possibly the indole alkaloids that are most important clinically are the anticancer bis-indoles vinblastine(Figure 5.2) and vincristine (Figure 5.2), which are found in *Catharanthus roseus*. These were introduced in the 1960s and have made a marked impact on remission of childhood leukemia and some other cancers. Other anticancer alkaloids derived from tryptophan are the indole ellipticine 20 and the quinoline camptothecin 21, the latter having greater importance as a template for analogues such as topotecan.

Many other types of alkaloids, their bitter taste is thought to act as a feeding deterrent to mammals, as they are often concentrated in parts of the plant vulnerable to attack (e.g., the high percentage of alkaloids in the bark of *Rauwolfia* roots). The deterrent property has been demonstrated for the simple indole gramine as regards sheep. It has also been pointed out that gramine has antifeedant activity against aphids, an example of general antifeedant activity regarding insects, shown by alkaloids.(Mukhopadhyay, 1981).

2.9 Chemosystematic Importance of Indole Alkaloids

Waterman has pointed out that the chemosystematic importance of the alkaloids is not great. The major interest concerning Indole alkaloids is that the Indole–secologanin Indole alkaloids are found in assorted genera of the Apocynaceae, Loganiaceae, and Rubiaceae of the Gentianales, with the Iboga type restricted to the Apocynaceae. These compounds are also found in the lesser families Alangiaceae, Nyssaceae, and Icacinaceae of the Cornales.(Sultana, 1992)

2.10 Alkaloids of Yohimbe

We are presenting the isolation and structure elucidation of constituents of 4 *Vinca* species occuring in Turkey, one of which (*Vinca herbacea)* has previously been

studied by our group (Boga, 2011) One of these species has recently been introduced to the world of botany by Koyuncu M (Koyuncu, 2011) and is endemic to Turkey.

During the chemical identification of this plant we obtained α- and β-Yohimbine which previously have not been isolated from *Vinca* species. Since the the occurance of a certain class of chemical compound in a plant family and/or species has a significant importance in plant taxonomy it will be useful to mention on the structure of "Yohimbinoids" in this chapter.

Yohimbehe bark, originally believed to be derived from a species of *Taberncemontana* (Apocynaceae), but now assigned to *Pausinystalia yohimba,* Pierre (Fam. Rubiaceas; syn. *Corynanthe yohimbe,* Schum.), a tree native to the Cameroons and French Congo, contains alkaloids on which pioneer work was done by Spiegel Some of the alkaloids are of uncertain individuality, *e.g.,* Spiegel's " yohimbenine "(Spiegel, 1915, 1926) and the unnamed base described by Danckwortt and Luy (Ohem, 1896)

The yohimbines comprise a group of natural, pentacyclic Indole alkaloids containing five chiral centers illustrated by Figure 2.11 (Ohem, 1896).

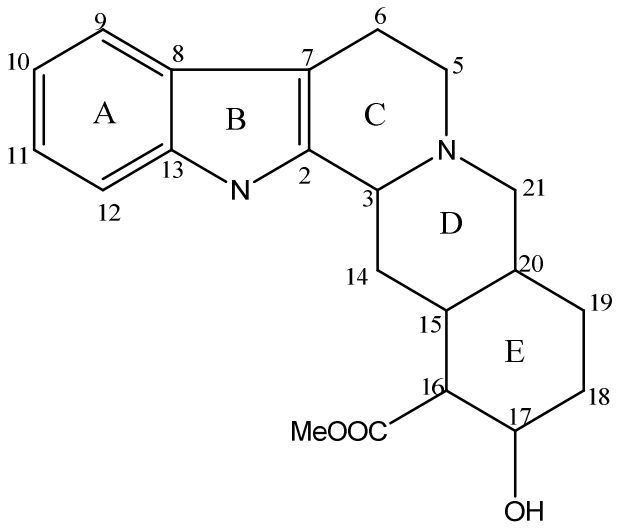

Figure 2.11: Chemical structure of Yohimbine (Ohem, 1896).

The Indole alkaloids under consideration have been categorized in the past on the basis of their ring D stereochemistry in terms of normal Figure 2.12(A), pseudo Figure 2.12(B)**,** allo Figure 2.12(C)**,** and epiallo Figure 2.12(D) configurations.

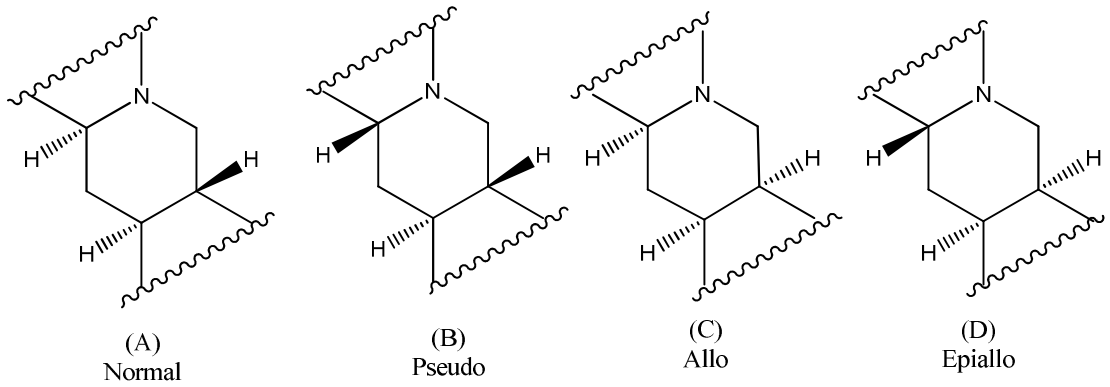

Figure 2.12: The categorization of Yohimbine alkaloids based on stereochemistry of ring D (Henry, 1949).

Normal type Yohimbine alkaloids includes: yohimbine; Figure 2.13(A), β-yohimbine; Figure 2.13(B), coryanthine; Figure 2.13 (C), Yohimbanr; Figure 2.13 (D) and Yohimbinone; Figure 2.13 (E).

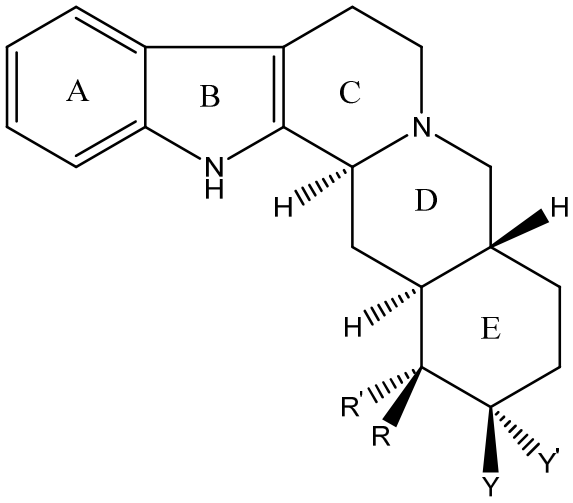

(A): R=Y=H; R'=CO_2Me; Y'=OH Yohimbine
(B): R=Y'=H; R'=CO_2Me; Y=OH β-Yohimbine
(C): R=CO_2Me, R'=Y=H; Y'=OH Coryanthine
(D): R=R'=Y=Y'=H Yohimbane
(E): R=H, R'=CO_2Me, Y+Y'=O Yohimbinone

Figure 2.13: The members of normal type Yohimbine alkaloids (Henry, 1949).

Pseudo type Yohimbine alkaloids includes: Pseudoyohimbine; Figure 2.14 (A) and Pseudoyohimbone; Figure 2.14 (B).

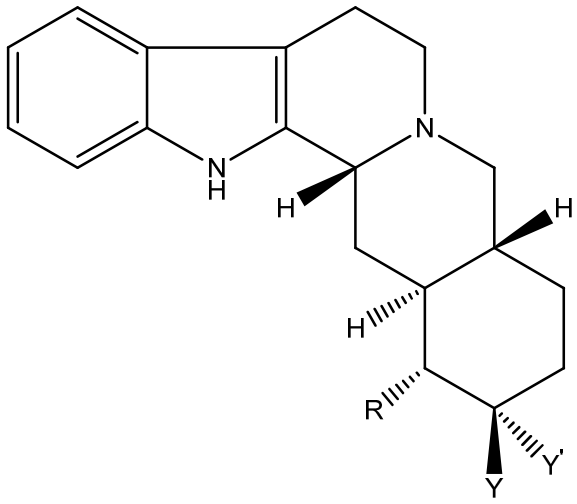

(A): R=CO_2Me; Y=H Y'=OH Pseudoyohimbine
(B): R=H, Y+Y'=O Pseudoyohimbone

Figure 2.14: Pseudo type Yohimbine alkaloids (Henry, 1949).

Allo type Yohimbine alkaloids includes: α-Yohimbine; Figure 2.15 (A), Alloyohimbine; Figure 2.15 (B), Alloyohimbane, Figure 2.15 (C), Isoreserpine, Figure 2.15 (D).

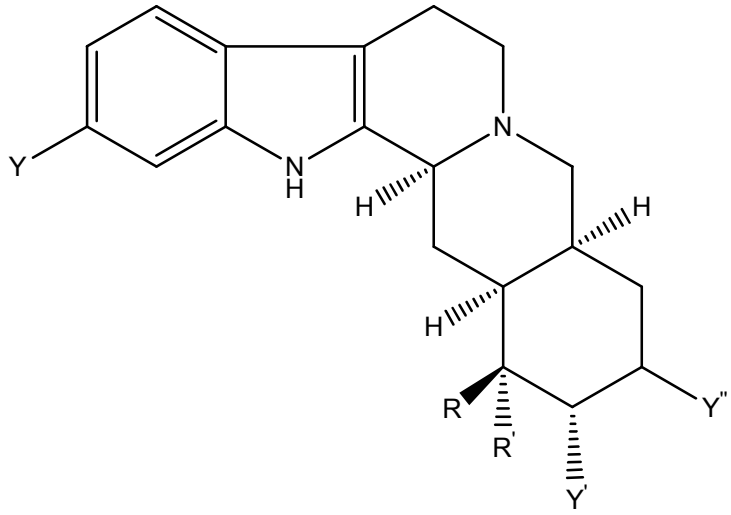

(A): R=CO_2Me; R'=Y=Y"=H; Y'=OH α-Yohimbine
(B): R=Y=Y"=H, R=H, R'=CO_2Me, Y'=OH Alloyohimbine
(C): R=R'=Y=Y'=Y"=H Alloyohimbane
(D): R=CO_2Me; R'=H, Y=Y'=OMe, Y"=OTMB Isoreserpine

Figure 2.15: Allo Type Yohimbine alkaloids (Henry, 1949).

Epi-Allo type Yohimbine alkaloids includes: 3-*Epi*-α-yohimbine; Figure 2.16 (A), Reserpine; Figure 2.16(B), Raunescine; Figure 2.16 (C), Isoraunescine; Figure 2.16 (D), Epialloyohimbane; Figure 2.16 (E), and Reserpate; Figure 2.16 (F).

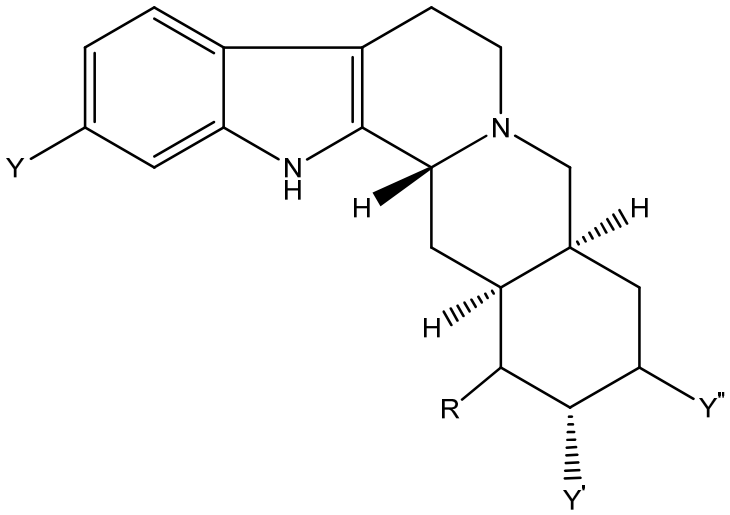

(A): R=CO_2Me; Y=Y"=H; Y'=OH 3-Epi-α-yohimbine
(B): R=CO_2Me Y=Y'=OMe, Y"=OTMB Reserpine
(C): R=CO_2Me, Y=H, Y'=OH, Y"=OTMB Raunescine
(D): R=CO_2Me; Y=H, Y'=OTMB, Y"= OH Isoraunescine
(E): R=Y=Y' =Y"=H Epialloyohimbane
(F): R=CO_2Me, Y=Y'=OMe, Y"=H Reserpate

Figure 2.16: *Epi*-Allo Type Yohimbine alkaloids (Henry, 1949).

Table 2.3: Physical properties of some yohimbinoid alkaloids.

Name	**Crystals and Solvent of Crystallisation**	**m.p.**	**$[\alpha]_D$ Py = pyridine A = alcohol**
Yohimbine (quebrachine)	Needles;	234-235°	+84 to 108°(Py) +50 to 55° A)
α-Yohimbine	Polyhedral: MeOH or EtOH + H_20	234-235°	-22° to -28° (A) -9.3° (Py)
β-Yohimbine	Leaflets : H_2Oor 2MeOH	235-236°	-54° (dry : Py)
allo Yohimbine	Leaflets ; 1 or 3 H_2O.	B. H_2O, 135-140°; B.3H_2O, 98-99° or 104-105°	-72-7° or -73-6° (Py)
Corynanthine	Hexagonal; 2H_2O	241-242° (dry)	-125° (A) - 73° (Py)

2.10.1 Pharmacological action

Yohimbine lowers blood pressure, increases the depth and frequency of respiratory movements and in toxic doses paralyses respiration, death being due to this cause in mammals, the heart remaining active for some time longer. It possesses local anaesthetic properties and resembles ergotoxine and ergotamine in sympatholytic

action. Though quebrachine has been shown to be identical with yohimbine, differences in pharmacological action have been noted. The other alkaloids of the group are stated to resemble yohimbine qualitatively in action, but Raymond-Hamet has observed differences in the action of Aspidospermine. Dawes (Dawes, 1946);. According to Edmunds, and Gunn (EDMUNDS, 1934) yohimbine is the most active of the group, closely followed by Aspidospermine; Quebrachamine and Aspidosamine. Kreitmair (Kreitmair, 1928) found α-yohimbine less toxic than yohimbine, equally potent as a local anaesthetic and similar in action on the genital organs of the dog. Various authors (Kreitmair, 1928) have stated that yohimbine exerts no estrogenic activity (Raymond, 1937). For method of evaluation also found that orynanthine is more active on the genital organs of the dog (Raymond, 1937) and on those of the rabbit cornea. The local anaesthetic action of yohimbine, cocaine and corynanthine is of the order 2 : 1 : 0.25 (Henry, 1949).

2.11 Vallesiachotamine

As mentioned in chapter condensation of secologanine with tryptamine affords strictosidine (3H-α) and vincoside (3H-β) (Figure 2.17).

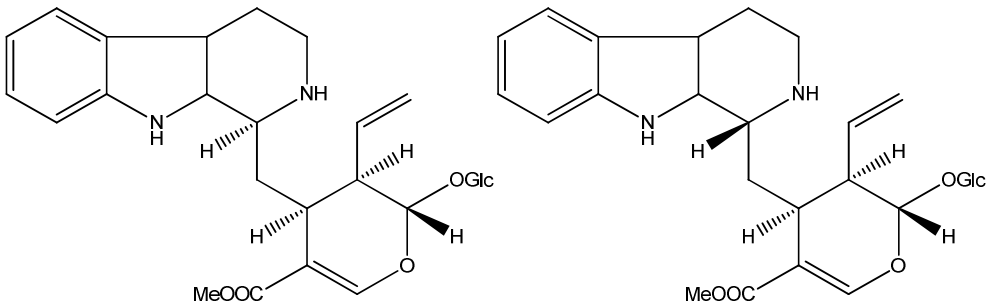

Strictosidine Vincoside

Figure 2.17: Chemical composition of Strychnine, the mother compound of Vallesiachotamine and Vincoside, (Arbain D, 1992).

Removal of sugar from Strictosidine under mild condition affords Vallesiachotamine and likewise Vincoside spontaneously gives its 3β epimer.

Vallesiachotamine was isolated from *Vallesia dichotoma* Ruis et. Pav. (Holker, 1959; Walser, 1965) and has been classified in modified Corynanthe (Hunterburine type) (Mukhopadhyay, 1981) alkaloids.

However duplication of some peaks in the NMR spectrum of Vallesiachotamine could be seen which has been attributed to the E\Z isomerization of the ethylidene group of vallesiachotamine**.** Wh**e**n some references mention on that Vallesiachotamine is a mixture of these two geometrical isomers (J. Edwin Saxton, 1983), some papers name them as Vallesiachotamine and Isovallesiachotamine (Figure 2.18) (Arbain D, 1992; Bolzani VS, 2001).

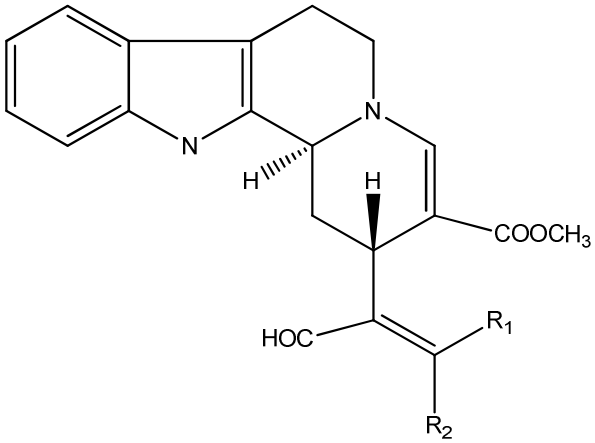

R_1	R_2	
CH_3	H	**Isovallesiachotamine**
H	CH_3	**Vallesiachotamine**

Figure 2.18: Chemical structure of Vallesiachotamine and its "Iso"mer (Bolzani VS, 2001).

3. Vinca L.

The genus *Vinca* L. **(**Apocynaceae) is native to Europe, northwest Africa and southwest Asia and comprises six species: *Vinca difformis* Pouret, *V. erecta* Regel & Schmalh, *V. pubescens* d'Urv., *V. herbacea* Waldst. & Kit., *V. major* L. and *V. minor* L.; the last three occur in Turkey (Stearn, 1973, 1978)

Low creeping evergreen or deciduous perennial subshrubs or herbs. Leaves opposite. Flowers large, solitary in leaf axils on long pedicels. Corolla infundibular, lacking appendages in throat but with a zone of hairs above insertion of stamens and a low ridge connecting corolla lobes at base, lobes spreading. Stamens included, inserted c. halfway up corolla tube; filaments short, bent forward the back; anthers with flat flap-like appendage at apx. Disc glands 2. Seeds glabrous, oblong, not comose.

3.1 *V. herbacea*

Vinca herbacea (Herbaceous Periwinkle) is a flowering plant native to eastern and southeastern Europe, from Austria south to Greece, and east to the Crimea, and also in southwestern Asia east to the Caucasus and Alborz mountains. It grows mainly in steppe habitats.

Herbaceous perennial, dying back completely top rootstock each winter, with ascending shoots to 20 cm, trailing shoots to 60 cm. leaves herbaceous, deciduous, very variable, narrowly elliptic, elliptic, lanceolate to ovate, 0.6-5x0.2-3 cm, base cuneate, apex acute, margin smooth, scabrid or shortly ciliate, with inconspicuous venis ascending at 10-35o from midrib; petiole 1-4mm. Calyx 3-10mm; lobes shortly ciliate or glabrous and smooth. Corolla pale blue to purple-blue; tube 1-2 cm, lobes 1-2 cm. Follicles 2.5-3.5 cm. Seeds 11-14 mm. Fl.3-5. Open sunny slopes, on sand, gravel, scree, fallow fields, rocks, scrub, very open woodland, 400-2000 m.

Scattered throughout Turkey & Islands: Tekirdağ: 14km E. of Tekirdağ, Istanbul: Değirmenköy, Bolu: Abant, Kastamonu: Kastamonu, Samsun: Havza (Sekizgöz), Gümüşhane: Gümüşhane, Çoruh: Artvin, Erzurum: S. Of İspir, İzmir: Tahtalı Daç

above İzmir, Eskişehir: 56 km from Eskişehir to Sivrihisar, Ankara: Ankara, Niğde: Malatya to Akça Da., 1000 m, Malatya: Baştaş, Maghda Da., Van: Bitlis, Antalya: S.W. of Avlan, Antalya: Hafis Paşa, Mut: Mağras Da., İçel: N. Side of Gülek Boğazı, Maraş: 10 km S. Of Maraş, Urfa: E. of Urfa (***Figure 3.1***).

Figure 3.1: *Vinca herbacea* (Url 1).

3.2 *V. major*

Vinca major, with the common names Large Periwinkle, Greater Periwinkle and Blue Periwinkle, is a flowering plant native to southern Europe, from Spain and southern France east to the western Balkans, and also in northeastern Turkey and the western Caucasus.

Evergreen subshurb, with arching shoots rising to 30 cm then curving downwards, trailing shoots to 100 cm. Leaves evergreen, blade mostly ovate but varying from broadly ovate to lanceloate, 2.5-9 x 2-6 cm, base cordate or turncate-rounded, apex acute or obtuse, margin ciliate, with veins spreading at 40-50o from midrib; petiole 5-15 mm. Calyx 6-18 mm; lobes ciliate. Corolla violet; tube 1.2-2 cm; lobes 1.2-2 cm. Follicles 2.5-3.5 cm.

Cultivated as an ornamental plant and sometimes naturalized: İstanbul: Yıldız Parkı, İstanbul: Ömerli to Şile, 10 km to Heriz, Bursa: Kumla, Hatay: Harbiye.

Subspecies

There are two subspecies, with geographically separate ranges:

•*Vinca major* subsp. *major*. Leaf petioles finely hairy, hairs short. Southern Europe.

•*Vinca major* subsp. *hirsuta* (Boiss.) Stearn (syn. *V. pubescens* d'Urv.). Leaf petioles densely hairy, hairs longer; petals much narrower. Caucasus, northeastern Turkey.

The closely related species *Vinca minor* is similar but smaller, with narrower, hairless leaves ***(*Figure 3.2*)***.

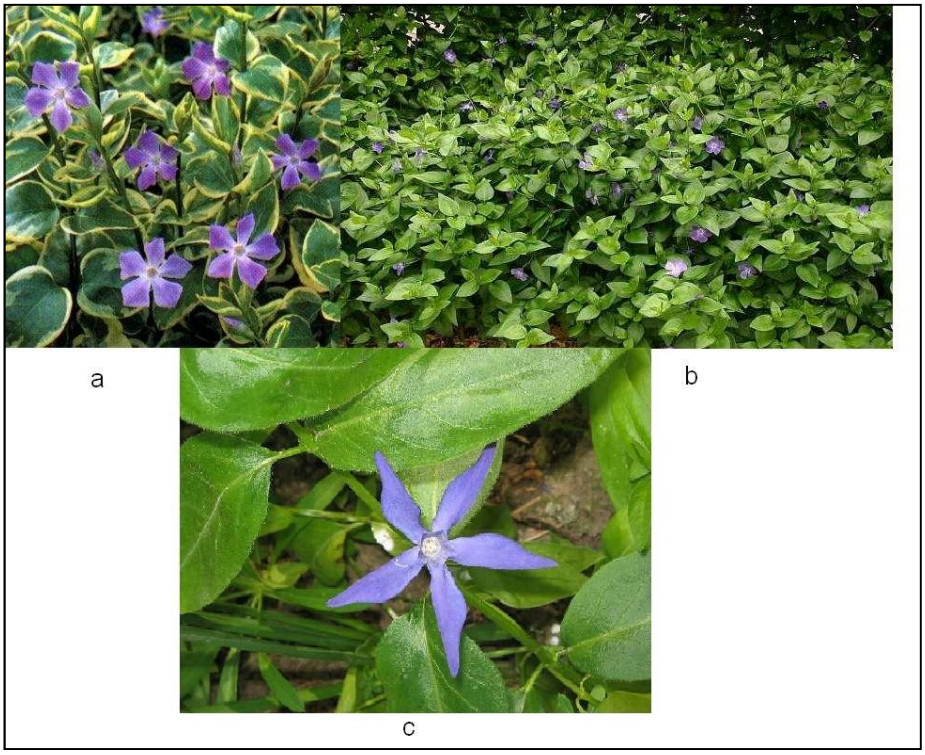

Figure 3.2: *Vinca major*(Url 1).

3.3 *V. minor L.*

Vinca minor, Lesser periwinkle and Dwarf periwinkle, is a plant native to central and southern Europe, from Portugal and France north to the Netherlands and the Baltic States, and east to the Caucasus, and also in southwestern Asia in Turkey. Other vernacular names used in cultivation include Small periwinkle, Common periwinkle, and sometimes in the United States, Myrtle or Creeping myrtle, although this is misleading, as the name myrtle normally refers to the Myrtus species. Wikipedia

Evergreen subshurb with flowering shoots to 15 cm, trailing shoots to 60 cm, making densely interwoven masses. Leave evergreen, blade mostly elliptic or lanceolate (but often oveate on trailing shoots), 1.5-4.5 x 0.5-2.5 cm, base usually cuneate, sometimes rounded, apex acute or obtuse, margin smooth and glabrous, with venis spreading from midrib at 40-60; petiole 2-10 mm. Calyx 3-4 mm, glabrous. Corolla usually blue-violet, sometimes white or reddish-purple; tube 9-11 mm, lobes 10-15 mm. Follicles 1.5-2 cm; seeds 6-9 mm.Cultivated and sometimes naturalized. İstanbul: Büyükdere, Park Camara, İstanbul: Kınalıada, Bolu: Abant***(Figure 3.3)***.

Figure 3.3: *Vinca minor* (Url 1).

Ethnomedicine

Ethnomedically, the dried leaves, aerial parts, and in some cases the entire plant of *Vinca* minor, are used to enhance blood circulation, including that of the brain, enhance metabolism in the brain, and to treat cardiovascular disorders.(Stearn, 1978)

3.4 *V. soneri* (Figure 3.4)

Perennial subschrubs with woody rootstock. Stem erect, simple, pilose, 25-50 cm. Trailing shoots absent. Leaves opposite, sessil or shortly petiolate, simple, entire, ovate-elliptic, 5-8 x 2.5-3.5 cm, base and apex acute, margine smooth and glabrous, beneath puberulant only on nerves-with veins spreading at 10-12 from midrib, petiol 0-1 mm long. Calyx 8-10 mm, lobes linear, glabrous. Corolla blue or pale-blue, lobes white-blue, tube 2-2.5 cm, lobes 1- 1.5 cm. Folicle 5-7 cm, seeds 10-12 mm, tuberculate. Flowering time: 5- 6. Dry stony slopes, 1200- 2800 m (Koyuncu et al.).

Figure 3.4 :*Vinca soneri*

Table 3.1: The morphological differences between *Vinca soneri* and *V. herbacea.*

Characters	*Vinca soneri*	*Vinca herbacea*
Stem	**25-50 cm**	**to 20 cm**
Trailing shoots	**absent**	**to 60 cm**
Leaves	**5-8** x **2.5-3.5 cm**	**0.6-5** x **0.2-3 cm**
	eliptic-ovate	narrowly elliptic, elliptic-lanceolate
Petiol	0-1 mm	1-4 mm
Calyx	8-10 mm	3-10 mm
Tube of corolla	**2-2.5 cm**	**1-2 cm**
Follicles	**5-7 cm**	**2.5-3.5 cm**
Flowering time	May-June	March-May

3.5 Indole Alkaloids Isolated from *Vinca herbacea, Vinca major and Vinca minor*

A literature summary of Indole alkaloids that have been isolated from three *Vinca* species are given in **APPENDIX F**

4. NANO MEDICINE

4.1 Introduction to Nano-Medicine

Nanotechnology is an area of science devoted to the design, construction, and utilization of functional structures on the nanometer scale (often 100nm or smaller). At the nanoscale, the properties of materials often differ from those of the corresponding bulk materials. In fact, fundamental characteristics of a given material can be precisely controlled by nanotechnology without changing its chemical composition—such as melting point, magnetic properties, or even a characteristic as basic as color. There are numerous applications for nanotechnology. Among them, the treatment, diagnosis, monitoring and control of biological systems have recently been referred to as ‘‘nanomedicine’’ by the National Institute of Health (Bethesda, MD, USA). Nanomedicine may involve a number of different types of nanodevices, including nanoparticles, nanomachines, nanofibers, sensors, and other nanoscale microfabrication-based entities .

Nanotechnology is now frequently used for various applications in fiber and textiles, agriculture, electronics, forensic science, space and medical therapeutics. However, biodegradable nanoparticles are frequently used to improve the therapeutic value of various water soluble/insoluble medicinal drugs and bioactive molecules by improving bioavailability, solubility and retention time. These nanoparticle–drug formulation reduces the patient expenses, and risks of toxicity.

Nanoencapsulation of medicinal drugs (nanomedicines) increases drug efficacy, specificity, tolerability and therapeutic index of corresponding drugs. These nanomedicines have many advantages in the protection of premature degradation and interaction with the biological environment, enhancement of absorption into a selected tissue, bioavailability, retention time and improvement of intracellular penetration.

Several disease related drugs/bioactive molecules are successfully encapsulated to improve bioavailability, bioactivity and control delivery. Nanomedicines of the dreadful diseases like cancer, AIDS, diabetes, malaria, prion disease and tuberculosis

are in different trial phase for the testing and some of them are commercialized (Weili Qiao, 2010).

4.2 Introduction to Nano-Drug Delivery Systems

Nanotechnology has opened the possibility of controlling and manipulating structures at the molecular level and led to the creation of novel surface architectures and materials.

Traditional biomedical applications incorporated the use of nanotechnology in a broad spectrum of areas. Among them, biosensors, tissue engineering, intelligent systems and nanocomposites are used in implant design and controlled release systems. Several nano-oriented approaches are being intended (e.g. nanoparticle engineering) in order to optimize the technological aspects of drugs. The use of these processes has dramatically enhanced dissolution rates *in vitro* and bioavailabilities *in vivo* of many drugs. Another important strategy is the design of nanocarriers. From the first liposomes developed by Gregoriadis and colleagues more than three decades ago until the current state-of-the-art, a pronounced increase in the variety of macromolecular-based approaches for drug delivery was observed. Among the technological alternatives, the most broadly implemented are polymeric nanoparticles, dendrimers, polymeric micelles and polymersomes.

Drug nanoformulations (nanodrug) are superior to traditional medicine with respect to control release, targeted delivery and therapeutic impact. These targeting capabilities of nanomedicines are influenced by particle size, surface charge, surface modification, and hydrophobicity. Among these, the size and size distributions of nanoparticles are important to determine their interaction with the cell membrane and their penetration across the physiological drug barriers. The size of nanoparticles for crossing different biological barriers is dependent on the tissue, target site and circulation. For the cellular internalization of the nanoparticles, surface charge is important in determining whether the nanoparticles would cluster in blood flow or would adhere to, or interact with oppositely charged cells membrane. Cationic surface charge is desirable as it promotes interaction of the nanoparticles with the cells and hence increases the rate and extent of internalization. For targeted delivery, persistence of nanoparticles is required in systemic circulation of the body. But conventional nanoparticles with hydrophobic surface are rapidly opsonized and

massively cleared by the fixed macrophages of the mononuclear phagocytic system (MPS) organs. For increasing circulation time and persistence in the blood, surface of conventional nanoparticles are modified with different molecules. Coating of hydrophilic polymers can create a cloud of chains at the particle surface which will repel plasma proteins. Finally, the performance of nanoparticles *in vivo* is influenced by morphological characteristics, surface chemistry, and molecular weight. Surface modified nanoparticles have anti-adhesive properties by virtue of the extended configuration on the particle surface which acts as steric barrier reducing the extent of clearance by circulating macrophages of the liver and promoting the possibility of undergoing enhanced permeation process.

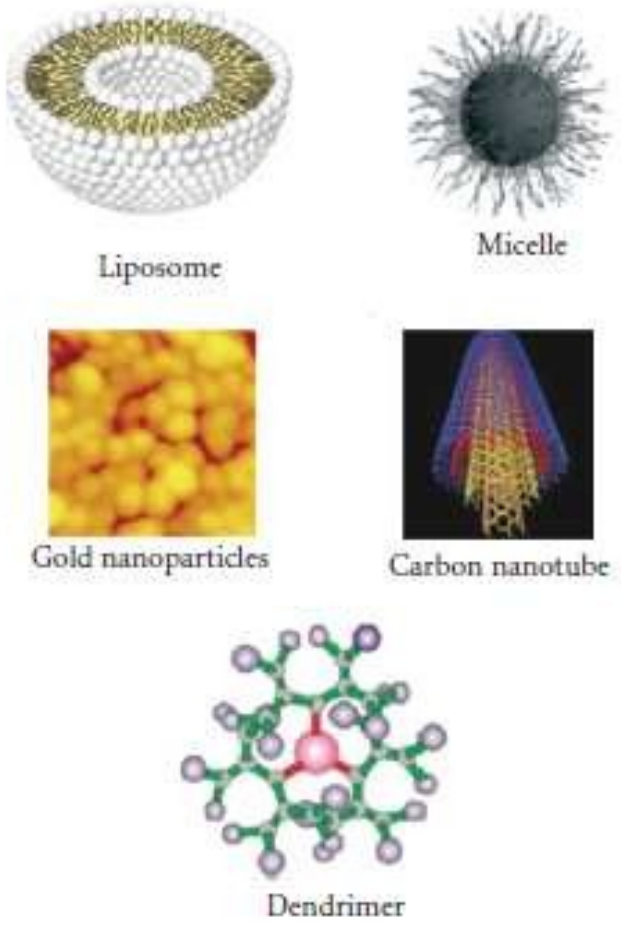

Figure 4.1 Different nanotechnology-based carrier systems (Weili Qiao, 2010).

Release mechanism can be modulated by the molecular weight of the polymer used. Higher the molecular weight of polymer slower will be the *in vitro* release of drugs. Careful design of these delivery systems with respect to target and route of

administration may solve some of the problems faced by new classes of active molecules. Biodegradable polymeric nanoparticles based drug delivery systems.

4.3 Different Nanotechnology-Based Nanocarrier Systems

Based on nanotechnology, nanocarriers synthesized from organic and inorganic materials have been developed, such as nanoparticles, micelles, carbon nanotubes, dendrimers and nanofibers (Figure 4.1). They have shown great potential in cancer therapy by enhancing the performance of medicines and reducing systemic side effect in order to gain therapeutic efficiency (Weili Qiao, 2010).

4.3.1 Micelles formed from amphiphilic block copolymers

The application of polymer made particles (micro and nano) as means for drug vehiculization was one of the most broadly investigated strategies during the last decades. Depending on the production methodology, nanocapsules or nanospheres can be obtained. While the former are vesicular systems where the solid or solubilized drug is surrounded by a polymeric membrane, the later comprise a solid matrix with different levels of porosity where the molecules are homogeneously distributed across the bulk or attached to the surface The different aspects of nanoparticles as well as the biomaterials employed for their production have been comprehensively reviewed by several research groups.

The general synthesis and encapsulation of biodegradable nanomedicines are represented in (**Fig. 4.2**). The drug molecules either bound to surface as nanosphere or encapsulated inside as nanocapsules (Kumari, Yadav, & Yadav, 2010).

The most broadly investigated polymers include the natural chitosan, alginate, gelatin and albumin and the synthetic polylactic acid (PLA), poly (lactic-co-glycolic) acid (PLGA), polycaprolactone (PCL), poly (cyanoacrylate) (PCA), poly (methacrylic acid-co-ethylacrylate) block copolymer as well as combinations with other materials such as poly(ethylene glycol) (PEG).

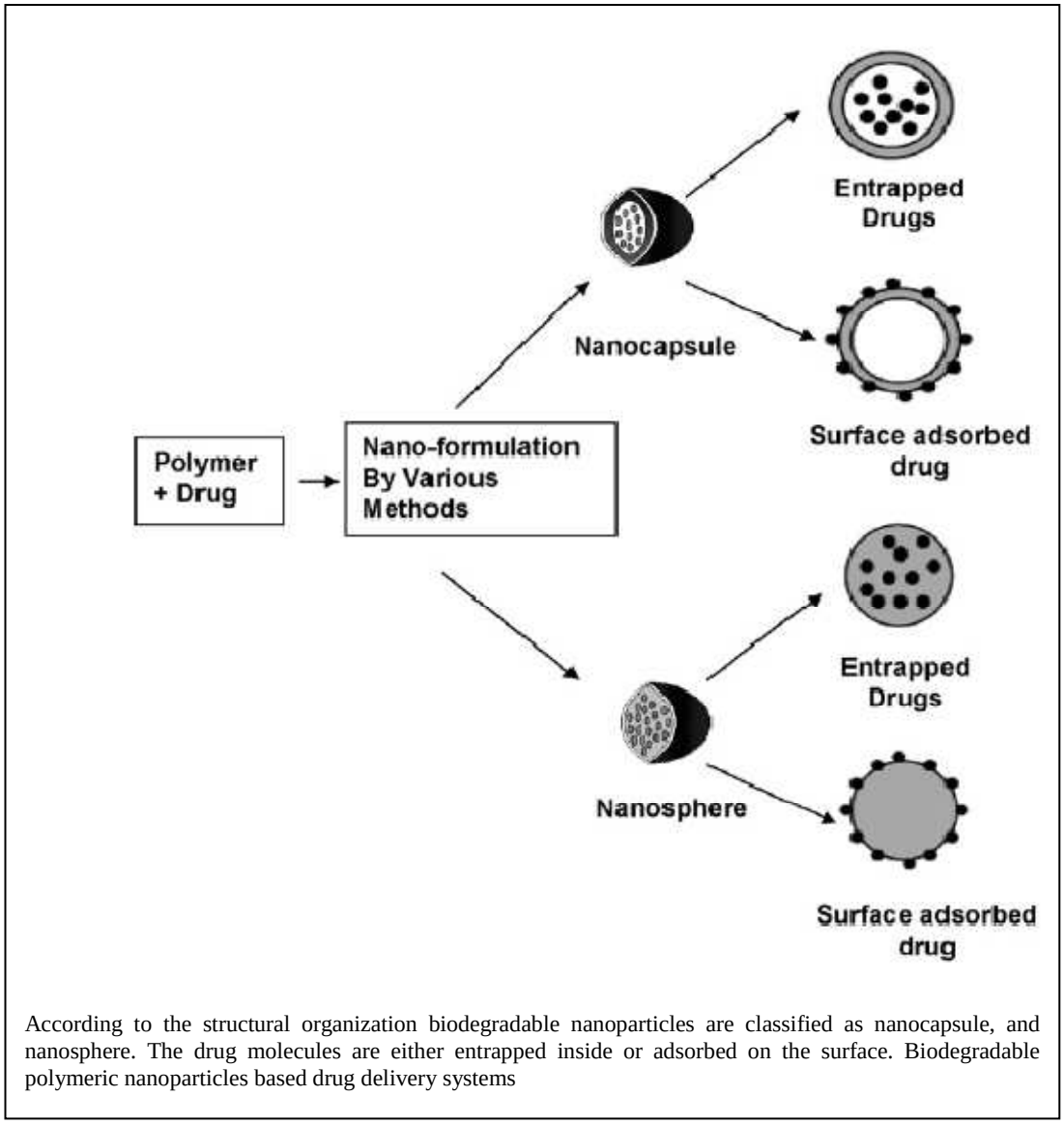

According to the structural organization biodegradable nanoparticles are classified as nanocapsule, and nanosphere. The drug molecules are either entrapped inside or adsorbed on the surface. Biodegradable polymeric nanoparticles based drug delivery systems

Figure 4.2: Type of biodegradable nanoparticles (Kumari et al., 2010).

Also, inorganic nanoparticles have been developed. In the case of highly hydrophobic drugs, increased entrapment can be also attained. From a pharmaceutical perspective, the application has been extended to formulations for a broad spectrum of administration routes including intravenous injection and pathologies (e.g., cancer). Polymeric micelles are nano-structures formed by the self-assembly of amphiphiles in water, above a minimal concentration called the critical micelle concentration or CMC. Polymeric micelles are composed by internal and external zones named core and shell, respectively. Due to the high molecular weight of the amphiphiles, they display higher stability (slower dissociation upon dilution) than micelles formed by regular surfactants (e.g. polyethoxylated castor oil or

Cremophor® EL, polysorbate 80 or Tween® 80), even at concentrations below the CMC, extending their circulation times in blood. Based on the core-drug interactions through chemical and physical forces, drugs display different release profiles. Also, polymeric micelles containing poly(ethylene oxide) as the hydrophilic component evade opsonization and uptake by the macrophages of the reticuloendothelial system (RES), prolonging circulation times in blood. Another aspect of relevance is the inhibition of efflux transporters like PGP.

Micelles formed from amphiphilic block copolymers have recently attracted significant attention in diverse fields of medicine and biology. In particular, polymeric micelles have been developed as drug and gene delivery systems as well as carriers for various contrasting agents in diagnostic imaging applications. In an aqueous environment, the hydrophobic blocks of the copolymer are expected to segregate into the core of the micelle, whereas the hydrophilic blocks form the corona or outer shell. Such a core-shell architecture of the polymeric micelles is essential for their utility as novel functional materials for pharmaceutical applications. The hydrophobic micelle core serves as a microenvironment for the incorporation of various therapeutic compounds; the corona, or outer shell, serves as a stabilizing interface between the hydrophobic core and the external medium.

As a result, polymeric micelles can be used as efficient containers for reagents with poor solubility and/or low stability in physiological environments. Interest in polymeric micelles for drug delivery has increased rapidly since the late 1980s. Most of the work has focused on classical micelles formed by intermolecular aggregation of amphiphilic polymers as the drug delivery vehicle, and the advantages of using micelle structures as a drug delivery system have been demonstrated.

The major factors that influence the performance of polymeric micelles for drug delivery are loading capacity, release kinetics, circulation time, biodistribution, size, and stability. Micelle stability is particularly important. Recent studies have shown that the *in vivo* antitumor activity of a drug incorporated into the polymer micelles is positively correlated with the stability of micelles *in vitro*. The formation of classical micelles is thermodynamically favorable only above a specific concentration of the amphiphilic molecules (Critical Micelle Concentration, CMC). Above the CMC, micelles are in dynamic equilibrium with the free copolymer molecules (unimers) in solution, continuously breaking and reforming. When the concentration of the

copolymer is below the CMC, micelles tend to disassemble. Such thermodynamic instability of micelles below the cmc is one of the concerns for their application *in vivo.* A delivery system is subject to a severe dilution upon intravenous injection into an animal or human subject.

In the bloodstream, under dilution, micelles begin to disassemble, causing changes in micelle structure and size. Therefore, controlling the release rate of drugs is difficult. Sudden dissociation of micelles may cause serious toxicity problems due to potentially large fluctuations in drug concentrations. The problem associated with the classical micelle structure can be overcome by developing molecules in which the lipophilic components are covalently bound together within the micelle core. Core polymerization is an effective method to prevent dissociation of the block copolymer micelle. Kataoka's group has successfully employed this idea. In their study, the micelles were prepared from an amphiphilic block copolymer in which the hydrophobic block contained a polymerizable end group. After micellation, the end groups on the hydrophobic block were polymerized to form a stable core for the star-shaped polymer structure. The resulting micelles showed fairly high stability and maintained small size. As anticipated, the core polymerized micelle showed excellent solubilization of rather large molecules such as Taxol. Another approach developed recently by Uhrich et al. with a three-arm star polymer composed of mucic acid substituted with fatty acid as the lipophilic inner block and with PEG as the hydrophilic outer block. This new type of molecule was capable of encapsulating a hydrophobic model drug in aqueous media. However, due to the structural constraints, the free volume of the hydrophobic core was limited, and only one or two drug molecules could be encapsulated in each micelle. A series of star block copolymers with the number of arms ranging from three to eight has also been synthesized. The arms were composed of block copolymer with PEG as the inner hydrophilic block and PCL as the outer hydrophobic block. The application of this type of copolymer as an injectable drug delivery system was reported. It was found that a reversible sol-gel transition process exists for this system, which is useful for drug delivery. However, such star copolymers do not form micelles in aqueous media because the hydrophilic block is located in the interior of the star. A recent paper described the synthesis of a four-arm star block copolymer of PCL and PEG by the same route and similar chemistry as reported in this paper. Another paper

described the preparation of a four-arm star PCL-b-PEG polymer with diethylzinc catalyst. However, the molecular weight distribution of the block copolymer was unacceptably wide. Many studies have been carried out using dendrimers as drug delivery systems. Star polymers with a dendrimer as the hydrophobic core and multiple PEG chains as the hydrophilic arms have been synthesized and investigated as unimolecular micelles for drug delivery by Fre´chet and Kono. It has been demonstrated that the micelles with larger dendrimer core have a higher encapsulation capability than those with smaller cores. However, due to the structural limitations involved in the synthesis of dendrimers of higher generation, and the relatively compact structure of the dendrimers, it is difficult to increase significantly the size of the hydrophobic dendritic core in the dendrimer-PEG star polymer. Therefore, such dendrimer systems have limitations in terms of drug-loading capacity and delivery of compounds of large size. In this paper, we describe the synthesis and micellar characterization of a novel amphiphilic star polymer. The core of this star polymer is a polyamidoamine (PAMAM) dendrimer; the inner block in the arm is lipophilic poly- (ε-caprolactone) (PCL), and the outer block in the arm is hydrophilic poly(ethylene glycol) (PEG). First, a star PCL polymer was synthesized using the PAMAM-OH dendrimer as the initiator for ring-opening polymerization of ε-caprolactone. A PEG polymer was then attached to the terminal group of PCL by an ester-forming reaction. In this star polymer the arms consist of polymers that are biocompatible and biodegradable. The star structure of the polymers was confirmed by several physicochemical methods. To establish this system as a suitable drug carrier, the micellar properties of the star amphiphilic polymer in aqueous media were studied by fluorescence techniques and dynamic light scattering. The solubilization capacity of star-PCL-PEG micelles was evaluated using several highly hydrophobic compounds, such as pyrene and water-insoluble dye molecules. A series of entrapment experiments showed that various drugs could be incorporated in such micelles. These results indicate that the star-PCL-PEG micelle system is a promising drug carrier for the delivery of lipophilic drugs (F. Wang, Bronich, Kabanov, Rauh, & Roovers, 2005).

Polymeric micelles, characterized as core-shell structured nanosize aggregations of amphiphilic polymer chains with hydrophobic inner core and hydrophilic corona, have aroused tremendous interest in pharmaceutical research. Generally, there are

two main principles for polymeric micelles to conduct drug delivery. First the hydrophobic core of micelles can act as the reservoir of drugs and meanwhile the hydrophilic corona has the capacity to stabilize micelles. Secondly, polymeric micelles are small enough (<200 nm) to evade from bioclearance, therefore have long blood circulation time which helps drug-loaded micelles to reach the action site or conduct controlled drug release. Furthermore, compared with lipid-based vectors such as liposomes and lipid nanoparticles, synthetic polymeric micelles have brilliant advantages in molecule design. By controlling the composition and the length of polymer chains, a variety of sized and shaped micelles could be obtained, which develop towards advanced drug delivery systems. Currently, a majority of explorations in polymeric micelles for drug delivery focuses on cancer therapy. Based on the well-known enhanced permeability and retention (EPR) effect, drug-loaded micelles could be accumulated around tumors and perform high tumor inhabitant. For this aim polymeric micelles should be carefully designed to achieve the appropriate size, stability and drug loading efficiency under control.

Polymer base is fundamental for the design of polymeric micellar drug delivery systems. Ideally polymers chosen for drug delivery should be biocompatible and can be easily tailored or functionalized. Polyphosphazene is a novel biocompatible and biodegradable inorganic polymer with two active chlorine side groups on each repeat unit. Compared with those popular biomaterials such as polycaprolactone (PCL) and poly(lactic acid) (PLA), the distinct advantage of polyphosphazene for drug delivery is the chlorine side groups on polyphosphazene can be readily substituted by other molecule/macromolecules, therefore, multi-functionalized polyphosphazenes with a variation of physical and chemical characteristics could be obtained. Pioneer researchers have fabricated several series of polyphosphazenes, and the biodegradation and biocompatibility of polyphosphazenes have been demonstrated. Other researchers further studied the biomedical application of polyphosphazenes such as nano-fibers and hydrogels (Zheng, Qiu, Yao, & Zhu, 2009). Our group has been focusing on the micellization of amphiphilic PCL-PEG polymers. In present work, we aim to construct a micellar system based on Star and Y shape amphiphilic PCL-PEG micelles for tumor targeting treatment.

Poly-ε-caprolactone (PCL)

PCL (poly-ε-caprolactone) is degraded by hydrolysis of its ester linkages in physiological conditions (such as in the human body) and has therefore received a great deal of attention for use in drug delivery. In particular, it is especially interesting for the preparation of long-term implantable devices, owing to its degradation slower than that of polylactide. PCL nanoparticles have been prepared mostly by nanoprecipitation, solvent displacement and solvent evaporation. Some of the molecules that have been successfully incorporated into PCL nanoparticles to increase their therapeutic value are described in Table 4.1 (Kumari et al., 2010).

Table 4.1: Some of the molecules that have been successfully incorporated into PCL nanoparticles to increase their therapeutic value.

Polymer	**Encapsulant**	**Encap. effic.**	**Synthesis methods**	**Therapeutic improvement**	**Release mechanism**	**Surface modification**	***in vivo***
Poly-ε-caprolactone (PCL)	Tamoxifen	90%	Solvent displacement	Preferrential tumor targeting and circulating drug reservoir		pluronics	Increased level of accumulation of the drug within tumor with time and extended their presence in circulation
	Clonazepam	72.6-95.1%	Solvent evaporation method	Drug release behaviour can be modulated by introducing thermo sensitive polymer	Diffusion		
	Saquinavir	60%	Solvent displacement method	Higher intra cellular saquinavir conc.	Diffusion	PEO	Rapid cellular uptake of rhodamine-123 encapsulated PEO-PCL nanoparticles was observed in THP-1 cells
	Taxol	20.79%	micelles	Higher taxol loading		MePEG	Decreased fasted glycemia in a dose dependent manner and nanoparticle strongly adhered to intestinal mucosa
	İnsulin	96%		Preservation of insulins' biological activity	Diffusion		
	Docetaxel	90%	Nanoprecipitaion method	Higher antitumor effect	Diffusion		Effectively kills BIG cells
	Vinblastine	48%	Emultion method	Slow drug release up to 20 days	Diffusion		Breast cancer cell line (MCF-7) showed efficient uptake

4.3.2 Micelles formed from phospholipids

Phospholipids are natural compounds consisting of a glycerol backbone linked by ester bonds to two fatty acid chains and one phosphoric acid. Phospholipids have two distinct regions – a long non-polar hydrocarbon tail and a polar phosphate head group. This gives the molecules amphiphilic properties. Amphiphiles are molecules characterized by the presence of both a hydrophilic and a hydrophobic region within a single molecule (Florence & Attwood, 2006). At low amphiphile concentrations in an aqueous medium, the amphiphiles exist as monomers in the bulk and the interface. As the amphiphile concentration increases, self-association occurs to minimize the unfavorable interactions between the aqueous phase and the non-polar region of the amphiphiles (Arleth, 2005; C. Lizano & Garc´ıa-P´erez, 2003). The type of aggregate formed depends on the numerous characteristics of the molecule like charge distribution, length of acyl chains, degree of unsaturation and size of the polar head group. When the amphiphiles have a large head group, they tend to have a more conical shape. These molecules self-assemble spontaneously above a certain concentration of the amphiphiles called the critical micellar concentration to form micelles, with their hydrophobic tails oriented towards a central hydrophobic core and the hydrophilic heads facing outwards (Arleth, 2005). Micelles are in dynamic equilibrium with their monomers in solution resulting in a constant exchange between monomers in solution and in those of the micelles (Florence & Attwood, 2006). It is the central hydrophobic core of these micelles that can be taken advantage of in delivering water insoluble drugs.

4.3.3 Sterically stabilized micelles

Phospholipids like distearoyl phosphatidylethanolamine (DSPE) conjugated to polyethylene glycol (PEG) at the polar head were synthesized and used to modify the surface of liposomes in the 1990’s (Allen, 1991; Klibanov, Maruyama, Torchilin, & Huang, 1990; Sejourne, Rubinstein, Suzuki, & AlkanOnyuksel, 1997; Sejourne, Suzuki, et al., 1997). This pegylation of DSPE in addition to making the molecule more water soluble also renders a more conical shape to the structure. This facilitates the formation of micelles when the concentration of monomers is above CMC (Arleth, 2005; Lasic, 1992; Lasic et al., 1992; Needham, McIntosh, & Lasic, 1992). PEG chains with molecular weight of 2000 and 5000 are typically used for this

purpose. The reason is PEG chains with MW less than 1000 do not provide sufficient polarity to the phospholipid molecule to form micelles, while chains with MW greater than 5000 make the phospholipid head group too bulky and water soluble. The structure of DSPE-PEG2000 is shown in (Figure 4.3).

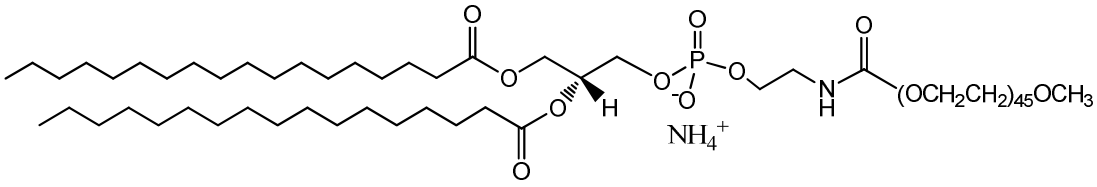

Figure 4.3: Chemical structure of DSPE-PEG2000 (Ashok, 2004).

DSPE-PEG2000 micelles also known as sterically stabilized micelles which offer numerous advantages as a carrier for the delivery of water-insoluble drugs. Firstly, SSM display high kinetic and dynamic stability due to very low CMC values of around 1µM (Ashok, 2004). This low CMC ensures thermodynamic stability even upon large dilution that occurs when administered into the body. Additionally, low CMC also ensures low monomer concentration. Since monomers of surfactants are primarily responsible for the toxicity caused, PEGylated lipids are safer compared to conventional surfactants such as bile salts, Tweens (20, 60 and 80) and Pluronics (Alkanonyuksel, 1994; Kabanov & Alakhov, 2002). Secondly, PEGylated lipids have a steric barrier on the surface due to the PEG shield. This steric barrier prevents the adsorption of proteins such as opsonins onto the particles, thus elongating the circulation half-life by reducing reticuloendothelial system (RES) uptake (H. Onyuksel, 2005; Lukyanov, 2002; Weissig, Whiteman, & Torchilin, 1998). Thirdly, SSM due to their small size with an average diameter of ~16 nm (Ashok, 2004; Dagar, 2003) are ideal for passive targeting to cancer tissue due to the (H. Onyuksel, 2005) Enhanced Permeation Retention (EPR) effect (Matsumura, 1986). This aspect will be discussed in further detail in section I.B.3.a. The PEG on the surface of SSM also provides the opportunity to surface graft targeting ligands for active targeting. Fourthly, SSM provide a unique hydrophobic gradient for the solubilization of drugs without the need for any chemical modification. Also SSM can be easily freeze-dried and reconstituted without the need for additional lyoprotectants and cryoprotectants, ideal for convenient manufacture and long term storage (H. Onyuksel, 2005). Finally, SSMs can be easily prepared from the PEGylated phospholipids which are biocompatible, biodegradable, relatively non-toxic and FDA approved for human use

(Working & Dayan, 1996). DSPE-PEG micelles have recently been studied as delivery systems for small molecules, peptides and imaging agents (Ashok, 2004) (Dagar, 2003; H. Onyuksel, 2005; Lukyanov, 2002; Y. Wang et al., 2010; Weili Qiao, 2010)

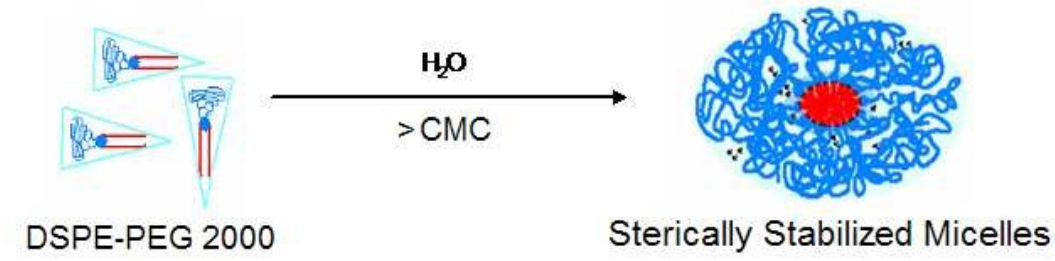

Figure 4.4: Formation of sterically stabilized micelles(Ashok, 2004).

4.3.4 Sterically stabilized mixed micelles

Sterically stabilized mixed micelles are a novel second generation modification of sterically stabilized micelles. They are prepared by the incorporation of a water insoluble phospholipid such as phosphatidyl choline (PC) into micelles formed from DSPE-PEG2000 (Figure 4.4). This results in an increased core fluidity providing an improved solubilization potential for certain drugs like paclitaxel (Dagar, 2003).

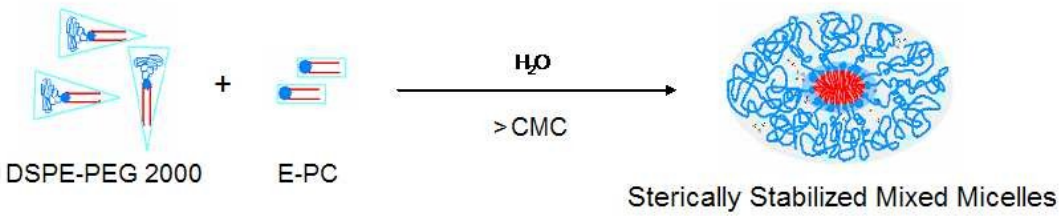

Figure 4.5: Formation of sterically stabilized mixed micelles (Ashok, 2004).

Depending on the ratio of PEGylated lipids and PC used, different morphological structures can be formed. Mixtures of low PC content along with PEGylated lipids form spherical micelles. As the PC content is increased there is a change from the spherical shape to rod-like micelles to disc-shaped aggregates. Further increase in the PC content causes micelle to vesicle transition observed by the formation of bi-layered vesicles (Arleth, 2005; Edwards, 1997; Hjelm, 1992; Hristova, 1995). It has been found that in case of DSPE-PEG2000 micelles, an increase of PC content greater than 25% led to the formation of rod-shaped particles (Ashok, 2004). To

achieve maximum solubilization using spherical mixed micelles alone, a molar ratio of 90:10 DSPE-PEG2000: E-PC was selected. Previous work using small angle neutron scattering (SANS) and small angle X-ray scattering (SAXS) have demonstrated that SSMM composed of DSPE-PEG2000 and E-PC (90:10) have aggregation number, size and shape similar to that of simple micelles composed of DSPE-PEG2000 alone (Ashok, 2004).

4.4 Pharmacokinetics and Biodistribution of Nanoparticles

The pharmacokinetic profiles of the parent drug and the drug encapsulated in the nanoparticles are often different. Therefore, it is very important to monitor the pharmacokinetics (PK) and biodistribution of nanoparticles to understand and predict their efficacy and side effects. The PK profile of the nanoparticles is mainly determined by their chemical and physical properties, such as size, charge, and surface chemistry.

4.4.1 PK study

PK study involves measuring drug concentrations in all major tissues after drug administration over a period of time until the elimination phase. It is necessary to monitor the drug concentration long enough to fully describe the behavior of the drug or nanoparticles *in vivo* (usually 3 × half-life). The PK profile in the blood can be fitted using various programs to obtain key PK parameters that quantitatively describe how the body handles the drug or nanoparticles. Important parameters include Cmax (maximum concentration), t1/2 (half-life), Cl (clearance), AUC (area under the curve), and MRT (mean resident time, average time that a molecule of a drug stays in the body). When a drug formulation shows prolonged blood circulation, an increased t1/2, a reduced Cl, an increased AUC, and an increased MRT are usually observed. On the other hand, if a formulation is quickly eliminated from the body, a low t1/2, a high Cl, a low AUC, and a low MRT are often obtained. PK data not only can help describe, but also can help predict the behavior or profile of the drug or nanoparticles. PK data are often used in deciding the dose and dose regimen for maintaining a desirable blood concentration for improved therapeutics with minimal side effects. The blood concentration of drugs is highly correlated with their efficacy and toxicity in most cases, especially for free drugs. However, to gain

insight into how the body handles the drug formulation and how the formulation may affect the efficacy and adverse effects, it is essential to obtain the tissue distribution information for the drug. A high level of accumulation of a drug in the target tissue often results in an enhanced therapeutic effect, and oppositely, a large amount of drug distributed to nontarget organs may cause unwanted toxicity. PK and tissue distribution studies that allow investigators to screen formulations for a given drug are extremely important during drug development. By optimizing the drug formulation, investigators can improve the drug delivery to the target tissue and reduce drug distribution to the nontarget tissues to obtain increased therapeutic activity with minimal side effects (Li & Huang, 2008).

4.4.2 Comparison of PK of free drugs and drugs encapsulated in nanoparticles

When a hydrophilic drug is intravenously (i.v.) injected into the body, without much protein binding, the drug is often quickly eliminated from the blood by renal filtration into the urine. In the case of a hydrophobic drug, the renal clearance is significantly reduced compared to that of the hydrophilic drugs due to an increased level of serum protein binding. The hydrophobic drugs are often transformed into hydrophilic metabolites in the liver and excreted into the bile or eliminated into the urine. When the drugs are encapsulated in nanoparticles, the drugs are protected from metabolizing enzyme in the liver before they are released and as well as from renal clearance due to the increased size. The cutoff size for renal excretion is approximately 5.5 nm according to recent research using quantum dots,1 and the nanoparticles are usually much larger. Reduced liver metabolism and renal clearance of drugs encapsulated in the nanoparticles often result in prolonged blood circulation with an increased chance of accumulation in the target tissue (Li & Huang, 2008).

4.4.3 Tissue selectivity of nanoparticles

The limited pore size of the endothelial wall in the tissue is the primary delivery barrier for nanoparticles but also allows selective accumulation in certain tissues. Unlike small molecule drugs that can diffuse through the capillary wall into the tissue, nanoparticles rely on the gaps between the endothelium to pass through the barrier. Tissues with a leaky endothelial wall usually contribute significant uptake of nanoparticles, including tumor, liver, spleen, and bone marrow. The increased rate of tumoral uptake of nanoparticles is based on a phenomenon termed the “enhanced

permeability and retention" (EPR) effect2 due to the increased capillary permeability in the tumor tissue (Li & Huang, 2008).

The Enhanced Permeability and Retention (EPR) effect is the property by which certain sizes of molecules (typically liposomes, nanoparticles, and macromolecular drugs) tend to accumulate in tumor tissue much more than they do in normal tissues. The general explanation that is given for this phenomenon is that, in order for tumor cells to grow quickly, they must stimulate the production of blood vessels. VEGF (Vascular endothelial growth factor) and other growth factors are involved in cancer angiogenesis. Tumor cell aggregates of size as small as 150-200 μm, start to become dependent on blood supply carried out by neovasculature for their nutritional and oxygen supply. These newly formed tumor vessels are usually abnormal in form and architecture. They are poorly-aligned defective endothelial cells with wide fenestrations, lacking a smooth muscle layer, or innervation with a wider lumen, and impaired functional receptors for angiotensin II. Furthermore, tumor tissues usually lack effective lymphatic drainage. All these factors will lead to abnormal molecular and fluid transport dynamics, especially for macromolecular drugs. Namely, this phenomenon was coined "enhanced permeability and retention (EPR)-effect" of macromolecules and lipids in solid tumors. The EPR-effect is even more enhanced by many pathophysiological factors involved in enhancement of the extravasation of macromolecules in solid tumor tissues. (Matsumura, 1986).The enhanced uptake in the liver, spleen, and bone marrow is largely attributed to the macrophages residing in the tissues, which are responsible for clearing particulates and macromolecules circulating in the blood.

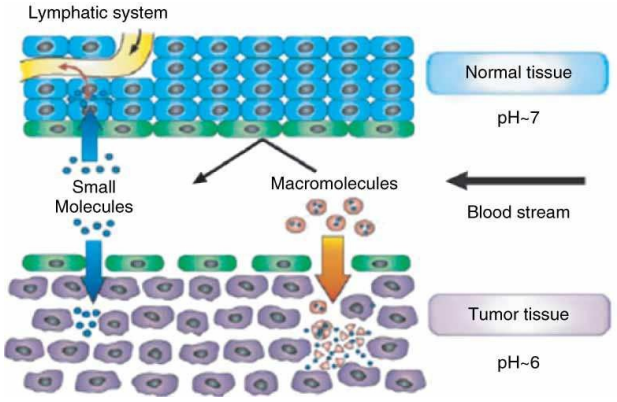

Figure 4.6: The illustration of EPR effect (Matsumura, 1986).

When nanoparticles are i.v. administered, a variety of serum proteins bind to the surface of the nanoparticles, which are recognized by the scavenger receptor on the macrophage cell surface and internalized, leading to a significant loss of nanoparticles from the circulation. The serum proteins binding on the nanoparticles are also termed “opsonins”,and the macrophages contributing the major loss of injected dose are also known as the reticuloendothelial system (RES) or mononuclear phagocyte system (MPS). Minimizing protein binding is the key point for developing a long circulation nanoparticle formulation.(Li & Huang, 2008)

4.5 Factors Influence PK of Nanoparticles

Opsonization is the major factor that induces MPS uptake of nanoparticles, and therefore, surface characteristics of nanoparticles greatly influence their PK. Generally, nanoparticles that have a mean diameter of approximately 100 nm with a neutral and hydrophilic polymer-extended surface exhibit prolonged blood circulation and an increased level of tumor delivery.

4.5.1 Surface-engineered nanoparticles as drug carriers

Over the last 12 years there has been a growing interest in the develpment of a drug carrier that is small enough for intravenous administration and has the ability to bypass the normal physiological defense processes of the organism.

The main challenge for administering particulate drug carriers into the vascular compartment is the achievement of sitee-specific drug delivery. Indeed, following its intravenous administretion, a drug substance will distribute through the body. As a consequence the amount of drug will reaching th target site maybe a only small fraction of the administered dose. Morover, adverse side effects may occur at nanotarget site.

Active research has been pursued since Ehlrich first considered the concept of “magic bullets” for the eradications of disease. For site-soecifirc drug delivery, should avoid indiscriminate inreactions with the Mononuclear Phagocyte System (MPS), selectively reach the disease site of action, and release the drug in its active form at suitable rate and in therapeutic amounts. The nanoparticles should be nontoxic elements. Such drug carriers could be of highest interest in cancer chemotherapy.

Many efforts have concentrated in recent years on the design of submicronic long-circulating drug carriers such as liposomes, lipid emultions, micelles, solid lipid nanoparticles. Among all of these systems we will focus on lipid base and polymeric nanoparticles which both are counted as solid colloidal particules ranging in size from 10 to 1000nm in which the drug is entrapped (Li & Huang, 2008).

4.5.2 Factors affect the fate of intravenously administered particles

Particle siz eand shape greatly influence organ distribution. To circulate through the smallest cappilaries, the particle size should be less than 5µm, and to avoid spleen filtering effects, the diameter should be less than 200 nm. Carrier surface properties such as charge and hydrophobicity play a major role in the interaction with the living organism. İt was established that hydrophobic particles are more avidly taken up by macrophages than by hydrophilic ones.

4.5.3 The role of Mononuclear Phagocyte System (MPS) in removing injected particles

The cells of MPS previously known as the reticuloendothelial system (RES) play a key role in the clearence of and body distribution of these particles. They are actively endocytic and posses on their surface a number of receptors for plasma proteins that are likely to adsorb on particles' surface. Among their variety of important biological functions MPS cells play a role in removing from blood invading bacteria, fungi and viruses or protein aggregates derived from tissue destruction. However MPS cells also recognise as foreign and efficiently clear injected particles from blood. This fast process can occur by an apperently nonspecific phagocytosis. However, uptake is tremendously triggered if the particles' surface is "decorated" with ligands that bind to one of the many receptors on the MPS cell surface.

The most preferred strategy to avoid the MPS phagocytic "barrier" are particle camouflage from MPS, for example by modifying the surface to allow a particle to "stealthily" circumvent phagocytic cells. To achieve this type of surface-engineered drug carrier interactions between carriers and blood should be taken into account(Li & Huang, 2008)

4.6 Nanoparticle Interactions With Blood

4.6.1 Opsonins

Immediately after intervenous administration, the nanoparticles encounter a high concentration of hundreds of plasma proteins. The adsorption of protein ligands that are capable of interacting with one or more receptors on MPS cells, thus promoting the particle uptake by these cells is called opsonization. In some cases plasma protein adsorption can also lead to exchange of lipid components with blood cells and lipoproteins. This phenomenon is believed not to take place with nanospheres which have rigid polymeric cores.

It is recognized generally that the fate of the injected particles is regulated by the composition and by the conformation of the protein layer that typically begins to form within seconds after contact with blood.

The phagocytosis is an irreversible process with mainly three steps: 1)Recognized by opsonins such as the complement protein, immunoglobulins G and M, fibronectin and apolipoproteins, or by specific or nonspecific receptors present at the surface of the macrophage plasma membrane; 2)Then adsorbed by these opsonins; 3)Finally, eliminated by the mononuclear phagocyte system (MPS). That means if wecould prevent the complement protein from activation, the phagocytosis may be inhibited subsequently. It was first pointed out by Vorman and Adams (Vorman, 1969) that the hundreds of proteins in plasma experience very different collision frequencies with respect to the exposed surface, depending on the concentration and diffusion coefficient of each protein (Table 4.1).

Table 4.2: Concentration (c) and diffusion coefficient (D) of some of the most concentrated plasma proteins.

Protein	Concentration, *c, (μM)*	*D* ($10^{-7}cm^2s^{-1}$)
Albumin	600	6.1
IgG	100	4.0
A-Antitrypsin	40	5.2
Transferrin	30	5.0
HDL	18	4.6
IgA	15	4
Complement3	9	4.5
Fibrinogen	7.5	2
LDL	2	2

If adsorption occurs, the protein can be more or less readily displaced by another one. As a consequence, the most abundant plasma proteins, such as albumin, adsorb first and as time progresses, are replaced by athers with a lower collision frequency but with a higher affinity for the surface.

More recently it has been pointed out that the collision and reversible attachment of protein to a substrate are followed by a series of conformatioanal adjustment to the surface, eventually ending with a quasi-irreversible fixation. The gain in entropy resulting from chain unfolding was found to be driving force behind adsorption, at times overwhelming charge repultions between the protein and the surface. As a consequence, the strucrural stability characterizing each protein has a strong influence over its adsorption. Hydrophobic surfaces have an ability to stabilize the nonpolar protein cores as they become exposed to water during water during unfolding. Fibrinogen is one of the most active plasma proteins. It becomes a powerful cell activator once it has undergone even modest conformatioanl changes.

The complement is generally considered to be one of the main opsonins involved in the uptake of intravenously adminstered particles. The complement system comprises about 20 blood proteins that can interact in a complex cascade involving specific binding and proteolytic activation steps. Complement can be activated by two major pathways. The “classical” pathway is initiated by the formation of an antigen/antibody complex; the “alternative” pathway involves the accelation of the spontaneous process of conversion of component C3 into its active form C3b;

From the immunological point of view, C3, as a major complement protein, plays a significant role in complement system. After opsonization, cleavage of C3 by C3 convertase would be activated into a large fragment of C3b and a small fragment of C3a. C3b provides specific recognition by type CR1 receptor on macrophages thus the evidence of C3 cleavage was obtained by quantified the C3 concentration, which was used as a way to characterize the avoidance of complement activation by NPs. (Shan et al., 2009)

Fibronectin has also a well-documented role in the uptake of particles. İt has been shown to bind to bacteria and to a variety of macromolecules, such as collagen, actin, DNA, or heparin. Some other reported opsonins are tuftsin and clotting factors.

4.6.2 Dysopsonins

In contrast to the opsonin family, certain blood components called dysopsonins were shown to inhibit phagocytic ingestion. Therefore, preadsorbing dysopsonins on nanoparticles prior to their i.v. administration appear to be a very attractive means of achieving long blood circulation times.

It has been shown that the presence of immunoglobulin IgA on surfaces inhibits ingestion by neutrophils and macrophages. The high hydrophilicity of this molecule was suggested to be apossible explanation its dysopsonic action. However the dysopsonic effects reported in vitro could not be confirmed in vivo. Precoating polystrene nanospheres with IgA did not reduce the uptake by peritoneal macrophages or the hepatic deposition.

Muir et al. (Moghimi, 1991; Muir, 1991)suggested that the principal factors that result in a dysopsonic action are two serum components, one with a molecular weight below 30,000 and another one with a molecular weight higher than 100,000. The competition between the two opposite phenomena, the reduction in opsonin adsorption and the selective adsorption of dysopsonins, is believed to be the key in controlling the particle uptake and hence their biodistribution (Baraton, 2003).

4.7 Role of Target Geometry in Phagocytosis

Exclusive use of spherical particles in drug delivery systems originated partly because of a presumption that size is the principal parameter of interest and partly because of difficulties in fabricating nonspherical particles of controlled dimensions. Use of spherical particles not only concealed the role of particle shape in phagocytosis but also created an inaccurate picture of the actual role of particle size because all parameters that describe size (volume, surface area, etc.) scale with particle radius, leaving one wondering as to which parameter is of fundamental consequence in phagocytosis.

A paper is reporting the results of investigation of the role of target geometry in phagocytosis using alveolar macrophages as model phagocytes and polystyrene (PS) particles of various sizes and shapes as model targets, that target shape at the point of first contact by macrophages, not size, decisively determines whether cells will proceed with phagocytosis or simply spread on the particle. Size, on the other hand,

primarily impacts the completion of phagocytosis when the target volume is larger than the macrophage volume.

This paper is reporting the synthesis of particles with 6 different shapes;

spheres (radius 1.0–12.5 μm), oblate ellipsoids (major axis 4 μm, aspect ratio 4), prolate ellipsoids (major axis 2–6 μm, aspect ratio 1.3–3), elliptical disks (EDs) (major axis 3–14 μm, aspect ratio 2–4, thickness 400–1,000 nm), rectangular disks (major axis 4–8 μm, aspect ratio 1.5–4.5), and UFOs (sphere radius 1.5 μm, ring radius 4 μm).

The paper reports that, Opsonized or nonopsonized particles were incubated with alveolar macrophages and observed under a light microscope (×100) with time-lapse video microscopy.

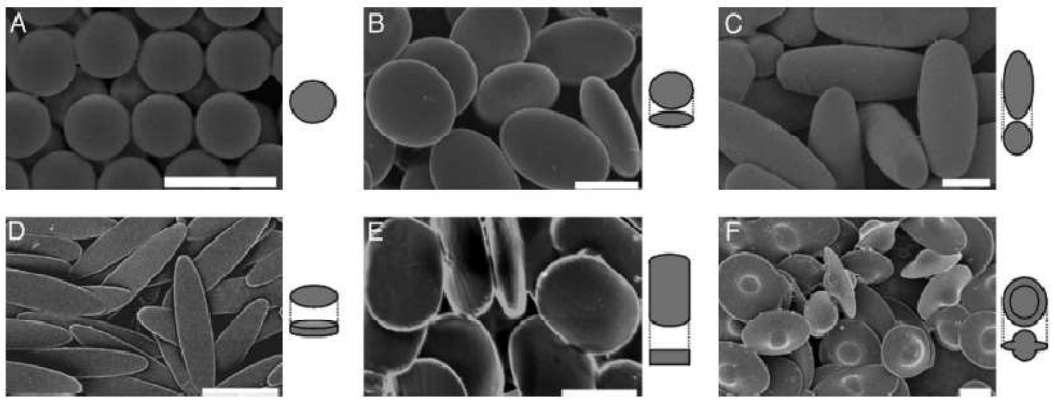

(*A*) Spheres. (*B*) Oblate ellipsoids (13%). (*C*) Prolate ellipsoids (7%). (*D*) Elliptical disks (9%). (*E*) Rectangular disks (5%). (*F*) UFOs (12%). Particles are monodispersed with average standard deviations of measured dimensions for each shape listed in parentheses. Aportion of this variation is due to2–5%standard deviation in the diameter of spheres used as starting materials. (Scale bars: 5 μm.)

Figure 4.7: Scanning electron micrographs and 3D illustrations of PS particles created for phagocytosis experiments) (Champion & Mitragotri, 2006).

IgG-opsonized particles are phagocytosed via Fc receptors, whereas nonopsonized particles adsorb proteins from the culture medium supplemented with heat-inactivated FBS during incubation and are phagocytosed through nonspecific scavenger receptors. In both cases internalization of particles is an actindependent process.Internalization of both opsonized and nonopsonized particles exhibited a strong dependence on local particle shape from the perspective of the phagocyte. Local shape varies not only for different particles but also for different points of initial contact on the same particle, except for spheres. For example, macrophages

that attached to EDs (major axis 14 μm, minor axis 3μm) along the major axis (discussed quantitatively below) internalized them very quickly, in <6 min (Figure 4.8 A). The macrophage membrane can be seen moving along the length of the particle in a coordinated, unified fashion. On the other hand, cells that attached to the same EDs along the minor axis or flat side did not internalize them, even after 2 h (Figure 4.8 B). They did, however, spread on the particle surface but with nonsynchronized, separate fronts moving in different directions at different times. Macrophages attached to the flat side of IgG-opsonized EDs exhibited more spreading than those attached to nonopsonized EDs, but the final result was the same: no phagocytosis. Because the particles used for these studies possessed identical properties (dimensions, surface area, volume, and chemistry), observations in Figure 4.8 A and B clearly show that the local particle shape at the point of initial contact, not the overall size, determined their phagocytic fate. Similar results were seen for all shapes including UFO-shaped particles, where internalization does not occur when cells attach to the concave region but internalization does occur after attachment to the dome or ring regions.

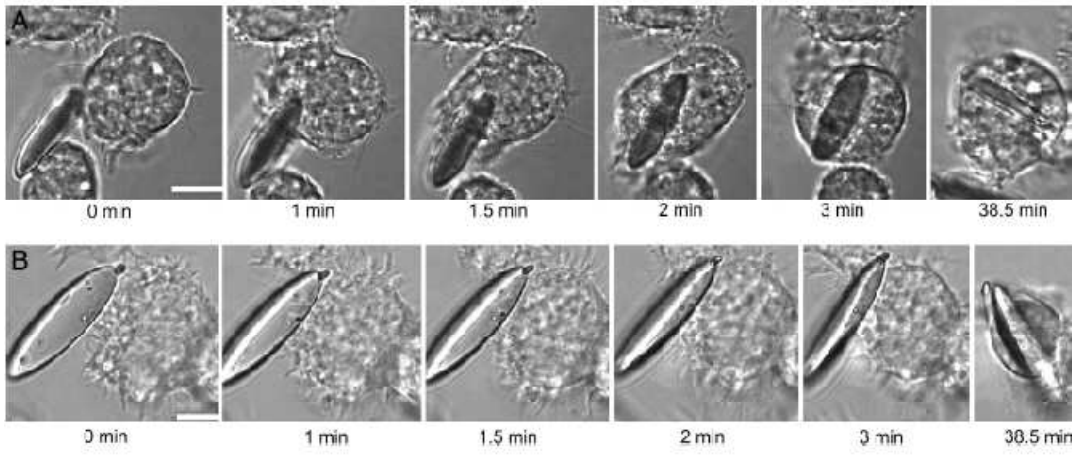

(*A*) Cell attaches along the major axis of an ED and internalizes it completely in 3 min. (*B*) Cell attaches to the flat side of an identical ED and spreads but does not internalize the particle. Continued observation indicated that this particle was not internalized for ~110 min. (Scale bars: 10 μm.) At least three cells were observed for each orientation of each particle type and size. Similar results were observed in all repetitions.

Figure 4.8: Time-lapse video microscopy clips spanning 39 min of macrophages interacting with identical nonopsonized ED particles (major axis 14 μm, minor axis 3 μm) from two different orientations (Champion & Mitragotri, 2006).

Furthermore this study reports Scanning electron microscopy images that provided more evidence for this orientation bias. As can be seen in the micrographs, the cell

membrane showed marked progression on EDs when approached along the major axis .In contrast, cells that attached to the flat side of EDs exhibited spreading but no engulfment of particles, even after 2 h .As a reference point, consistent engulfment was observed on spheres **(Fig. 4.9).**

Further insight into orientation-dependent particle phagocytosis was gained by staining macrophages for polymerized actin at various times during phagocytosis. Actin polymerization is the principal mechanism by which macrophages push the leading membrane edge and engulf particles. Initially, an actin cup, comprised of a dense actin network, forms beneath the particle.

As additional actin polymerization and remodeling occur and the membrane progresses, the actin cup is transformed into an actin ring around the particle that pushes the membrane along the particle until it is internalized (14–16). Spheres and EDs that attached to macrophages along the major axis exhibited an actin cup at short times that later transformed to a ring around the particle as phagocytosis progressed (**Figure 4.9**, F and D, respectively).

Macrophage attachment to the flat side of EDs, despite actin polymerization at points of contact and spreading, did not exhibit an actin cup or ring .Formation of an actin cup is a clear indicator of initiation of internalization and was observed only at certain local shapes.

This phase diagram shows whether or not internalization was initialized and completed for particles with different combinations of Ω and V*, the ratio of particle volume to macrophage volume. The authors indicate that initiation of internalization could be judged by formation of an actin cup or ring (**(Fig. 4.9 E and F)**, and completion could be judged by closure of the membrane. The diagram shows three regions: the successful phagocytosis region ($\Omega \leq 45°$, $V^* \leq 1$) where phagocytosis is initiated and completed quickly, the attempted phagocytosis region ($\Omega \leq 45°$, $V^* > 1$) where phagocytosis is initiated but not completed within the period of observation, and the spreading region ($\Omega > 45°$) where particle attachment takes place and macrophages spread on the particle but phagocytosis is not initiated. This diagram clearly shows that initiation of phagocytosis is governed by Ω whereas V* primarily influences completion.

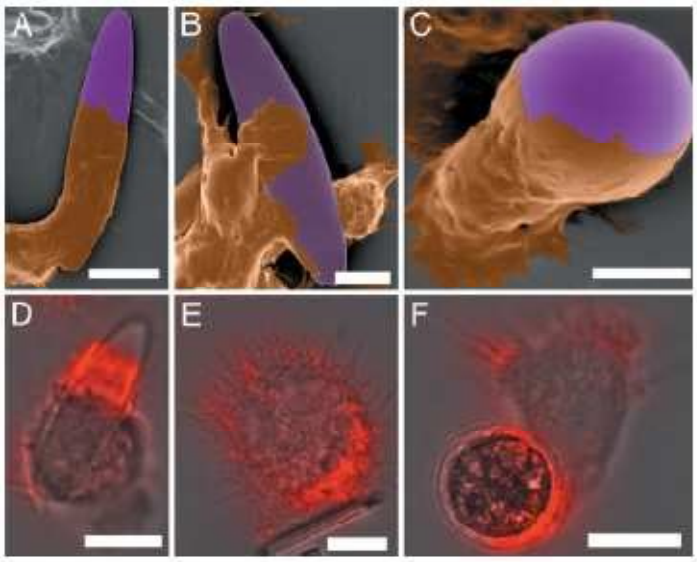

Micrographs (*A–C*) of cells and particles were colored brown and purple, respectively. (*A*) The cell body can be seen at the end of an opsonized ED, and the membrane has progressed down the length of the particle. (Scale bar: 10 µm.) (*B*) A cell has attached to the flat side of an opsonized ED and has spread on the particle. (Scale bar: 5 µm.) (*C*) An opsonized spherical particle has attached to the top of a cell, and the membrane has progressed over approximately half the particle. (Scale bar: 5 µm.) (*D–F*) Overlays of bright-field and fluorescent images after fixing the cells and staining for polymerized actin with rhodamine phalloidin. (*D*) Actin ring forms as remodeling and depolymerization enable membrane to progress over an opsonized ED by new actin polymerization at the leading edge of the membrane. (*E*) Actin polymerization in the cell at site of attachment to flat side of an opsonized ED, but no actin cup or ring is visible. (*F*) Actin cup surrounds the end of an opsonized sphere as internalization begins after attachment. (Scale bars in *D–F*: 10 µm.) At least five cells were observed for each orientation of each particle. Similar results were observed in all repetitions.

Figure 4.9: Scanning electron micrographs and actin staining confirm time-lapse video microscopy observations (Champion & Mitragotri, 2006).

Macrophages phagocytosed particles as large as themselves when approached from the preferred orientation ($\Omega \leq 45°$). However, when approached from the undesired orientation ($\Omega > 45°$), they did not internalize particles with volumes as small

as 0.2% of the cell volume. Similar bias has also been seen during phagocytosis of pathogens based on limited anecdotal literature. It remains to be seen whether the orientation bias of phagocytosis disappears at extremely small particle volumes ($V^* << 0.002$) (Champion & Mitragotri, 2006).

4.8 Modeling The Interaction Between Proteins and PEG-Grafted Surfaces

Several methods of camouflaging or masking NPs (NPs) have been employed for particles surface modification through physical or chemical attachment in terms of neutralize the NPs surface charge or provide a repulsive steric barrier to prevent the flocculation of particles and decrease opsonization by blood components. Poly(ethylene glycol) (PEG) has uncharged hydrophilic characteristic, and high

steric stabilization with non-toxic resulting in dramatically changing the charge of biomaterials, which thus has been a major strategy to decrease the nonspecific interactions of complexes with serum components, and thereby increase blood circulation time.

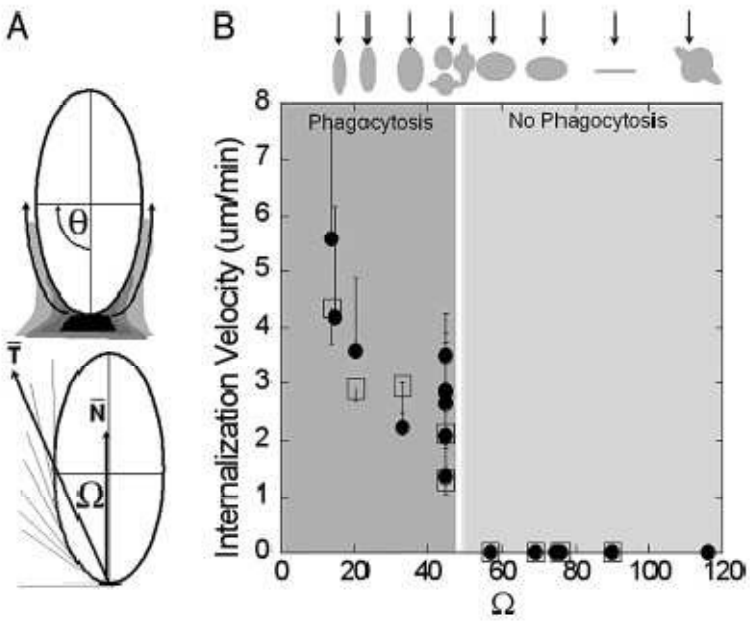

(*A*) A schematic diagram illustrating how membrane progresses tangentially around an ED. **T** represents the average of tangential angles from θ=0 toθ=2. Ω is the angle between **T** andmembranenormal at the site of attachment, **N**. (*B*) Membrane velocity (distance traveled by the membrane divided by time to internalize, *n* ≥ 3; error bars represent SD) decreases with increasing Ω for a variety of shapes and sizes of particles.

Figure 4.10: Definition of Ω and its relationship with membrane velocity(Champion & Mitragotri, 2006).

Previously PEG chains has been introduced into hydrophobic poly(ε-caprolactone) (PCL) Nanoparticles (NPs) to improve the hydrophilicity of NPs and prolong the longevity of polymeric NPs in blood stream. In this study Results have been showen that, after intravenous (i.v.) administration, the longevities of PCL-PEG NPs in blood circulation were prolonged approximately 7.2-fold as long as that of the naked nanoparticles.

Some studies (Shan et al., 2009) found that the negative charge on the particles surface may be a potential activator of human complement system. Therefore, the PEG chains on the NPs surface neutralized the zeta potential, the results of mentioned study are shown in Table 4.3 .

Table 4.3: The neutralization of surface of nano-particle by PEG.

Samples	Size distribution (nm)	PDI	ζ potential (mV)
PCL	183.4±10.7	0.188±0.029	−27.17±2.92
PCL-PEG	159.6±15.8	0.159±0.020	−6.046±3.76

resulting in suppressing complement activation. On the other hand, it has been conformed that the brush-like PEG chains may sterically prevent the deposition of C3b onto the surface of NPs and reduce interaction with phagocytic cells membrane. The results of that study is demonstrated in Figure 4.11.

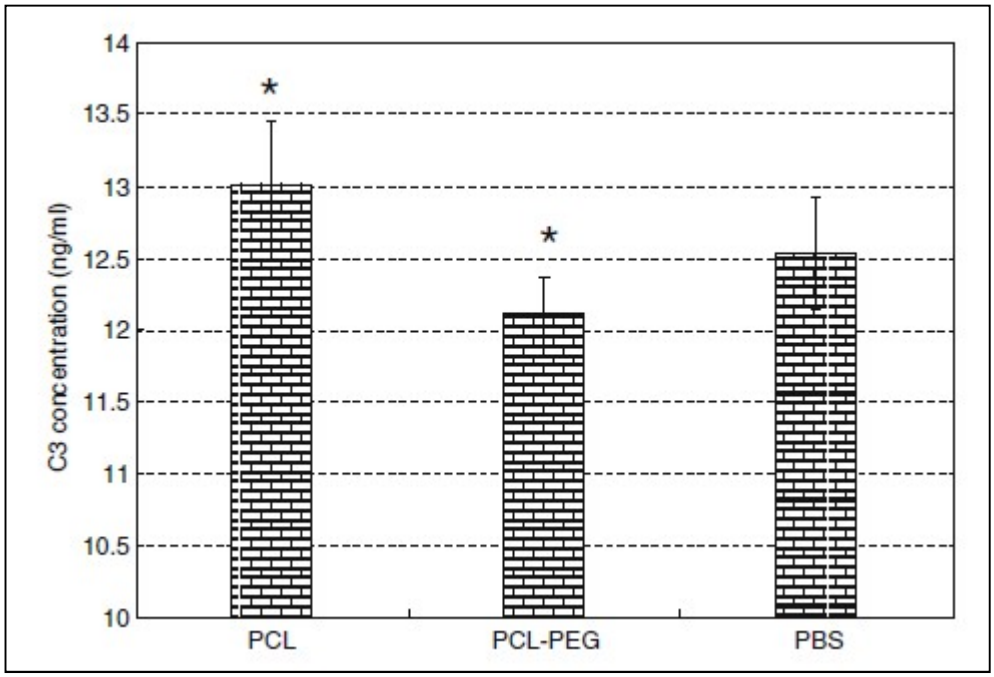

Figure 4.11: Complement C3 concentrations of human serum after incubation with PCL or PCL-PEG NPs. *p<0.05 .vs. PBS (Shan et al., 2009).

It has been mentioned that the PCL NPs were prone to cause complement activation. On the contrary, compared with naked PCL NPs, the PEG copolymers had a lower degree in C3 cleavage than the negative control PBS did (Shan et al., 2009).

As discussed before, the RES tissues play an important role in determining the disposition of NPs, which are expected to be involved in the tissue uptake, retention, andmpossible metabolism of PCL and PCL-PEG NPs. The above preliminary investigations in biodistribution has been provided important information that the hydrophilic PEG chains mask NPs from the plasma protein. The trend showed that naked PCL NPs accumulated more in liver, but with the PEGylation NPs, this final accumulation was shift toward the spleen.

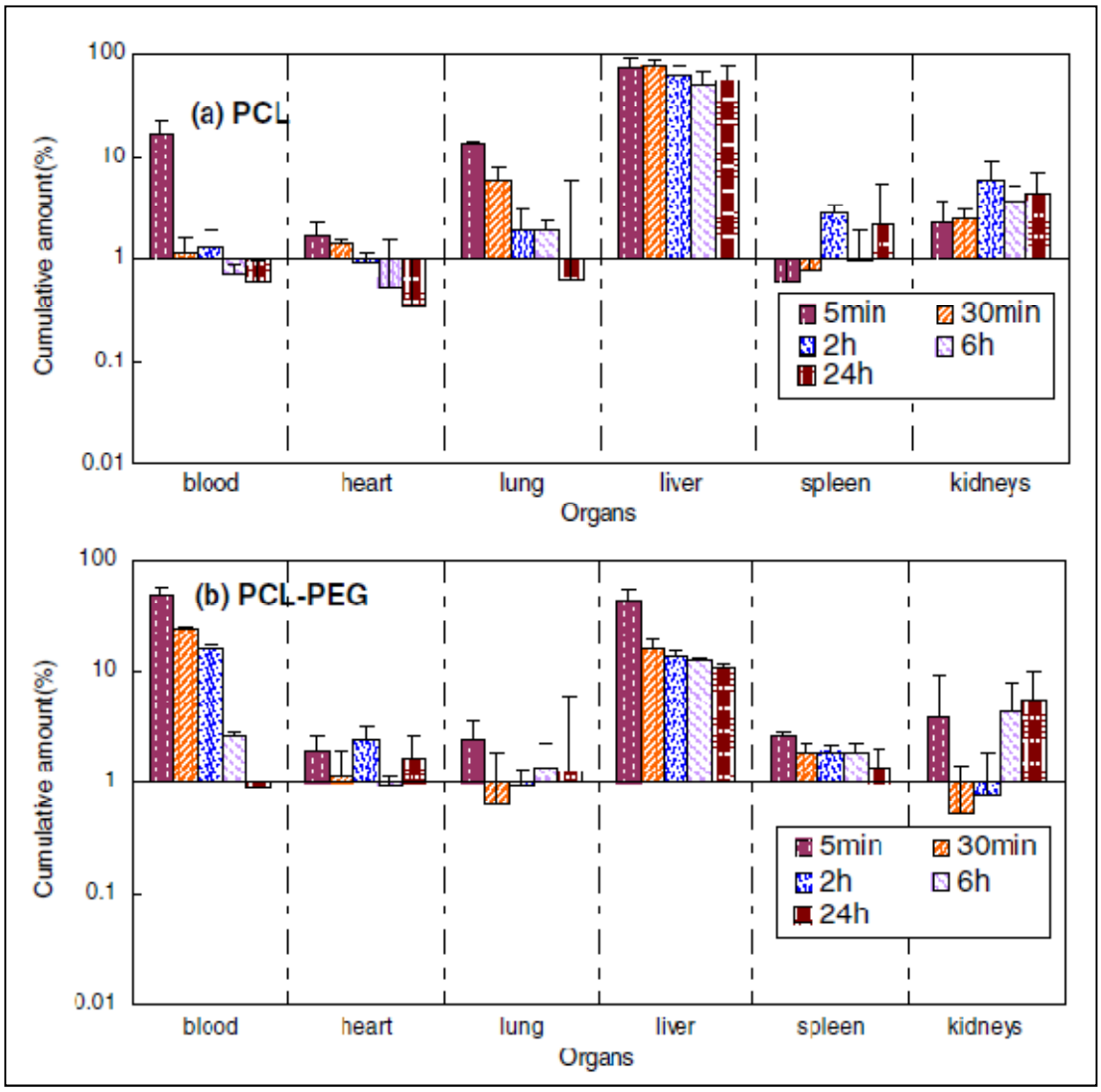

Figure 4.12: The accumulation for the naked PCL (a) and PCL-PEG (b) NPs in various organs at predetermined time (5 min, 30 min, 2 h, 6 h, 24 h and 48 h) (Shan et al., 2009).

In the case of naked PCL NPs, the sequestration in the RES tissues is very rapid and considerable, typically in a first 5 min, 90% of NPs were captured by phagocytosis. Furthermore, the uptake NPs were eliminated by metabolism rapidly, with only 25% of original injected dose residual after 48 h later, decreased for 65%. On the contrary, PEGylated NPs had a more steady experience with 45% found in the RES in 5 min after injection.

During 48 h of blood circulation, the accumulation in the RES decreased for 33%. The in vivo biodistribution data accompanied with the evidence of uptake by macrophages showed substantial difference in phagocytosis uptake between PCL and PCLPEG NPs. During the formation of PCL-PEG NPs, the hydrophobic chain of

PCL can incorporate with each other, while the hydrophilic chain of PEG chain, remaining on the surface, protrude to the outer phase and form a conformational hydrophilic “cloud-layer” over the NPs that protect the particles from each other and various plasma proteins.

As a result, the PEGylation NPs could avoid uptake by mononuclear phagocyte system (MPS). Indeed, the most marked inhibition of phagocytosis was owing to the hydrophilicity and steric effect of PEG chains, which ensure the particles a longer half-life time in blood stream.

Although the description of the adsorption protein is unknown, these observations imply that, under the protection of PEG chains to NPs, quiescent macrophages are not sufficiently activated yet by some blood component adsorb on NPs surface.

Nanoparticles That Have a Mean Diameter of Approximately 100 nm Show Prolonged Blood Circulation and a Relatively Low Rate of MPS Uptake.

Liu et al. (D. Liu, Mori, & Huang, 1992) have investigated the biodistribution of liposomes of different sizes (30-400 nm) in blood, liver, spleen, and tumor. They i.v. injected the radioisotope-labeled liposomes into the mice and examined the recovered dose in those tissues 4 h later. It was found that approximately 60% of the injected liposomes between 100 and 200 nm in size were detected in the blood, while only 20% of the ID for liposomes greater than 250 nm or less than 50 nm in size was recovered in the blood. For liver uptake, liposomes of approximately 100 nm exhibited only 20% ID accumulation, and particles greater than 250 nm in size had ~25% ID found in the liver.

Approximately 60% ID was recovered in the liver for liposomes with a diameter of less than 50 nm, which was smaller than the pore size of liver fenestrae (100 nm), and easily penetrated through the endothelial wall, resulting in an enhanced liver uptake. In the case of spleen uptake, liposomes less than 100 nm in size exhibited minimal spleen uptake, whereas an increase in particle size led to an increase in the rate of spleen uptake. For the liposomes approximately 400 nm in size, 40-50% ID was found in the spleen 4 h after injection. The tumoral uptake data were tightly correlated to those of the blood PK, in which liposomes with a diameter between 100 and 200 nm showed a 4-fold higher rate of uptake in the tumor compared to the liposomes greater than 300 nm or less than 50 nm in size.

Allen's group also demonstrated (Moreira, 2001)a similar result, in which liposomes with a diameter of approximately 120 nm exhibited a 10-20-fold increase in the rate of tumoral uptake compared to those with a diameter of approximately 170 nm.19 In this particular tumor model, the cutoff size range was even narrower. Torchillin et al. found that using micelles with a mean diameter of 10 nm to deliver paclitaxel did not show any EPR effect compared to the free drug. However, when the micelles were modified with a targeting antibody, significantly improved tumoral uptake was discovered. For very small particles, they can easily pass through the leaky capillary wall in the tumor but can also be easily pushed out from the tumor into the blood. Therefore, small particles have good permeability but poor retention. After conjugation with a targeting ligand, the retention in the tumor was greatly enhanced, leading to improved tumoral uptake.

Figure 4.13 summarizes the effect of size on the tumor targeting of nanoparticles. The research into the influence of size on PK was mainly studied in the liposome field since liposomes of a certain size can be prepared with a narrow size distribution by the membrane extrusion method (Li & Huang, 2008).

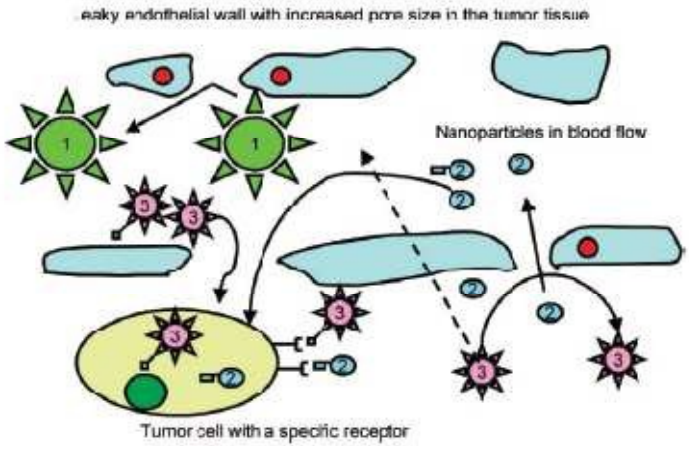

Figure 4.13: The effect of size on the tumor targeting, (Li & Huang, 2008).

4.9 Drug Loading and Release Mechanisms

A successful nanoparticle system may be the one which has high loading capacity to reduce the quantity of the carrier required for administration. Drug loading into nanoparticles is achieved by two methods: one by incorporating the drug at the time of nanoparticle production and second by adsorbing the drug after the formation of nanoparticles by incubating them in the drug solution. Drugs can be loaded onto

nanoparticles by adding them to a solution that contains previously prepared nanoparticles or by adding them to the reaction mixture during the polymerization process. These two methods provides solid solution for the drug encapsulation in the polymer, dispersion of the drug in the polymer, adsorption of the drug onto the surface of the nanoparticles and chemical binding of the drug to the polymer. The amount of bound drug and the type of interaction of drug and nanoparticles depend on the chemical structure of the drug as well as the polymer and the conditions of drug loading. The determination of the adsorption isotherm is one possible way to detect the type of binding and the binding rate (mg drug/mg nanoparticle). Adsorption isotherms for the nanoparticle/drug delivery system is used to give vital information on the best possible formulation, the drug binding capacity onto the surface of nanoparticles and the drug adsorbed. Linear sorption isotherms characterize solid solutions and Langmuiror S-type isotherms characterize surface adsorption. Because nanoparticles are colloidal systems, precise determination of the drug content is a major problem. Therefore, the most reliable way to separate thenano particles from the solution containing unbound drug is ultracentrifugation or gel filtration. From the amount of drug bound, the encapsulation efficiency (EE) of the drug can be calculated by using the formula:

$$EE = \frac{\text{Amount of Drug Bound}}{\text{Total amount of drug used for nanoparticle production}} \quad \textbf{(4.1)}$$

The drug release mechanisms are equally important as the drug polymer formulation because of the proposed application in sustained drug delivery. For manipulation of the rate and the timing of the drug release from nanoparticles, a good understanding of the mechanisms of drug release is needed. There are five possible methods for drug release: (a) desorption of drug bound to the surface, (b) diffusion through the nanoparticle matrix, (c) diffusion through the polymer wall of nanocapsules, (d) nanoparticle matrix erosion, or (e) a combined erosion–diffusion process. The kinetic analysis of drug release from nanoparticles can be described by a biexponential function

$$C = Ae^{-\alpha t} + Be^{-\beta t} \quad \textbf{(4.2)}$$

where C is the concentration of drug remaining in the nanoparticles at time t, A and B are system characteristic constants (A is used for diffusion control system and B for erosion control system), and ¸ and ˇ are rate constants that can be obtained from semilogarithmic plots. In general drug release rate depends upon solubility, diffusion and biodegradation of the matrix materials. The drug release mechanisms can be modified by the choice of polymer matrices.

Drug release also depends upon the loading efficiency of drug and size of nanoparticles. Larger particles have a smaller initial burst release than smaller particles. The drug loading capacity is directly proportional to burst and release rate of nanoencapsulated drug molecule. In the case of nanospheres, where the drug is uniformly distributed, the release occurs by diffusion or erosion, of the matrix under sink conditions. If the diffusion of a drug is faster than matrix erosion the mechanism of release is largely controlled by a diffusion process. The rapid initial release or burst is mainly attributed to weakly bound or adsorbed drug to the large surface of nanoparticles. The addition of other polymers to PLA based polymers can also be used to control drug release. For example, PEG has been polymerized into a PLA homopolymer creating a PLA–PEG–PLA copolymer. The drug release continued to increase as the total molecular weight of the copolymers decreased. The initial burst can be decreased in the absence of lower molecular weight polymers (Kumari et al., 2010).

4.10 The Importance of Cancer Therapy Based on Nanomaterials and Nanocarrier Systems

Cancer is one of the leading causes of death worldwide; it claimed 7.6 million deaths (13.1%) in 2005 out of 58 million deaths from all causes. In 2002, estimated 6.72 million people worldwide were newly diagnosed with any the most 10 prevalent forms of solid cancers; of these, 4.15 million died within the same year.

Based on projections, the death toll will rise to 9 million cancer deaths in 2015.

Chemotherapy, surgery and radiotherapy continue to be the mainstay treatments of cancer. Over 700 FDA approved drugs have entered into clinical practice during the last 30 years; these are classified into six major groups that include the platinum coordination complex, antimicrotubule agents (*vinca* alkaloids, taxanes),

antimetabolites (methotrexate, fluoropyrimidines, cytocine arabinose, gemcitabine), antitumor antibiotics (actinomycin D, mitomycin C, bleomycin, anthracyclines, podophylotoxines, camptothecines), alkylating agents, and others including a number of biological drugs or monoclonal antibodies that target specific pathways such as EGFR or angiogenesis (Boulikas, 2008).

Cancer occurs at a molecular level when multiple subsets of genes undergo genetic alterations, either activation of oncogenes or inactivation of tumor suppressor genes. Then malignant proliferation of cancer cells, tissue infiltration, and dysfunction of organs will appear. Tumor tissues are characterized with active angiogenesis and high vascular density which keep blood supply for their growth, but with a defective vascular architecture. Combined with poor lymphatic drainage, they contribute to what is known as the enhanced permeation and retention (EPR). Tumor genes are not stable with their development and often show genovariation. The inherent complexity of tumor microenvironment and the existence of P-glycoprotein (Pgp) usually act as barriers to traditional chemotherapy by preventing drug from reaching the tumor mass. Meanwhile, delivery of the therapeutic agents *in vivo* shares physiological barriers, including hepatic and renal clearance, enzymolysis and hydrolysis, as well as endosomal/lysosomal degradation. In addition, the efficiency of anticancer drugs is limited by their unsatisfactory properties, such as poor solubility, narrow therapeutic window, and intensive cytotoxicity to normal tissues, which may be the causes of treatment failure in cancer.

Accordingly, there is a great need for new therapeutic strategies capable of delivering chemical agents and other therapeutic materials specifically to tumor locations.

With the development of nanotechnology, the integration of nanomaterials into cancer therapeutics is one of the rapidly advancing fields. It can revolutionize the treatment of cancer. Nanotechnology is the creation and utilization of materials, devices, and systems through the control of matter on the nanometer scale.

Nanocarrier systems can be designed to interact with target cells and tissues or respond to stimuli in well-controlled ways to induce desired physiological responses. They represent new directions for more effective diagnosis and therapy of cancer.

4.10.1 The importance of nano-micelles in cancer therapy

Nano micelles are usually formed into core-shell structures by spontaneous assembly when their concentration is above critical micelle concentration (CMC). They have a number of unique features, including nanosize, easy manipulation of surface chemistry, core functionalities, as well as ease of fabrication, making them suitable as carriers for encapsulation, and delivery of water insoluble agents. The micelles have a solid-like inner core, which serves as a potent nanocontainer of hydrophobic compounds for solubilization of chemotherapeutics, including docotaxel (B. Liu et al., 2008), paclitaxel (Park, 2008) camptothecin (H. Onyuksel, 2005) ,and dequalinium (DQA) (Lizano et al., 2003) While polyionic complex micelles and cationic polymer micelles can incorporate and protect anionic gene or protein with low rate of cellular uptake and low physiological environment stability, such as vascular endothelial growth factor (VEGF), siRNA (Kim, 2009)and luciferase reporter gene.

Thanks to their hydrophilic shell, polymer micelles play an important part in escaping the recognition of RES and prolonging the blood circulation of drugs. The small size (<100 nm) allows micelles for efficient accumulation in pathological tissues with permeabilized vasculature via the enhanced permeability and retention (EPR) effect. However, the physiological factors, such as the density and heterogenesity of the vasculature at tumor sites, interstitial fluid pressure, and transport of macromolecules in the tumor interstitium, are responsible for the extent of micelles extravasations.

Stimuli-responsive polymeric micelles are often designed for controlled release of drug into tumor tissue with external stimuli trigger, like temperature, pH, ultrasound, and special enzymes (Weili Qiao, 2010).

Table 4.4. Stimuli that can be utilized to control the behavior and properties of micelles.

Stimuli	Stimuli origin	Examples	References
pH	Decreased pH in cancer site caused by hypoxia and massive cell death	Tumoral acidic extracellular pH targeting of pH-responsive micelles encapsulated doxorubicin for cancer therapy	(J. Ko, 2007)
Temperature	Increased temperature in cancerous tissues owing to their high metabolic activities. External applied heating	Self-assembled, thermosensitive micelles for controlled doxorubicin delivery	(Nakayama, 2006)
Magnetic field	Locally applied magnetic field	Folate-encoded and Fe304-loaded polymeric micelles for dual targeting of cancer cells	(Yang, 2008)
Ultrasound	Locally applied ultrasound	Ultrasonic release of doxorubicin from pluronic P105 micelles	(Husseini, 2002)
Redox potential	Increased concentration of glutathione inside many cancerous cells	Poly(ethylene glycol)-modied thiolated gelatin nanoparticles for glutathione-responsive intracellular DNA delivery	(Torchilin, 2009)

5. VINORELBINE (VLB)

The *Vinca* alkaloids are a subset of drugs that are derived from the periwinkle plant, *Catharanthus roseus* (also *Vinca rosea*, *Lochnera rosea*, and *Ammocallis rosea*).

There are four major *Vinca* alkaloids in clinical use: Vinblastine, vinorelbine, vincristine, vindesine and newly synthesized one; Vinflunine (Figure 5.2).

Since we were trying to upload one of these *Vinca* alkaloids to nano-micelles in which the core part is consisting of nonpolar environment, we had to choose the most nonpolar one in order to place the drug in the core of formulation, otherwise localization of the drug in the shell would have lead to the fast release of drug from carrier which is not favorable in cancer targeting.

Table 5.1: Water solubility of *Vinca* alkaloids calculated by a software (Development, (© 1994-2010 ACD/Labs)).

Alkaloid	**Solubility in pH7** μg/ml
Vincristine	20
Vinblastine	6.3
Vinorelbine	0.75

Vinorelbine has the least functional groupin among mentioned *Vinca* alkaloids so seems to be the most nonpolar one. Along with this, its side effects in chemotherapy (below) makes it the most appropriate candidate to use it in preparing the new targeting nano-formulation to use in cancer therapy.

Lung cancer is one of the most commonly diagnosed malignancies in developed countries and is a growing problem in developing countries. There are two major types of lung cancer: non-small cell lung cancer (NSCLC) and small cell lung cancer (SCLC). NSCLC makes up approximately 80% of all lung cancer cases and has a limited response rate to current chemotherapeutic agents, with tumor shrinkage in only 20% of patients and a two-year survival rate between 10% and 16%. One major reason for this unsatisfactory outcome of chemotherapy is compromised drug delivery to the lung cancer tissues due to high interstitial fluid pressures (IFP) within the tumor. Systemically administered chemotherapy cannot be adequately delivered

into solid tumors because of the immature vasculature with abnormal architecture and leaky, heterogeneous vessel walls as well as the high IFP within tumor tissues. Furthermore, a lack of tumor specificity allows anti-cancer drugs to distribute indiscriminately to normal organs and tissues. Thus, cancer cells are exposed to a lower concentration of the drug than normal cells, resulting in not only decreased effectiveness but also increased toxicity. Therefore, it is important to develop a strategy to enhance the amount of drugs delivered to tumor tissues in a targeted way while sparing normal tissues (Chang, 2009).

Vinorelbine is currently used in salt form (Bitartarate) in chemotherapy, so according to our knowledge the water solubility of its base form is not reported in literature. Its calculated water solubility and LogP are 0.75mg/ml and 4.69 respectively which were satisfying enough to start using this drug in nano formulation investigations. However, the real water solubility value was obtained experimentally was completely different (mentioned on Results and Discussion).

In the other hand it is very important for a drug to carry all functional groups on just one surface or in a localized position on the whole surface in order to upload succesfully to the core. Otherwise, charge distribution will lead to localization on shell. Vinorelbine's structure carries almost all functional (chargable) groups in a very localized manner:

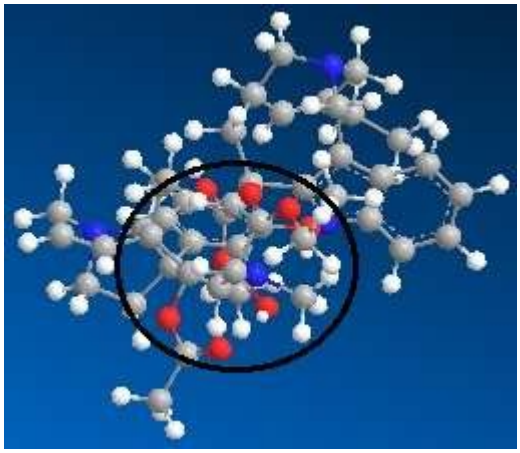

Figure 5.1: 3D illustration of the structure of VLB and the localization of its functional groups.

So, we chose Vinorelbine to prepare a new targeting nano-formulation for cancer therapy.

5.1 History

Vinorelbine was invented by the Pharmacist Pierre Potier and his team from the CNRS in France in the 1980s and was licensed to the oncology department of the Pierre Fabre Group and was first reported in Onkologie, vol. 4, issue 1, p; 7-12, 1991 (Krikorian, 1991).

The drug was approved in France in 1989 under the brand name Navelbine for the treatment of bronchial cancer. It gained approval to treat non-small cell lung cancer in 1991. The drug is now primarily used to treat this cancer. Vinorelbine received approval by the United States Food and Drug Administration (FDA) in December 1994 sponsored by Burroughs Wellcome Company. Pierre Fabre Group now markets Navelbine in the U.S. The drug went generic in the U.S. in February 2003.

In Europe is approved to treat non-small cell lung cancer, breast cancer and, in some countries, prostate cancer.

Since 2004 an oral formulation has been marketed and registered in Europe for the same settings. It has been shown a similar efficacy and safety profile between both intravenous and per os formulations, avoiding local toxicity induced by the intravenous vinorelbine (Krikorian, 1991).

5.2 Mechanism of Action:

All *Vinca* alkaloids are administered intravenously (IV). After injection, they are eventually metabolized by the liver and excreted. They work in a cellcycle specific manner, halting mitosis of affected cells and causing cell death. The mechanism of action involves binding to the tubulin monomers and keeping the microtubules (spindle fibers) from forming (Ngan et al., 2000; Okouneva, 2003). This is where the mechanis of action of taxanes are to stabilize tubulin polymers but also to disrupt additional cellular processes and to induce apoptosis (X. M. Liu, Wang, L. G., Kreis, W., Budman, D. R., & Adams, L. M. , 2001).

The mitotic spindle is a specialized structure required for exact chromosome segregation in mitosis. Spindle formation is dependent on the reorganization of interphase microtubule network, regulated by cell cycle-regulatory mechanisms. The centrosome (known as the microtubule organizing center) is involved in the

formation of spindle poles during mitosis, which ensures the distribution of the correct number of chromosomes to daughter cells. Aberrant centrosome duplication could cause centrosome amplification and chromosomal instability.

These alkaloids also seem to interfere with cells' ability to synthesize DNA and RNA. Although the plant has medical uses, it can produce many serious side effects if smoked or ingested (Boulikas, 2008).

5.3 Targeting Stem Cells by Vinorelbine

One of the virtues of vinorelbine is the fact that it may can be easily combined with other cytotoxic and may be suitable for use in special populations such as the elderly and/or frail patients. Another rationale for using this agent is that, unlike doxorubicin or paclitaxel, vinorelbine has not been proven to be the substrate of ABC transporters, which are highly expressed in cancer stem cells (cancer stem cells express high levels of drug transporters such as ATP-binding cassette (ABC) transporters, which actively efflux drugs from cells, thus protecting them from cytotoxic agents). However, based on cancer stem cells concept, the effect of vinorelbine on malignant stem is still limited since it is a cell-cycle specific drug inhibiting cell growth during metaphase. To circumvent the problem, a sesquiterpene lactone parthenolide (PTL) is introduced. PTL is derived from feverfew (tanacetum parthenium), an herbal medicine that has been traditionally used for the treatment of migraine and rheumatoid arthritis. Recent studies have demonstrated that PTL possesses anti-tumor property in different cell lines through multiple signal pathways. In particular, a study showed that PTL was able preferentially to ablate primitive leukemia cells without affecting normal stem and progenitor cells. These findings indicate PTL may represent a novel class of agents for targeting cancer stem cells (Y. Liu, Lu, W.-L., Guo, J., Du, J., Li, T., Wu, J.-W., Wang, G.-L.,, 2008).

5.4 Side Effects

For the treatment of non-small cell lung cancer NSCLC, VLB is administered at a dose of 20 to 25 mg/m2 alone or in combination with cisplatin or gemcitabine. VLB is also administered at a dose of 25 mg/m^2 alone or combined with cisplatin or trastuzumab in patients with inoperable, advanced, and recurrent breast cancer, who

have previously received anthracyclines and taxanes. Vinorelbine has been reported to cause venous discoloration and chemical phlebitis proximal to the site of injection, as well as localized rashes and urticaria, blistering, and skin sloughing. It is a vesicant and venous irritant like other *Vinca* alkaloids. Factors that influence the development of phlebitis include the quality of the vein selected, the size and type of catheter used, the duration of infusion, and the pH and osmolality of the drug solution. The Japanese package insert for VLB recommends dilution with 50 mL of normal saline or 5% glucose and administration over less than 10 min, followed by flushing of the vein but the effectiveness of this protocol has not been evaluated.

Vinorelbine has some other side-effects that can limit its use: Lowered resistance to infection, bruising or bleeding, constipation, diarrhea, nausea, numbness or tingling in hands or feet (peripheralneuropathy), tiredness and a general feeling of weakness (asthenia), granulocytopenia, leucopenia, and thrombocytopenia, with granulocytopenia being the primary dose-limiting toxicity.

Acute reaction, such as dyspnea, chest pain and wheezing has been reported during administration but can be prevented in some cases by premedication with corticosteroids.

A stable oral dosage form of vinorelbine (Navelbine Oral) developed in 1994 by Pierre Fabre Medicament is also available. However, Depierre et al. (Depierre et al., 2001)found a high rate of early deaths (10%) due to complicated neutropenia toxicity when patients were given a weekly dose of 80 mg/m2 by mouth; accordingly, the dose had to be reduced to 60 mg/m^2/week to continue the study (Kohno, 2008).

5.5 Reported Nano Vinorelbine Formulations:

The company Hanna Biosciences Inc. has prepared a liposomal formulation for vinorelbine-tartarate and the phase I studies started in 2006 and is almost enden in 2010. They have 2 very important disadvantages in comparing with our DSPE-PEG and Polymeric Micelles:

During preparation of this liposomal formulation, they use Inophore and in another stage they use MgSO4 which removing both of them is very hard and they add two steps of cleaning and purifying these two compounds to the processes (Semple et al., 2005).

Another study is reporting enhanced therapeutic and reduced side effect of vinorelbine by using Peptide attached liposomes. This study is only trying to show the effect of a very specific peptide; PC5-2 to target breast cancer cells and uses Vinorelbine as an example drug to show the efficacy of the mentioned peptide. Maybe because of that reason this paper deos not mention of the method of preparing liposome so we are not able to compare our formulation with the reported nano-vinorelbine formulation (Chang, 2009).

The last study that reports preparing a nano formulation old Vinorelbine is a paper presented by Wang et al. This paper is using the water soluble form of Vinorelbine; Vinorelbine-tartarate as model water soluble drug. In this study Poly (ethylene glycol)-phosphatidylethanolamine (PEG-PE) (we called the same material DSPE-PEG in our thesis) has been used as drug delivery system. The authors are reporting a very high encapsulation efficacy and saticfying in vitro release period.

Interestingly this study is reporting using micelles for encapsulation of hydrophiic drugs. According to our knowledge liposomes are the most appropriate drug delivery systems in order to carry water soluble drugs. Although this paper is reporting different evidences that proofes the incorporation of the water soluble drugs with the hydrophilic head group of phosphatidylethanolamine, the water soluble drug is more possible to incorporate with the PEG layer. Unfortunately all results that have been mentioned as the evidence of incorporating drug with the core part of micelle could be seen when the drug is incorporated with the PEG layer too (Y. Wang et al., 2010).

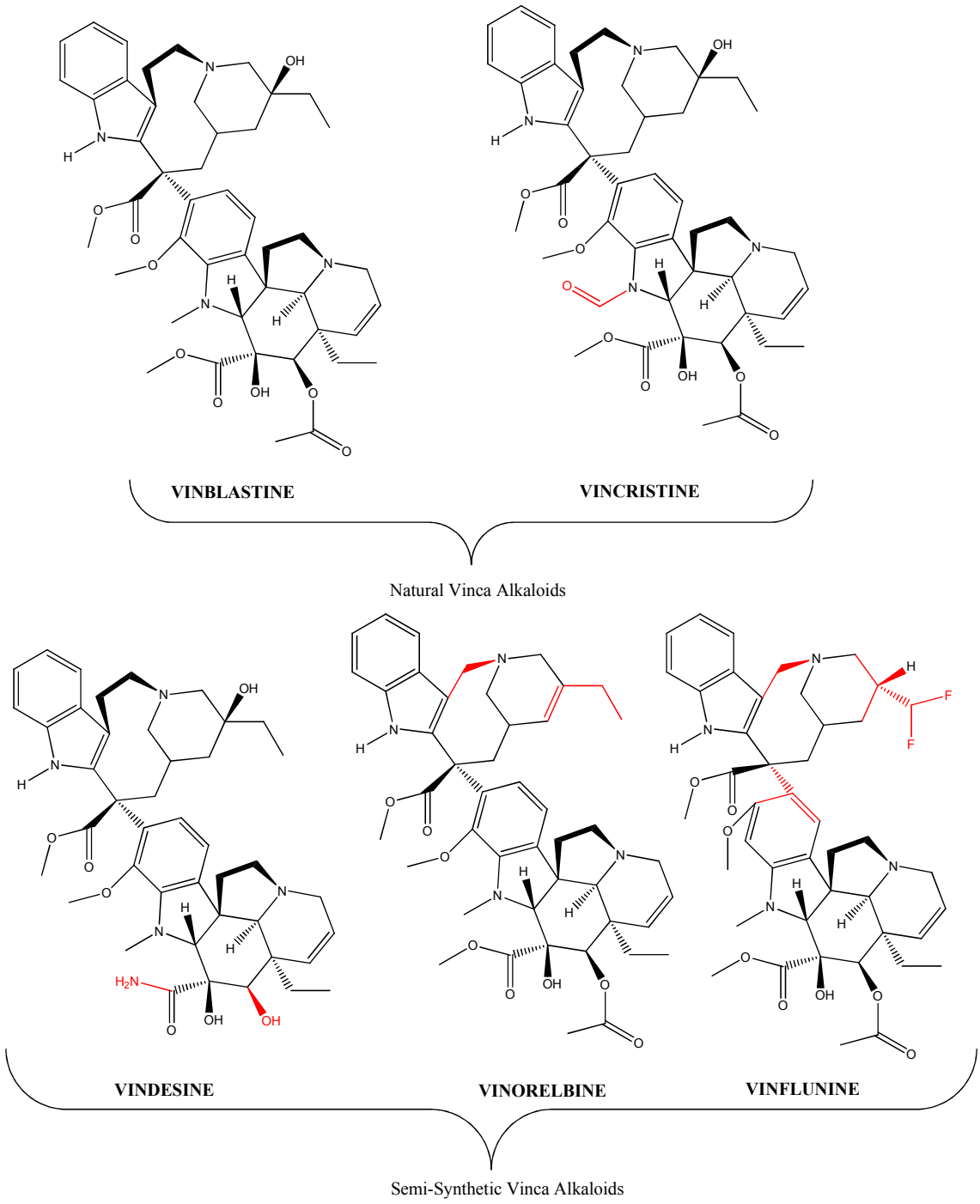

Figure 5.2: Currently used *Vinca* alkaloids in chemotherapy, (Boulikas, 2008).

6. THE BASICS OF THE METHODS USED IN THIS STUDY

6.1 The Methods Used in Chemical Isolation of Plant Materials

6.1.1 Chromatography

Among the chemical methods of plant examination, chromatographic analysis plays a very important role, and it has been introduced to all the modern pharmacopoeias. Because of numerous advantages of the chromatographic methods (such as their specificity and a possibility to use them for qualitative and quantitative analysis), they comprise an integral part of the medicinal plant analysis.

The following chromatographic methods are most frequently applied in phytochemical analysis: one- and two-dimensional paper chromatography, one- and twodimensional thin layer chromatography (TLC; also called planar chromatography), high-performance column liquid chromatography (HPLC), gas chromatography (GC), and column chromatography (CC). These methods can also be used for the isolation of the individual components from the component mixtures on a preparative and micropreparative scale (Waksmundzka-Hajnos, 2008).

Chromatography is based on differential migration rates of components of a liquid or gas as it moves past adsorptive materials. Practically any soluble or volatile substance can be purified by chromatography. Some combination of adsorbant, conditions and carrier fluid will allow us to apply a mixture of materials to a column of adsorbent and to flush so that differential migration rates separate the materials to a column of adsorbent and to flush so systems have *stationary phase* (which can be solid or liquid) and a *mobile phase* (usually liquid or gas) (Raaman, 2006).

6.1.2 Column chromatography

In column chromatography both phase are placed in a column container. Column chromatography involves ion-exchange, molecular sieve, adsorption and partition phenomenon.

Column chromatography can function with quite impure feed streams, but an undesired byproduct in high concentrations may give peaks that overlap with those

of the desired product. Loading relates to capacity of the adsorbent, and overloading results in dispertion through the column and little or no purification. A run starts with concentrate at the top of the column, then a solvent (eluent) flushes materials through the column. Molecules have different attractions to the adsorbing materila and move at different rates through the column to its exit.

With light loading of small columns, resolution of peaks is often excellent so that very high purity is obtained. Heavier loading produces longer tails so that one material contaminates another. The dispertion of flow in large columns can lead to severe cross contamination of material (Raaman, 2006).

6.1.3 Thin layer chromatography:

TLC is a chromatographic technique widely used for qualitative analysis of organic compounds, isolation of the individual compounds from multicomopnent mixtures, quantitative analysis, and preparative-scale isolation. Many kinds of TLC and highperformance TLC (HPTLC) precoated plates are commercially available, e.g., those with the inorganic adsorbent layers (silica or silica gel and alumina); organic layers (polyamide, cellulose).

Sorbents applied in TLC have different surface characteristics and, hence, different physicochemical properties. Moreover, there is a wide choice of mobile phases that can be used to separate mixture components; these belong to various selectivity groups and, thus, have different properties as proton donors, proton acceptors, and dipoles. In TLC, ultraviolet (UV) absorption of the mobile phase solvents does not play a significant negative role in detection and quantification of the analytes, because the mobile phase is evaporated from the plate prior to the detection. High viscosity of a solvent can be viewed as a sole property limiting its choice as a mobile phase component. These plate and mobile phase characteristics

allow a choice from among an unparalleled abundance of TLC systems that offer a broad spectrum of separation selectivities, which is particularly important when complex mixtures of the plant extracts have to be separated.

The advantages of TLC are particularly important with plant extracts, which are very complex mixtures of the structurally differentiated chemical compounds. Such extracts very often contain polar (e.g., tannins and phenols) and nonpolar (lipids,

chlorophylls, and waxes) ballasts, apart from a fraction of active substances that is of main importance for phytochemistry and pharmacognosy.

TLC enables separation of a crude plant extract without an earlier purification. For example, in a normal phase system a nonpolar fraction moves with the mobile phase front (or it can be prewashed with a nonpolar mobile phase prior to the development of a chromatogram), and the polar fraction remains strongly retained near to the origin; then the fraction of interest is separated in the central part of the chromatogram (Hajnos, 2008).

6.1.4 TLC techniques used in identification of Indole alkaloids

6.1.5 Stationary phases

Most TLC procedures for separating Indole alkaloids use an adsorbent stationary phase such as silica gel G, often with fluorescent agent added, since all Indole alkaloids will absorb UV light and can be observed as quenching zones when examined under UV light.

6.1.6 Mobile phases

A very large number of mobile phases have been used to separate Indole alkaloids

and can be found in the standard reference sources. Solvents employed reflect the polarity of the alkaloids under investigation. The majority of Indole alkaloids are tertiary bases with fairly low polarity, so that mixtures containing a major part of a less polar solvent (e.g., chloroform, toluene) with a small proportion of a more polar solvent (e.g., acetone, ethanol, methanol) are frequently cited. Since tertiary Indole alkaloids share the amphiphilic properties of most other alkaloids, resulting in elongated ‘‘streaked’’ zones, sometimes called ‘‘tailing,’’ a base is often added to the solvent mixture to ensure that the noncharged form of the alkaloids is predominant and that the zones are more compact. For less polar systems, diethylamine, in proportions up to 10% v:v, is used but in other cases ammonia solution, either concentrated (13.5 M) or in a more dilute form can be used, often in conjunction with ethyl acetate and propan-2-ol.

6.1.7 Detection reagents

Most detection of Indole alkaloids is carried out by first observing under UV light 254 nm for the presence of fluorescent or quenching zones. If the latter are sought, then a layer with added fluorophor (e.g., silica gel GF254) should be used. The Cinchona alkaloids in particular give a very strong bright blue fluorescence under UV 365 nm and can be detected at very low concentrations. Many of the ergot alkaloids give a blue fluorescence under UV light at both 254 and 365 nm. It is very common to follow examination under UV light with the use of a chemical chromogenic reagent but there are a few instances of biological detection methods also being applied.

6.1.8 Chemical detection methods

Dragendorff's reagent (potassium iodobismuthate solution) will give an orange color against a yellow background for all Indole alkaloids, based on the precipitate complex of the alkaloid and the bismuth metallic component of the reagent.

The colors of zones for some Indole alkaloids obtained by spraying with Dragendorff's reagent can be made more intense by subsequent spraying with 10% sodium nitrite solution.15 Iodoplatinate reagent works on a similar principle and gives a slightly greater range of colors comprising pink, brown, and violet (Hajnos, 2008).

6.2 Methods Used in Preparation of Nano Vinorelbine Formulations:

6.2.1 Surfactant micelle characterization using dynamic light scattering (DLS)

Dynamic Light Scattering (DLS) is a technique used for particle sizing of samples, typically in the sub-micron range. The technique measures the time-dependent fluctuations in the intensity of scattered light from a suspension of particles undergoing random, Brownian motion. Analysis of these intensity fluctuations allows for the determination of the diffusion coefficients, which in turn yield the particle size through the Stokes- Einstein equation.

Conventional DLS instruments use a detection angle of 90° and this optical configuration may not be sensitive enough for the successful measurement of surfactant micelles. The Zetasizer Nano range of instruments incorporates non-

invasive back scatter (NIBS) optics . The scattered light is detected at an angle of 173° and this novel optics arrangement maximizes the detection of scattered light while maintaining signal quality. This provides exceptional sensitivity that is required for measuring the size of nanoparticles, such as surfactant micelles, at low concentrations.

DSPE-PEG 2000 and Polymeric micellar samples prepared in a concentration 1000 and 100 times higher than their CMC respectievely (Birdi, 1997; Cosgrove, 2005; Everett, 1988).

6.2.2 The principals of Differential Scanning Calorimeter (DSC) and its relation with polymer characterization and drug delivery systems:

DSC is a technique which is part of a group of techniques called Thermal Analysis (TA). Thermal Analysis is based upon the detection of changes in the heat content (enthalpy) or the specific heat of a sample with temperature. As thermal energy is supplied to the sample its enthalpy increases and its temperature rises by an amount determined, for a given energy input, by the specific heat of the sample. Most DSC instruments are of the heat-flux design, a schematic of which is shown below.

Small, flat samples are contained in shallow pans, with the aim of making a good

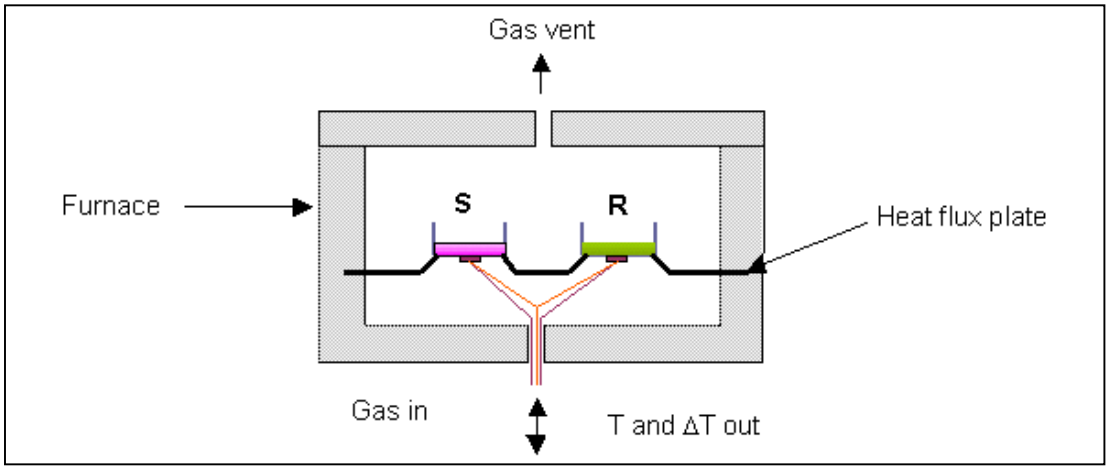

Figure 6.1: Basic Components of a DCS Instrument (Kastantin, 2009).

thermal contact between sample, pan and heat flux plate. Symmetrical heating of the cell, and therefore **S** and **R**, is achieved by constructing the furnace from a metal of high thermal conductivity.

6.2.3 Crystallization of a polymer sample and the recording of this event by using DSC

Above the glass transition, the polymers have a lot of mobility. They wiggle and squirm, and never stay in one position for very long. When they reach the right temperature, they will have gained enough energy to move into very ordered arrangements, which we call crystals, of course.

When polymers fall into these crystalline arrangements, they give off heat. We can see this drop in the heat flow as a big dip in the plot of heat flow versus temperature:

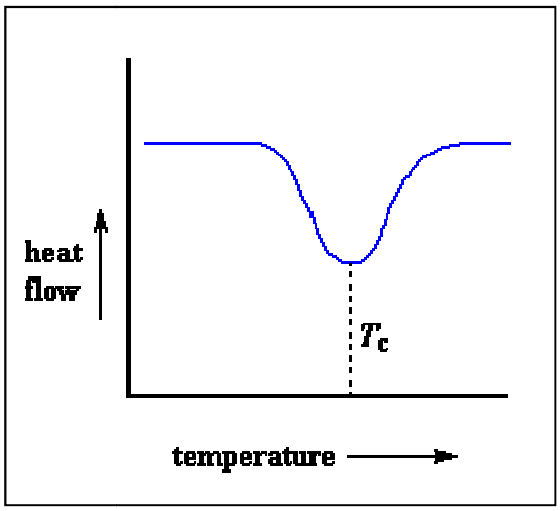

Figure 6.2: General view of the crystallization thermogram of a polymer, **(**Kastantin, 2009**).**

The temperature at the lowest point of the dip is usually considered to be the polymer's crystallization temperature, or T_c. Also, we can measure the area of the dip, and that will tell us the latent energy of crystallization for the polymer.

6.2.4 The meaning of "crystal" in polymeric materials and the relation of crystallization temperature with the loaded drug in drug delivery systems:

The kind of crystal we're talking about here is any object in which the molecules are arranged in a regular order and pattern.

Most of Polymers can't always stretch out so straightly. In fact, very few polymers can stretch out perfectly straight, and those are ultra-high molecular weight polyethylene, and aramids like Kevlar and Nomex. Most polymers can only stretch out for a short distance before they fold back on themselves.

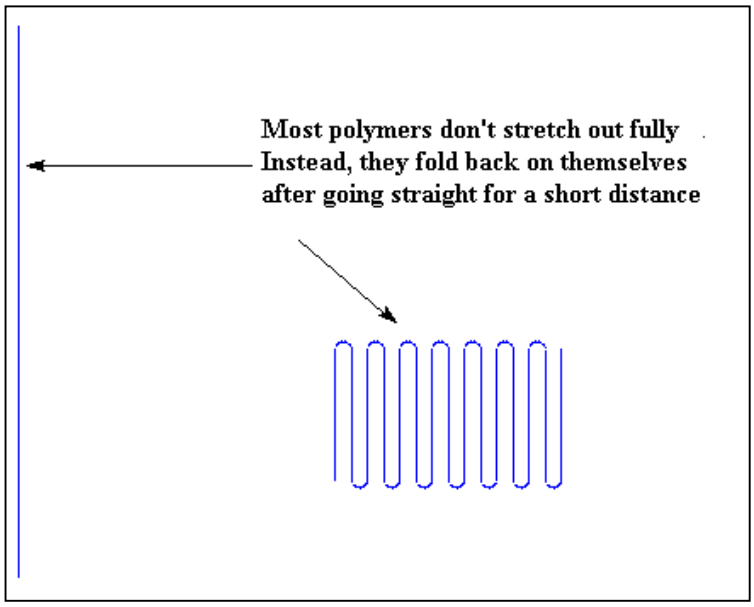

Figure 6.3: Folding of polymers in solid state, **(**Kastantin, 2009**).**

For polyethylene, the length the chains will stretch before they fold is about *100 angstroms*.

But not only do polymers fold like this. Polymers also form stacks of these folded chains. There is a picture of a stack, called a lamella, right below.

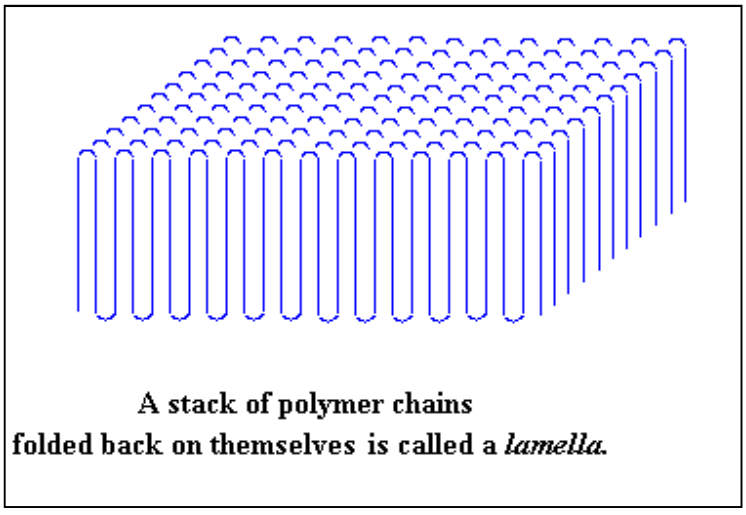

Figure 6.4: The stack of polymers which causes the crystallization thermogram in DSC spectrum, **(**Kastantin, 2009**).**

This is the point in which we see the *Crystallization Temperature.* In this temperature, (after giving enough heat to the material,) material gains enough energy to form stacks of folded chains.

Of course, it isn't always as neat as this. Sometimes part of a chain is included in this crystal, and part of it isn't. When this happens we get the kind of mess. Lamella is no longer neat and tidy, but sloppy, with chains hanging out of it everywhere. *This amorphism causes a decrease in crystallization temperature.*

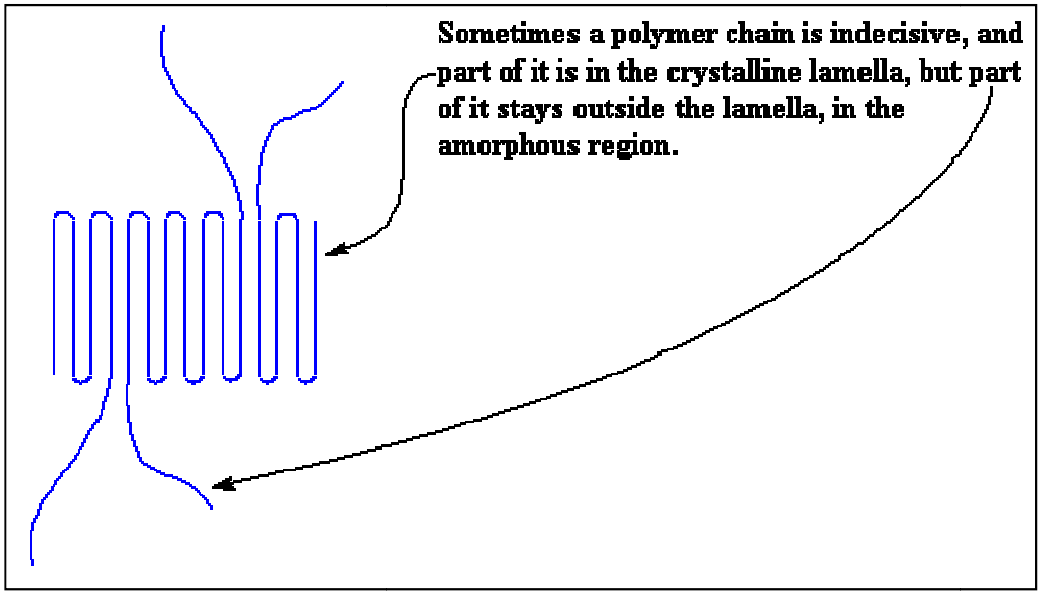

Figure 6.5: The reason of decrease in crystallization temperature, **(**Kastantin, 2009**).**

6.2.5 The partial interdigitation induced by drugs in lamellar systems and its evidence in DSC researchs (similar to plactisizers)

In polymer science plasticization is the inter mingling of the "solvent" between the polymer chains causing the polymer to become more flexible.

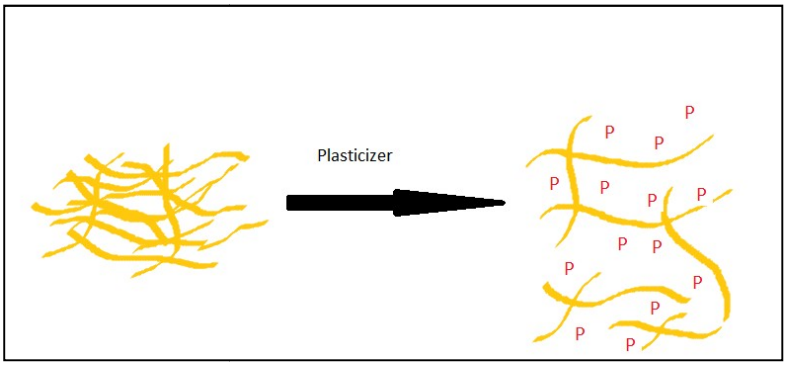

Figure 6.6: Adding the plasticizer and reduction in crystallization temperature (Whypych 2009).

According to the free volume theory, the addition of the plasticizer to the polymer creates a large free volume in the polymer and so diminishing the crystallization temperature of the plasticized polymer.

The presence of drug in lipid based lamellar drug delivery systems induces partial interdigitation as it is depicted by the increase of ΔH and reduction of crystallization temperature. As it is reported in the literature, the main cause of intergiditation is an increase in the lateral area between the lipid headgroups with a formation of voids in the hydrophobic core. By interdigitation the system gains energy due to the stronger van der Waals interactions in the interior of the membrane bilayers and due to an entropy gain by replacing the highly ordered water molecules at the interface with the polar part of the amphiphilic molecules (Galipeau, 1995; Kastantin, 2009; Koukoulitsa, 2006; Lv et al., 2009; Maswadeh et al., 2002; Sullivan, 2004; Ward, 2005; Whypych).

6.2.6 Reversed-phase High Performance Liquid Chromatography (RP-HPLC)

Reversed phase HPLC (RP-HPLC or RPC) has a non-polar stationary phase and an aqueous, moderately polar mobile phase. One common stationary phase is a silica which has been treated with RMe_2SiCl, where R is a straight chain alkyl group such as $C_{18}H_{37}$ or C_8H_{17}. With these stationary phases, retention time is longer for molecules which are less polar, while polar molecules elute more readily. An investigator can increase retention time by adding more water to the mobile phase; thereby making the affinity of the hydrophobic analyte for the hydrophobic stationary phase stronger relative to the now more hydrophilic mobile phase. Similarly, an investigator can decrease retention time by adding more organic solvent to the eluent. RPC is so commonly used that it is often incorrectly referred to as "HPLC" without further specification. The pharmaceutical industry regularly employs RPC to qualify drugs before their release.

Structural properties of the analyte molecule play an important role in its retention characteristics. In general, an analyte with a larger hydrophobic surface area (C-H, C-C, and generally non-polar atomic bonds, such as S-S and others) results in a longer retention time because it increases the molecule's non-polar surface area, which is non-interacting with the water structure. On the other hand, polar groups, such as -OH, $-NH_2$, COO^- or $-NH_3^+$ reduce retention as they are well integrated into water. Very large molecules, however, can result in an incomplete interaction between the large analyte surface and the ligand's alkyl chains and can have problems entering the pores of the stationary phase.

Retention time increases with hydrophobic (non-polar) surface area. Branched chain compounds elute more rapidly than their corresponding linear isomers because the overall surface area is decreased. Similarly organic compounds with single C-C-bonds elute later than those with a C=C or C-C-triple bond, as the double or triple bond is shorter than a single C-C-bond.

Another important component is the influence of the pH since this can change the hydrophobicity of the analyte. For this reason most methods use a buffering agent, such as sodium phosphate, to control the pH. The buffers serve multiple purposes: they control pH, neutralize the charge on any residual exposed silica on the stationary phase and act as ion pairing agents to neutralize charge on the analyte. Ammonium formate is commonly added in mass spectrometry to improve detection of certain analytes by the formation of ammonium adducts. A volatile organic acid such as acetic acid, or most commonly formic acid, is often added to the mobile phase if mass spectrometry is used to analyze the column eluent. Trifluoroacetic acid is used infrequently in mass spectrometry applications due to its persistence in the detector and solvent delivery system, but can be effective in improving retention of analytes such as carboxylic acids in applications utilizing other detectors, as it is one of the strongest organic acids. The effects of acids and buffers vary by application but generally improve the chromatography (S. Ahuja & Dong, 2005; Satinder Ahuja & Rasmussen, 2007).

6.2.7 A short review of MTT assay:

The **MTT assay** and the **MTS assay** are colorimetric assays for measuring the activity of enzymes that reduce MTT or close dyes (XTT, MTS, WSTs) to **formazan** dyes, giving a purple color. A main application allows to assess the viability (cell counting) and the proliferation of cells (cell culture assays). It can also be used to determine cytotoxicity of potential medicinal agents and toxic materials, since those agents would stimulate or inhibit cell viability and growth. **MTT** (3-(4,5-Dimethylthiazol-2-yl)-2,5-diphenyltetrazolium bromide, a yellow tetrazole), is reduced to purple formazan in living cells. A solubilization solution (usually either dimethyl sulfoxide, an acidified ethanol solution, or a solution of the detergent sodium dodecyl sulfate in diluted hydrochloric acid) is added to dissolve the insoluble purple formazan product into a colored solution. The absorbance of this

colored solution can be quantified by measuring at a certain wavelength (usually between 500 and 600 nm) by a spectrophotometer (Mosmann, 1983).

7. MATERIALS AND METHODS

Materials used in Synthesis of PCL_4 -PEG_4 and PCL_2-PEG Polymers are not included

1.1. Materials:

- DSPE-PEG_{2000} ; MW2810, Cat #`PE 18:0/18:0-PEG2000, Lot # 882032-01/907
- Acetonitrile, Methanol (HPLC grade) Ficsher scientific
- TFA (HPLC grade) Ficsher scientific
- Chloroform-Methanol-Ethanol- Acetonitrile, Ficsher scientific
- Vinorelbine; Cat# AL-4176 Altan Biochemicals. MW: 778.932
- Plastic cuvettes
- Amicon® Ultra-4 Centrifugal Filter Tubes (Millipore)
- Spectra/Por 3 Molecularporous Dialysis Membrane, Spectrum, MWCO 6000-8000, part no. 132720
- Spectra/Por 1 Molecularporous Dialysis Membrane, Spectrum, MWCO 3500, part no. 132720
- MCF-7 cell lines ($6x10^4$ cells/ml).
- Media: DMEM Dulbeccos Modified Eagle Medium, High Glucose 1X. Lot# 12430
- Phosphate buffer saline (PBS) (preparation method mentioned below)
- Media: DMEM Dulbeccos Modified Eagle Medium, High Glucose 1X. Lot# 12430
- Fetal bovin serum
- MTT, Sigma Aldrich Cat# M2003

- Merck: 1.07730.1000 Silica gel 60 GF254, 1.07734.1000 Silica gel 60 (0.063-0.200 mm), Merck 1.05554.0001 TLC Silica gel 60 F_{254}
- Argon Tube

Preparation of Reagents and Buffers:

Table 7.1: Chromogenic Spray Reagents for Indole Alkaloids (Hajnos, 2008).

Common Name	Formula	Treatment after Spraying	Notes
Dragendorff's reagent	Solution A: 0.85 g basic bismuth nitrate dissolved in 10 mL glacial acetic acid and 40 mL water with Heating Solution B: 8.0 g potassium iodide dissolved in 30 mL water Mix solutions A and B in 1:1 ratio then add to glacial acetic acid and water in 1:2:10 ratio	Observe in daylight	Gives an orange color with many types of alkoloids.
Cerium(IV) sulfate 1 g	Ammonium cerium(IV) sulfate dissolved in 100 ms 85% phosphoric acid	Heat at 105^0C for 10 min; observe in daylight	Variations of formula exist

Table 7.2: The formulation of 1xPBS Buffer (Medicago, 2010).

1	8 g NaCl
2	0.2 g KCl
3	1.44 g Na_2HPO_4
4	0.24 g KH_2PO_4
5	in 800 ml of distilled H_2O
6	Adjust the pH to 7.4 with HCl. Add H_2O to 1 liter. Sterilize by autoclave

7.1 Instruments:

- Schimadzu Prominence HPLC unit

- HPLC Column: Zorbax-300SB, C18, 4.6x250mm,5µm, 300A, lot# WSB 0752003, Agilent Technologies.
- Zeta Potential/Particle Sizer, NICOMP 380 ZLS
- Labconco Freezone 6 Freezdrier
- Beckman Coulter /Du 800 Spectrophotometer
- Beckman Coulter GS-6R Centrifuge (for centrifuging filter tubes)
- Fischer scientific Micro Centrifuge 235 C (for centrifuging regular tubes)
- 400 MHz Bruker AVANCE-400 spectrometer (Department of Medicinal Chemistry and Pharmacognosy, University of Illinois at Chicago) and Varian Mercury (^{1}H: 400 MHz, ^{13}C: 100 MHz) Boğaziçi University Advanced Technologies R&D
- Perkin Elmer, Jade DSC Instrument
- Eliza Reader Molecular Devices Spectro Max340 PC
- Rota Evaporator, Büchi and Heidolph
- Vortex IKA MS3 basic
- Ultrasonic Bath (Fisher Scientific FB 15051)
- UV cabin and light (Camag)

8. EXPERIMENTAL

In this study we

A) Isolated and identified *Vinca* alkaloids from three *Vinca* species.

B) Uploaded the hydrophobic anticancer drug Vinorelbine to 3 different Nano-Drug Delivery Systems all of wich have the ability of making micelles and carrying hydrophobic drugs. These Drug delivery systems are:

1- Micelles made of the lipid-polymer conjugate Distearoyl Phosphatidylethanolamine-PolyEthylene Glycole 2000 (DSPE-PEG 2000). The material is obtained commercially.

2- Star shape Poly- ε-Capro Lactone$_4$ - PolyEthylene Glycole$_4$ (PCL$_4$-PEG$_4$).

3- Y Shape Poly- ε-Capro Lactone$_2$- PolyEthylene Glycole(PCL$_2$-PEG).

The latter two polymers have been synthesized by "Gürkan Hızal, Ümit Tunca Polymer Research Group", Istanbul Technical University- Faculty of Scıence and Letters, Department of Chemistry. So we just give a short illustration of the method of synthesizing these two polymers:

8.1 Methods:

8.1.1 Methods used in synthesizing star shape PCL$_4$-PEG$_4$

a-Synthesis of 1-2,2,5-trimethyl [1,3]dioxane- 5-carboxylic acid

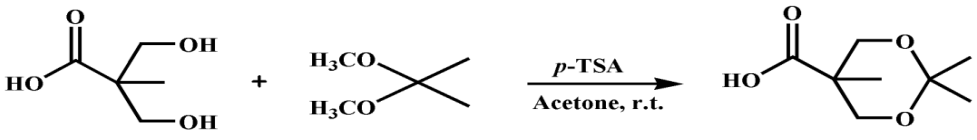

(8.1)

b- benzyl 2,2,5-trimethyl-[1,3]dioxane-5-carboxylate

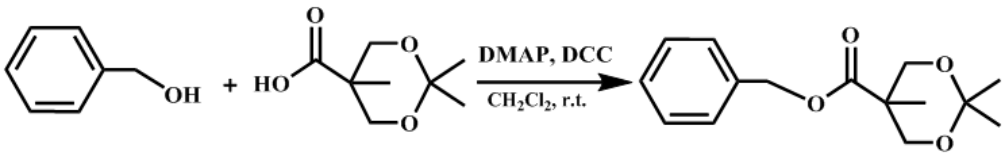

(8.2)

c- Reduction of Product

d- Synthesis of 2-(benzoylcarbonyl)-2-metilpropane-1,3-diyl-bis(2,2,5-trimethyl-1,3-dioxane-5-carboxylate

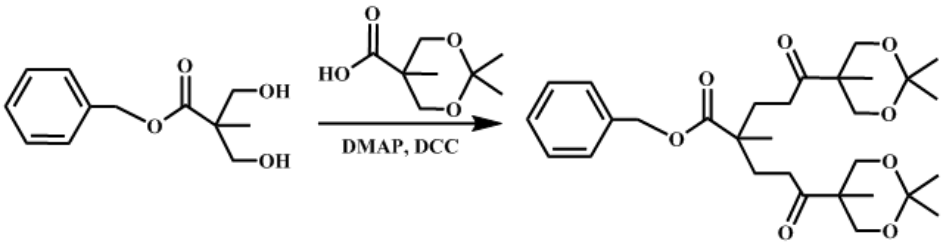

(8.3)

e-Reduction of Product

f- Synthesis of Star PCL polymer

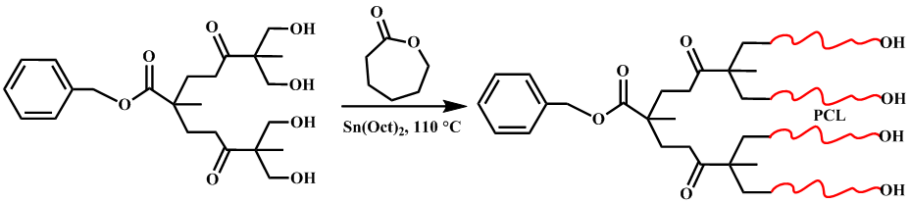

(8.4)

i-Synthesis of Azide PCL

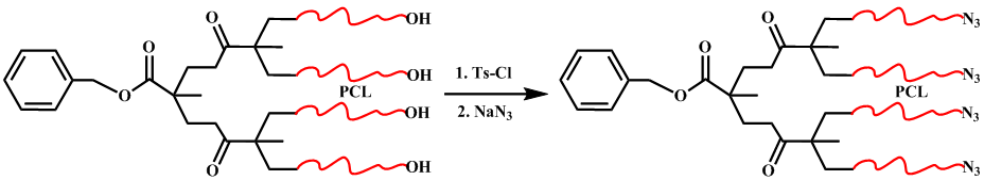

(8.5)

j- Synthesis of Azide PEG

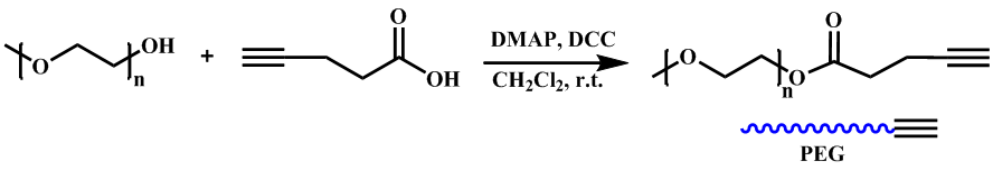

(8.6)

k- Final Synthesis of Star PCL-PEG (A_4B_4)

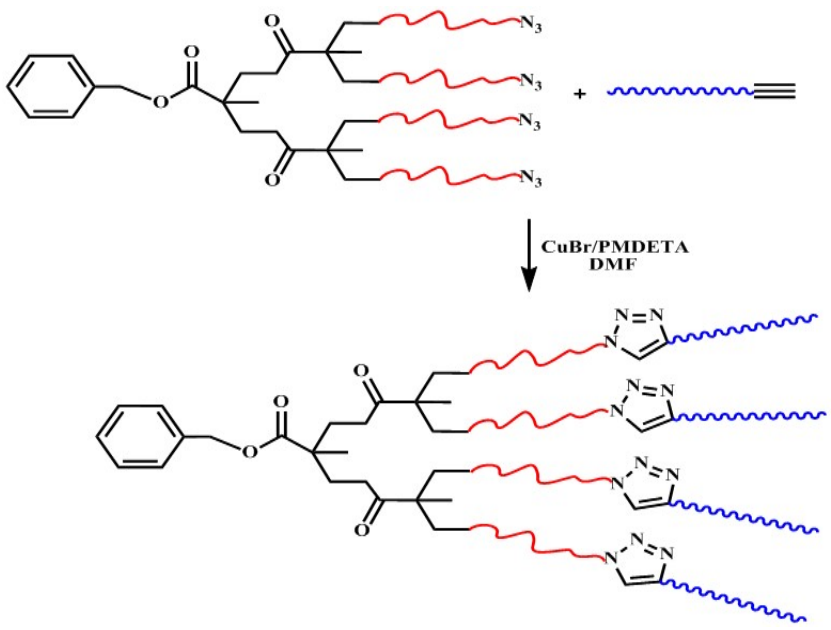

(8.7)

8.1.2 Synthesis of Y shaped Polymer

a- Synthesis of 2,2,5-trimethyl [1,3]dioxan- 5-carboxylic acid

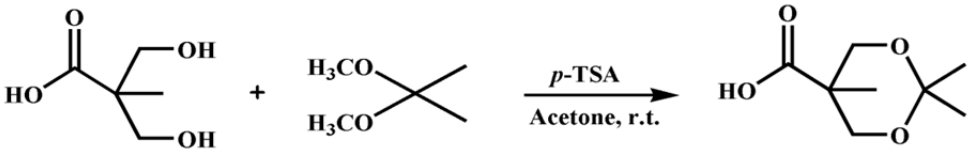

(8.8)

b- Synthesis of antrasen-9-il-methyl 2,2,5-trimethyl-1,3-dioxane-5-carboxylate

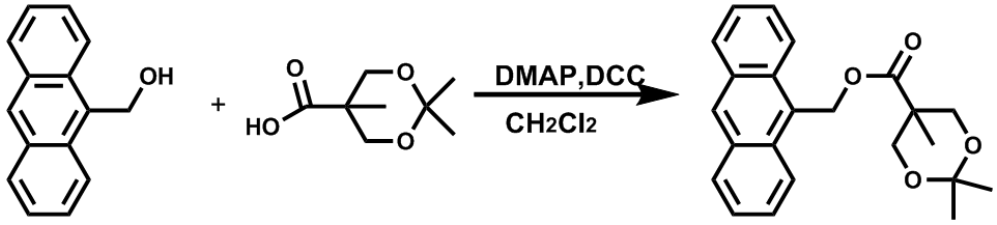

(8.9)

c- Reduction of Product

d4- Coupling of PCL

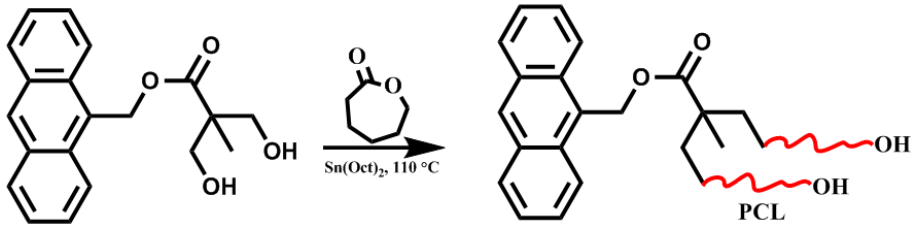

(8.10)

e- PEG Modification

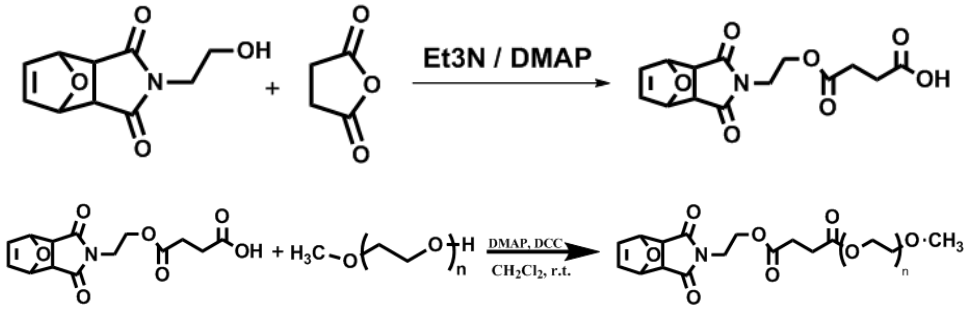

(8.11)

f- Synthesis of Poli *ε*-caprolactone-*b*-poliethilene glycol co-polymer

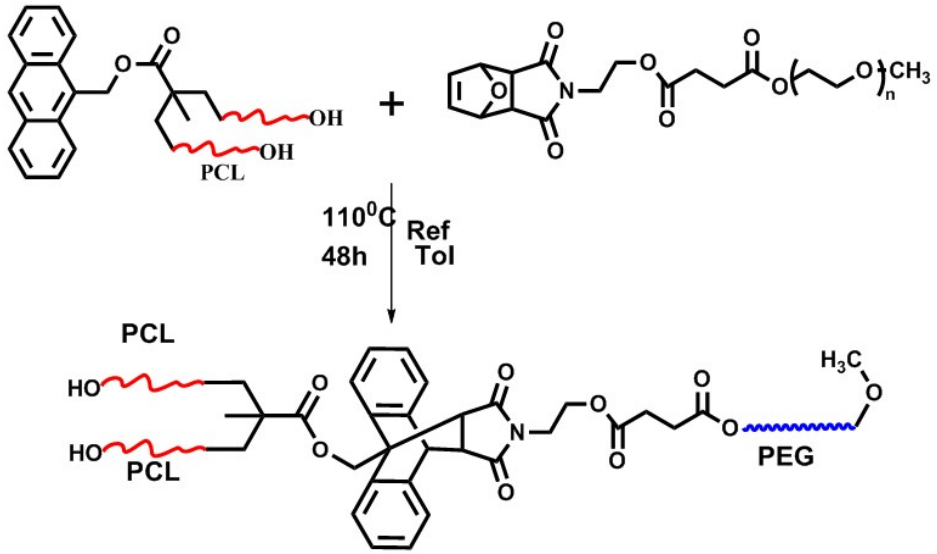

(8.12)

In all steps, synthesized compounds were characterized by NMR, GPC, DSC and Mass Spectrometric measurements.

8.1.3 Methods applied in isolation of alkaloids

Plant Material:

Table 8.1: The collected locations of *Vinca* species.

Name	Plant Part	Collected From	Weight (kg)
Vinca soneri	Aerial Parts	Erzincan-Kemaliye-Sirakanaklar	1.2
Vinca major	Aerial Parts	The Garden of Ankara University, Faculty of Science	0.24
Vinca minor	Aerial Parts	The Garden of Ankara University, Faculty of Science	0.15

All plants were dried in shadow and grounded.

Extraction:

The extraction method applied to above mentioned plants is the same.

Most alkaloids are present in the raw plants in the form of salts of organic acids.(Hesse, 2002) The extracted alkaloids may remain salts or change into bases. Base extraction has been achieved by processing the raw material with Ethanol twice in room temperature. The Ethanolic extract has been evaporated under vacuum. In all cases we obtained a green adhesive gum was obtained. The viscous residue dissolved in water (as little as possible, generally around 250ml). The aquous solution treated with weak acidic solution (%1 acetic acid in water, obtained pH= 4.2). We accept that Alkaloids are in salt form in aquous phase so we could extract the non-basic content by using an organic solvent like Dichloromethane. A base is then added to convert alkaloids to basic forms (pH= 8.3 by using %25 NH_3 in water) which are extracted with organic solvent(Hesse, 2002). The amount of obtained extracts areas listed in table below.

Table 8.2: The amount of the extracts.

Name	Basic Extract (g)	Asidic Extract(g)	Aquous Extract (remaining after extractions)
Vinca soneri	1.29	41.76	59.2
Vinca major	1.54	10.08	22.36
Vinca minor	0.54	8.2	15.8

The basic extract obtained from *Vinca sonerii* applied to Silica Gel column and the basic extracts of *Vinca minor* and *major* were applied to Aluminium column chromatography. The applied solvent system is as the table below. The amount of solvent applied is proportional to the amount of the fractions is being washed from the column at moment of application.

Table 8.3: The applied solvent system in column chromatography of *Vinca soneri.*

	Added Solvent	Isolated fraction
DCM*	%100	1-5
Aceton	%2	5-8
Aceton	%5	8-11
Aceton	%10	12-13

Table 8.4 (Contd.): The applied solvent system in column chromatography of *Vinca soneri.*

	Added Solvent	Isolated fraction
Aceton	%25	13-17
Aceton	%50	17-21
Aceton	%75	21-26
Aceton	%100	26-29
MeOH	%2	29-30
MeOH	%5	31-34
MeOH	%10	34-37
MeOH	%25	38
MeOH	%50	39
MeOH	%75	40
MeOH	%100	41

Table 8.5: The applied solvent system in column chromatography of *Vinca minor* and *major.*

	Added Solvent	Isolated fraction
P.E.*	%100	1-5
$CHCl_3$	%2	5-8
$CHCl_3$	%5	8-11
$CHCl_3$	%10	12-13
$CHCl_3$	%25	13-17
$CHCl_3$	%50	17-21
$CHCl_3$	%75	21-26
$CHCl_3$	%100	26-29
MeOH	%2	29-30
MeOH	%5	31-34
MeOH	%10	34-37
MeOH	%25	38
MeOH	%50	39
MeOH	%75	40
MeOH	%100	41

Alkaloid existance has been surveyed in the obtained fractions by using Dragendorf Reagent. Fractions carrying alkaloid were further purified using Praparative Thin Layer Chromatography (Preparative TLC). Aluminium based Silica Gel or neutral Aluminium precoated sheets have been used. The used plate type and isolation solvent has been reported under Results chapter.

8.1.4 Methods applied in preparation and characterization of Nano-VLB formulations:

As we mentioned in general information part, in order to achieve a succesfull targeted drug delivery it is important to obtain micelles with certain physical

properties like size (under 200nm), acceptable CMC, compatibility to industrial production processes and the most important stability at *in vivo* conditions. The latter factor is important in targetting cancer side. Since we aim to use EPR effect it is important for drug delivery system to carry the drug till the point of cancer tissue.

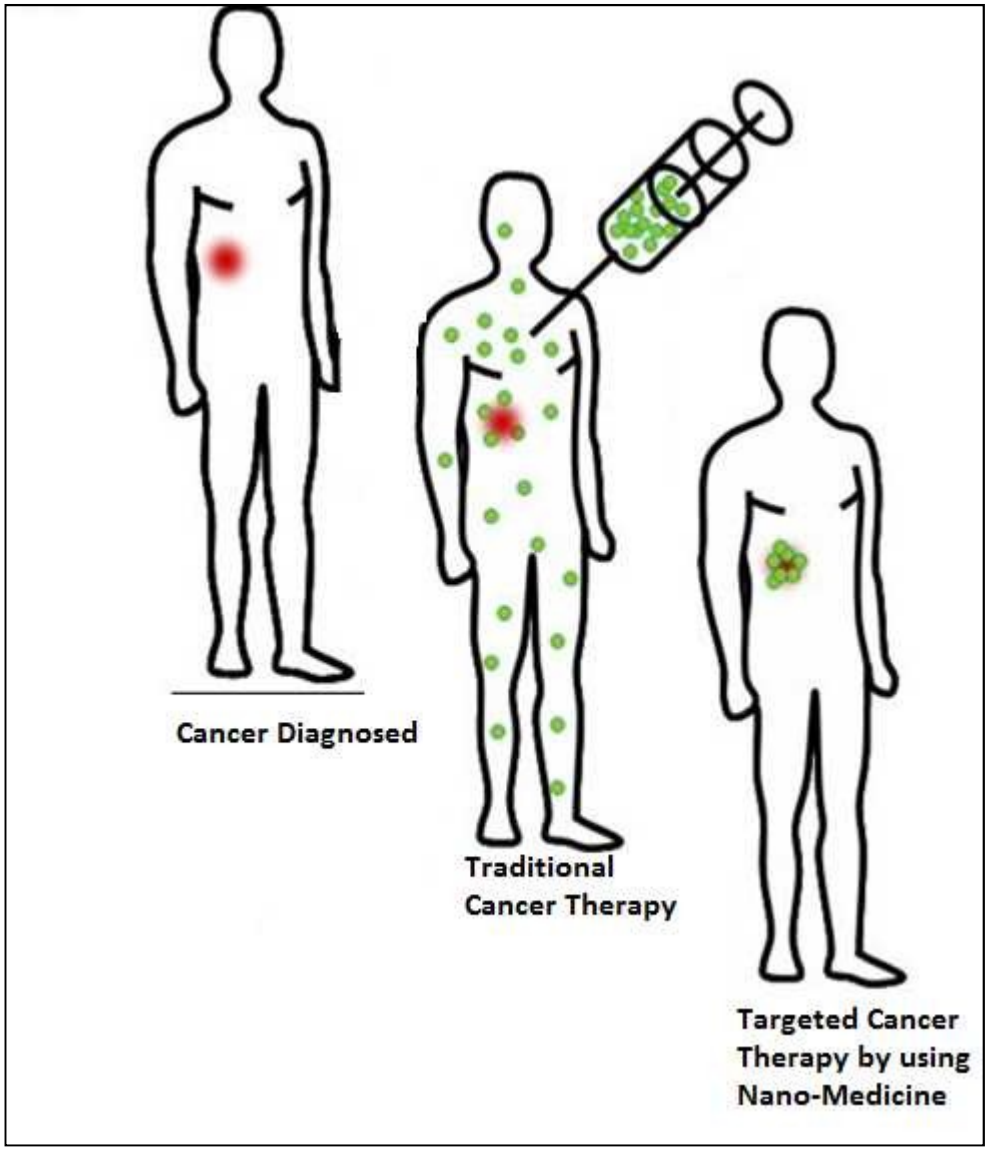

Figure 8.1: Targeted drug delivery to the tumor side.

All methods mentioned below have done by considering these factors.

8.1.5 Nano-VLB-SSM formulation:

8.1.6 Determination of the purity of commercially available Vinorelbine:

According to the recorded NMR Spectrum the sample is completely pure.

- The most common impurity in natural and/or semisynthetic compound is the isomeric form of related compound. Generally the concentration of isomeric form(s) is less than mother compound and makes bothering little peaks beside main peaks. Obviously the sample is purified from isomeric forms during production, because all peaks are in the same ratio of height and shape.
- All peaks are assignable to the protons of Vinorelbine so sample hasn't been contaminated by any non isomeric impurities as well.
- The table of assigned protons is as follows (Ribet, 2001):

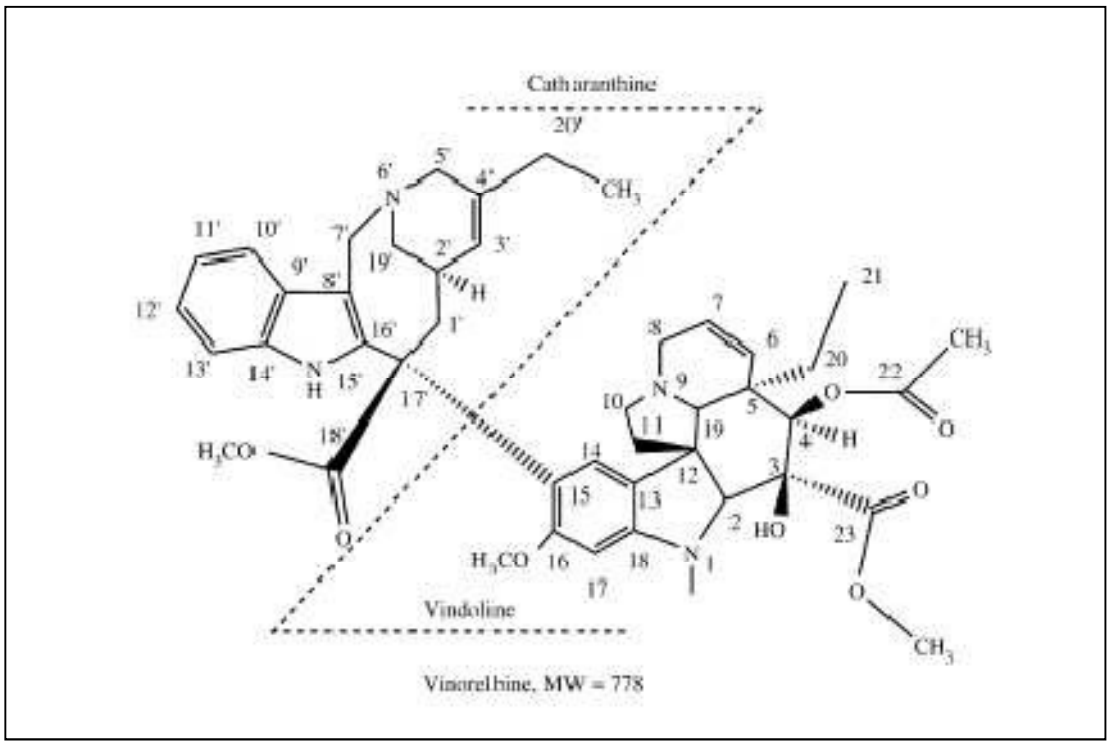

Figure 8.2: The structure of Vinorelbine (Ribet, 2001).

Table 8.6: The results of NMR assay to proof the purity of VLB.

H No	Group	ppm
21	CH_3	0.73
21′	CH_3	1.08
b-20	CH	1.25
a-20	CH	1.72
2′	CH	1.87
20′	CH_2	2.05
11	CH	2.05
a-8	CH	2.59
a-1′	CH	2.59
a-19′	CH	2.82
b-1′	CH	2.86
b-8	CH	3.06
b-10	CH	3.22
a-10	CH	3.33
b-19′	CH	3.64
23′	$COOCH_3$	3.71

H No	Group	ppm
2	CH_2	3.73
24	$COOCH_3$	3.78
25	OCH_3	3.85
a-5′	CH	3.85
b-5′	CH	3.96
a-7′	CH	4.04
b-7′	CH	4.44
6	CH	5.27
4	CH	5.38
3′	CH	5.77
6	CH	5.27
4	CH	5.38
3′	CH	5.77
7	CH	5.85
14	CH	6.09
17	CH	6.39
10′ 11′ 12′ 13′ 14′	CH	7.17
	NH	7.80
	C_3- OH	8.52

8.1.7 HPLC method optimization for Vinorelbine in base form:

The aim of this study was to determine the best mobile phase for Vinorelbine (in base form) concentration measurements in our lab settings using Schimadzu Prominence HPLC unit.

Applied General Parameters (Jehl et al., 1990; Puozzo, Ung, & Zorza, 2007; Robieux, 1996; Vendrig, 1988):

- Detection wavelength: 267nm
- Sample concentration: 100µg/ml.
- Injection volume: 20µl
- TFA concentration: %0.05 in water and %0.05 in MeOH; Totally 0.1 *v/v*

A gradient of MeOH starting from %20 achieving %100 in 20 minutes is applied to the system:

HPLC Time Table:

Table 8.7: HPLC program time table for VLB.

Time	Pump	Action	%MeOH
0.01	Controller	Start	
0.02	Pumps	Pump AB Conc	20
20	Pumps	Pump AB Conc	100
25	Pumps	Pump AB Conc	100
30	Pumps	Pump AB Conc	20
35	Pumps	Pump AB Conc	20
30.01	Controller	Stop	

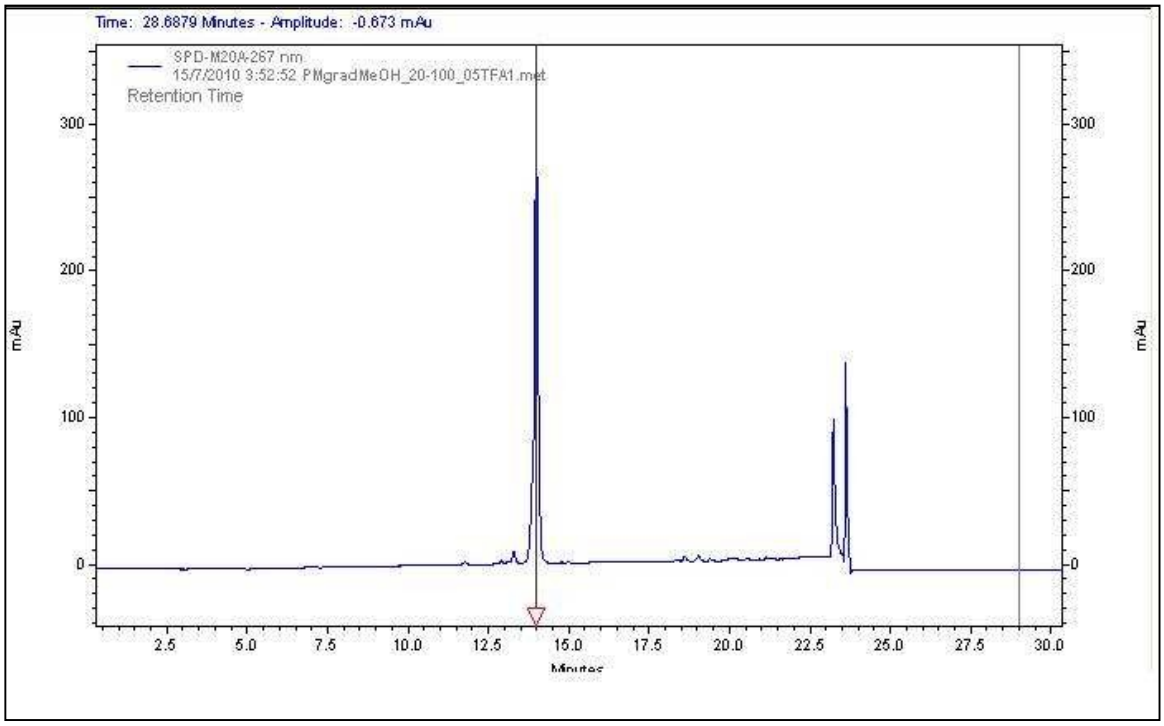

Figure 8.3: HPLC chromatogram of VLB

- The intensity of peak is high enough however a ‘‘pre-peak’’ is seen in base part of main peak
- The retention time is acceptable

- The only problem with this mobile phase is the more or less significant ‘‘pre-peak’’.

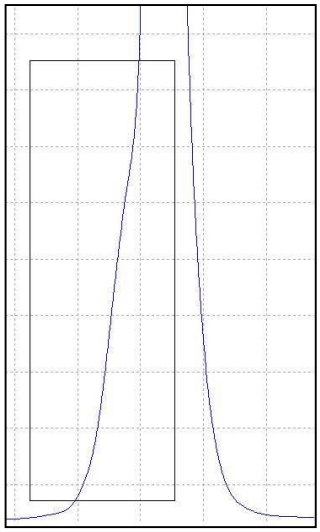

Figure 8.4: The ghost peak was seen in chromatogram of VLB.

- Considering that sometimes high concentration of sample causes this problem some samples in lower concentrations have been tested but this pre-peak was still recognizable. So this has been accepted as the nature of peak of Vinorelbine.

- During the optimization of a mobile phase for VLB a peak was seen around 24th minute of Chromatogram;

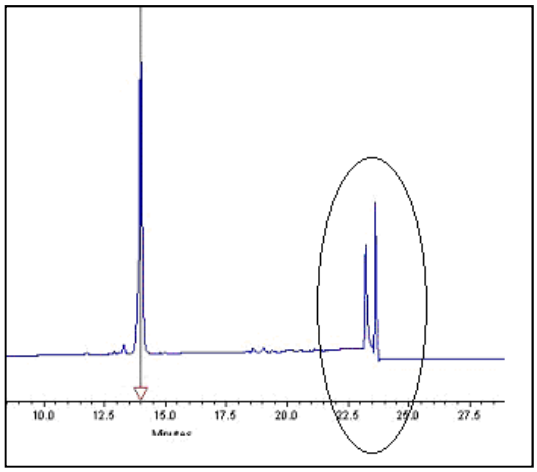

Figure 8.5 The ghost peak was seen in chromatogram of VLB.

This was accepted as impurity but during the process of obtaining concentration curve it has been seen that the height of this peak is always the same and doesn’t change with the height of the sample peak. Starting from this point we came to the

conclusion that this is not a impurity but maybe it is a “ghost peak” which is popular when TFA is included to mobile phase. Generally its common to see those peaks when the organic solvent reaches the point %100. To verify this idea a run without sample has been done and the same peak in the same point has been recognised.

So this peak is not an impurity.

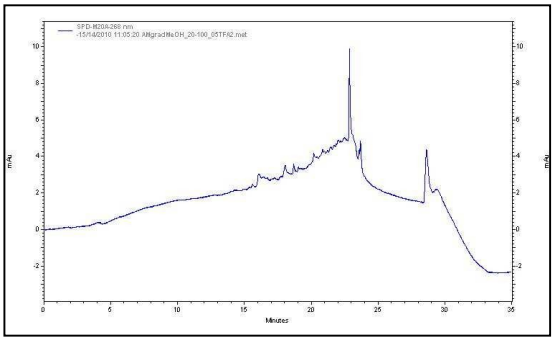

Figure 8.6: The ghost peak was seen in chromatogram of VLB.

8.1.8 Preparation of calibration curve of Vinorelbine (VLB) using HPLC

- VLB concentrations: 100, 75, 50, 25 and 12.5µg/ml
- Injection sequences: 3 times each concentration
- Mobile phase, MeOH and Water, each containing %0.05 TFA (v/v)

Table 8.8: Absorbance and area under curve per each injection.

Conc. (µg/ml)	Rep.	Abs(mAu)	Area (%)	Average of Areas
12.5	1	40.23	339737	
12.5	2	36.41	337604	**339737**
12.5	3	35.68	315608	
25	1	73.90	711400	
25	2	75.38	708379	**701825**
25	3	76.31	685696	
50	1	152.53	1406120	
50	2	177.39	1434691	**1417211**
50	3	168.71	1410823	
75	1	234.43	2145092	
75	2	233.85	2108867	**2129935**
75	3	228.92	2135847	
100	1	299.00	2710300	
100	2	338.83	2839339	**2760766**
100	3	339.14	2732660	

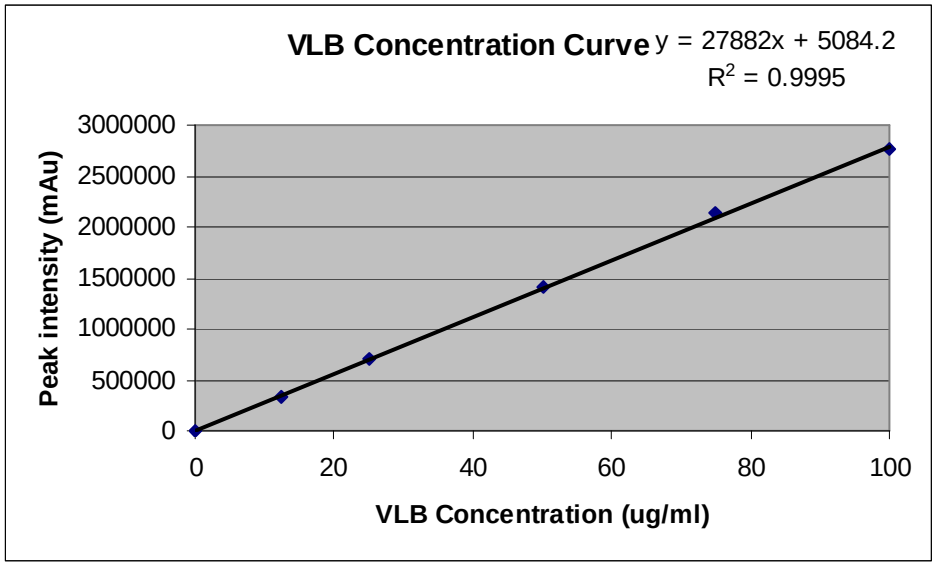

Figure 8.7: VLB's concentration curve.

8.1.9 DSPE-PEG2000 Sterically Stabilized Micelles (SSM)(drug loaded and free micelles):

Sterically Stabilized Micelles' Critical Micelle Concentration (CMC) has been reported as 1µM/ml(Ashok, 2004). In vitro characterization of PEGylated phospholipid micelles for improved drug solubilization: effects of PEG chain length and PC incorporation (Ashok, 2004). In DLS and Solubility experiments the SSMs has been prepared in concentration of 1mM (CMCx1000). In case of release and stability investigations this concentration has been scaled up to 10mM. In cell culture studies the concentration of SSM has been scaled up proportional to the amount of Vinorelbine used in determination of IC_{50}.

The method for preparing 50 and 500µg VLB in 1mM SSM has been described below as two examples:

Stock solutions to be prepared: DSPE-PEG will be kept constant at 1mM (2.81mg/ml)

Table 8.9: Stock solutions to be prepared to synthesize DSPE-PEG 2000 micelles.

Stock #	**DSPE-PEG_{2000} (mg)**	**Vinorelbine (µg)**	**Final volume (ml) (dis. in MeOH)**	**Name**
1	9.835	-	3.5	Stock DSPE-PEG
2	-	560	1.12	Stock Vinorelbine

Table 8.10: The ratios of stocks to be mixed to obtain 50 and 500ugVLB/1mM SSM.

Sample #	DSPE-PEG_{2000} Stock (ml)	Amount of Vinorelbine (ml)	Amount of MeOH will be added	Final volume	Final Concentration	Name
1	1	1	-	2	500µgVLB/1mM SSM	sample
2	1	0.12	0.88	2	50µgVLB/1mM SSM	sample
3	1	-	1	2		standard

8.1.10 Preparation of solubilized Vinorelbine in SSM

The above amounts of Vinorelbine and DSPE-PEG measured into the respective 100ml round bottom flasks and 1 ml Methanol added to DSPE-PEG standard solution. The methanol evaporated in a rotary evaporator, at 45^{o}C, 150rpm and 630 mmHg preassure under argon. The film obtained further dried in vacuum overnight.

1ml of isotonic PBS buffer (10mM, pH 7.4) added and flasks vortexed for 2 minutes at maximum speed on a thermolyne (maxi mix II) vortex until all the film is dispersed. Then bath sonicated for 5 minutes. The sample and standard transferred to a NICOMP tube flushed with argon and sealed and left for equilibration in the dark at room temperature for 2 hours (25^{o}C).

8.1.11 Determination of drug delivery system capacity; solubility of Vinorelbine (VLB) in SSM:

The objective of this experiment was to determine the amount of Vinorelbine that is solubilized in DSPE-PEG micelles in a concentration of 1mM. Consequently we will find the amount of Vinorelbine in buffer. This is the most important part of characterization of VLB-SSM formulation.

Concentrations of prepared samples:

Table 8.11: Samples prepared to study in DLS investigations.

Sample #	Amount of Vinorelbine (µg/1ml of 1mM DSPE-PEG)
1	50
2	100
3	200
4	350
5	500
6	1000
7	2000
8	3000

As we will discuss in results part, generally or normally when we add a certain amount of drug to a system which contains any micellar nano-drug delivery system, the drug solublizes in buffer in amounts equal to its water solubility. The excess amount will be incorporated with micelles and further addings of the drug to the system will cause an aggregation or precipitation in system. So by centrifuging the system and measuring the amount of drug in supernants we could measure the exact amount of solublized drug in Micelles.

Interestingly even adding 3mg of VLB to the system didn't make any aggregation. So we decided to make more studies to understand what is the position of VLB in SSM and waht is its exact amount in SSM and PBS.

In the other hand we try to understand what prevents the VLB precipitation and what makes it such soluble in SSM.

8.1.12 Investigation of the possibility of forming micelles by free Vinorelbine:

Sometimes the hydrophobic drug makes its own micellar system and becomes soluble in water (Taylor, 1982). To understand if this event comes true in our system or not we made one more experiments; searching for drug micelles with DLS. In order to understand does the VLB make its own micelles or not a concentration of 2mg/ml has been prepared.

8.1.13 Investigation of the solubility of Vinorelbine (VLB) (base form) in PBS by pre-solving it in organic solvents

Previously has been seen that VLB is not soluble in water or PBS (Reported by Science Finder using a calculation program). During making the VLB- SSM formulation a very high solubility has been seen. To figure out if this is the solublization power of SSM or VLB's water solubility is higher than what references report, a solution of VLB in Organic solvent has been prepared by following the procedure of making SSM formulation.It is possible that by following the SSM preparation procedure, VLB gains a higher solubility than normal conditions. In this order certain amounts of VLB has been dissolved in MeOH and evaporated under vacuum by using rotary evaporator. The flasks have been kept under vacuum in vacuum desiccator overnight. The day after 1ml of PBS buffer has been added to

each sample. Vortexed for 2 minutes and sonicated for 5 minutes. The UV absorbance has been measured by using UV spectrophotometer.

Table 8.12: U.V. absorbance of different concentrations of VLB solublized in PBS after making film.

Sample No	**µg VLB**	**ml MeOH added**	**Total vol. ml**	**Final vol. ml**	**Final conc. µg/ml**	**U.V. absorbance**
1	2000	2	2	1	**1000**	**2.7624**
	ml of previous slvnt.					
2	1	1	2	1	**500**	**2.7624**
3	1	1	2	1	**250**	**2.8971**
4	1	1	2	1	**125**	**2.1060**
5	1	1	2	1	**62.50**	**1.0262**
6	1	1	2	1	**31.25**	**0.4494**
7	1	1	2	1	**15.63**	**0.1776**
8	1	1	2	1	**7.82**	**0.1004**
9	1	1	2	1	**3.90**	**0.0677**
10	1	1	2	1	**1.95**	**0.0320**

As it could be seen in the table above the water solubility of VLB is around 250µg/ml. To obtain more accurate results the concentrations between 250 and 500 has been prepared in $CHCl_3$ as below and Again the solubility of VLB is around 250µg/ml. :

Table 8.13: U.V. absorbance of different concentrations of VLB solublized in PBS after making film.

Sample No:	**µg VLB**	**ml $CHCl_3$ added**	**Total ml**	**Final cons. µg/ml**	**U.V. absorbance**
1 *Stock Solution*	2500	5	5	**500**	**2.8983**
	ml of stock sl.				
2	0.9	0.1	1	**450**	**2.8605**
3	0.8	0.2	1	**400**	**2.8983**
4	0.7	0.3	1	**350**	**2.8983**
5	0.6	0.4	1	**300**	**3.1616**
6	0.5	0.5	1	**250**	**3.2407**
7	0.4	0.6	1	**200**	**2.9397**

8.1.14 Separation the drug associated with SSM from free drug in buffer by centrifuging:

Using regular centrifuge process:

Different concentrations of Vinorelbine has been uploaded to 1mM DSPE-PEG200 and centrifuged for 10 minutes. Samples from supernatants has been collected and

injected to HPLC. Also samples from bottom part of tubes have been collected and injected as well but at the end of HPLC assay there was no difference between the concentration of supernatants and precipitates meaning that nothing is precipitated.

Using Centrifugal filter tubes:

As second trial centrifuge tubes with filters in middle has been used. Certain concentrations of VLB in 1 mM SSM (1 ml) has been prepared and transferred to centrifuge tubes. The best centrifuge period has been calculated considering the centrifuge instrument's radius. The time period is important because we don't need too much centrifuge force. A short period in which only the free drug in PBS finds the possibility of passing through filter and the VLB associated with micelle stays stable will be enough.

Certain procedures necessitate precise centrifugation conditions, which must be specified in terms of relative centrifugal force (RCF) expressed in units of gravity (times gravity or × *g*). Many microcentrifuges only have settings for speed (revolutions per minute, RPM), not relative centrifugal force. Consequently, a formula for conversion is required to ensure that the appropriate setting is used in an experiment. The relationship between RPM and RCF is as follows:

$g = (1.118 \times 10\text{-}5)\ R\ S^2$

Where *g* is the relative centrifugal force, R is the radius of the rotor in centimeters, and S is the speed of the centrifuge in revolutions per minute. Values of RCF in units of times gravity (× *g*) for common microcentrifuge rotor radii appear in the following conversion table. As an example, centrifugation of a sample at 5,000 RPM in a microcentrifuge that has a rotor with a radius of 7 cm will deliver a centrifugal force of 1,957 × *g*. **("Url- 2 <http://www.piercenet.com>„" accessed at 09.08.2011).**

Filtrates have been injected to HPLC using the method mentioned above.

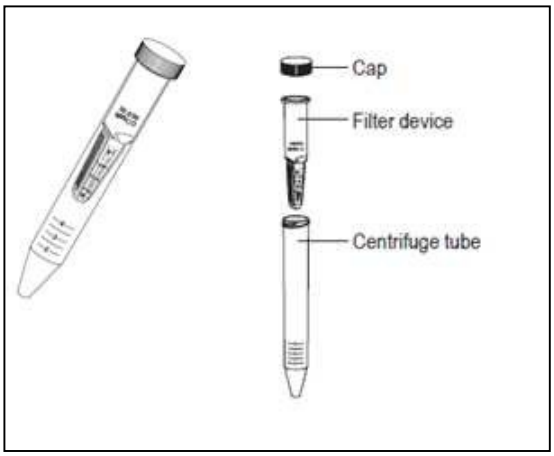

Figure 8.8: The main parts of centrifugal filter tubes (Url- 2).

The prepared concentrations and obtained results are as below:

Table 8.14: The prepared concentrations and obtained results of centrifuging VLB-SSM formulations by using filter tubes.

Vinorelbine (μg/ml) in 1mM DSPE-PEG200 (1ml)	**%VLB associating with SSM (1mM) 1st Trial**	**%VLB associating with SSM (1mM) 2nd Trial**	**%VLB associating with SSM (1mM) 3rd Trial**
50	93.2	94.8	100
150	92.7	94.7	90.7
250	91.4	95.0	92.4
500	90.7	90.9	90.4
750	84.44	85.4	86.34

A control sample consisting of 4mgVLB/1ml MeOH has been centrifuged to check the error of method and error is near to "0". No Vinorelbine is absorbed by filter.

8.1.15 Study the stability of Vinorelbine-SSM formulation after lyophilization

In case of introducing VLB-SSM as a new cancer therapy agent to the industry, it is important to emphesise the method of storing the material. We suggest lyophilizing the formulation and rehydrating it before use. The objective of this experiment is to measure the amount of Vinorelbine before and after Lyophilization and measure the size of SSMs in the same conditions to determine the stability of formulation.

The amount of Vinorelbine corporated with SSM has been measured by using HPLC before and after lyophilization. The HPLC method is mentioned above. The stability of size of SSM has been determined by using DLS. The latter assay has been repeated 2,3,5,7 and 15 days after Lyophilization and rehydration.

8.1.16 Drug release studies by dialysis of Sterically Stabilized Phospholipid Micelles containing Vinorelbine (SSM-VLB)

To perform dialysis, 3 ml of the VLB-SSM dispersion was transferred into dialysis membrane tubing, which was then be placed into 300 ml of dialysis medium (PBS buffer) at 37^{o}C under constant slow stirring and kept in dark through out the experiment. Two milliliter of dialysis medium was drawn at 0.5, 1, 2, 3, 4, 6, 8, 10, 12, 20, 22,24, 28, 48, 72 and 90 hours of the experiment. One milliliter was used for immediate drug measurement while the other milliliter saved in case of necessary lyophilization to concentrate the sample more for HPLC measurement. Samples will also be taken from the dialysis membrane tubing before and after the experiment. Release studies will be conducted for 24 hours without any change or replacement of dialysis medium (Cho, 2004; Johnston, 2006; Michalowski, 2004; Morris, 2008; Zheng, Qiu, Yao, & Zhu, 2009).

Applied General Parameters:

- Total PBS media: 300ml
- Total amount of formulation: 15mg VLB in 30mM SSM, Total Volume 3ml
- Dialysis temperature: 37^{0}C.
- Sampling periods0.5, 1, 2, 3, 4, 6, 8, 10, 12, 20, 22,24, 28, 48, 72 and 90
- Sampling volume: 200µl
- HPLC Method: as mentioned above

8.1.17 Characterization of Vinorelbine-SSM Formulation by Using Differential Scanning Calorimetry (DSC)

Previously we showed that the VLB-SSM formulation is stable after lyophilization. We assume that in a VLB-SSM formulation, after lyophilization, the amount of drug which is associated with micelles will be kept in dry micelle (maybe with some lost). Based on this assumption and by following some logical steps we designed the route of our investigation:

The interdigitation of VLB with SSMs will cause a difference in DSC results in compare with that of Free SSMs.

If we obtain 2 separated crystallization point for DSPE and PEG using DSC, loading the drug will cause changes in both or just one of these crystallization points according to the settlement of the drug in the core or on the shell of SSMs.

If we obtain the DSC spectrum of VLB-SSM formulation in buffer prior to lyophilization, comparing the crystallization temperature of VLB-SSM in buffer (liquid sample) with the solid lyophilized sample will tell us a lot.

Liquid Samples' DSC thermogram has been recorded by using special pans are available to measure the thermal behaviour of samples in water or buffer.

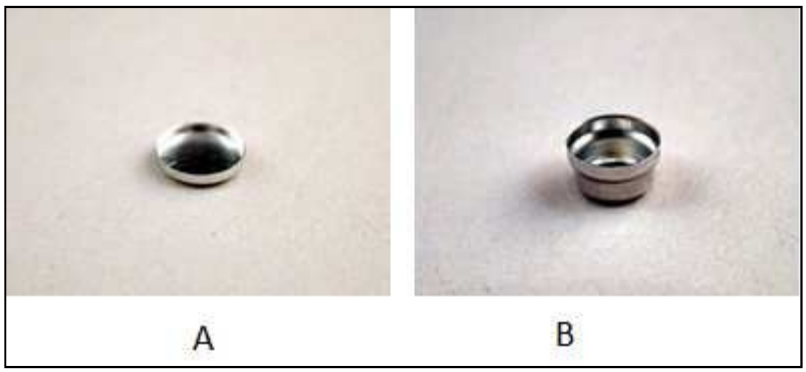

Figure 8.9: DSC Pans available for A; Solid samples and B; Liquid samples (Kastantin, 2009).

It is noteworthy that in a sample which contains Buffer salts + Drug Delivery System+ Drug+ Water, the mass of buffer salts and water covers a very high ratio of the mass of total system. So the amount of drug delivery system and drug itself is pretty low in comparing with other components of system so it is hard to observe very significant and huge peaks as we saw in solid materials. To overcome this challenge we made both concentrations in 10 times higher concentration, 500µg and 5000 µg VLB in 10 mM SSM (in 1ml PBS). 70µl of each formulation has been used in DSC assays.

8.1.18 Cell culture investigation of Vinorelbine in the three different drug delivery systems: DSPE-PEG and PCL-PEG polymers.

The purpose of this experiment is to determine whether Vinorelbine solubilized in simple micelles has similar cytotoxic activity against MCF-7 human breast cancer cell line, as compared to a solution of Vinorelbine itself.

Applied General Parameters (Dagar, 2003; Onyueksel, 2009; Onyuksel, 2009):

- Complete media has applied to 96 well plates in 190µl volume
- 3 different drug delivery systems has been used SSMs, Y shaped PCL_2-PEGs and Star shaped PCL_2-PEG_2s.
- The concentration of VLB in SSM is in the same ratio of 500µg VLB/ 1 mM Lipid. The concentration of VLB in Polymers is %5 VLB in %95 Polymer (w/w). As a result in the highest concentration of formulations, 500ug VLB has been uploaded to
- The final concentration of VLB in all cases were as:16, 8, 0.8, 0.08, 0.008, 0.0008 µg/ml
- Before adding VLB-delivery system, all of delivery systems have been applied to well plated in amount of 2µl to keep the drug delivery system above CMC. The concentration of all delivery systems has been fixed to 100 times above CMC
- In case of adding drug in drug delivery system the drug-delivery system has added on empty delivery system in 8µl volume
- VLB in 10% DMSO has been added on complete media in amount of 10 µl
- All drug delivery systems has been used in their highest concentrations (empty) as controls
- %10 DMSO and PBS are used as Controls too. The amount of all controls were 10µl.
- Measurements were done in 24, 48 and 72 hours and each were repeated 3 times.

MTT Method Application (Allahverdiyev, 2004; Davydov, 2002)

- MTT has been applied in the concentration of 1mg/ml in the volume of 100µl to each well

Before applying MTT, the medium has been aspirated from wells and all wells has been washed by PBS for three times.

8.1.19 Nano-VLB-polymer formulation

8.1.20 Preparation of polymeric micelles:

Polymeric Micelles have been prepared by using two different methods.

8.1.21 Preparation of free polymeric micelles:

The star-PCL_4-PEG_4 and PCL_2-PEG polymer was dissolved in DMF at ~100 mg/ mL and stirred overnight at room temperature. Water was added in a dropwise fashion to both of the polymers' solution in DMF. The addition of water was continued until the desired water content was achieved (13% of DMF in the final mixture). The obtained solution was stirred overnight and then dialyzed against double distilled water using Spectra/Por 1 Molecularporous Dialysis Membrane, Spectrum, MWCO 3500. The dialysate water was exchanged every hour for the first 4 h and then every 6 h for the next 12 h (Lv et al., 2009; F. Wang et al., 2005; Ward, 2005; Zheng et al., 2009).

Its noteworthy that the amount of water that must be added on DMF solution of polymers prior to dialysis, has been determind by trying different ratios of water/ DMF and the ratio %67/ 13 water/ DMF has been found to afford the polymeric micelles with the best size and stability.

8.1.22 Preparation of drug loaded polymeric micelles:

Solid Extraction: A measured volume of a methanol solution of Vinorelbine (VLB)

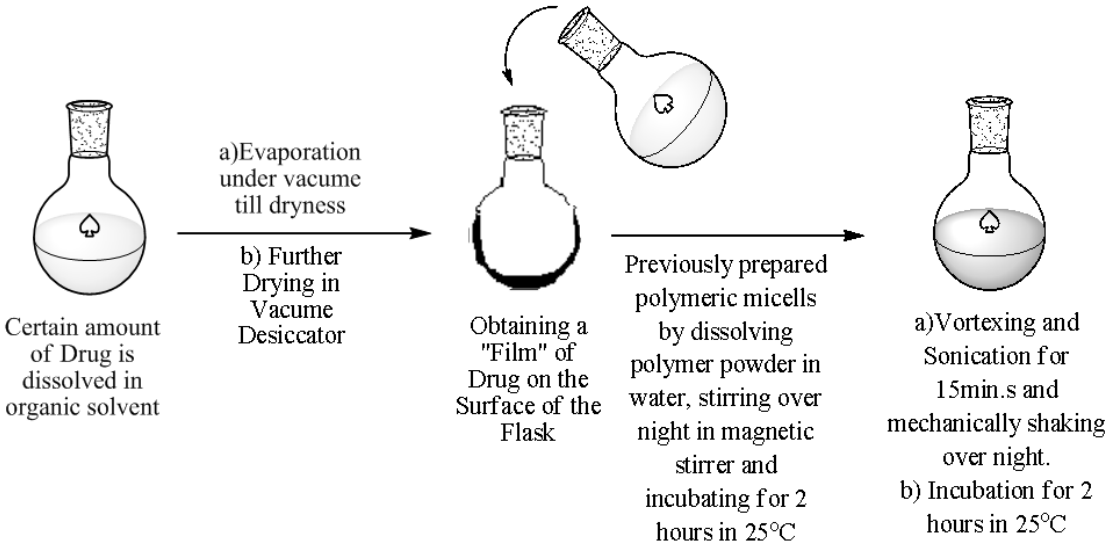

Figure 8.10: Preparation of drug loaded polymeric micelles.

was added to a 100ml flask and the solvent was removed under vacuum, leaving a solid film of Vinorelbine. A pre-prepared polymer micelle solution (by using Dialysis) was agitated with VLB for 15 mins mechanically shaked over night. The day after dryg loaded micelles were incubated in 25^{o}C for 2 hours (Lv et al., 2009; Zheng et al., 2009).

8.1.23 Determination of the Critical Micelle Concentration (CMC) of polymeric micelles.

The same method has been applied to determine CMC of both Star and Y Shape polymers. The method is briefly as below.

- The apparent critical micelle concentration was determined using pyrene as a fluorescent probe.
- Sample solutions were prepared by adding known amounts of pyrene in acetone to each of a series of empty vials. The amount of pyrene was chosen so as to give a pyrene concentration in the final solution of $6x10^{-7}$ M.
- After the evaporation of acetone, solutions of star-PCL_4-PEG_4 nd Y shaped PCL_2-PEG of various concentrations in phosphate buffer saline were added to the probe.
- Samples were equilibrated upon shaking overnight at the desired temperature. Steady-state fluorescence spectra were recorded at 336 nm for emission *i*ex, and for excitation spectra, *ì*em was 390 nm.
- From obtained flourescence graphic, the values I_3/ I_1 has been calculated by dividing the height of the peak at 390 to that of 336.
- The point of crossing of tangents of curve in the graphic of concentration vs I_3/ I_1 gives the point of Critical Micelle Concentration (Lv et al., 2009; F. Wang et al., 2005; Ward, 2005; Zheng et al., 2009).

8.1.24 Determination of Vinorelbine concentration associated with polymeric micelles by using Eliza Reader

During our studies on polymeric formulations of Vinorelbine we had the opportunity of measuring the concentration of Vinorelbine in micelle only by using Elisa Reader.

Firstly we prepared certain concentrations of Vinorelbine and we obtained the concentration curve by reading max. U.V. absorbance at 286nm. Consequently we prepared decreasing concentrations of Vinorelbine in vials and evaporated it under reduced preassure to obtain a thin film of Vinorelbine in vial. The pre-made polymeric micelle in PBS in the constant concentration of 5mg/ml (~CMCx1000) has been added on VLB films and agitated for 15 min.s and physically shaked over night.

The day after the polymeric VLB formulations left in 25^{o}C for 2 hours and centrifuged at 6000rpm for 30 mins. The supernants transferred to clean holders and 10 times diluted with methanol to prevent any aggregation of the drug in PBS.

All other methods used for characterization of polymeric micelles are similar to the reported methods used for DSPE-PEG micelles.

9. RESULTS AND DISCUSSION

9.1 Results of Isolation and Structure Elucidation of *Vinca* Alkaloids from *Vinca* Species

9.1.1 Identification of some compounds from *Vinca herbacea*

This PhD thesis does not cover structure elucidation of Vinca herbacea. However we decided to mention our newly published results for identification of chemical constituents (Boga et al. 2011) of this species to serve a collected report of all structures that have isolated from Turkish Vinca species to the readers.

An alkaloidal extract of the aerial parts of *V. herbacea* (herbaceous periwinkle) afforded six Indole alkaloids, and their structures were elucidated as 10-methoxyraucaffrinoline (1) 11-methoxyburnamine (2), picrinine, burnamine, caboxine A and elegantine using intensive 1D- and 2DNMR techniques and mass spectrometric analyses (Figure 9.1) (Atta-ur-rahman, 1995; Bhattach.J & Pakrashi, 1972).

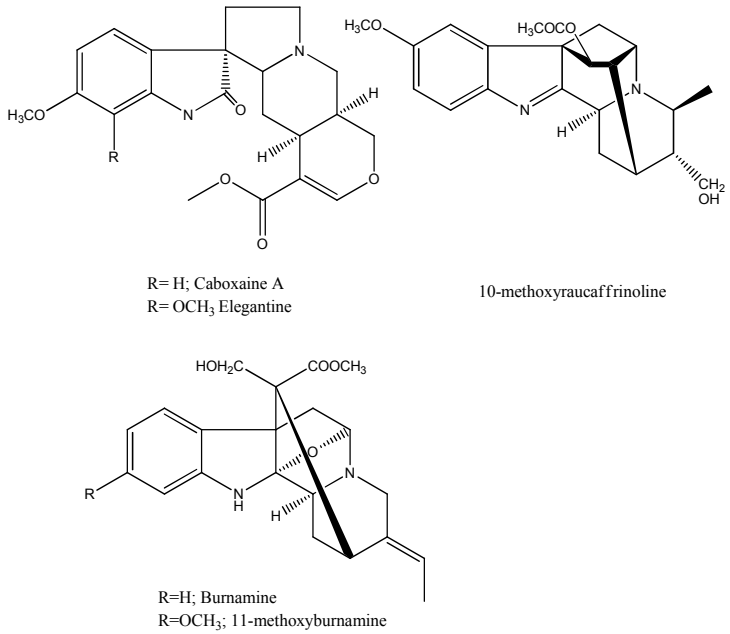

Figure 9.1: Indole alkaloids isolated from *Vinca herbacea.*

Table 9.1: ^{1}H and ^{13}C NMR spectroscopic data for 10-methoxyraucaffrinoline and 11-methoxyburnamine.

	1		**2**	
Position	**^{1}H-NMR**	**^{13}C-NMR**	**^{1}H-NMR**	**^{13}C-NMR**
2	-	181.7		106.9
3	4.07 d (9.36)	57.4	3.63 brd (2.50)	52.0
5	3.64 dd (6.24, 4.90)	51.5	4.80 brs	87.8
6	1.63 d (11.70) 2.75 dd (11.70, 4.70)	38.0	2.4 dd (14.00, 1.80) 3.30 d (14.00)	45.0
7	-	65.3	-	54.0
8	-	138.3	-	126.3
9	7.02 d (2.73)	111.2	6.73 d (8.40)	125.6
10	-	158.1	6.68 dd (8.40, 2.0)	108.2
11	6.89 dd (8.58, 2.73)	113.0	-	160.0
12	7.50 d (8.19)	121.3	6.93 d (2.0)	97.2
13	-	150.4	-	not observed
14	1.53 dd (14.04, 5.07) 1.92 dd (14.82, 9.75)	22.0	1.98dt (14.40, 2.50) 2.05 brd (14.32)	22.1
15	2.47 dd (5.70, 5.07)	26.8	3.49 brt (1.20)	33.8
16	2.35 dd (6.24, 5.85)	49.6	-	58.1
17	5.00 s	79.0	3.47 d (12.10) 3.70 brd (12.12)	65.0
18	1.26 d (7.02)	18.6	1.57 d (6.24)	13.6
19	3.67 dd (11.0, 8.0) 3.72 dd (11.0, 5.10)	62.2	5.37 brq (6.24)	121.1
20	1.48 ddd (9.10, 8.0, 5.1)	46.0	-	138.1
21	2.52 dd (9.00, 6.90)	53.4	3.14 brd (18.0) 3.79 brd (18.0)	47.2
$OCO\underline{CH_3}$	2.17 s	21.4	-	-
$O\underline{CO}CH_3$	-	170.1	-	-
$CO\underline{OCH_3}$	-	-	3.72 s	52.4
$\underline{CO}OCH_3$	-	-	-	174.1
OCH_3	3.82 s	55.9	3.77 s	54.3

In another study on *Vinca herbacea* collected from Ankara (M. Kartal et al.) afforded six Indole alkaloids; Reserpinine, Elegantine (isomajidine), Caboxine A, Vincamajine, N-methyl, 14-15 dehydroaspidospermidine, Carpanaubine (or iso-Carpanaubine) besides a triterpene Ursolic acid (unpublished data).

9.1.2 Identification of Vallesiachotamine

The fractions 8-9 were obtained by washing the alkaloid extract of *Vinca soneri* on Si-gel column by using Dichloromethane, Acetone (95:5). The combined fractions were dried under reduced preassure and the dried residue was dissolved in dichloromethane by mild heating. Cooling down the solvent afforded crystals of Vis-1.

The alkaloid extract of *Vinca minor* subjected to a si-gel column resulted in obtaining 40 fractions. The 17th fraction was obtained by proceeding the column by using Petroleum ether, chloroform (P.E., $CHCl_3$ (50:50)). The obtained fraction was further purified on prep. TLC, and mobile phase was $CHCl_3$. The purified compounds were named Vim-1 (and its structure was characterised as Vallesiachotamine) and Vim2, (its structure was characterised as iso-Vallesiachotamine)

Vis-1(8mg) and Vim-1(4mg).

Vallesiachotamine,

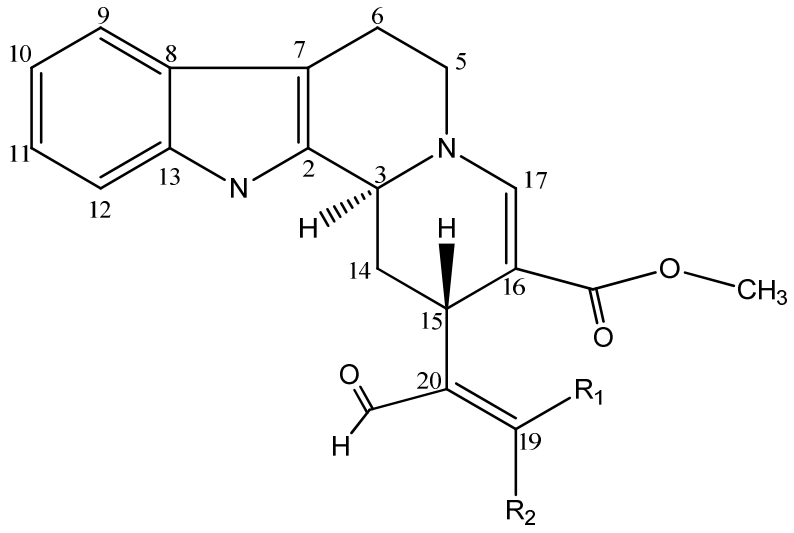

R_1	R_2	
(1) H	CH_3	Vallesiachotamine
(2) CH_3	H	Isovallesiachotamine

Figure 9.2: Vallesiachotamine and its isomer.

Table 9.2: ^{1}H-NMR and ^{13}C-NMR assignment of Vallesiachotamine and iso-Vallesiachotamine (Appendix A).

C No	^{1}H-NMR		Multiplicity *J* (Hz)	^{13}C-NMR	HMBC
	Vallesiachotamine	iso-Vallesiachotamine		Vallesiachotamine	Vallesiachotamine
2	-		-	132.4	-
3	4.48	4.16	brd (1;11)	49.2	-
5α	3.73	3.73	dd (4;11)	51.06	-
5β	3.70	3.70	dd (4)		-
6α	2.94	2.94	m	22.02	-
6β	2.81	2.81	brd (1;15)		-
7	-		-	108.53	-
8	-		-	136.2	-
9	7.30	7.30	dd(1;8)	110.9	C-8, C-10
10	7.11	7.11	brt(1;7)	119.81	C-8, C-9
11	7.16	7.16	brt(1;7)	122.13	C-13, C-12
12	7.48	7.48	d(1;8)	118.15	C-13, C-11
13	-		-	136.2	-
14α	1.94	1.74	dt(7;13)	34.14	-
14β	2.18		brt (13;1)		-
15	4.02	4.02	brd (6)	28	-
16	-		-	168.3	-
17	7.68	6.10	s	147.4	COH, C-5, C-3, C-15
18	2.10	2.03	d(7)	15.02	C-19, C-20
19	6.68	6.47	q (7)	152.6	C-18, COH
20	-		-	146.4	-
OCH_3	3.64	3.64			

The first isolated alkaloid from *V. soneri* and *V. minor* identified as an di-substituted Indole alkaloid by the observation of four aromatic methine proton signals, resonated at δ 7.11, 7.16. 7.30 and 7.48. The characteristic two broadened triplets and two broadened doublets indicated a non-substituted benzene of the Indole ring. The presence of a double bond was observed by a methine proton signal at δ 7.68 (s) and its corresponding carbon signal at δ 147.4 based on an HMQC correlation. Since

there was no second olefinic proton in the ^{1}H-NMR spectrum, the trisubstituted nature of the double bond was deduced and located between C-16 and C-17 which clearly followed by ^{13}C- NMR and HMBC experiments. In the presence of a carbonyl moiety, such as a carboxymethyl attached to the olefinic proton at C-16 led to the observation of a significant down field chemical shift of H-17, resonated at about δ 7.68 as a singlet besides a methoxy signal at 3.64 which could be attributed to Vallesiachotamine. One of the other most characteristic signal of Vallesiachotamine is aldehyde proton observed at δ 9.4, besides a neighbooring olefinic proton appeared at 6.68 as a quartet with a *J* value of 7Hz, indicating a coupling with a methyl protons at 2.10 ppm. This aldehyde bearing ethylenic side chain must be attached to C-15. Indeed H-15 signal was observed as a broadened doublet at 4.02 (*J*=6 Hz) confirming Vallesiachotamine structure (Mukhopadhyay, 1981; Sultana, 1992). All the spectral data and literature comparision verified of Vis-1 to be Vallesiachotamine which was isolated from both *Vinca* species *V. soneri* and *V. minor* for the first time.

9.1.3 Identification of α-Yohimbine

The fractions 21-26 were obtained during elution dichloromethane, acetone (DCM, Ace (25:75)) of the alkaloid extract of *Vinca soneri* on Si-gel column and purified through preparative thin layer chromatography. DCM, Ace (70:30) was used as a mobile phase which afforded four different pure compounds, named as: Vis.2, 3, 4 and 5.

Vis 3(5mg):

^{1}H-NMR of the alkaloid exhibited four aromatic methine signals resonated at δ 6.95, 7.025, 7.27, 7.37 which indicated a possible Indole ring moiety in the structure attributing to H-10, H-11, H-12 and H-9, respectively. Their corresponding carbons were assigned by HMQC experiment, observing the signals at δ 118.30, 120.47, 110.61 and 117.09. Its skeleton followed by all carbon signals as well as proton signals and deduced to be a yohimbine type alkaloid. The lack of a skeletal methyl moiety was supported yohimbine structure.

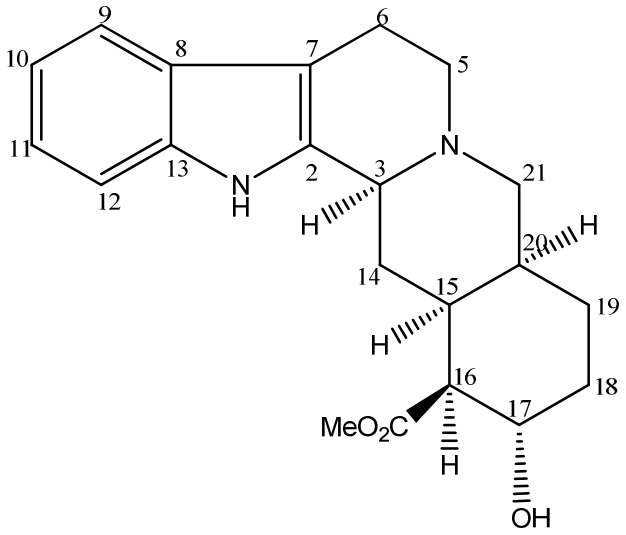

Figure 9.3: α-Yohimbine.

The most characteristic signals were observed at δ 3.41 as a broaden doublet (*J* =11Hz) for H-3, and δ 4.24 as a doublet of doublet (2.7 and 5.6 Hz). The former was significant for C-3 proton with α-stereochemistry. The latter was assigned to H-17 which should be attached to an oxygenated carbon. H-16 was determined based on *J* coupling values of the signal appeared at δ 2.35 and a COSY experiment. H-16 and H-17 signals were significant signals which indicated a yohimbine structure of this alkaloid. Their carbons were observed at δ 52.41 and 67.22. The presence of an carboxy methyl ester group at C-16 followed by ^{1}H-NMR (δ 3.76 as a singlet) and ^{13}C-NMR (δ 50.75) and carbonyl signal at 173.92 ppm. The carbon NMR experiments (BB and APT) displayed 21 carbon signals consisting of six methylene, nine methyne, five quaternary carbon atoms and one methoxyl methyl carbon. The methoxyl carbon was observed at 50.75 ppm.

Besides Indole skeleton's nitrogen, the presence of a second N atom clearly followed by its neighboring three carbon atom signals at δ 60.49 (C-3), 52.79 (C-5) and 60.93 (C-21) and they were assigned by HMQC and HMBC experiments. This carbon frame was supported the yohimbine skeleton.

As indicated in previous pages yohimbine alkaloids categorized into four different type of configurations (normal, pseudo, allo and *epi*-allo). Among them, β-yohimbine belongs to normal type yohimbin alkaloids while α-yohimbine included to allo-type alkaloids.

Table 9.3: ^{1}H-NMR and ^{13}C-NMR assignments of α-Yohimbine (Appendix B).

C $_{No}$	^{1}H-NMR	Multiplicity *J* (Hz)	^{13}C-NMR	COSY	HMBC
2			134.17		
3	3.41	brd (11)	60.49	H-14α,14β	
5α	2.62	d of t (4; 12)	52.79	H-5β	C-3
5β	3.1	dd (6;11)		H-5α	C-3,C-2,C-1,C-7
6α	2.98	m	20.96		
6β	2.72	dd(5;15)			C-7
7			106.31		
8			126.91		
9	7.37	d(8)	117.09	H-10	
10	6.95	t(8;1)	118.30		
11	7.025	t(8;11)	120.47		
12	7.27	d(8)	110.61		
13			136.69		
14α	1.17	q(11;7)	32.24	H-14β,H-3	C-2,C-134,C-15
14β	2.46	td (3;1)		H-14α,H-3,H-15	
15	2.00	dq (2.7; 3)	36.02	H-14β	
16	2.35	dd(11.7;2.7)	52.41		
17	4.24	dd(2.7;5.6)	67.22	H-16,H-18	
18α	1.9	dd(4;13.5)	32.03		
18β	1.66	m(2;4;13.3)			
19	1.36-1.39	m	22.82		
20	1.52	dpentet(2.6;11.0)	39.76	H-21α	
21α	2.26	t(10.9)	60.93	H-21β	
21β	2.92	dd(3;11.4)		H-21α,H-20	
CO<u>OCH$_3$</u>	3.76	s	50.75		
<u>CO</u>OCH$_3$			173.92		

The only skeletal difference between normal- and allo-type yohimbines is the configuration of hydroxyl group at C-17. In this structure, to identify its configuration we have considered coupling constant values of H-17 with H-16 protons and H_2-18. The appearance of chemical shift of H-17 at δ 4.24 as a dd and its coupling values (Table 9.3) was indicative of β- configuration of H-17. All carbon and proton NMR data confirmed the structure to be α- yohimbine (Robert et al., 1983).

9.1.4 Identification of β-Yohimbine

Vis-5(5mg):

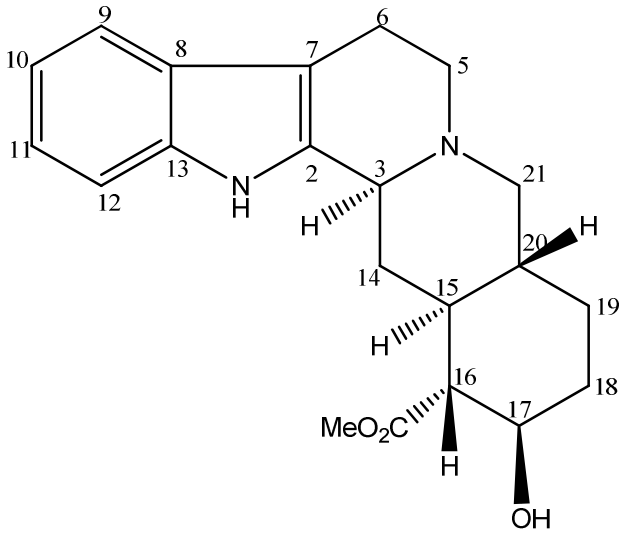

Figure 9.4: β-yohimbine.

Third compound from *V. soneri* revealed similar spectral data to those of α-yohimbine. It exhibited 21 carbon signals having the same nature of protonated carbons with same numbers. Its Indole ring protons were resonated almost at the same frequency (Figure 9.4). C-3 proton was observed at δ 3.3 as an overlapped signal by MeOH signal which was determind by an HMQC experiment. Its *J* value followed by coupling constant value of one of C-14 protons at δ 1.20 brt (*J* = 11.3 Hz). Consequently the *J* value of H-3 should be 11.3 Hz which indicated α-stereochemistry of H-3. In fact, except for pseudo- and *epi*allo-yohimbines, normal and allo yohimbines always have H-3 with α stereochemistry.

The main difference between α and β yohimbines was observed for H-17 proton. When a β-hydroxyl group was attached to C-17, H-17 was resonated at δ 3.74 as dd (*J*= 3.52 and 10.77Hz) in case of β- Yohimbine while in α-yohimbine (C-17, α-OH) it was observed at δ 4.24 with smaller *J* couplings.

It should be noted that C-17 signal was observed at 71.58 ppm in β-hydroxylated cases in yohimbine structures. Thus, all spectral data confirmed the structure to be β-yohimbine (Robert et al., 1983).

9.4: ^{1}H-NMR and ^{13}C-NMR assignment of β-Yohimbine (Appendix C).

C $_{No}$	^{1}H-NMR	Multiplicity *J* (Hz)	^{13}C-NMR
2			133.89
3	3.3	Overlapped by MeOH	59.91
5α	2.64	ddd (4.30;11.3;11.5)	52.77
5β	3.12	dd (5.5;11.3)	
6α	2.96	m	20.98
6β	2.72	dd(4.5;15.4)	
7			106.44
8			126.87
9	7.38	d(8)	117.80
10	6.96	t(8,1)	118.2
11	7.04	t(8,11)	120.60
12	7.28	d(8)	110.5
13			136.69
14α	1.32	d	33.10
14β	2.16	d	
15	1.52	dd (5)	36.02
16	2.16	dd (5.7; 10.6)	57.4
17	3.74	dd(3.52;10.77)	71.5
18α	2.06	dd(4,14)	33.68
18β	1.4	d	
19α	1.20	dd(3,…)	27.7
19β	1.7	t of d (3,13)	
20	1.48	m	39.4
21α	2.18	dd(4,10.5)	60.55
21β	2.98	dd(3;10.8)	
CO_2CH_3	3.80	s	51
	2.64	ddd(4.30;11.3;11.5)	

9.1.5 Identification of Picrinine

Vis-31

The positive APCI-MS spectrum of Vis-31 revealed a molecular ion peak at *m/z* 339.40 $[M+H]^{+}$ for $C_{20}H_{22}O_3N_2$.

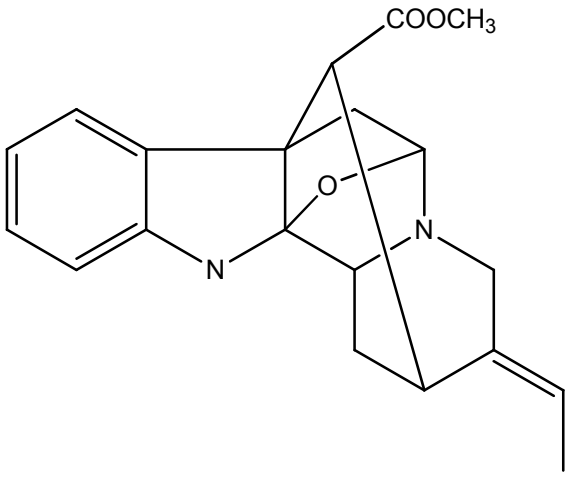

Figure 9.5. Chemical structure of Picrinine.

Table 9.5: ^{1}H-NMR and ^{13}C-NMR assignment of Picrinine (Appendix D).

C $_{No}$	^{1}H-NMR	Multiplicity *J* (Hz)	^{13}C-NMR
2			106.13
3	3.68	m	52.75
5	4.92	m	87.20
6	2.29 3.42	dd (3.0; 14) d(14)	44.10
9	6.78	d (7.41)	111.70
10	6.80	td (1.2; 7.4)	121.66
11	7.10	td (1.2; 7.4)	128.70
12	7.13	brd (7.4)	126.6
14	1.92	m	21.92
15	3.31	d (2.5)	32.95
16	2.45	d (3.5)	58.01
18	1.49	dd (1.7;7)	14.02
19	5.44	brq (7)	121.27
20			137.85
21	3.16 3.81	brd (17.6) td (18.33)	47.02
$COOCH_3$	3.66	s	51.13
$\underline{C}OOCH_3$			174.02
N-H	1.84	brs	

Its ^{1}H-NMR spectrum exhibited Indole ring protons at δ 6.78, 6.80, 7.10 and 7.13 with characteristic multiplicities indicating a nonsubstituted benzene of the Indole ring. The presence of an ethylenic side chain at C-20 was observed by the signals at δ 5.44 as br quartet (*J* =7 Hz) along with a doublet of doublet at δ 1.49 (*J*= 1.7 and 7 Hz) which resembled sarpagine related type indol alkaloids. The smaller *J* value of the latter signal originated from allylic coupling of Me-18 with one of the allylic protons. The vinylic proton at δ 5.44 showed three bond away correlation with a

carbon, appeared at δ 31.65 assigning to H-15 at δ 3.31 (d, *J* = 2.6 Hz). This proton was also showed a gHMBC correlation with C-19, and vice-versa. Another characteristic proton signal was observed at 4.92 ppm as a narrow multiplet, its corresponding carbon was determined to be at 87.20 ppm, attributable a carbon probably located between a nitrogen and oxygen atoms. The proton signal at 4.92 showed a three bond correlation with a quaternery carbon signal appeared at 51.25 which was assigned to C-7, therefore the signal at 4.92 was determined to be H-5. Another carbon signal resonated at 106.13 ppm, also assigned to a carbon either between two oxygenes or between an oxygen and a nitrogen atoms. Based on g-HMBC correlation as well as literature data, the signal was deduced to be C-2. In fact, it was also located between nitrogen and oxygen atoms, however, its rigid situation as a bridge-head carbon caused more downfield resonance compared to C-5. H-15 also exhibited a three bond away correlation with a carbonyl carbon of the ester group indicating location of the ester group at C-16 and verifying the assignment of the proton at δ 3.31 belong to C-15 as well as its vicinity to C-20. C-3 proton signal resonated at δ 3.68 as a broadened doublet (*J* = 11.20 Hz) which coupled to H-14 protons (1.92, m) observed by a COSY experiment. All the experimental data allowed to determine of the structure as picrinine (Atta-ur-rahman, 1995; Batista, 1996) which has been isolated from some *Vinca* species as well as some other Apocynaceae family plants .

9.1.6 Identification of 11-Hydroxypolyneuridine

Elution of the alkaloid extract of *Vinca major* on neutral Aluminium column by using EtOAc, MeOH (95:5) was afforded fraction 34 which was further purified by a second column chromatography. The fraction 19 of the latter column was purified by using preparative TLC. The mobile phase was Toluene- Acetone- Diethylamine (40:5:5) and 5 compounds were obtained. First compond was named Vmaj-1.

Vmaj-1(3mg):

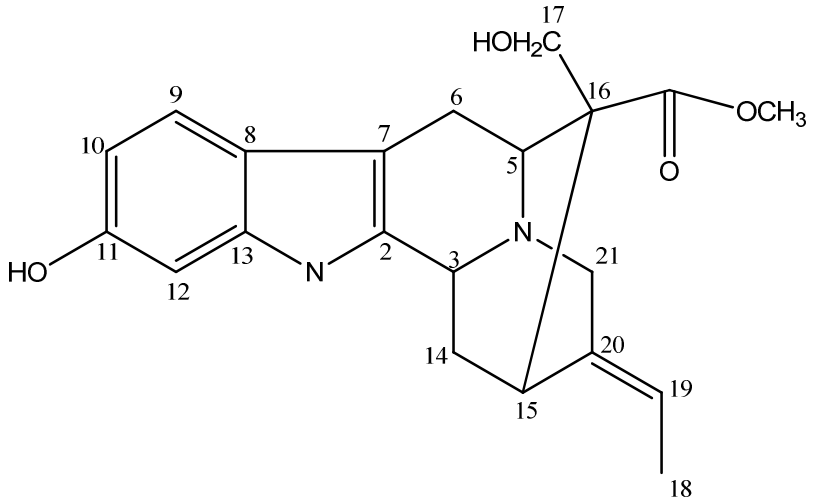

Figure 9.6: 11-hydroxypolyneuridine.

This alkaloid has also an Indole skeleton as expected. However it was a mono substituted benzene ring exhibiting aromatic signals at δ 6.62, 6.76 and 7.10 corresponding to H-10, H-12 and H-9, therefore the compound should carry a substituent at C-11, probably being a hydroxyl or methoxyl group, but HMBC experiments indicated hydroxyl moiety rather than methoxyl moiety. One of the characteristic signal for its skeleton was observed at δ 5.45 as a broadened quartet (*J* =6.7Hz) along with a vinylic methyl doublet appeared at δ 1.70 as a doublet which belong to an ethylenic side chain attached to C-20 as seen in sarpagine type Indole alkaloids.

The three carbons attached to the nitrogen atom were observed at δ 50.80 (C-3), 57.75 (C-5) and 54.53 (C-21). Their protons were assigned by HSQC experiments (Table 9.6). In addition, the presence of a hydroxymethylene and carboxy methyl groups in the structure followed by ^{1}H and ^{13}C NMR signals (Table 9.6). Based on HMBC experiments both their location was deduced to be at C-16. Particularly C-5 proton showed three bond correlations hydroxymethylene carbon which appeared at 67.41 and carboxymethyl carbonyl observed at 173.02 verifying their location at C-16. All spectral data and literature comparison indicated that Vmaj-1 must be a polyneuridine derivative.

Table 9.6: ^{1}H-NMR and ^{13}C-NMR assignment of 11-Hydroxypolyneuridine (Appendix E).

C $_{No}$	^{1}H-NMR	Multiplicity *J* (Hz)	^{13}C-NMR	COSY	HMBC
2			130.93		
3	4.3	d(10)	50.80		
5	2.9	brd(4)	57.75		
6α	2.81	dd(5,16)	nd		C-5, C-16, C-7
6β	3.35	dd(2,16)			
7			103.93		
8			131.93		
9	7.1	dd(9)	110.97		C-11, C-13
10	6.62	dd(2,9)	110.47		
11			149.88		
12	6.76	d(2)	101.86		C-8
13			127.00		
14α	2.72	q of d (1,5,13)	28.56		C-17
14β	1.92	t (12)			
15	3.27	brd(3)	28.77		C-21, C-3
16			51.11		
17α	3.78	d(9)	67.41		
17β	3.65	d(10)			$\underline{C}OCH_3$
18	1.7	d (6.7)	11.87		C-19
19	5.45		117.41		
20			137.22		
21α	3.58	d(16)	54.53		
21β	3.69	d(16)			
$CO\underline{O}CH_3$	3.00	s	50.43		
$\underline{CO}OCH_3$			173.02		

On the basis of HMBC correlations, a hydroxyl group should be located at C-11, thus 11-hydroxypolyneuridine was isolated for the first time from nature (Atta-ur-rahman, 1995; Kogure, 2005; Marinibettolo, 1980).

9.2 Results of Characterization of Nano-VLB Formulations

9.2.1 Results of characterization of nano-VLB-SSMs

9.2.2 Results of solubility of Vinorelbine (VLB) in SSM:

There was no precipitation in any of samples and time history graphic was so clear too.

A hydrophobic drug has certain water solubility. Normally in a micellar drug delivery system drug molecules prefer to be dissolved in water in an amount equal to its water solubility. Adding more amount of drug causes the incorporation of hydrophobic core of the micelle with the hydrophobic drug. By the addition of higher amount of drug causes the precipitation of drug in the holder.

As it could be seen there is no Vinorelbine agrregation or precipitation even by adding 3000µg VLB to the system.

There are two possibilities:

1-Since the hydrophilic functional groups on VLB molecule is much localised, it is possible for VLB to make its own dimers or micelles in or out of micelle and increase the water solubility.

2- It is noteworthy that micelle size is going smaller and smaller by adding more and more vinorelbine. Previously it has been reported that the size of Sterically Stabilized Mix Micelles' (SSMM) is smaller than normal SSMs. The reason is that a "unimer" of DSPE localises in between two DSPE-PEG"unimers" in the "polymeric" micelle structure and gives the PEG part to fold more than before. We know that the size of PEG layer encloses a very important part of the size of all of micell. Therefore more folding in PEG layer causes the whole micelle go smaller and smaller.

We shall pay attention on that some times 2-3 nm difference in size is not important in DLS measurements. We repeated our assays at least 3 times and calculated the Standard Deviation. The change in size of micelle by addition of more VLB is in range of meaningfullness.

The results has been repeated for 3 times, and particle size measurements have been repeated for 3 subsequent days and then one week after. When the particle size was

stable for 1mg VLB/1mM lipid, the size of micelles containing 2 and 3 mg VLB were increasing after first day.

It seems that the VLB units settled in between two DSPE unimers, leave their position after some days and cause an enlargement in micellar size.

Starting from this point we need to understand if VLB makes its own micelles or incorporates with the DSPE core of the SSMs.

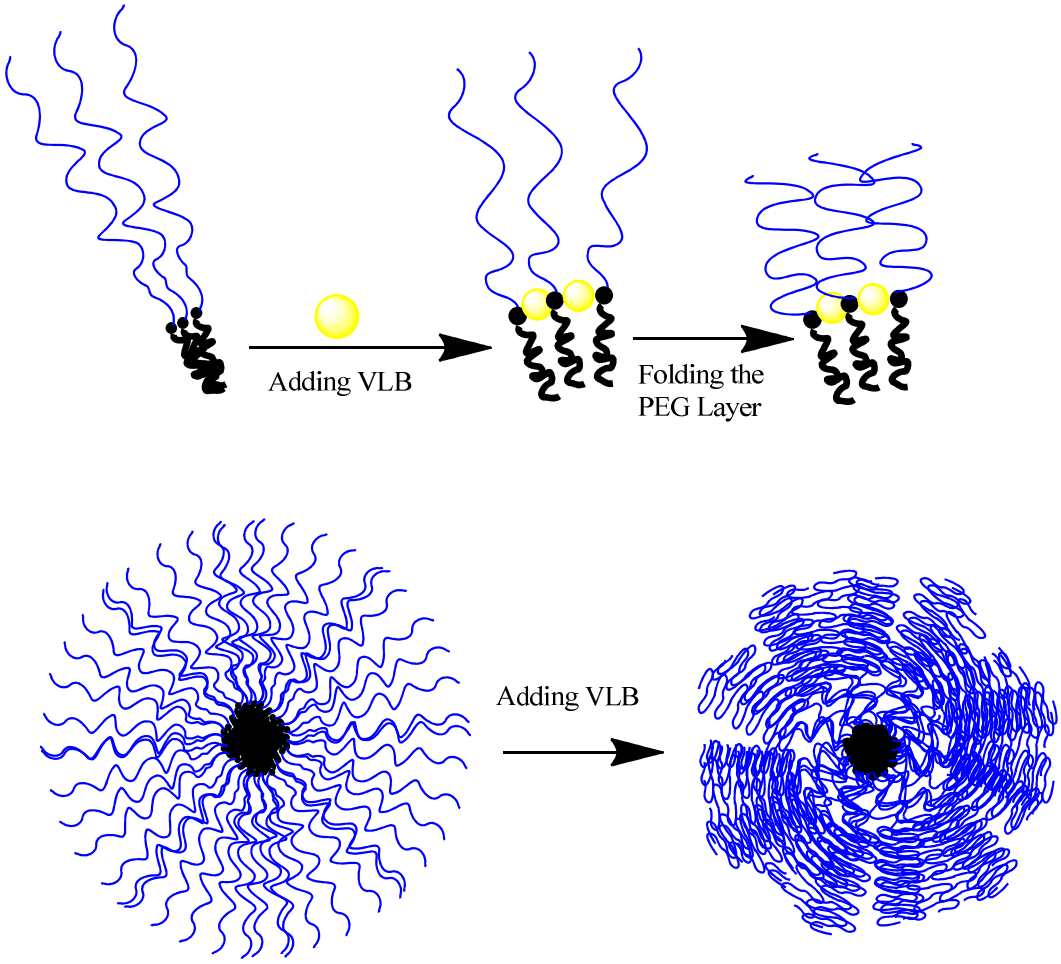

Figure 9.7: Localization of VLB in between 2 DSPE-PEG unimers and observation of a decrease in size of particle.

Table 9.7: The results of particle sizing of different formulations of VLB-SSM by using DLS.

VLB conc. in 1mM lipid (1ml)	INT-WT and VOL-WT	Time History
50	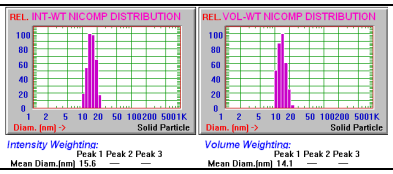	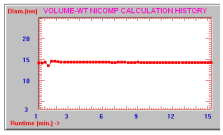
100	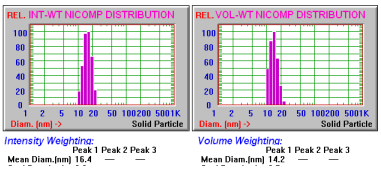	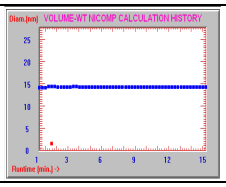
200	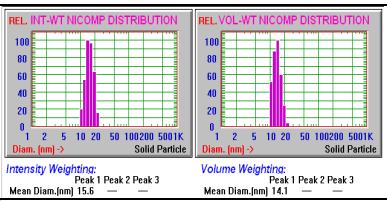	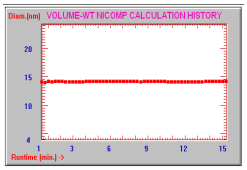
350	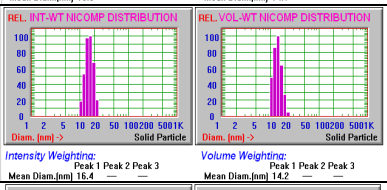	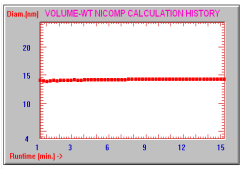
500	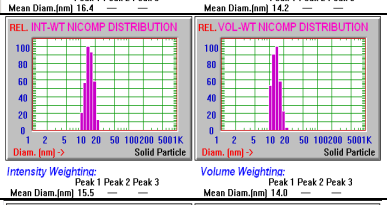	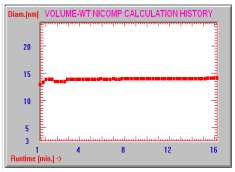
1000	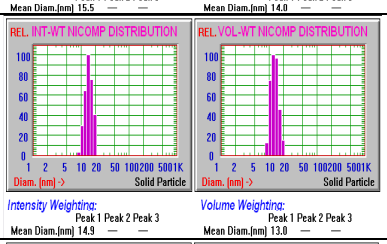	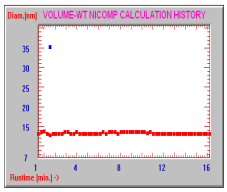
2000	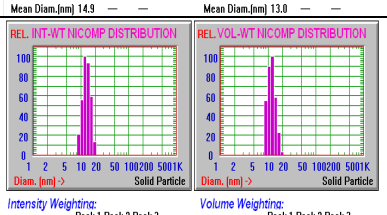	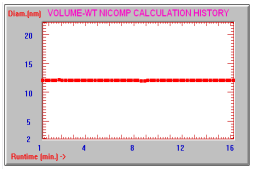
3000	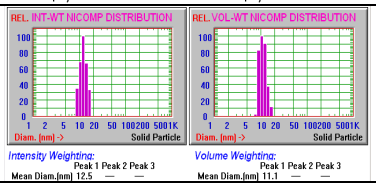	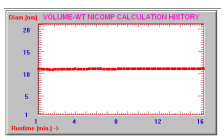

Table 9.8: The relationship between amount of VLB associated with SSM and micelle size.

VLB conc. (µg/1mM SSM)	Micelle size (nm) First day	Micelle size (nm) 3rd day
50	14.02	14.2
100	14.16	14.2
200	14.42	14.2
350	14.24	14.2
500	13.9	14.2
1000	13.4	13
2000	12.02	12.9
3000	11.04	12.1

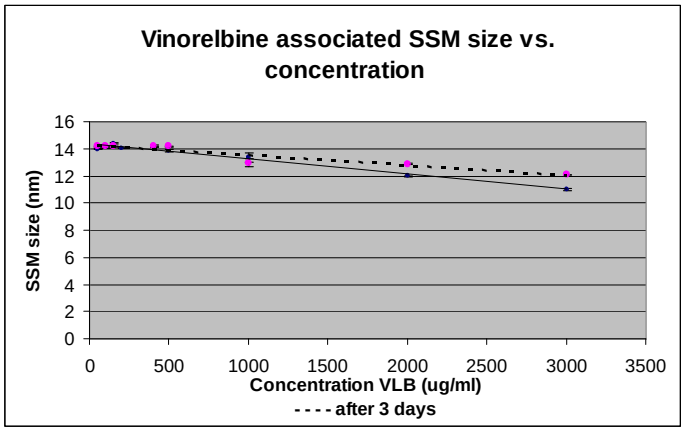

9.2.3 The UV study of VLB associated with SSM:

We assume that if Vinorelbine associated with SSM is in molecular level its UV absorbance will be equal to that of free VLB in molecular level in in buffer. In this assay, we repeated the UV absorbance measurments 3 times in a day and once again after three days. The reason is explained under the "Results" part.

Table 9.9: Free Vinorelbine concentration curve in PBS in UV spectrophotometer.

VLB Conc. µg/ml	U.V. absorbance
125	**2.106**
62.5	**1.0262**
31.25	**0.4494**
15.63	**0.1776**
7.82	**0.1004**
3.9	**0.0677**
1.95	**0.032**
0	**0**

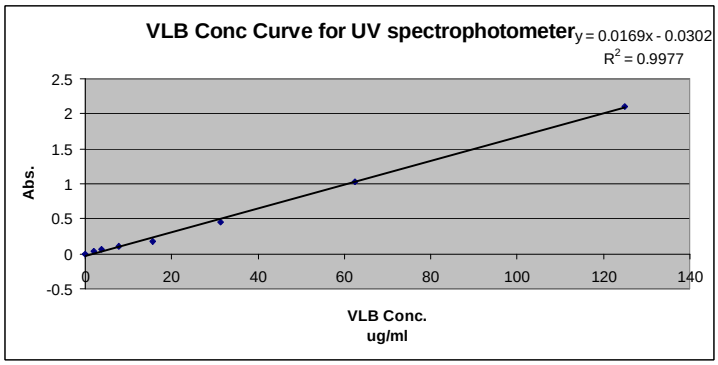

y = 0.0169x - 0.0302

9.2.4 UV Absorbance of 1mM SSM associated Vinorelbine in different concentrations:

After identification of UV absorbance of VLB in PBS, we have measured the same concentrations of VLB in 1mM SSM. If the VLB is in molecular level in SSMs we should get the same absorbance that VLB showed in PBS with SSM-VLB formulation.

Table 9.10: UV absorbance of 1mM SSM associated Vinorelbine in different concentrations.

VLB conc. (µg/ml) in 1 mM DSPE-PEG 2000	UV absorbance First day	UV absorbance First day (2nd trial)	UV absorbance First day (3rd trial)	UV absorbance After 3 days (the same for all formulations)
50	1.8097	1.2205	1.2264	2.1632
150	2.8204	3.8698	3.8698	3.1095
250	3.8996	3.8698	3.8698	3.8876
350	3.8996	3.8698	3.8698	3.8876
500	3.8996	3.8698	3.8698	3.8876
1000	4.5000	4.5000	4.5000	4.5000
1500	4.5000	4.5000	4.5000	4.5000
2000	4.5000	4.5000	4.5000	4.5000
3000	4.5000	4.5000	4.5000	4.5000

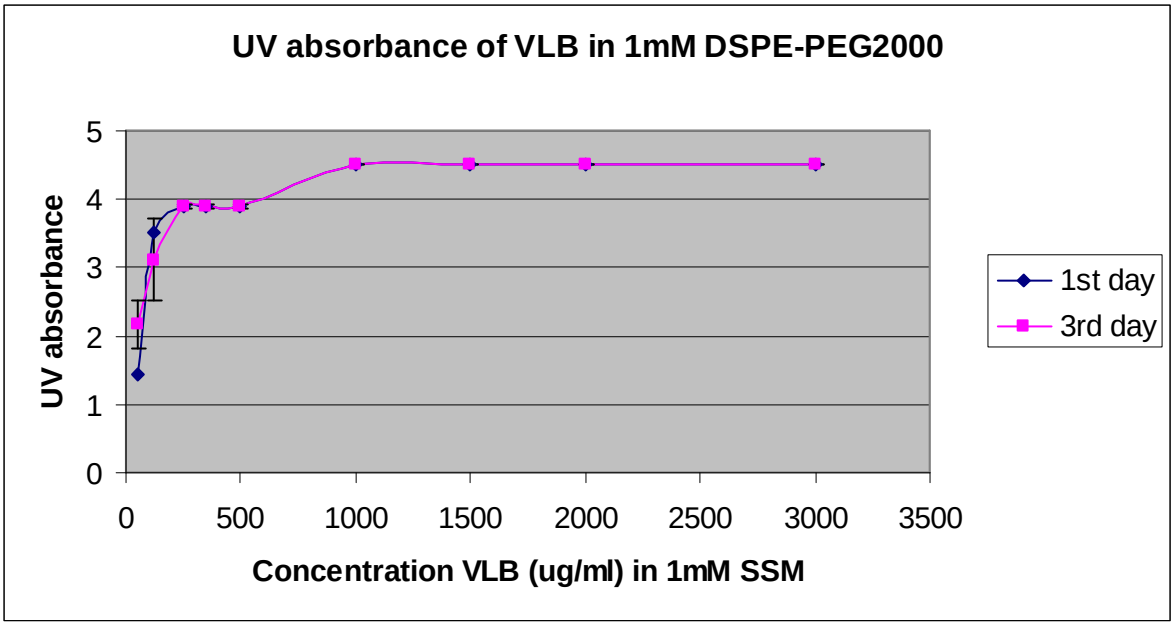

Figure 9.8: UV absorbance of VLB in 1mM DSPE-PEG 2000.

As a result of above study, its impossible to use the free VLB conc. curve equation to find out the amount of VLB in SSM or to prove that VLB is in molecular level in SSM or not. For example if we use the equation to find the amount of VLB associated with SSM in the first line equation (50µgVLB/1mM lipid): $y = 0.0169x - 0.0302$, $1.8097 = 0.0169x - 0.0302 \rightarrow x = 106.9$ µg/ml. But this is impossible because we used only 50 µg/ml VLB in making this formulation.

But starting from this point we could come to the conclusion that in all concentrations of VLB a part or all of the drug is associated with SSMs and that is why the UV absorption of a certain amount of VLB is much more higher than the same amount of free drug.

9.2.5 Results of Investigation of the Possibility of Forming Micelles by Free Vinorelbine:

A concentration of 2 mg/ml has been prepared by using the method reported in Table 8.9 and Table 8.10, and the existence of particles has been studied in NICOMP particle sizer, but no significant result has been obtained:

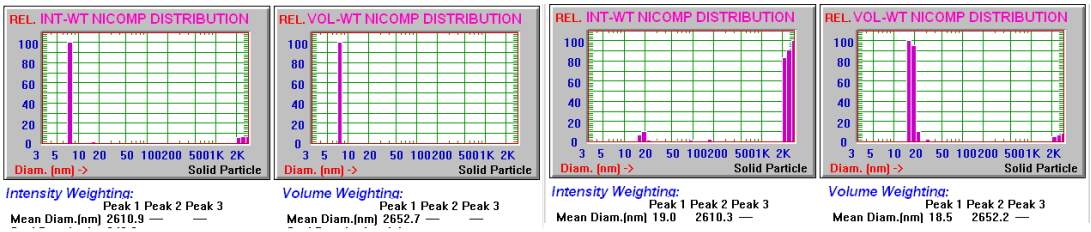

Figure 9.9: DLS investigation of 2 mg VLB in PBS.

However in time history diagram some particles with stable sizes (2600 and 1000 nm) show up but disappear as soon as we dilute this concentration to 1mg/ml:

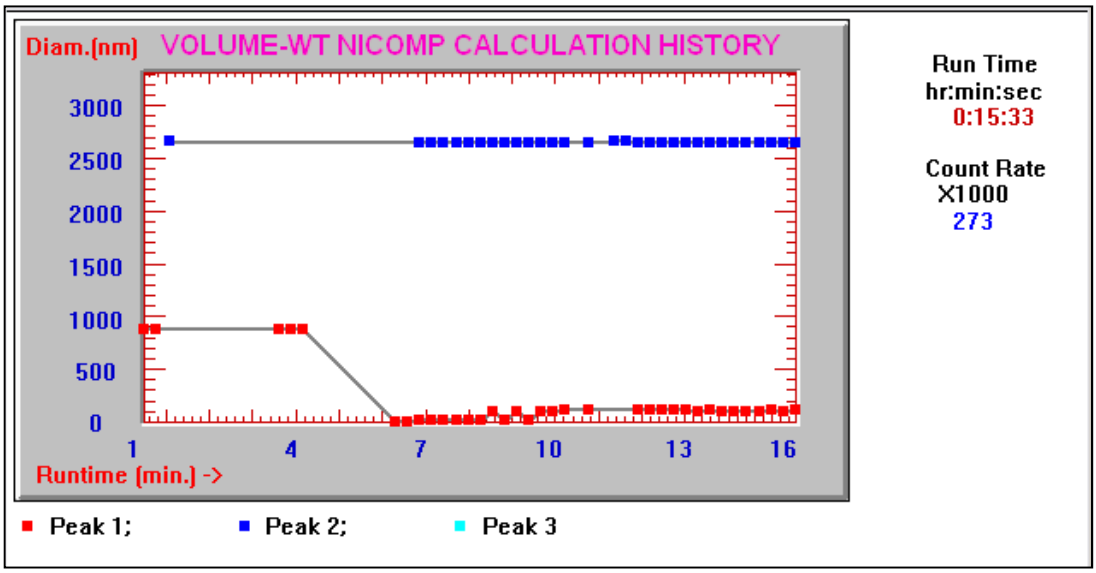

Figure 9.10: Time history diagram in DLS investigation of 2 mg VLB in PBS.

But when we incorporate the same amount of drug with 1mM SSM the solvent is completely clear and these particles are disappeared:

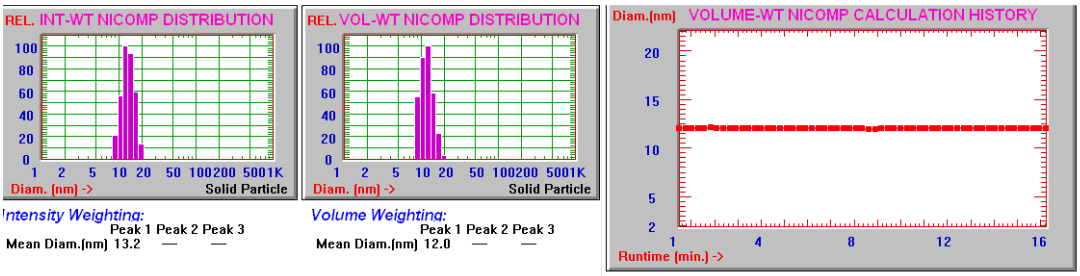

Figure 9.11: DLS investigation of 2 mg VLB associated with DSPE-PEG.

As a result either Vinorelbine is makes its own micelles or not, this is a clear proof of the association of the drug with micelles. But as we will mention in DSC results, eventually we came to the conclusuion that VLB does not make its own micelles in water and the particles detected by NICOMP particle sizer are not real particles. Generally, this happens in particle sizing assays carried out in highly diluted systems.

9.2.6 Results of separation of the amount of drug associated with SSM from free drug in buffer by centrifuge

As mentioned in Methods part, using normal centrifuge tubes, no difference was observed between the concentration of supernatants and precipitates, which meanes there is neither a precipitation during centrifuge procedure nor latent aggregation in system.

By using Centrifugal Filter Tubes the results are as follows:

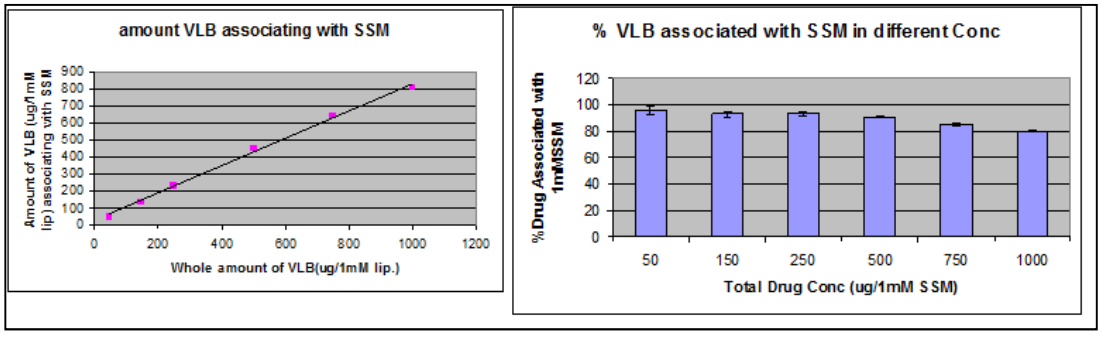

Figure 9.12: Amount of VLB associated with SSM followed by centrifuge assay.

Three very important results are obtained:

1- The more Vinorelbine the more association between SSM and drug. As seen in the left hand graphic, increasing the amount of drug causes more association and consequently less drug has been filtrated in centrifuge tubes.

2- We have calculated the percentage of drug is associated with SSMs, as illustrated in the right hand graphic. The amount of VLB associated with DSPE-PEG raises up starting from low concentration up to 500µg and faces a little decrease after increasing its concentration from 500µg to 1mg. Probably 500µg VLB concentration in the system is the highest point of association of SSM with drug and above this point in 1mM SSM concentration, the drug delivery system is saturated with with drug and it starts to be solved in buffer.

3- The most important result: If we shall choose the most appropriate formulation 500µg VLB in 1mM SSM would be the best in which the physical properties of formulation is stable even after 3 days and also is the highest amount of stable incorporation of the drug with SSM.

Earlier reports support our results. Previously by using "Differential Scanning Calorimetry" it has been shown that the most favored position of Vinorelbine (VLB) in lipid bilayer is at the interface part of polar and non-polar groups of phospholipids bilayer *(C.Koukoulitsa et al. Chemistry and Physics of Lipids 144 (2006) 85-95)*. The same study exhibited the amphoteric property of Vinorelbine should be a reason for its association with model lipid bilayer. According to this study, Vinorelbine is characterized by an extensive hydrophobic area covering both catharantine and vindoline moieties and hydrophilic groups predominated in vindoline moiety.

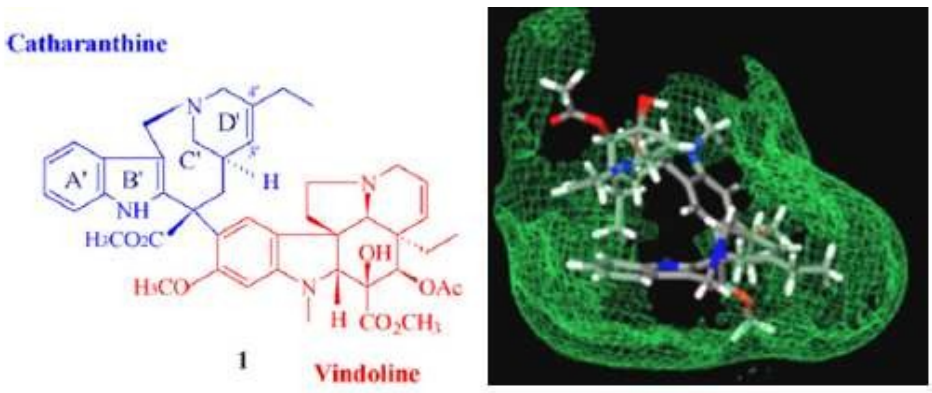

Figure 9.13: The amphoteric property of Vinorelbine (Koukolitsa, 2006).

There is always a second possibility that must be concidered. Sometimes the existance of a latent aggregate in the system causes a shift in the size diagram of particles. For example if we have two different particles with 20 and 2000 nm diameters, the larger particle causes a left hand shift in the size diagram of the smaller particle. This causes in measurement of the size of the smaller particle as 18-17 nm. About our results, it is possible that VLB is making it's own micelles (or soluble aggregates) and this floating aggregates are pushing the DSPE-PEG2000 micells' size daigram to left and results in the sizing them as 11-12 nm.

By using centrifuge assays, we showed that this hypothesis does not really come true. However we discard the possibility of presence of latent aggregates in the system by choosing the 500 µg VLB/ 1mM SSM as the most stable formulation in which there is no decrease in size of micelles.

9.2.7 Results of the stability of Vinorelbine-SSM formulation after lyophilization:

Concentration changes before anf after lyophilization and rehydration :

Table 9.11: The amount of VLB in SSM, measured by HPLC.

VLB amount before lyophilization (µg/ml)	VLB amount after lyophilization
4487.715302	3992.526628
4485.582259	3993.453780
6411.449000	4884.277000

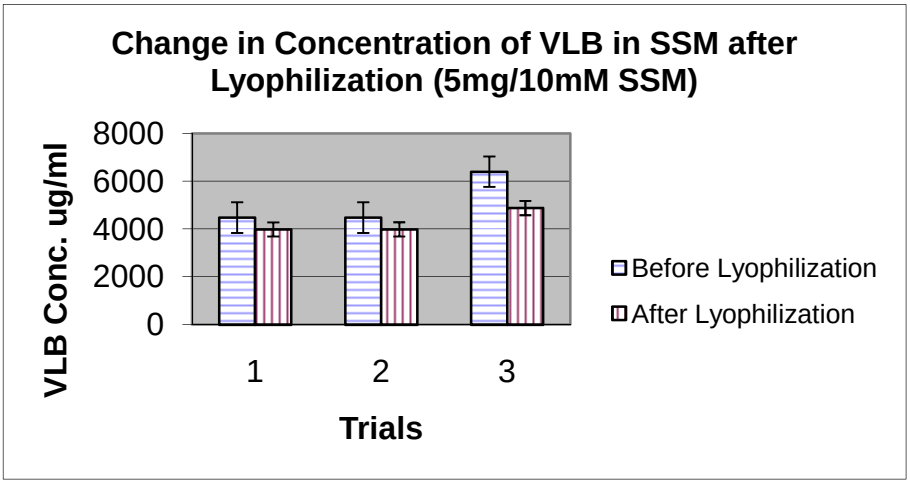

Figure 9.14: Changes in concentration of VLB in SSM after lyophilization.

Table 9.12: Size changes before and after lyophilization.

before lyophilization	after lyophilization
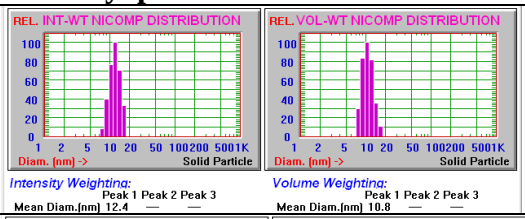	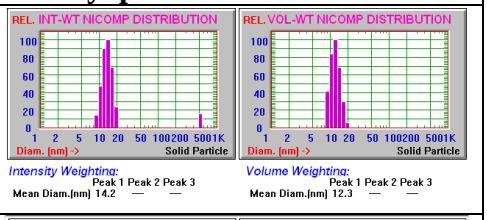
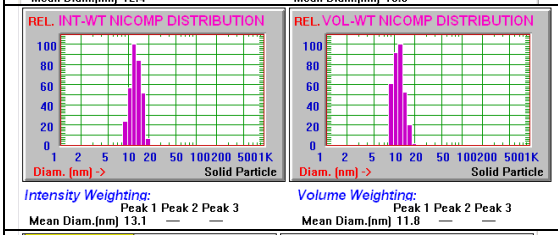	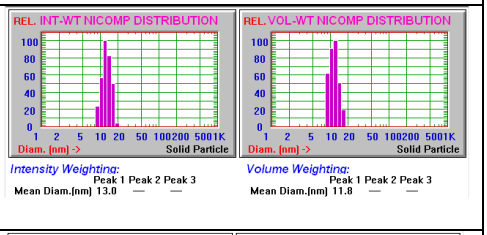
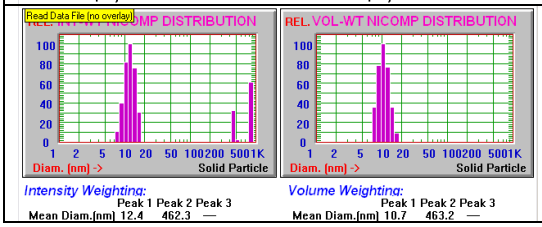	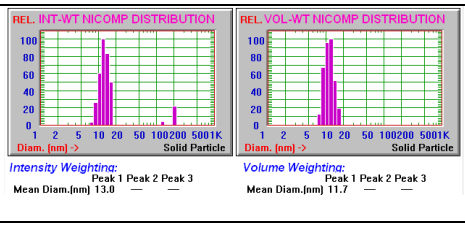

Table 9.13: Differences in size of micelles before and after lyophilization.

Particle size nm before lyophilization	Particle size nm after lyophilization
10.8	12.3
11.8	11.8
10.7	11.7
Standard Deviation	Standard Deviation
0.60827625	0.32145503

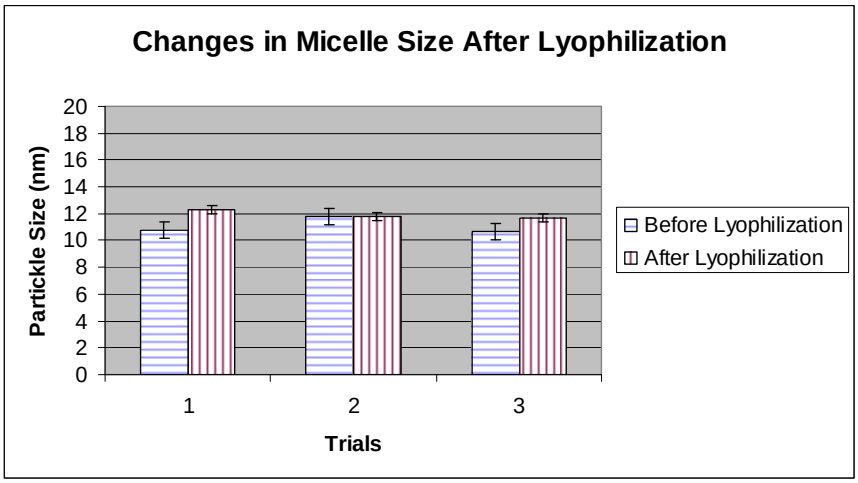

Figure 9.15: Changes in micelle size after lyophilization.

Table 9.14: Changes in micellar size in 2,3,5,7 and 15 days after lyophilization.

2nd day	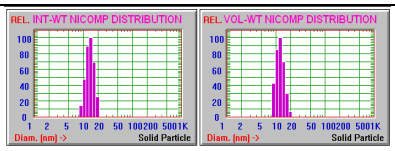	7th day	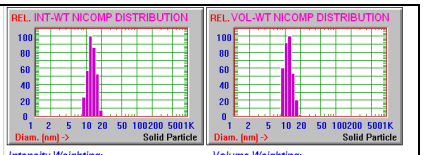
3rd day	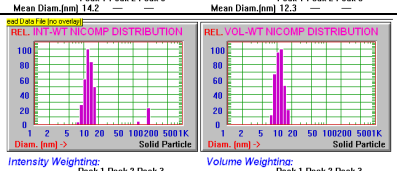	15th day	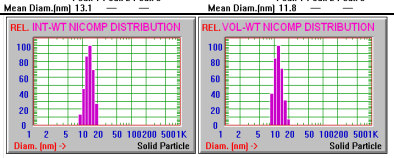
5th day	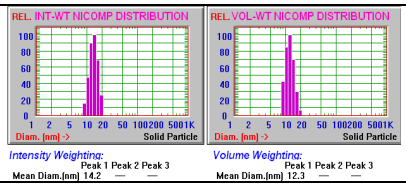		

The Physical Result of Lyophilization:

We were also able to get a fluffy material of formulation after lyophilization as could seen in photos:

Figure 9.16: The physical results of lyophilization.

As it could seen there is no significant change in size and amount of Vinorelbine in 500µg VLB/1mM SSM formulation after and before lyophilization.

9.2.8 Results of drug release studies by dialysis of Sterically Stabilized Phospholipid Micelles containing Vinorelbine (SSM-VLB)

First Release Study:

Table 9.15: First VLB-SSM release results.

Time(H)	% release
0	0
0.5	-0.15
1	1.47
2	3.11
3	5.15
4	6.36
6	5.7
12	11.82
21	16.56
24	18.79
30	18.94
48	25.58

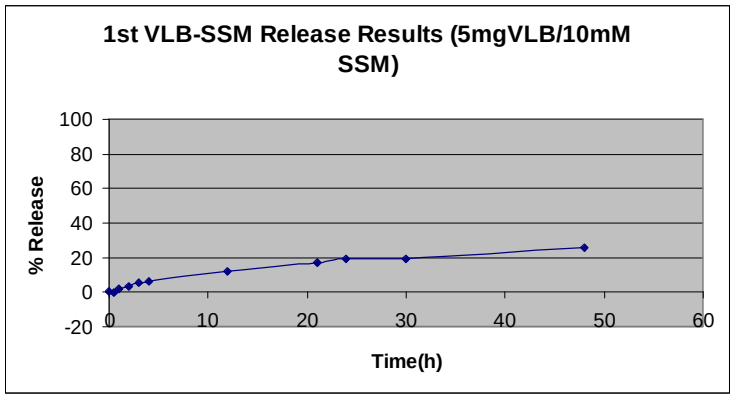

As it could seen the very first sample of release (0.5h) was not sufficient to be detected. To solve this problem in the second and third trials, 1ml of media has been sampled and lyophilized. The lyophilized sample was dissolved in 200µl of MeOH to obtain 5 times higher absorbance. Thus, the 5 times concentrated sample was used in calculations.

Second Release Study:

Table 9.16: Second VLB-SSM release results.

Time (h)	% release
0	0
0.5	0.12
1	1.49
2	3.50
3	5.45
4	6.50
6	7.10
12	11.73
24	15.10
28	18.30
48	20.1
72	22.29
90	35.71

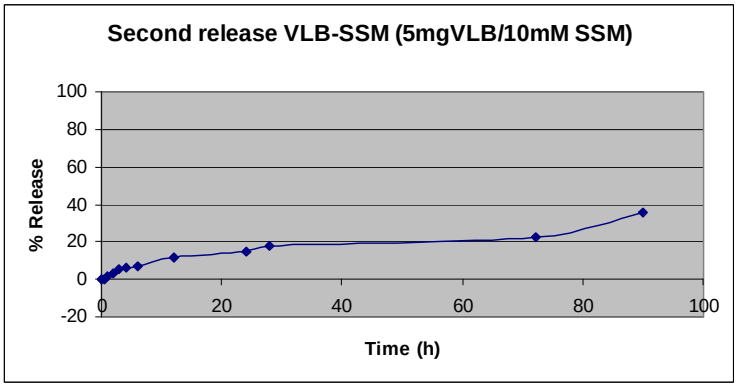

3rd Dialysis Study:

Table 9.17: Third VLB-SSM release results.

Time (h)	% release
0	0
0.5	0.7
1	1.47
2	4.6
3	6.15
4	6.36
12	11.81
18	9.61
22	13.15
24	15.94
48	26.42
53	32.53
96	82.66
117	99.06

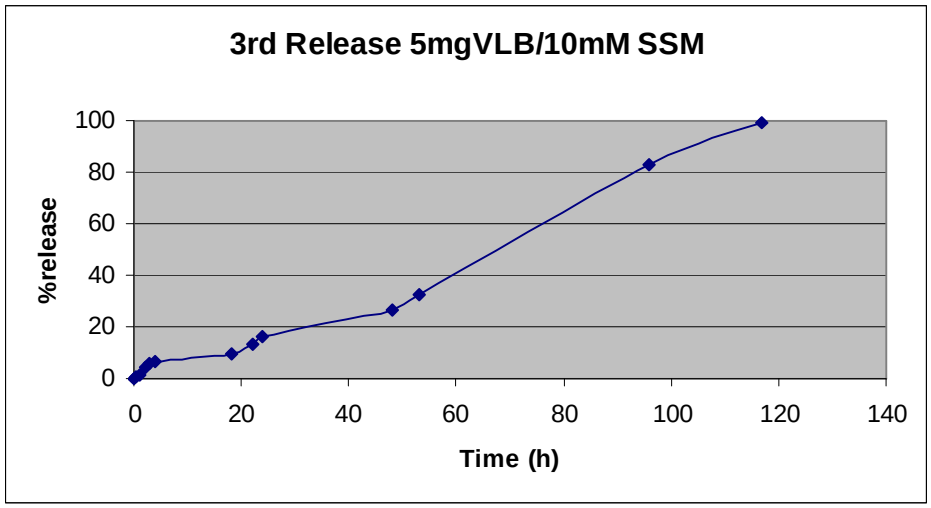

Total Release Results:

Table 9.18: Total release results.

Time (h)	0	0.5	1	2	3	4	12	24	48
%Release	0	0.22	1.47	3.73	5.58	6.40	11.79	16.61	24.03
STDV	0	0.434319	0.011547	0.772679	0.51316	0.080829	0.051962	1.934089	3.432162

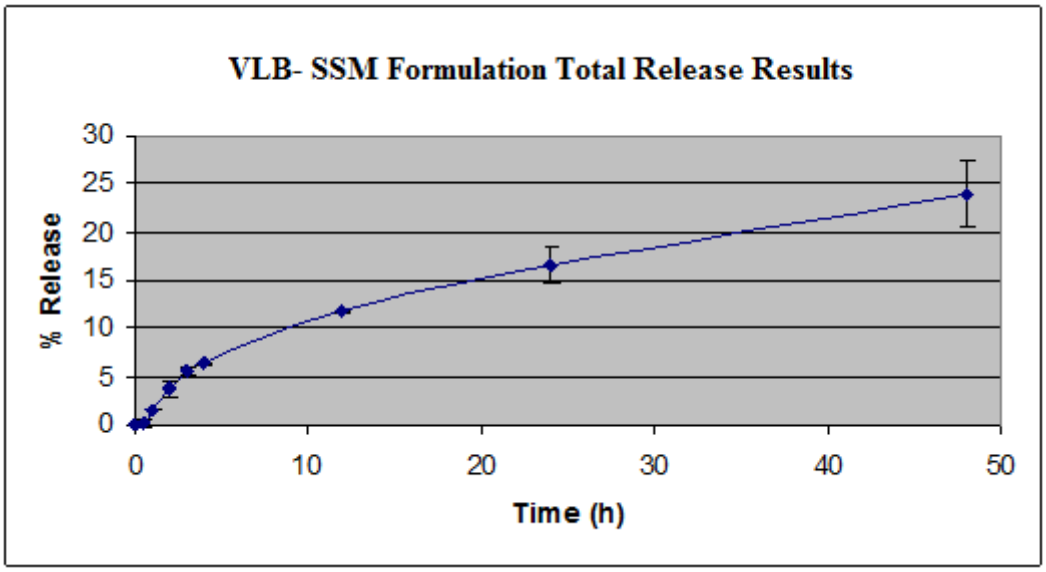

Figure 9.17: VLB-SSM Total release result.

The release from VLB-SSM formulation is slow enough to keep drug stable until the drug delivery system reaches the cancer cell side, and it then releases.

Also the “very slow release” period confirms the tight corporation of the drug with DSPE part of the micelle.

9.2.9 Results of DSC assays of SSM-VLB formulation:

9.2.10 _Results of Solid Samples

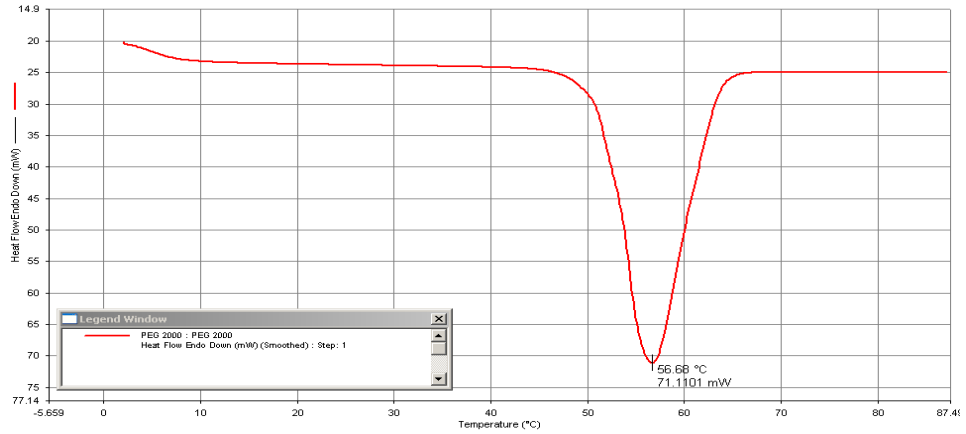

Figure 9.18: DSC thermogram of PEG 2000.

As shown in the above figure, PEG 2000 shows a crystallization temperature at 56^{o}C.

The dip point is obtained herein is due to the stock of polymers as seen below and mentioned before (Fig.6.4).

This crystallization temperature decreases to 52^{o}C in case of DSPE-PEG2000 sample:

In Figure 9.19 a new peak in 48^{o}C has shown up. We didn’t have naked DSPE to compare its Thermogram with obtained spectrum.However the Thermogram of Dipalmitoyl Phosphatidyl Choline (DPPC) which is structurally very near to DSPE as 41 ^{o}C.

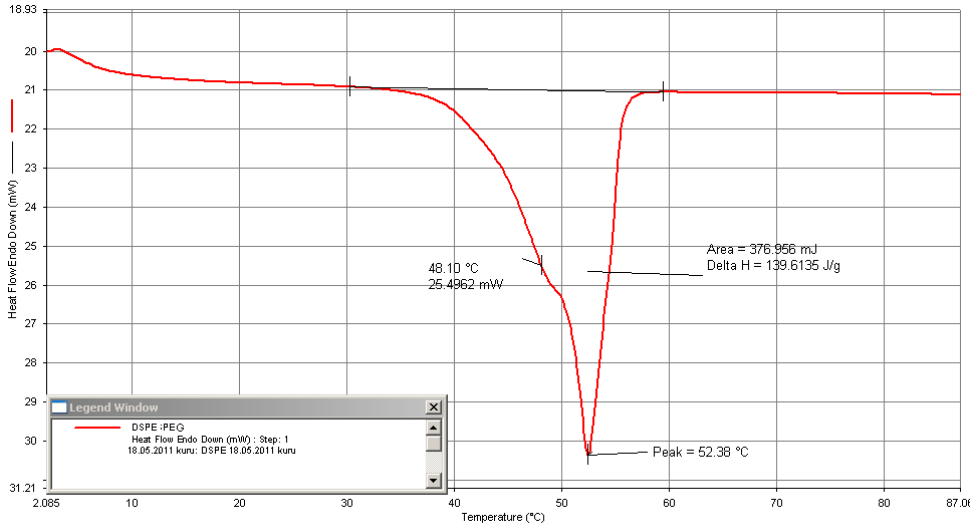

Figure 9.19: DSC thermogram of solid DSPE-PEG 2000 (obtained commercially) before making SSM.

So it seems that the spectrum in 48 ^{o}C is related to DSPE. Probably DSPE is also making some stacks possibly not as organized as PEG, but ordered enough to give a crystallization thermogram.

The decrease in crystallization temperature of PEG probably is due to attachment to DSPE. During the Click Reaction both materials loose energy equal to the binding energy and this causes a reduction in crystallization temperature. On the other hand binding of PEG to DSPE causes a disruption in the structure of above mentioned polymeric stock and this is another reason for the decrease in crystallization energy.

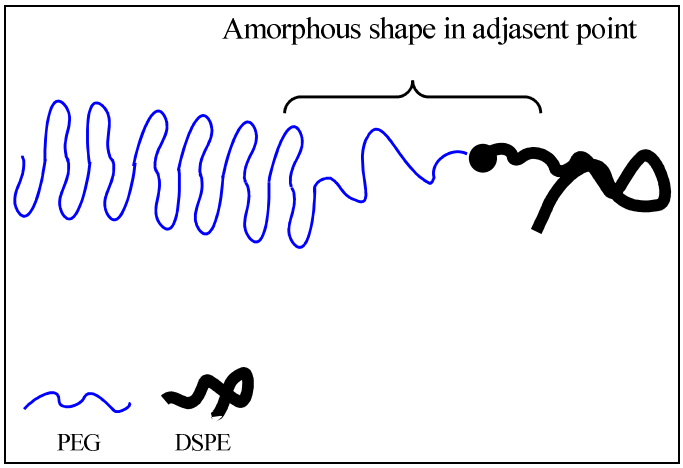

Figure 9.20: Unfolding of PEG at the point of attachment to DSPE and decrease in crystallization temperature.

The Illustrated Reason of Reduced Crystallization Temperature of PEG after Binding to DSPE

A very interesting result is obtained from the Thermogram of DSPE-PEG after making SSM. The film making procedure has been followed and the obtained free SSM formulation obtained has been freeze dried. The result is as seen below:

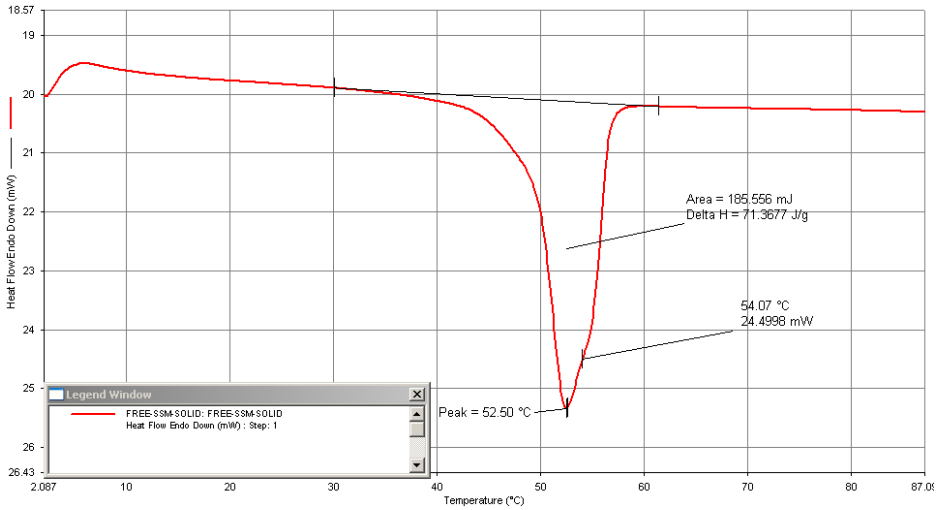

Figure 9.21: DSC Thermogram of solid DSPE-PEG 2000 after making SSM.

It seems that we lose the crystallization thermogram of DSPE after making film and lyophilization. This probably is related to the amorphous shape which hydrophobic DSPE gains after dealing with water. As we mentioned on, amorphous material don't show crystallization temperature.

Other result which obtained from this thermogram is the second peak related to PEG. PEG gave 2 different peaks; 52 ^{o}C and 54 ^{o}C. The crystallization peak at 52 ^{o}C is the same with DSPE-PEG before film making and the shoulder at 54 ^{o}C is related to PEG stocks that found the opportunity of making crystals again after lyophilization whole around the micelles.

Results of Solid Samples of VLB associated with SSM:

As mentioned above, we measured the water solubility of Vinorelbine (VLB) as 250µg/ml. In order to determine the behaviour of Vinorelbine in Sterically Satabilized Micellar (SSM) system, we chose two different concentrations of VLB, one below its water solubility; 50µg/ml and the second above it; 500µg/ml. In both cases the concentration of SSM was 1mM.

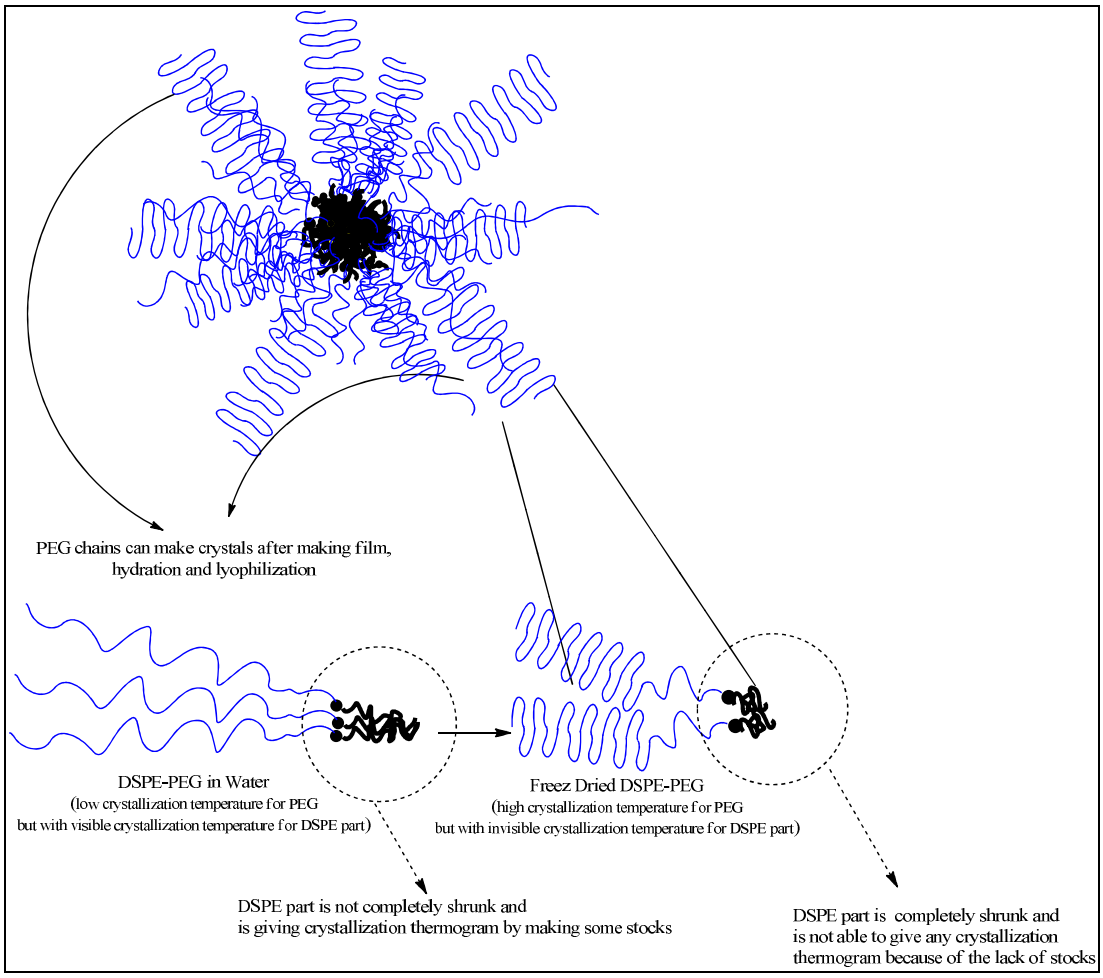

Figure 9.22: The illustration of changes in SSM structure after lyophilization.

Thermogram of 50µg VLB associated with 1mM SSM:

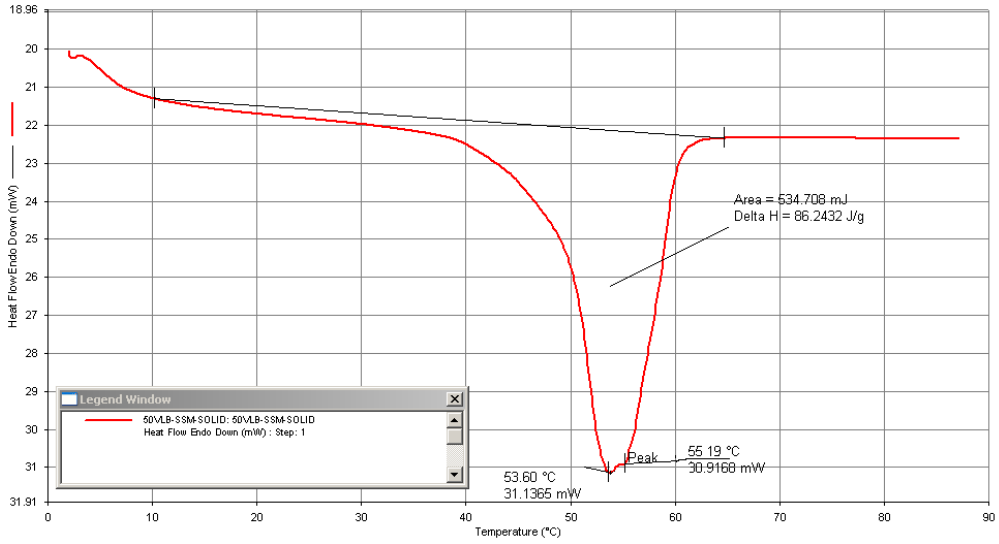

Figure 9.23: Thermogram of 50µg VLB associated with 1mM SSM after lyophilization.

The area under peak (ΔH) has been enhanced (71.36J/g for Free SSM and 86.24J/g for 50µg VLB associated with SSM). Since this is the freez dried sample we assume that the enhancement of the thermogram is due to the association of VLB with the core part, eventhough there is no significant change in the core part of Thermogram (around 46^{o}C).

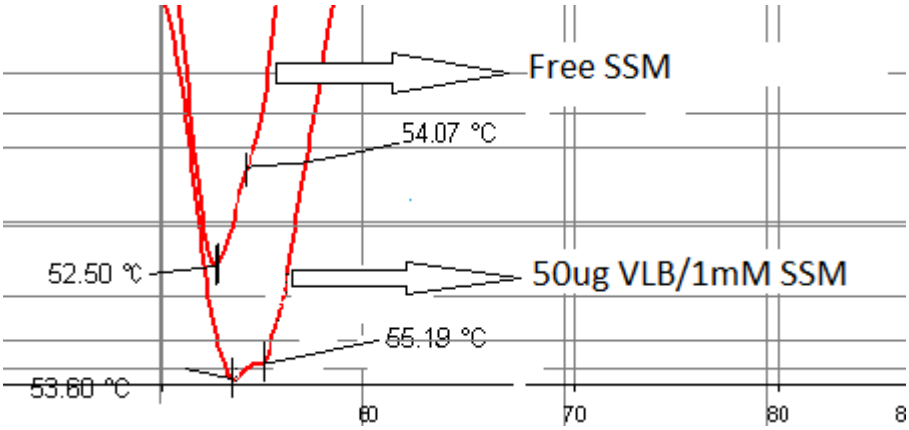

Figure 9.24: Thermogram of 50µg VLB associated with 1mM SSM in comparing with the free SSM, both after lyophilization.

Thermogram of 500µg VLB associated with 1mM SSM:

The thermogram showes a very significant change both in ΔH (123.99 J/g for 500µgVLB-SSM and 71.36J/g for the free SSM) crystallization thermogram. This indicates the association of VLB with SSM completely in core part since there is a significant change in DSPE thermogram at 46^{o}C.

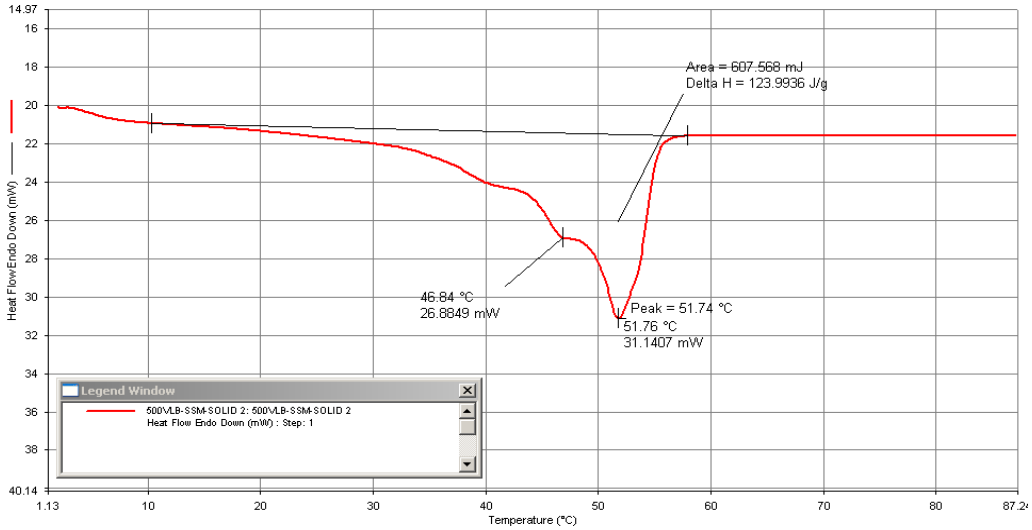

Figure 9.25: Thermogram of 500µg VLB associated with 1mM SSM after lyophilization.

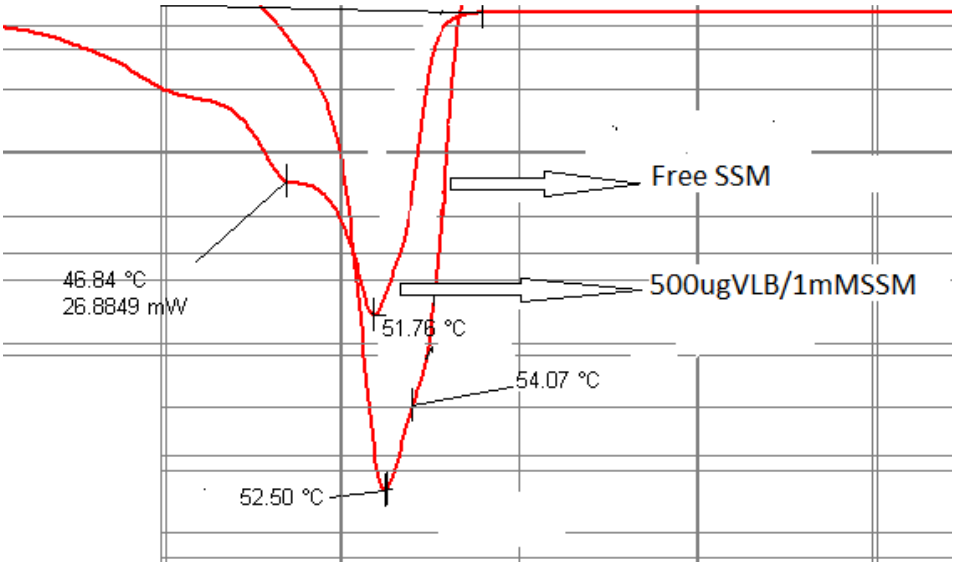

Figure 9.26: Thermogram of 500µg VLB associated with 1mM SSM in comparing with free SSM after lyophilization.

As we mentioned above the presence of drug in lipid based lamellar drug delivery systems induces partial interdigitation as it is depicted by the increase of ΔH and reduction of crystallization temperature.

9.2.11 Results of Liquid Samples

The Thermogram of the free SSM (10mM) in Buffer:

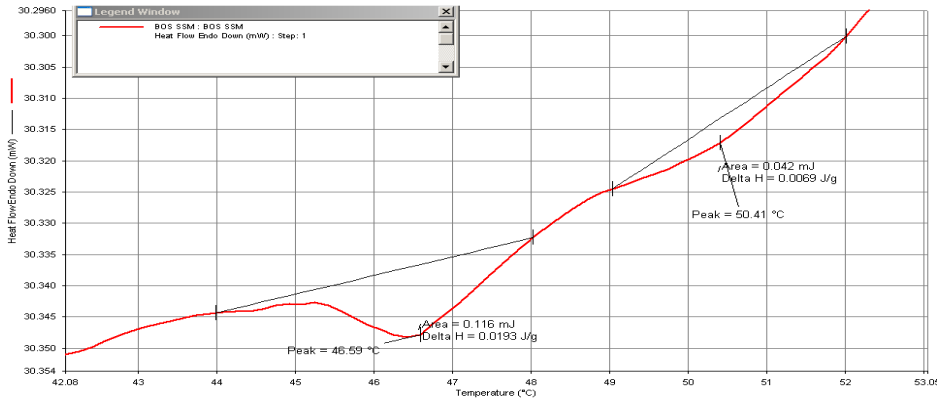

Figure 9.27: The thermogram of free SSM (10mM) in buffer.

As we mentioned on Figure **9.22** in liquid media DSPE chains are able to make stacks and we could see this at 46^{o}C as the crystallization thermogram of core part. Also there is a significant decrease in the crystallization thermogram of PEG layer. In Figure **6.4**, we showed how polymers give crystallization dip and in Figure **9.22** we saw how PEG chains are sprinkled in water and give crystallization thermogram

in lower point. Here in buffer media, obviously PEG layer is freer in comparing with its lyophilized shape and exhibits the crystallization temperature at 50^{o}C instead 52 ^{o}C and 54 ^{o}C (Figure **9.21**).

The Thermogram of 50µg VLB/1mM SSM (500µgVLB/10mM SSM) in Buffer:

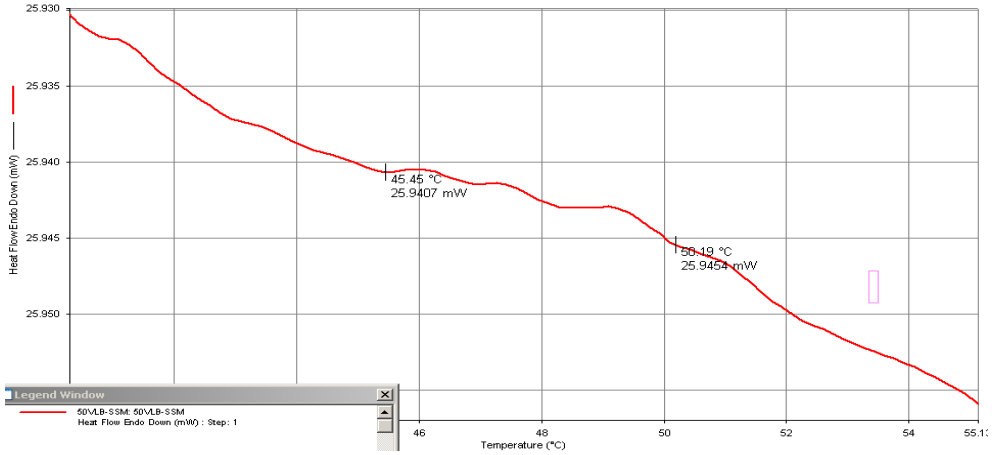

Figure 9.28: The thermogram of 50µg VLB/1mM SSM (500µgVLB/10mM SSM) in buffer.

Because of the low concentration of VLB-SSM in whole system the crystallization thermograms are not significant; we assigned the exact temperatures by following the similar points in solid samples.

There is a shift in core part from 46^{o}C to 45^{o}C which could indicate the localization of VLB in core. As we mentioned before this could be a sign of intedigitation of VLB with the DSPE layer. This is where there is no change in PEG layer's crystallization temperature and this evident confirms the localization of VLB in core not on PEG layer (50 and 50^{o}C) (Figure **9.28** and Figure **9.27**).

The Thermogram of 500µg VLB/1mM SSM (5000µgVLB/10mM SSM) in Buffer:

Using 500µg VLB gives us more significant peaks. Again when there is almost no change in PEG layer (50^{o}C in comparing with 50 and 50^{o}C) there is a shift in crystallization temperature of DSPE layer; 45^{o}C (46^{o}C in free SSM).

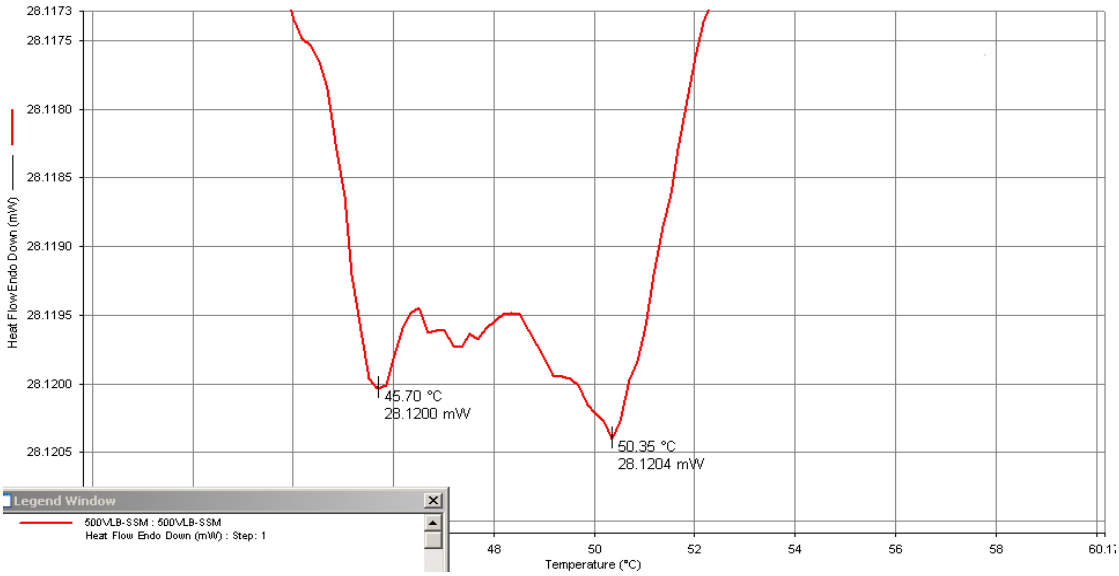

Figure 9.29: The thermogram of 500µg VLB/1mM SSM (5000µgVLB/10mM SSM) in buffer.

When we use 500µg VLB in 1mM SSM both in solid and liquid phases we obtain very good results which showes a complete incorporation of drug in SSM in core part.

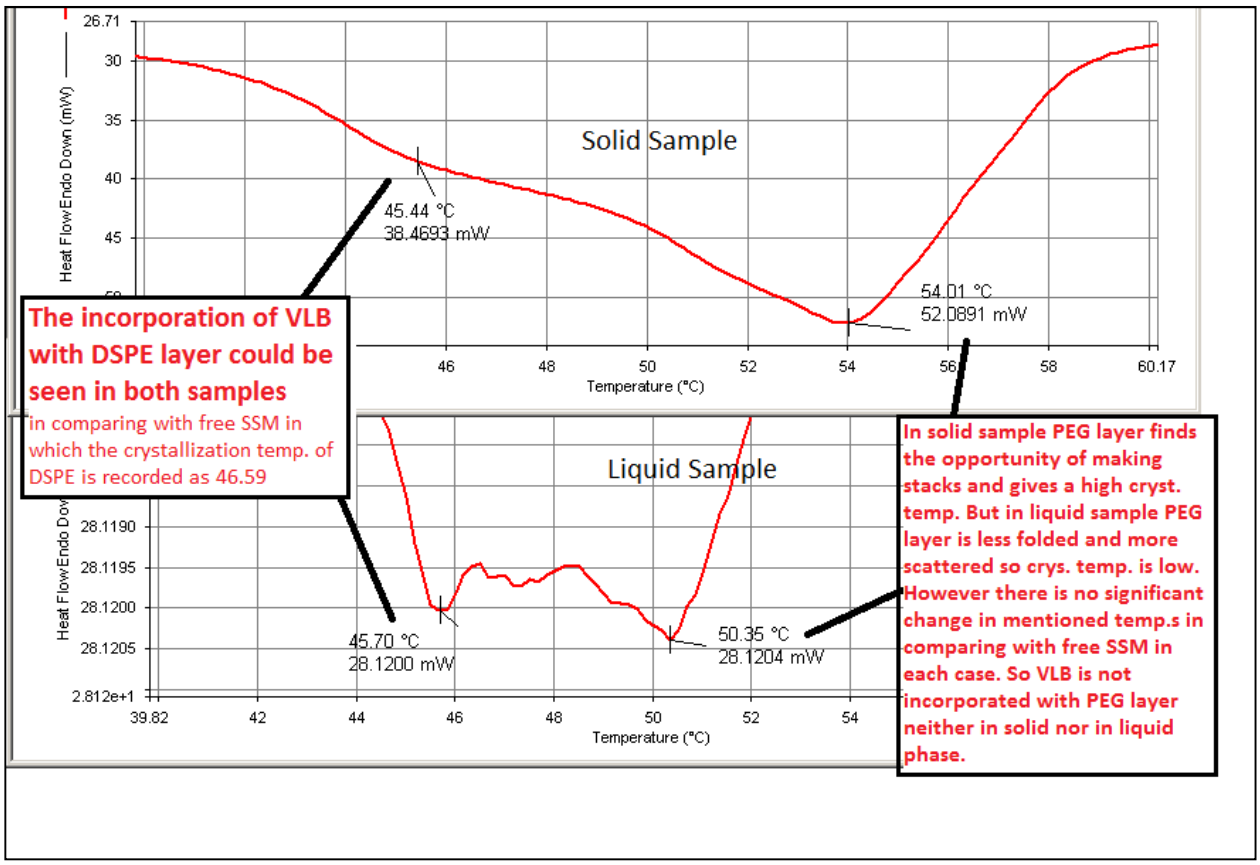

Figure 9.30: The thermogram of 500µg VLB/1mM SSM (5000µgVLB/10mM SSM) after lyophilization (solid) and in in Buffer (liquid).

The Thermogram of solid Vinorelbine:

To ensure that Vinorelbine's DSC spectrum does not interfere with SSM's thermogram, we recorded thermal behaviour of the free dug.

Interestingly no crystallization or melting point was seen in VLB's thermogram. However there was an exothermic peak at 42^{o}C which indicates the "decomposition" or "degradation"of the drug during heating.

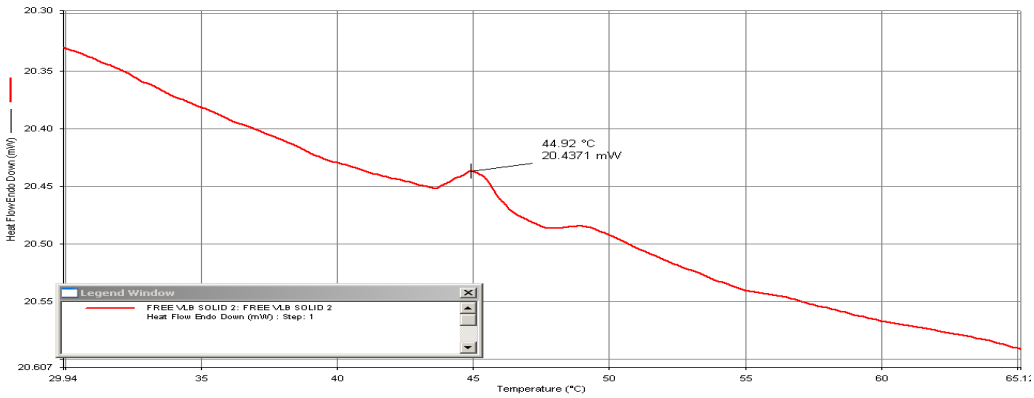

Figure 9.31: The thermogram of solid Vinorelbine.

We don't see this exothermic peak in the thermogram of VLB-SSM samples. This is probably due to the protection of the drug by the covering shell of SSM. If this assumption is correct this evidence again confirms the incorporation of VLB with core part. The settlement of VLB on shell wouldn't protect the drug from degradation and would give us the exothermic peak in all samples.

In the other hand this thermogram showes us that Vinorelbine has an amorphous compound. It is in chrystalline form neither in molecular level nor in drug delivery system.

In solid samples PEG layer finds opportunity to make stacks and gives a high crystallization temperature. But, in liquid samples PEG layer is less folded and more scattered, so crystallization temperature is lower than solid phase. However, there is no significant change in mentioned temps in comparison with free SSM in each case. So, VLB is incorporated with PEG layer neither in solid nor in liquid phase.

The DSPE layer is able to make kind of stack in water, so gives a crystallization peak around 46^{o}C. However, it seems that a kind of deformation happens in the core of micelle during the lyophilization and this event prevents the recording of DSPE crystallization peak at solid samples (after lyophilization). But, fortunately we see the

DSPE crystallization peak when we incorporate 500µg VLB with 1mM micelle both in solid and liquid phases. Probably, the interdigitation of VLB with core gives enough energy to the system and the DSPE crystallization peak shows up again in thermogram.

As a result, although we were not able to measure the exact amount of VLB incorporated with the core of SSM we successfully showed the loading of VLB to DSPE part of the micelles.

9.2.12 Results of characterization of polymeric micelles

9.2.13 Results of determination of the Critical Micelle Concentration (CMC) of polymeric micelles:

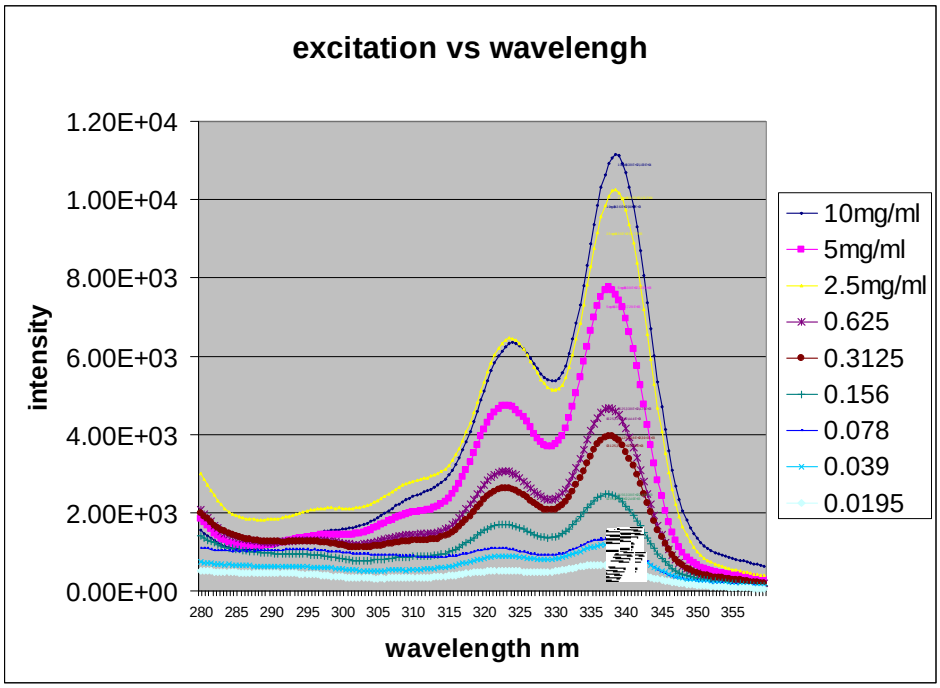

Figure 9.32: Excitation vs wavelength in determining the CMC value of Star-PCL-PEG.

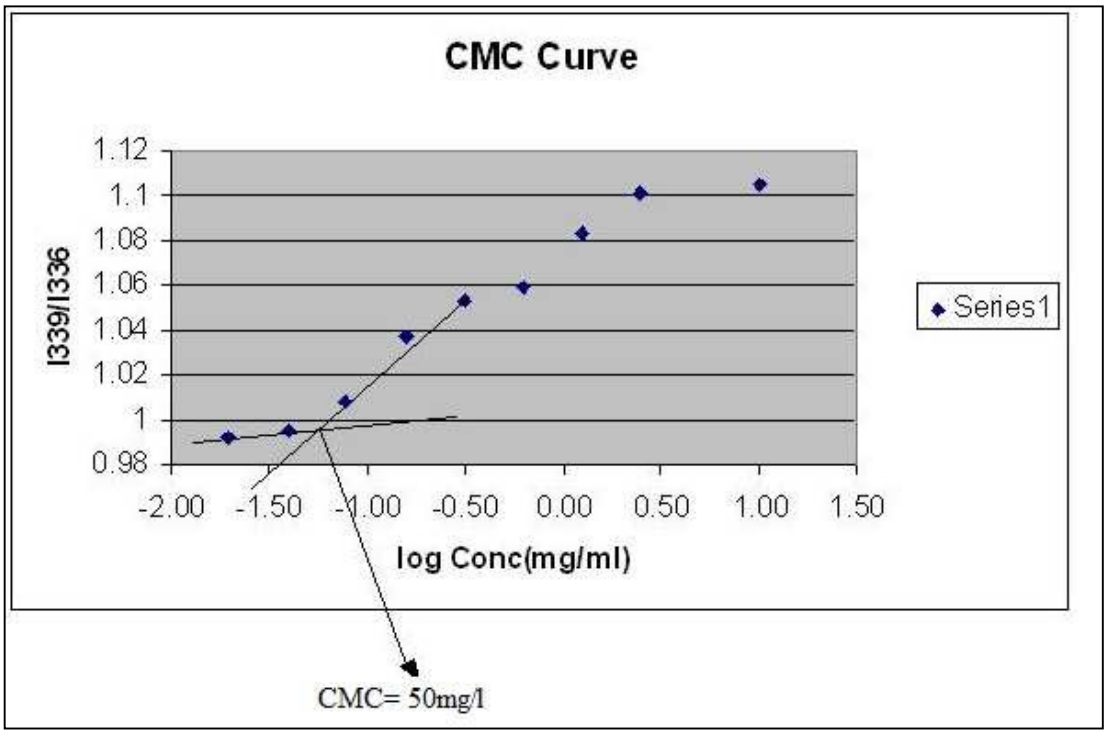

Figure 9.33:CMC graph of Star-PCL-PEG.

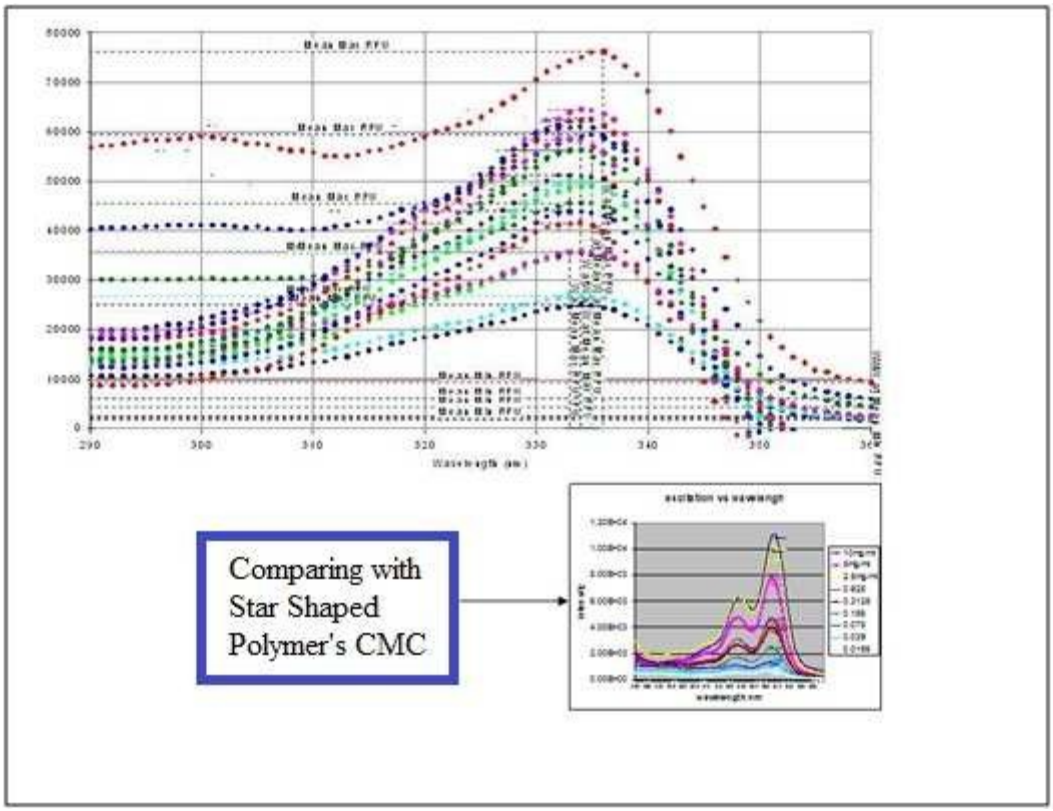

Figure 9.34: : Excitation vs wavelength in determining the CMC value of Y-Shaped-PCL-PEG.

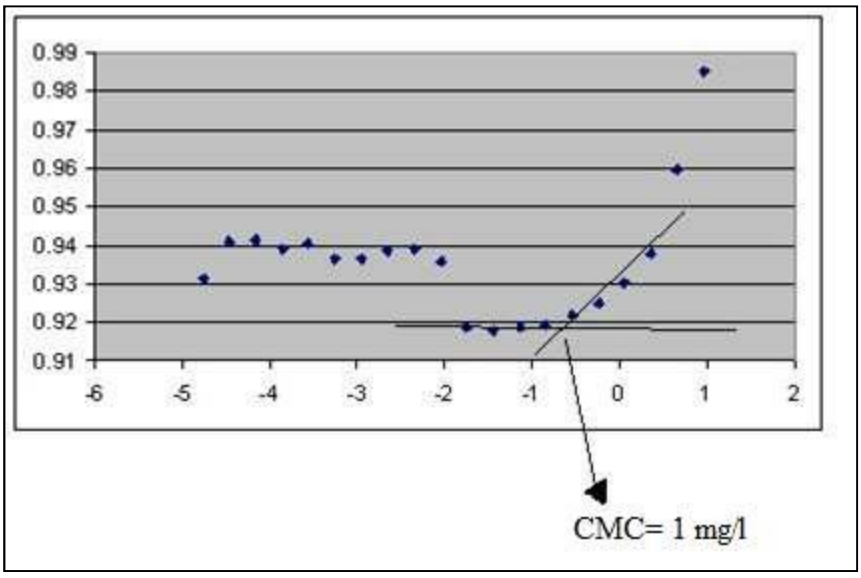

Figure 9.35: CMC graph of Y shaped-PCL-PEG.

The CMC of Star Shaped polymer has been calculated as 50mg/l which is in the borders of acceptable CMC ranges.

That was the reason we tried to synthesize the second polymer.

As we showed in synthesizing part of thesis, we used a benzene ring as dendrimer in the 4 arm star shape polymer. Probably this ring is causing a steric hindrance for unimers to get along and make micelles.

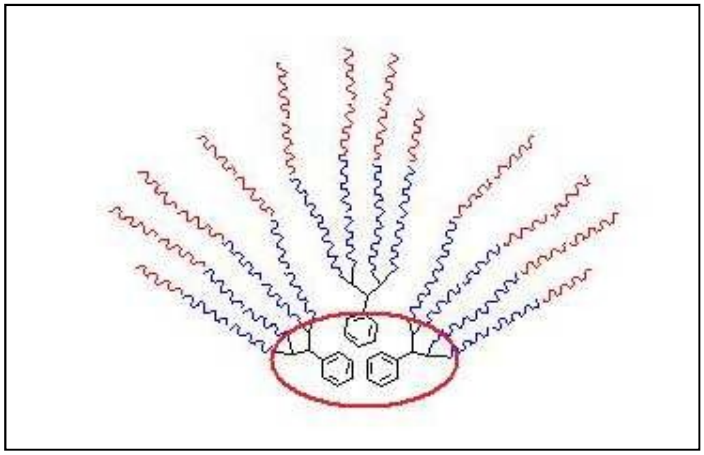

Figure 9.36: The steric hinderance in making micelles made by benzene rings.

Although this is a very sofisticated illustration, and in reality the size of benzene ring in comparing with the length of PCL and PEG parts is ignorable, we need to consider that there is no attracting force in between benzene rings and also in comparing with other polymeric micellar systems that have been reported, our unimers do not make a

network in the corona of micellar system. So we decided to synthesize a polymer with “Chain Form” corona and ended up with Y Shape PCL_2-PEG.

As it could seen the CMC of the second polymer is 1mg/l which is accepted as an excellent CMC value in previous papers.

Although the CMC is very satisfying in Y Shaped Polymer, we faced a problem with this material.

In Pyrene fluorescence of Star Shape polymer there is a point after which pyrene shows no fluorescenece. This means all pyrene molecules are aggregated and non of them are in molecular level insizde of polymeric micelle (Chattopadhyay, 1984).

In contrast the fluorescence of pyrene in micelles made by Y-Shaped polymer never goes to zero and whatever the concentration of polymer is, pyrene is giving some flourescence even under CMC point. That’s the reason the CMC graphic is that odd.

The reason of this extra ordinary behaviour of pyrene maybe is due to some aggregates that are made by Y shaped polymers under CMC. Under CMC although there is no Micellar aggregation in system there are some amorph aggregates that entrap pyrene and helps it to give fluorescence. This situation has been reported by some other groups too (Jones, 1999). This is what nedds to be confirmed by DLS assays.

9.2.14 Results of particle sizing assay of VLB-polymeric micelles formulation:

The results of DLS assay support the CMC results. The size of Star Shaped polymer is 59nm. However under CMC we have aggregations with ~250nm size.

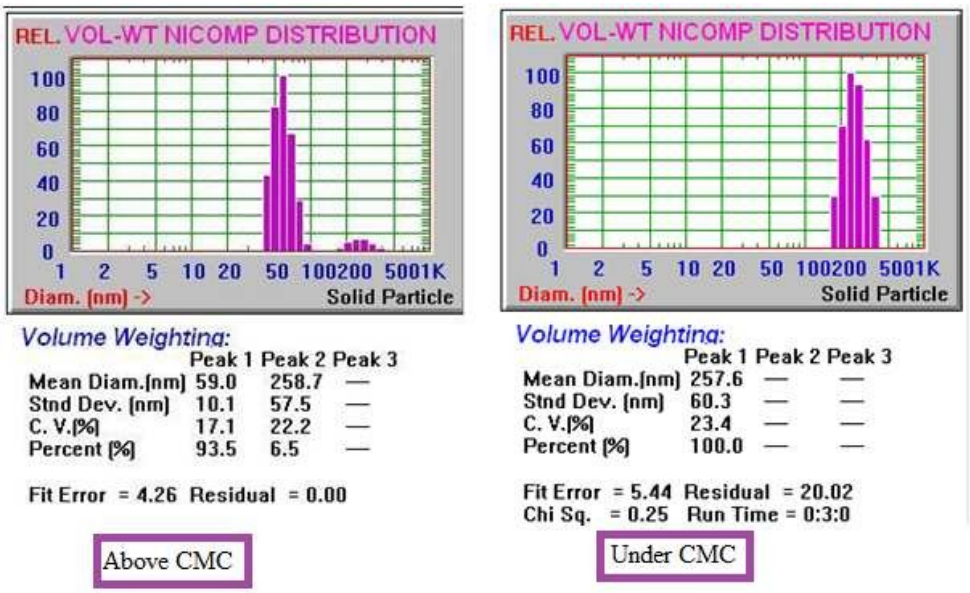

Figure 9.37: Results of DLS investigation of the size of Star-PCL-PEG.

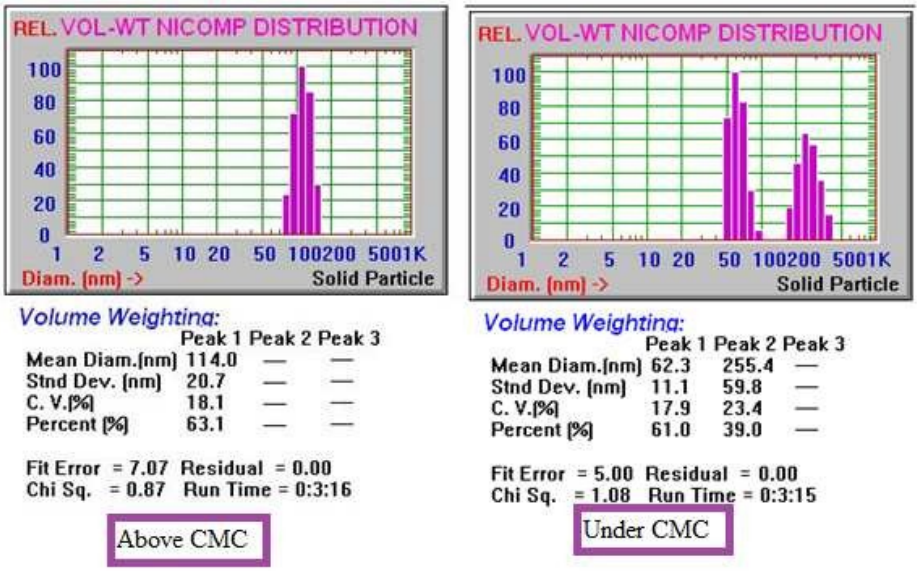

Figure 9.38: Results of DLS investigation of the size of Y shaped-PCL-PEG.

The micellar size is around 114nm and under CMC we find an aggregate at 62 and 255 nm.

9.2.15 Results of solubility of Vinorelbine (VLB) in polymeric micelles:

Dealing with polymers, we didn't face the extra ordinary solubilization case of Vinorelbine in SSM. Vinorelbine reached a certain solubility capacity in Polymeric micelles and then started making aggregates.

The rsults are as below and were similar for both polymers:

Table 9.19: Results of Solubility of Vinorelbine (VLB) in polymeric micelles.

Total VLB (ug/ml)	VLB ug/ml associated with 5mg/ml Polymer
50	50
100	100
150	150
200	200
250	250
300	250
350	250
400	150
500	150

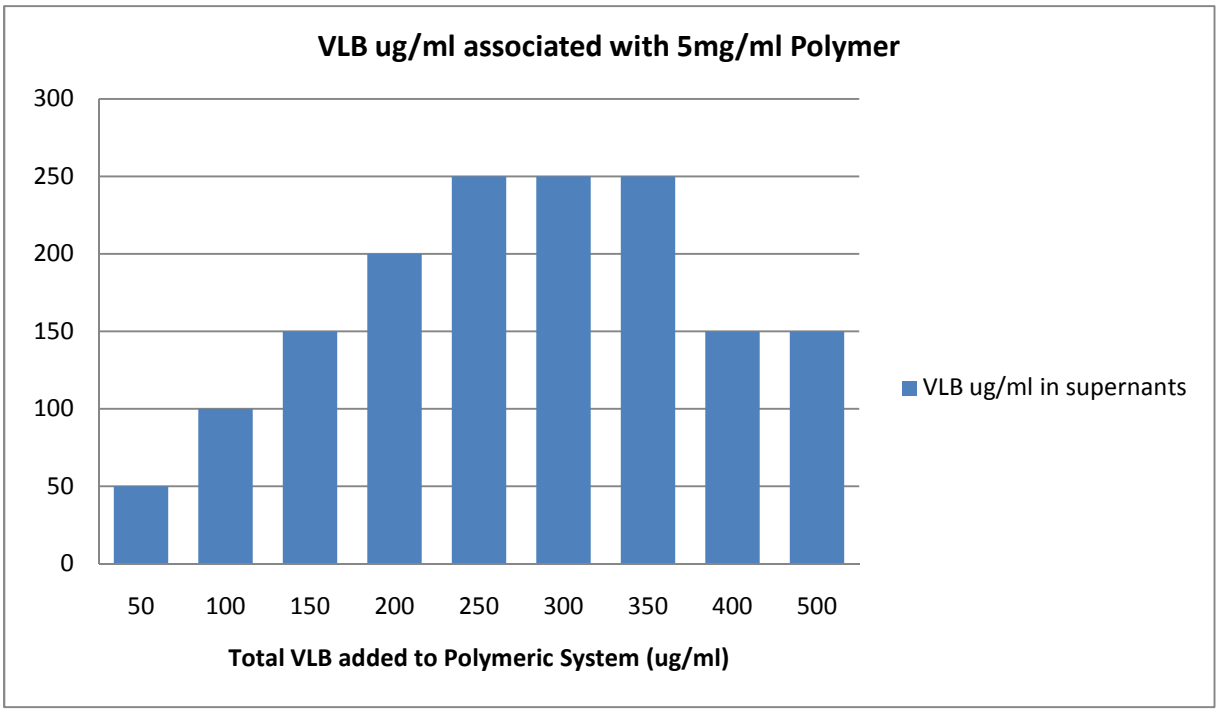

Figure 9.39: The results of determining the max. Amount of VLB carried by polymeric micelles

As a result 5mg Polymer is able to carry 250µg VLB which is equal to %5 of Polymer's mass.

Table 9.20: The comparision of mass of different drug delivery systems carrying 500µg VLB.

	SSM	**Star- PCL_4 -PEG_4**	**Y- PCL_2 -PEG**
500µg VLB is soluble in:	1mM= 2.81 mg	10 mg	10 mg

9.2.16 Results of drug release studies by dialysis of PCL-PEG-VLBs

The samples obtained from dialysis bath has been diluted using MeOH (x10) and the U.V. absorbance has been recorded by using Eliza Reader at 286nm. Since the dialysis results of two different polymers are very similar we don't report the same results twice.

Table 9.21: Results of Drug Release Studies by Dialysis of Polymeric Micelles Containing Vinorelbine (PCL-PEG-VLB).

% Release VLB/Pol micelle

Hour	%Release
0	0
0,5	10,32
1	14,35
2	16,36
3	19,68
4	25,22
6	32,23
9	38,45
12	39,67
24	42,44
48	60

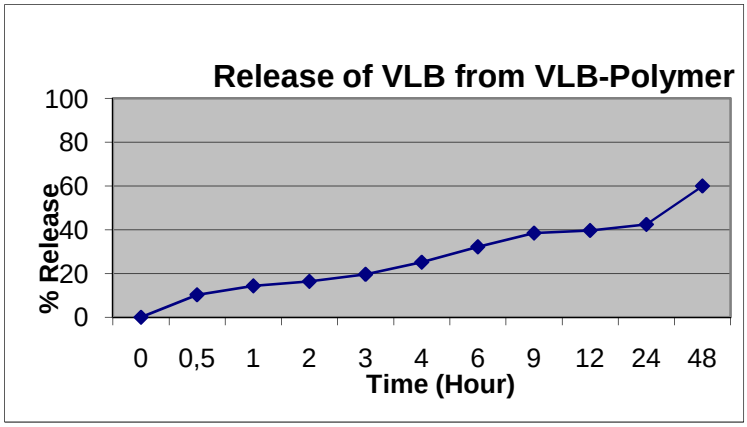

The release period of VLB-Polymer formulation is slow enough to be used in cancer tharapy by using targeted drug delivery.

9.2.17 Results of the ınvestigation of cytotoxic activity of Nano-VLB formulations:

9.2.18 VLB-SSM

Cytotoxic activity of VLB in SSM after 24 hours

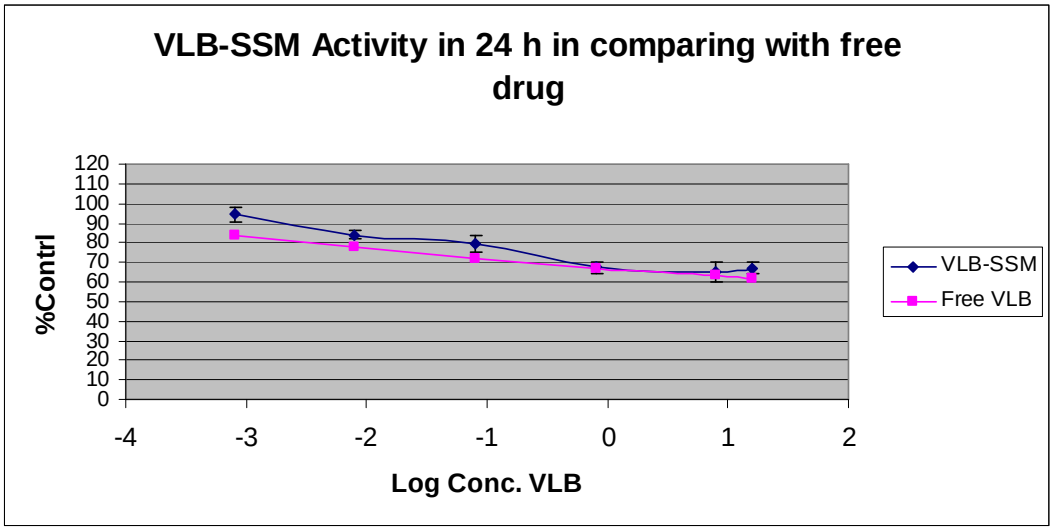

Figure 9.40: VLB-SSM cytotoxic activity after 24 h.

Table 9.22: VLB-SSM cytotoxic activity after 24 h.

VLB CONC.	% CONTROL 24h	STDV
16ug VLB/32uM (89.92ug) SSM	66.9	3.044667
8ug VLB/16uM (44,96 ug) SSM	65.24297	5.017679
0.8ug VLB/1.6uM (4,496 ug) SSM	67.18352	3.268222
0.08ug VLB/0.16 uM (0,496 ug) SSM	79.68791	4.109966
0.008ug VLB/0.016 uM (0,0496 ug) SSM	83.90033	2.155281
0.0008ug VLB/0.0016 uM (0,00496 ug) SSM	94.38791	4.00357

Cytotoxic activity of VLB in SSM after 48 hours

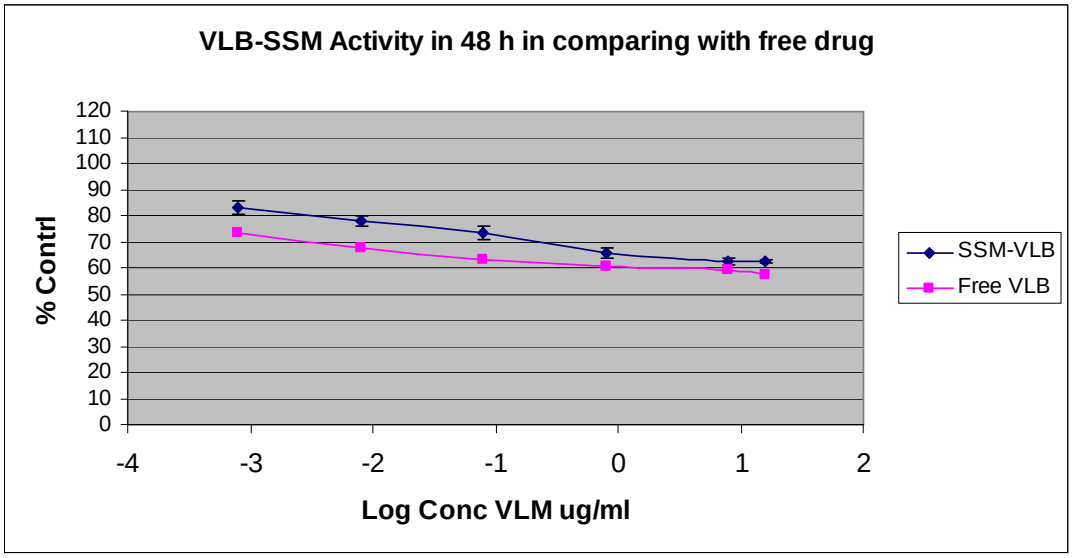

Figure 9.41: VLB-SSM cytotoxic activity after 48 h.

Table 9.23: VLB-SSM cytotoxic activity after 48 h.

VLB CONC.	% CONTROL 48h	STDV
16ug VLB/32uM (89.92ug) SSM	62.36667	0.665833
8ug VLB/16uM (44,96 ug) SSM	62.53333	1.28582
0.8ug VLB/1.6uM (4,496 ug) SSM	65.8	1.915724
0.08ug VLB/0.16 uM (0,496 ug) SSM	73.56667	2.466441
0.008ug VLB/0.016 uM (0,0496 ug) SSM	77.93333	2.11266
0.0008ug VLB/0.0016 uM (0,00496 ug) SSM	83.2	2.535744

Cytotoxic activity of VLB in SSM after 72 hours

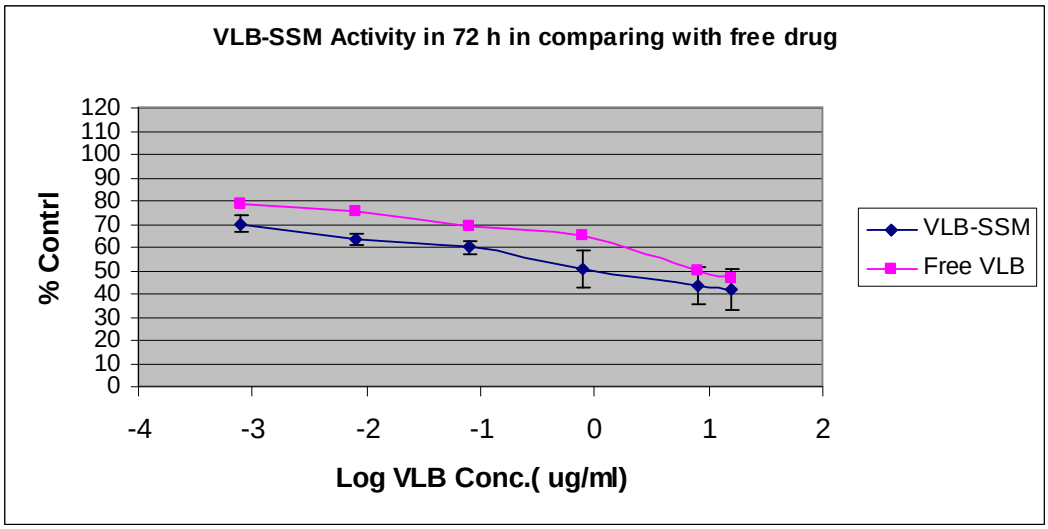

Figure 9.42: VLB-SSM cytotoxic activity after 72 h.

Table 9.24: VLB-SSM cytotoxic activity after 72 h.

VLB CONC.	% CONTROL 72h	STDV
16ug VLB/32uM (89.92ug) SSM	41.5	8.884256
8ug VLB/16uM (44,96 ug) SSM	43.5	8.019823
0.8ug VLB/1.6uM (4,496 ug) SSM	50.6	8.070239
0.08ug VLB/0.16 uM (0,496 ug) SSM	59.67853	2.790698
0.008ug VLB/0.016 uM (0,0496 ug) SSM	62.90565	2.469391
0.0008ug VLB/0.0016 uM (0,00496 ug) SSM	69.93202	3.62307

9.2.19 VLB-Y Shaped polymer

VLB-Y Shaped Polymer Cytotoxic Activity after 24 Hours

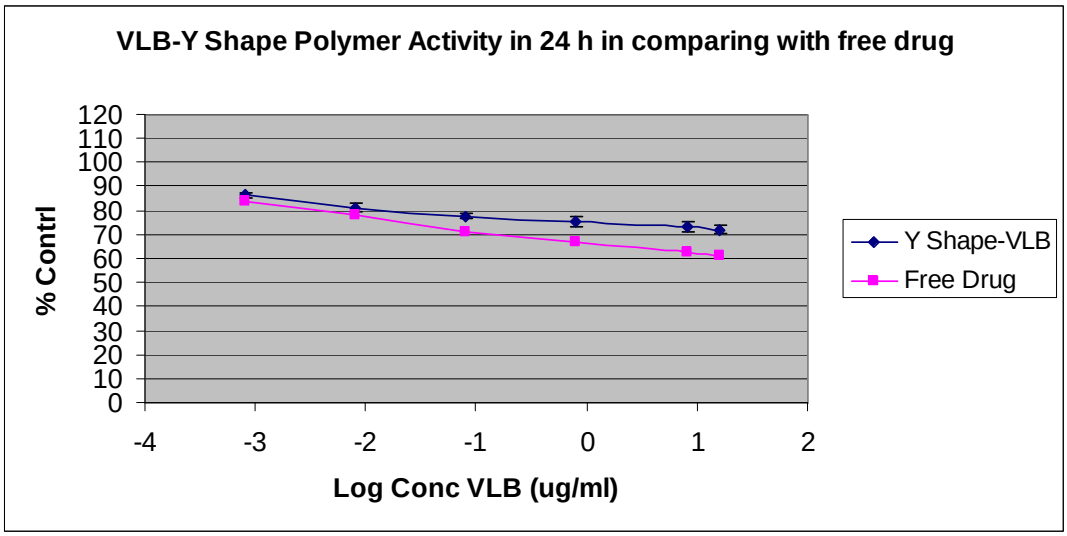

Figure 9.43: Cytotoxic activity of VLB-Y Shaped PCL-PEG polymer in 24 h.

Table 9.25: Cytotoxic activity of VLB-Y Shaped PCL-PEG polymer in 24h.

VLB CONC.	% CONTROL 24h		STDV
16ug VLB/320ug Y sh. Pol	72.31111		2.005917
8ug VLB/160ug Y sh. Pol	73.28018		1.992692
0.8ug VLB/16ug Y sh. Pol	75.54301		2.081594
0.08ug VLB/1.6ug Y sh. Pol	77.93651		0.797287
0.008ug VLB/0.16ug Y sh. Pol	81.36111		1.809108
0.0008ug VLB/0.016ug Y sh. Pol	86.53147		1.111877

VLB-Y Shaped Polymer Cytotoxic Activity after 48 Hours

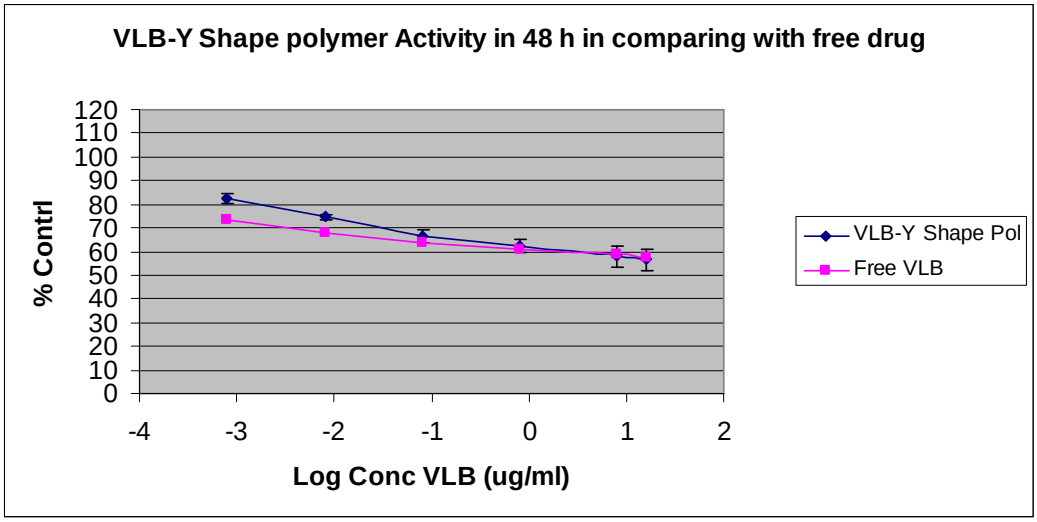

Figure 9.44: Cytotoxic activity of VLB-Y Shaped PCL-PEG polymer in 48 h.

Table 9.26: Cytotoxic activity of VLB-Y Shaped PCL-PEG polymer in 48 h.

VLB CONC.	% CONTROL 48h	STDV
16ug VLB/320ug Y sh. Pol	56.76667	4.574203
8ug VLB/160ug Y sh. Pol	58.2	4.503332
0.8ug VLB/16ug Y sh. Pol	62.14533	2.8327
0.08ug VLB/1.6ug Y sh. Pol	66.50059	2.786869
0.008ug VLB/0.16ug Y sh. Pol	74.5826	1.283188
0.0008ug VLB/0.016ug Y sh. Pol	82.71622	1.932373

VLB-Y Shaped Polymer Cytotoxic Activity after 72 Hours

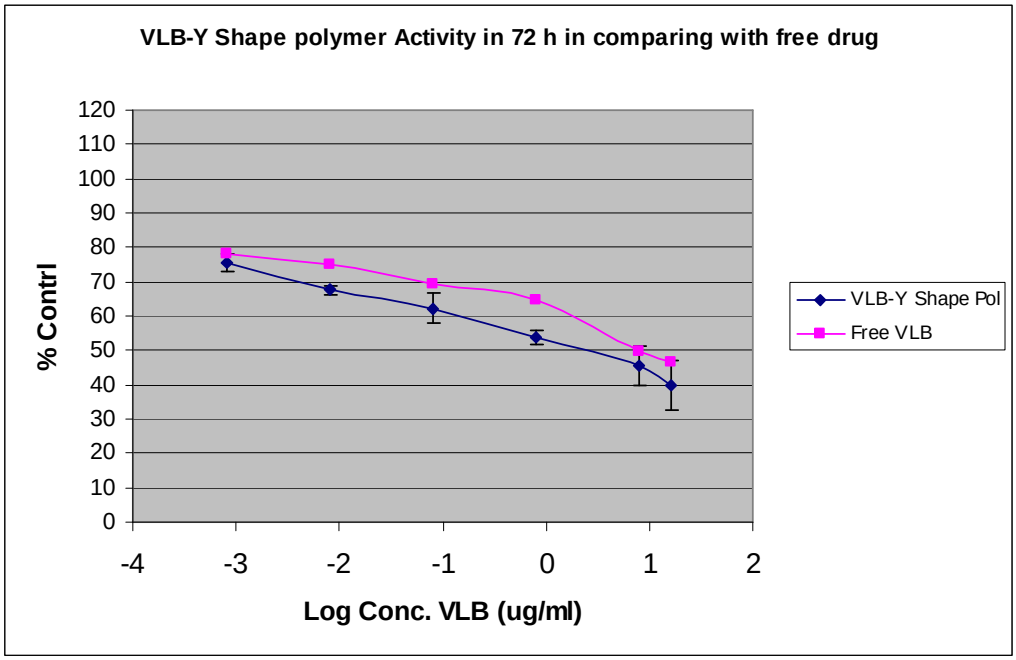

Figure 9.45: Cytotoxic activity of VLB-Y Shaped PCL-PEG polymer in 72 h.

Table 9.27: Cytotoxic activity of VLB-Y Shaped PCL-PEG polymer in 72 h.

VLB CONC.	% CONTROL 72h	STDV
16ug VLB/320ug Y sh. Pol	39.79096	7.178032
8ug VLB/160ug Y sh. Pol	45.47006	5.834016
0.8ug VLB/16ug Y sh. Pol	53.68362	2.073716
0.08ug VLB/1.6ug Y sh. Pol	62.25989	4.395596
0.008ug VLB/0.16ug Y sh. Pol	67.58418	1.358241
0.0008ug VLB/0.016ug Y sh. Pol	75.58757	2.504597

9.2.20 VLB-Star Shaped polymer

Star Shaped Polymer Cytotoxic Activity after 24 Hours

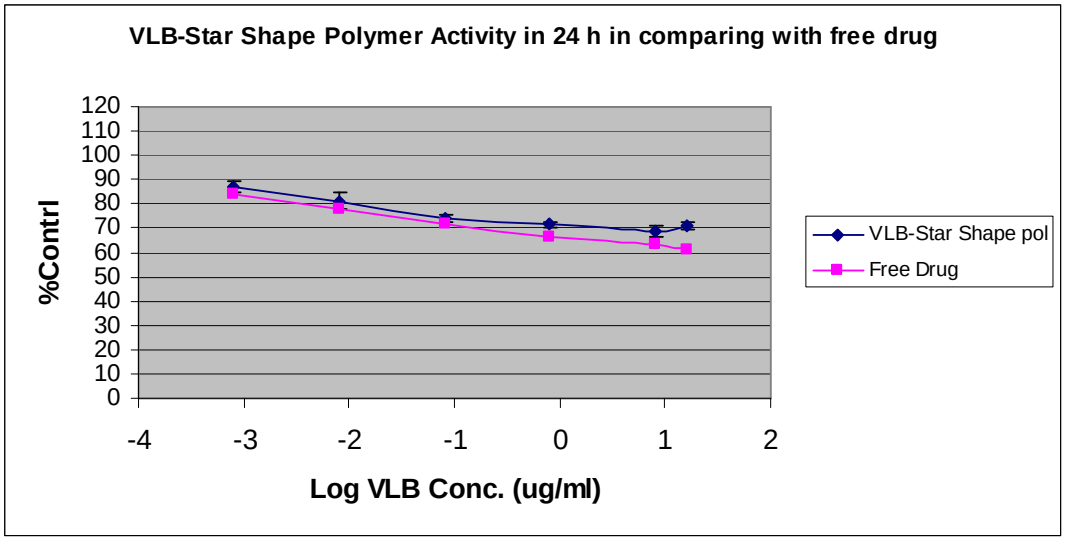

Figure 9.46: Cytotoxic activity of VLB-Star Shaped PCL-PEG polymer in 24 h.

Table 9.28: Cytotoxic activity of VLB-Star Shaped PCL-PEG polymer in 24 h.

VLB CONC.	% CONTROL 24h	STDV
16ug VLB/320ug Star sh. Pol	71.13333	1.41892
8ug VLB/160ug Star sh. Pol	69.03333	2.182506
0.8ug VLB/16ug Star sh. Pol	71.5	1.322876
0.08ug VLB/1.6ug Star sh. Pol	74.16667	1.607275
0.008ug VLB/ 0.16ug Star sh. Pol	81.06667	3.426855
0.0008ug VLB/0.016ug Star sh. Pol	87.3	2.306513

Star Shaped Polymer Cytotoxic Activity after 48 Hours

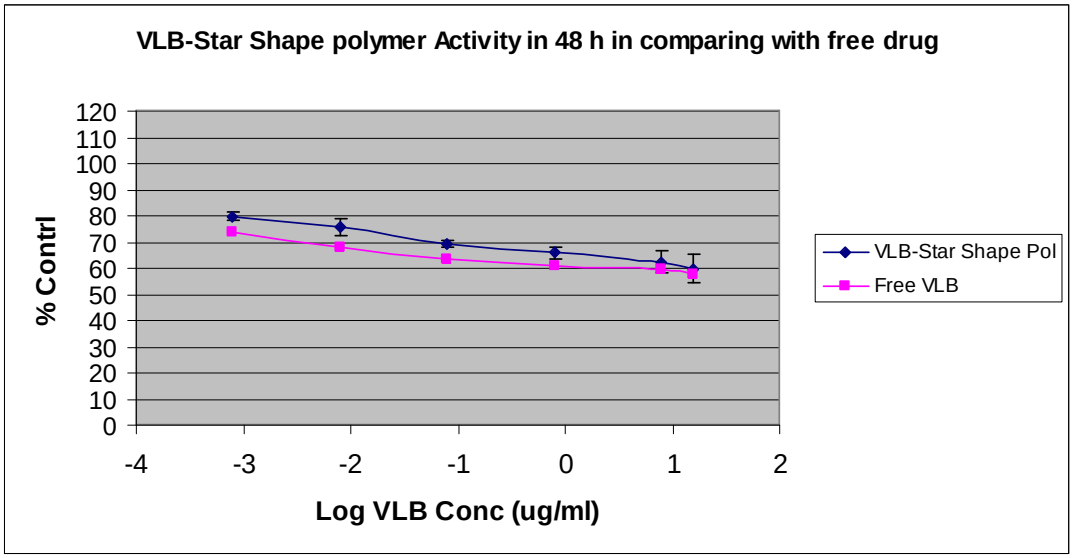

Figure 9.47: Cytotoxic activity of VLB-Star Shaped PCL-PEG polymer in 48 h.

Table 9.29: Cytotoxic activity of VLB-Star Shaped PCL-PEG polymer in 48 h.

VLB CONC.	% CONTROL 48h		STDV
16ug VLB/320ug Star sh. Pol	59.6		5.670979
8ug VLB/160ug Star sh. Pol	62.2		4.084116
0.8ug VLB/16ug Star sh. Pol	65.48889		2.542382
0.08ug VLB/1.6ug Star sh. Pol	69.1		1.4
0.008ug VLB/ 0.16ug Star sh. Pol	75.46667		3.233162
0.0008ug VLB/0.016ug Star sh. Pol	79.53333		1.501111

Star Shaped Polymer Cytotoxic Activity after 72 Hours

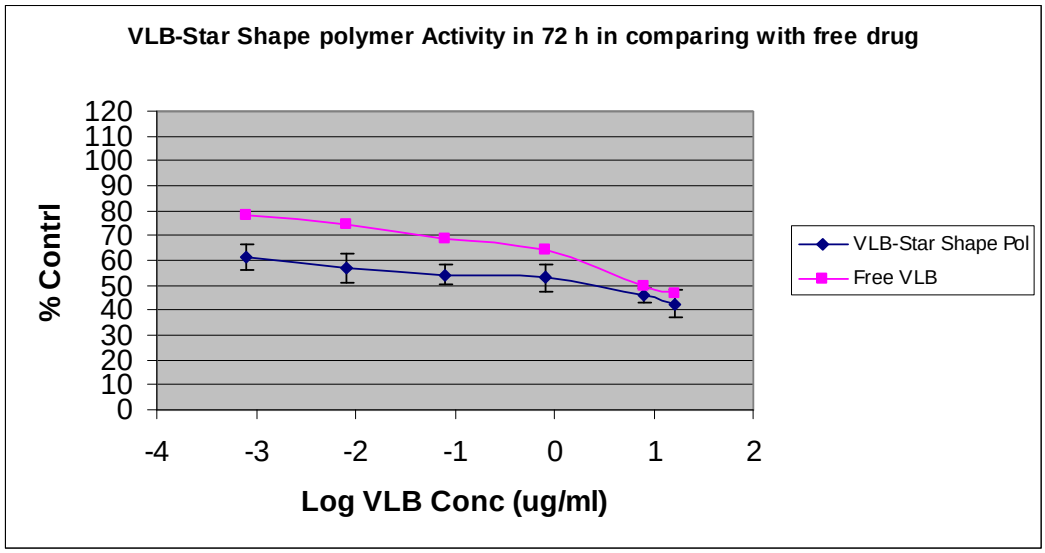

Figure 9.48: Cytotoxic activity of VLB-Star Shaped PCL-PEG polymer in 72 h.

Table 9.30: Cytotoxic activity of VLB-Star Shaped PCL-PEG polymer in 72 h.

VLB CONC.	% CONTROL 48h		STDV
16ug VLB/320ug Star sh. Pol	42.8		5.8
8ug VLB/160ug Star sh. Pol	46		2.73913
0.8ug VLB/16ug Star sh. Pol	53.2		5.694212
0.08ug VLB/1.6ug Star sh. Pol	54.5		3.814149
0.008ug VLB/ 0.16ug Star sh. Pol	57.2		5.642694
0.0008ug VLB/0.016ug Star sh. Pol	61.37391		5.301546

VLB in %10 DMSO after 24 h

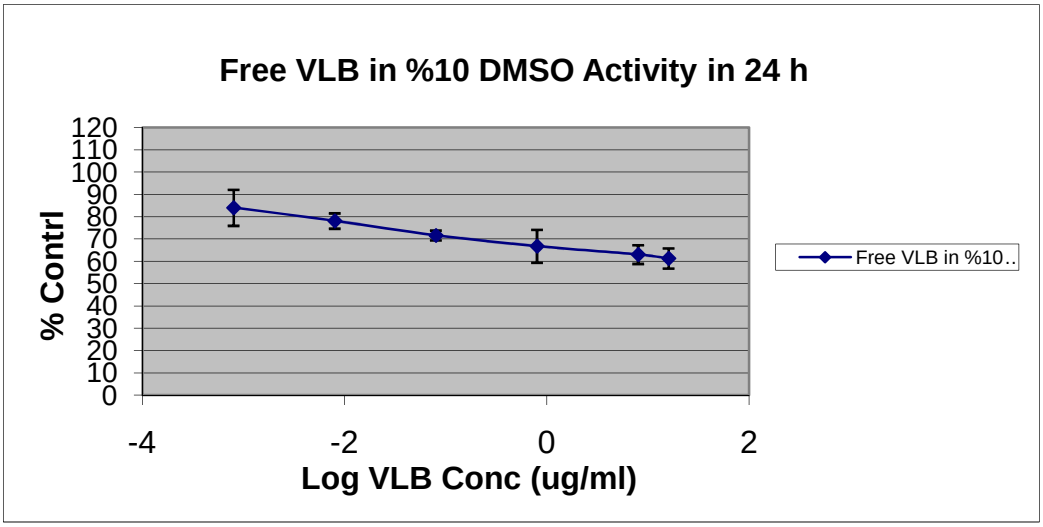

Figure 9.49: Cytotoxic activity of free VLB in 24h.

Table 9.31: Cytotoxic activity of free VLB in 24h.

VLB CONC.	% CONTROL 48h		STDV
16ug VLB/%10 DMSO	61.34534		4.544604
8ug VLB/%10 DMSO	63.09525		4.193084
0.8ug VLB/%10 DMSO	66.84642		7.373908
0.08ug VLB/%10 DMSO	71.64132		2.183458
0.008ug VLB/%10 DMSO	78.14511		3.433965
0.0008ug VLB/%10 DMSO	84.07831		8.065308

VLB in %10 DMSO after 48 h

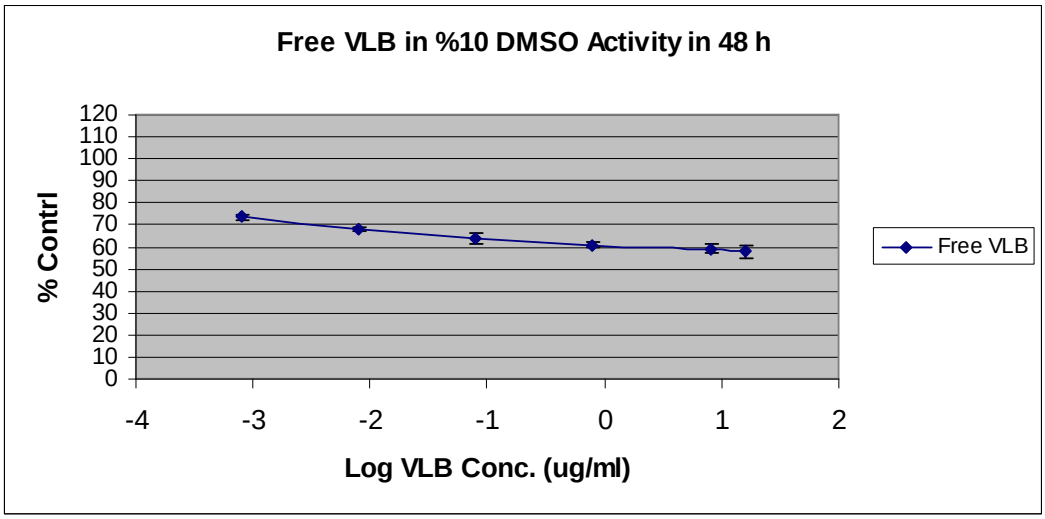

Figure 9.50: Cytotoxic activity of free VLB in 48h.

Table 9.32: Cytotoxic activity of free VLB in 48h.

VLB CONC.	% CONTROL 48h		STDV
16ug VLB/%10 DMSO	36.74044		3.160696
8ug VLB/%10 DMSO	51.11143		2.177919
0.8ug VLB/%10 DMSO	67.24581		1.270171
0.08ug VLB/%10 DMSO	69.53089		2.615977
0.008ug VLB/%10 DMSO	70.44066		0.80829
0.0008ug VLB/%10 DMSO	70.04371		1.305118

VLB in %10 DMSO after 72 h

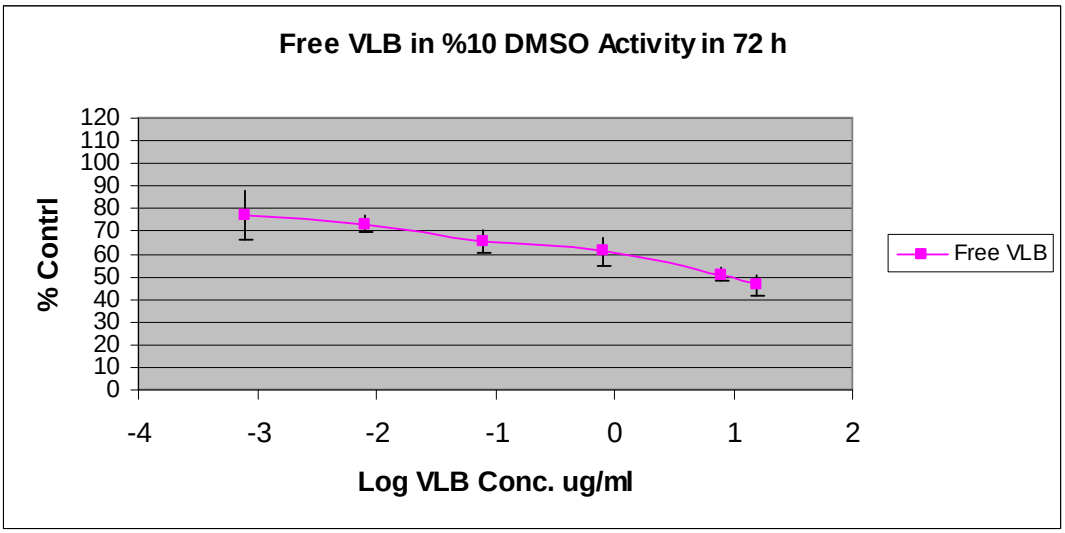

Figure 9.51: Cytotoxic activity of free VLB in 72h.

Table 9.33: Cytotoxic activity of free VLB in 72h.

VLB CONC.	% CONTROL 72h		STDV
16ug VLB/%10 DMSO	46		4.71593
8ug VLB/%10 DMSO	50.6		2.986637
0.8ug VLB/%10 DMSO	61		6.237788
0.08ug VLB/%10 DMSO	65.66667		5.040172
0.008ug VLB/%10 DMSO	72.93333		3.682843
0.0008ug VLB/%10 DMSO	77.2		10.78518

Controls:

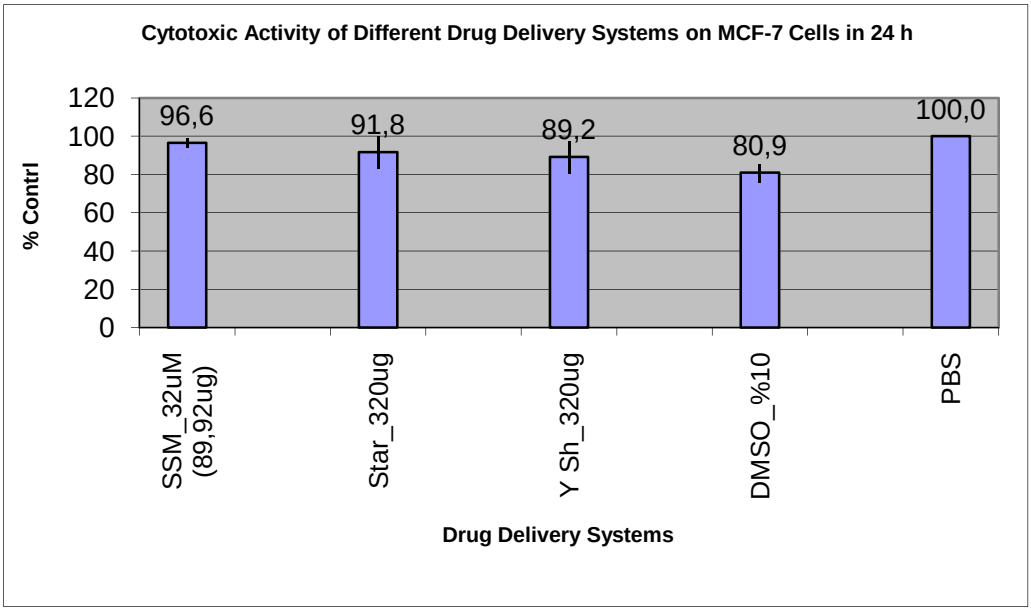

Figure 9.52: Cytotoxic activity of different drug delivery systems on MCF-7 in 24 h.

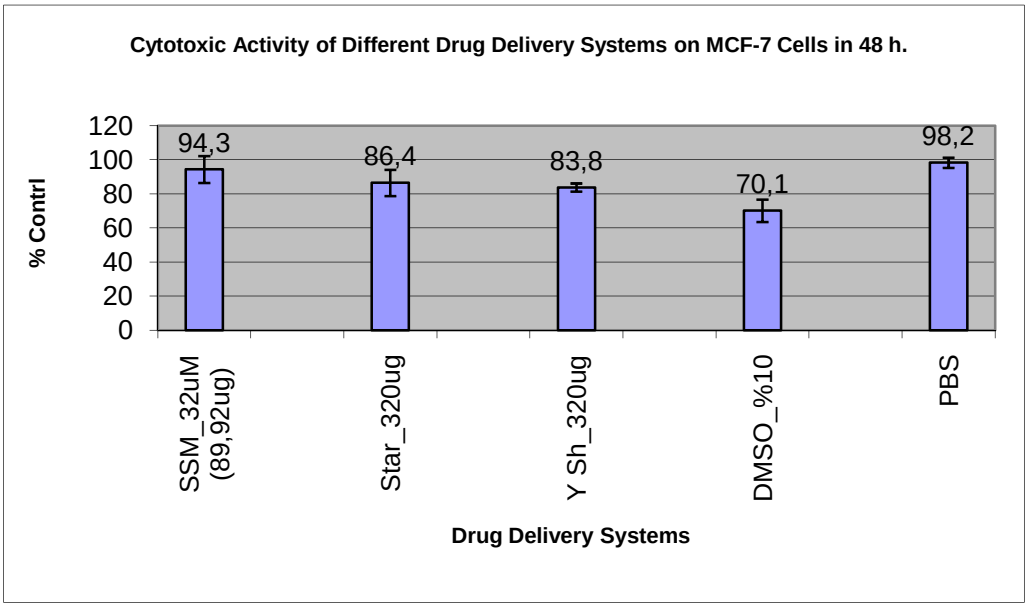

Figure 9.53: Cytotoxic activity of different drug delivery systems on MCF-7 in 48 h.

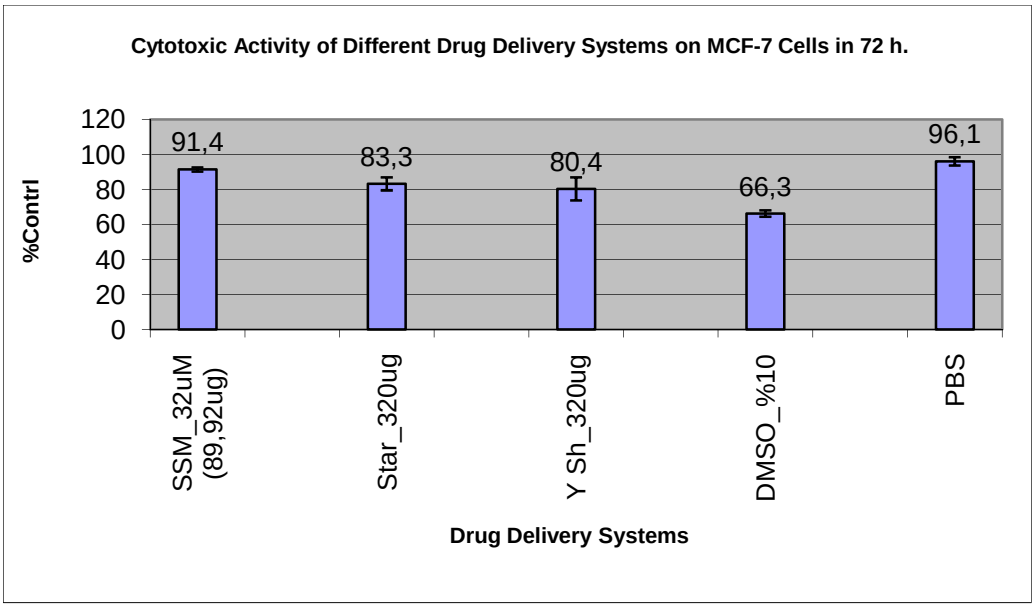

Figure 9.54: Cytotoxic activity of different drug delivery systems on MCF-7 in 72 h.

Determination of IC_{50} of 3 Different Formulations of Vinorelbine in 72 h.

Table 9.34: Determining IC50 of 3 different formulations of Vinorelbine in 72 h.

Formulation	IC50	STDV
Free VLB	8.127951	0.71593
VLB-SSM	1.199619	0.309321
VLB-Y Shaped Pol	1.956646	0.5907
VLB- Star Shaped Pol	1.337767	0.4173

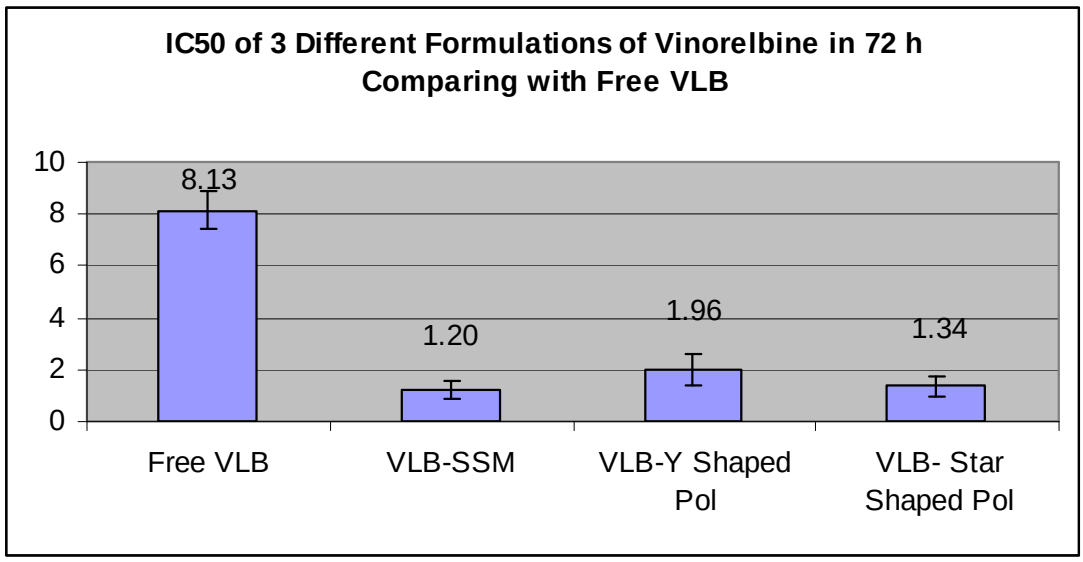

Figure 9.55: IC50 of 3 different formulations of Vinorelbine in 72 h in comparing with free VLB.

Cytotoxic Activity Discussion:

The cytotoxic activity of different Nano-formulations of Vinorelbine shows improvement comparing with Free Vinorelbine. This improvement is %85.24 for VLB-SSM, %75.92 for VLB-Y Shape Pol. and %83.54 for VLB-Star Shape Pol.

10. CONCLUSION AND RECOMMENDATIONS

10.1 Conclusion of Results Obtained from Plant Analysis*:*

In this study we report the isolation and structure elucidation of *Vinca* alkaloids obtained from Turkish *Vinca* species which consist of Vallesiachotamine, α-Yohimbine, β-Yohimbine, Picrinine from *Vinca soneri*, Vallesiachotamine and iso-Vallesiachotamine from *Vinca minor,* and 11-Hydroxypolyneuridine was isolated as a new compound from *Vinca major*. The fourth species growing in Turkey is *V. herbacea,* our investigation on it afforded Indole alkaloids, 10-Methoxyraucaffrinoline, 11-Methoxyburnamine, Picrinine, Burnamine, Caboxine A and Elegantine. Our results on the study of *V. herbacea* has been just published in 2011 (Boğa et al.).

Since *Vinca soneri* has newly been introduced to the world of science by Turkish scientists (Koyuncu, 2011) it was important to confirm the relationship of this species to *Vinca* L. Because α- Yohimbine and β-Yohimbine are being reported for the first time from a *Vinca* species. This could be an evidence for the novelity of *V. soneri* which differed from other *Vinca* species while the presence of Picrinine which is a common chemical constituent of *Vinca* species, also found in the other three species investigated in this study,l verified that the species *soneri* should belong to the genus *Vinca* L.

The synthesis of yohimbine derivatives have attracted a significant attention (Brown, 2000; D. J. Mergott & Jacobsen, 2005; D. J. Z. Mergott, S. J.; Jacobsen, E. N., 2008; Mustafa, 2005; Yoshino, 2008) due to their aphrodisiac and CNS stimulant activity. Early studies suggest that the alkaloid stimulated the respiratory center in small doses, while depressed respiration in large doses. It is generally considered an α_2-adrenergic blocking agent. According to Goodman and Gilman, the activity of Yohimbine may arise from being an relatively selective inhibitor of α_2-adrenergic receptors, enhancing neural release of norepinephrine at concentrations less than those required to block postsynaptic α_1 receptor. Yohimbine also blocks peripheral 5-HT receptors. Aphrodisiac activity has also been attributed to the enlargement of

blood vessels in the genitalia, transmission of nerve impulses to genital tissue, and an increased reflex excitability in the sacral region of the spinal cord. Yohimbine is also reported as a monoamine oxidase inhibitor; it also possesses a weak calcium channel blocking effect (Wiley-Blackwell, 2010).

So, the newly introduced plant *Vinca soneri* could be presented as a new source of Yohimbine derivatives and could further be used in biological and chemical assays.

10.2 Conclusion of Results Obtained from Synthesis and Characterization of nano-Vinorelbine (nao-VLB) Formulations

In this study we report synthesis and characterization of three different nano-VLB formulations. Vinorelbine is a dimeric *Vinca* alkaloid and is a chemotherapeutic agent which is used in the treatment of non-small cell lung cancer and breast cancer 0, p.71). This agent has numerous side effects (Chapter 5.4, p.74), therefore we have prepared nano-VLB formulations by uploading Vinorelbine to the micellar drug delivery systems. By this way, we will be able to target cancer tumors and this will cause a reduction in the side effects of commercially available Vinorelbine (4.2, p.36, Chapter 4.10, p.66).

It is important to prepare a formulation which has the appropriate size, not detectable by MPS, with a prolonged release period, enhancing cytotoxic effect in comparision with free Vinorelbine and is not toxic to the healthy cells, as well (4.4 p: 48, Chapter 4.5, p: 51, Chapter 4.6 p:53, Chapter 4.7 p:55, Chapter 4.8 p:59, Chapter 4.9, p: 64 and Chaper 4.10, p: 66).

We then prepared three different nano-VLB formulations all of which form micelles in aqueous systems;

1-VLB-SSM Formulation (Chapter 4.3.3, p:45), Sterically Stabilized Micelles are well known targeted drug delivery systems with a very low CMC value (1µM) (Chapter 4.3.3, p:45). Their size is ~15 nm (Chapter 4.3.3, p:45), and by uploading of the drug the size is reduced to ~11nm 8.1.11, p:108). The most stable formulation was found to be 500µgVLB/1mM SSM formulation. In this formulation, release period is long enough (%35.7 release after 90h) (Chapter 8.1.16 p: 113) to be effective in cancer side. We also showed that it is stable enough after lyophilization without using any surfactant which is suitable to store for a certain period 8.1.15, p:112). And lastly VLB-SSM formulation has a cytotoxic activity ~6.7 times better

than free VLB. Together with all of these results by using DLS and DSC we came into a conclusion that VLB settles in the core of sterically stabilized micelle in between 2 DSPE units and this property gives an extra ordinary stability to the formulation (9.2.9, p:145). There is always a second possibility that must be concidered. Sometimes the existance of a latent aggregate in the system causes a shift in the size diagram of particles. In our results, it is possible that VLB is making it's own micelles (or soluble aggregates) and this floating aggregates are pushing the DSPE-PEG2000 micells' size daigram to left and results in the sizing them as 11-12 nm.

By using centrifuge assays, we showed that this hypothesis does not really come true. However we could discard the possibility of presence of latent aggregates in the system by choosing the 500 µg VLB/ 1mM SSM as the most stable formulation in which there is no decrease in size of micelles.

2- VLB-star shape PCL_4-PEG_4 (VLB-Star Poly) and 3- VLB-Y shape PCL_2-PEG (VLB-Y Poly) formulations: While PCL and PEG are very well known biodegradable materials, the synthesis and structure of the unimers are completely new 8.1.1, p:95). We measured the CMC value of VLB-Star Poly and VLB-Y Poly as 50mg/L and 1mg/L, respectively. Both are acceptable values for polymeric nano drug delivery systems. However, the latter CMC value is ideal for a targeted drug delivery system 9.2.13, p:154). The size of these two micelles are 59 nm for VLB-Star Poly and 114 nm for VLB- Y Poly. Both micelles exhibited to have acceptable sizes to achieve passive targeting (Chapter 4.3.1, p:43). However, both polymers are making aggregates under CMC value which is considered as a handicap for drug delivery systems, because the pharmacokinetic of aggregates would be completely different from micelles. Both polymeric micelles are able to carry VLB maximum in an amount equal to 5% of polymer weight (5% VLB/95%Pol (w/w)). The release period is sufficient (%60 release in 48h), but is not as long as VLB-SSM formulation. Cytotoxic activity of VLB-Poly formulations are enhanced in comparing to the free VLB (~ 4.1 times for VLB-Y Poly and ~6 times enhancement for VLB- Star Poly) (Chapter 9.2.19-9.2.20 and p:184).

As a conclusion, although the characterization of all nano-VLB formulations revealed sufficient results, the best results are obtained by VLB-SSM formulation which might be due to the lipophilicity of Vinorelbine (Koukoulitsa, 2006). This

property causes a high affinity of drug to the sterically stabilized micelles which is the main reason of high solubility, prolonged release and a better cytotoxic activity of VLB-SSM formulation.

REFERENCES

Ahuja, S., & Dong, M. W. 2005. *Handbook of pharmaceutical analysis by HPLC*: Elsevier Academic Press.

Ahuja, S., & Rasmussen, H. 2007. *HPLC method development for pharmaceuticals*. Amsterdam; Boston: Elsevier, Academic Press.

Alkanonyuksel, H. R., S.; Chai, H. B.; Pezzuto, J. M. 1994. A mixed micellar formulatıon suitable for the parenteral administration of taxol. *Pharmaceutical Research, 11*(2), 206-212.

Allahverdiyev, A. D., N.; Ozguven, M.; Koltas, S. 2004. Antiviral activity of the volatile oils of Melissa officinalis L. against Herpes simplex virus type-2. *Phytomedicine, 11*(7-8), 657-661.

Allen, T. M. H., C.; Martin, F.; Redemann, C.; Yauyoung, A. 1991. Liposomes Containing Synthetic Lipid Derivatıves Of Poly(Ethylene Glycol) Show Prolonged Circulatıon Half-Lives Invivo. [Article]. *Biochimica Et Biophysica Acta, 1066*(1), 29-36.

Arbain D, B. L., Putra MM, Sargent MV, Syarif M.1992. A new glucoalkaloid from Uncaria glabrata. *J Chem Soc Perkin Trans, 1*, 665-667.

Arleth, L. A., B.; Onyuksel, H.; Thiyagarajan, P.; Hjelm, R. P. 2005. Structure and growth behavior of hairy mixed micelles formed by pegylated and non-pegylated phospholipids in aqueous media. [Meeting Abstract]. *Abstracts of Papers of the American Chemical Society, 229*, U662-U662.

Ashok, B., Arleth, L., Hjelm, R. P., Rubinstein, I., Onyuksel, H. 2004. In vitro characterization of PEGylated phospholipid micelles for improved drug solubilization: Effects of PEG chain length and PC incorporation. *Journal of Pharmaceutical Sciences, 93*(10), 2476-2487. doi: 10.1002/jps.20150

Atta-ur-rahman, S., A. Nighat, F. Bhatti, M. K. Kurucu, S. Kartal, M. 1995. Alkaloids from *Vinca major*. *Phytochemistry, 38*(4), 1057-1061.

Baraton, M. I. 2003. *Synthesis, Functionalization and Surface Treatment of Nanoparticles, .* California American Science Publishers.

Batista, C. V. F. S., J.; Verpoorte, R.; Rech, S. B.; Henriques, A. T. 1996. Indole alkaloids from Rauwolfia sellowii. *Phytochemistry, 41*(3), 969-973.

Bhattach.J, & Pakrashi, S. C. 1972. Elegantine, a new oxindole alkaloid from *Vinca-elegantissima* hort .27. *Tetrahedron Letters*(2), 159-&.

Birdi, K. S. 1997. *Handbook of Surface and Colloid Chemistry*. Boca Raton, FL.: CRC Press.

Boğa, M., Kolak, U., Topçu, G., Bahadori, F., Kartal, M., & Farnsworth, N. R. ,2011. Two new indole alkaloids from Vinca herbacea L. *Phytochemistry Letters*4/4, Under Press.

Bolzani VS, Y. M., Furlan M, Cavalheiro AJ, Araújo AR, Silva DHS, Lopes MN 2001. Secondary metabolites from Brazilian Rubiaceae plant species: Chemotaxonomical and biological significance. *Recent Res Devel Phytochem 5*, 19-31.

Boulikas, T. T., L. 2008. Microtubule-targeted antitumor drugs: chemistry, mechanisms and nanoparticle formulations. *Gene Therapy and Molecular Biology, 12*, 313-357.

Brown, R. T. P., S. B.; Richards, P. 2000. Enantiospecific synthesis of (-)-3-iso-19,20-dehydro-beta-yohimbine from secologanin: a route to normal and pseudo stereoisomers of yohimbine. *Tetrahedron Letters, 41*(30), 5627-5630.

C. Lizano, V. W., V. P. Torchilin, P. Sancho, A. I., & Garc´ıa-P´erez, a. M. P. 2003. In vivo biodistribution of erythrocytes and polyethyleneglycol-phosphatidylethanolamine micelles carrying the antitumour agent dequalinium. *European Journal of Pharmaceutics and Biopharmaceutics, 56*, 153–157.

Champion, J. A., & Mitragotri, S. 2006. Role of target geometry in phagocytosis. *Proceedings of the National Academy of Sciences of the United States of America, 103*(13), 4930-4934.

Chang, D. L., C.T.; Wu, C. H.; Wu, H. C. 2009. A Novel Peptide Enhances Therapeutic Efficacy of Liposomal Anti-Cancer Drugs in Mice Models of Human Lung Cancer. *PLoS ONE, 4*(1), e4171.

Chattopadhyay, A. L., E. 1984. Fluorımetrıc determınatıon of crıtıcal micelle concentratıon avoidıng ınterference from detergent charge. *Analytical Biochemistry, 139*(2), 408-412.

Cho, Y. W. L., J.; Lee, S. C.; Huh, K. M.; Park, K. 2004. Hydrotropic agents for study of in vitro paclitaxel release from polymeric micelles. *Journal of Controlled Release, 97*(2), 249-257.

Cordell, G. A. 1981. *Introduction to Alkaloids, A Biogenetic Approach*. N.Y.: Wiley Interscience Publications

Cosgrove, T. 2005. *Colloid Science: Principles, Methods and Applications*. Blackwell, Oxford, UK.

Dagar, S. K., A.; Rubinstein, I.; Blend, M. J.; Onyuksel, H. 2003. VIP grafted sterically stabilized liposomes for targeted imaging of breast cancer: in vivo studies. *Journal of Controlled Release, 91*(1-2), 123-133.

Davydov, M. V., S.; Polotsky, B.; Gerasimov, S.; Machaladze, Z.; Allahverdiyev, A.; Nojin, S.; Bouidenok, Y. 2002. Mediastinal lymphadenectomy improves survival in surgically treated patients with non-small cell lung cancer. *International Journal of Cancer*, 414-415.

Dawes, G. S. 1946. Synthetic Substitutes for Quinidine. *British Medical Journal, 1*(4436), 43-45.

Depierre, A., Freyer, G., Jassem, J., Orfeuvre, H., Ramlau, R., Lemarie, E., . . . Trillet-Lenoir, V. 2001. Oral vinorelbine: Feasibility and safety profile. *Annals of Oncology, 12*(12), 1677-1681.

Development, A. C. ((© 1994-2010 ACD/Labs)). (ACD/Labs).

EDMUNDS, C. W., and GUNE, J. A. 1934. *Cuishny's Pharmacology and Therapeutics*. London.

Edwards, K. J., M.; Karlsson, G.; Silvander, M. 1997. Effect of polyethyleneglycol-phospholipids on aggregate structure in preparations of small unilamellar liposomes. *Biophysical Journal, 73*(1), 258-266.

Everett, D. H. 1988. *Basic Principles of Colloid Science*. Cambridge, UK: The Royal Society of Chemistry.

Finlayson, J. 1892. Hippocrates. *Glas. Med. Jour, 37*, 4.

Florence, A. T., & Attwood, D. 2006. *Physicochemical principles of pharmacy*: Pharmaceutical Press.

Galipeau, R. J. 1995. *Predicting the Effects of Contact Materials and Their Environments on Thermoplastics Through Chemical Compatibility Testing*. Paper presented at the ANTEC conference.

H. Onyuksel, O. M. K., V. Sethi and I. Rubinstein. 2005. Sterically stabilized phospholipid micellar human vasoactive intestinal peptide: A novel disease-modifying drug for rheumatoid arthritis. *Arthritis and Rheumatism, 52*(9), S262-S262.

Hajnos, M. W. S., J.; Kowalska, T. 2008. *Thin Layer Chromatography in Phytochemistry*. NewYork: CRC press.

Henry, T. A. 1949. *The Plant Alkaloids*. Philadelphia • Toronto: The Blakiston Company,.

Hesse, M. 2002. *Alkaloids: Nature's Curse or Blessing?* : Wiley-VCH.

Hjelm, R. P., P. Thiyagarajan, H. Alkan-Onyuksel. 1992. Organization of phosphatidylcholine and bile salt in rodlike mixed micelles.. *J. Phys. Chem., 96*, 8653-8661.

Holker, J. S. E., Cais, M., Hochstein, F. A., and Djerassi, C. 1959. Alkaloid Studies XXII. The Alkaloids of Vallesia Dichotoma. *J. Org. Chem, 24*, 314.

Hristova, K., and D. Needham. 1995. Phase behaviour of a lipid/polymerlipid mixture in aqueous medium. *Macromolecules, 28*, 991-1002.

Husseini, G. A. R. N. Y. C., T. D. A. ; Pruitt, J. D.; and Pitt, W. G. 2002. Kinetics of ultrasonic release of doxorubicin from pluronic P105 micelles,. *Colloids and Surfaces B: Biointerfaces, 24*, 253–264.

J. Edwin Saxton, P. 1983. *The Indoles: the monoterpenoid indole alkaloids*: John Wiley and Sons.

J. Ko, K. P., Y.-S. Kim, et al.,. 2007. Tumoral acidic extracellular pH targeting of pH-responsive MPEG-poly(β-amino ester) block copolymer micelles for cancer therapy. *Journal of Controlled Release, 123*, 109–115.

Jehl, F., Debs, J., Herlin, C., Quoix, E., Gallion, C., & Monteil, H. 1990. DETERMINATION OF NAVELBINE AND DESACETYLNAVELBINE IN BIOLOGICAL-FLUIDS BY HIGH-PERFORMANCE LIQUID-CHROMATOGRAPHY. *Journal of Chromatography-Biomedical Applications, 525*(1), 225-233. doi: 10.1016/s0378-4347(00)83397-6

Johnston, M. J. W. S., S. C.; Klimuk, S. K.; Edwards, K.; Eisenhardt, M. L.; Leng, E. C.; Karlsson, G.; Yanko, D.; Cullis, P. R. 2006. Therapeutically optimized rates of drug release can be achieved by varying the drug-to-lipid ratio in liposomal vincristine formulations. *Biochimica Et Biophysica Acta-Biomembranes, 1758*(1), 55-64.

Jones, M. C. L., J. C. 1999. Polymeric micelles - a new generation of colloidal drug carriers. *European Journal of Pharmaceutics and Biopharmaceutics, 48*(2), 101-111.

Kabanov, A. V., & Alakhov, V. Y. 2002. Pluronic (R) block copolymers in drug delivery: From micellar nanocontainers to biological response modifiers. *Critical Reviews in Therapeutic Drug Carrier Systems, 19*(1), 1-72.

Kastantin, M., Ananthan, A., Badriprasad, K., Karmali, P., Ruoslahti, E., Tirrell, M. 2009. Effect of the Lipid Chain Melting Transition on the Stability of DSPE-PEG(2000) Micelles. *Langmuir, 25*(13), 7279-7286.

Kim, A. A. A. M. S. H. L. S. H. 2009. Penetration and efficacy of VEGF siRNA using polyelectrolyte complex micelles in a human solid tumor model in-vitro. *Journal of Controlled Release, 137*, 130–135.

Klibanov, A. L., Maruyama, K., Torchilin, V. P., & Huang, L. 1990. Amphipathic Polyethyleneglycols Effectıvely Prolong The Circulation Time Of Liposomes. [Article]. *Febs Letters, 268*(1), 235-237.

Kogure, N. N., C.; Kitajima, M.; Takayama, H. 2005. Six new indole alkaloids from Gelsemium sempervirens Ait. f. *Tetrahedron Letters, 46*(35), 5857-5861.

Kohno, E. M., S.; Nishikata, M.; Noboru Okamura, N.; Matzno, S.; Kuwahara, T. and Matsuyama, K. 2008. Methods of preventing vinorelbine-induced phlebitis: an experimental study in rabbits. *Int J Med Sci., 5*, 218–223.

Koukoulitsa, C. K., I.; Demetzos, C.; Mavromoustakos, T. 2006. The role of the anticancer drug vinorelbine in lipid bilayers using differential scanning calorimetry and molecular modeling. *Chemistry and Physics of Lipids, 144*(1), 85-95.

Koyuncu. 2011. *Turkish Journal of Botany*.Under Press

Kreitmair, E. 1928. *Merck's Jahresb., 42*.

Krikorian, A. B., F. 1991. Vinorelbine (Navelbine ® 1). A New Semisynthetic Vinca Alkaloid. *Onkologie, 4*, 7-12.

Kumari, A., Yadav, S. K., & Yadav, S. C. 2010. Biodegradable polymeric nanoparticles based drug delivery systems. *Colloids and Surfaces B: Biointerfaces, 75*(1), 1-18. doi: 10.1016/j.colsurfb.2009.09.001

Lasic, D. D. 1992. Mıxed micelles in drug delivery. *Nature, 355*(6357), 279-280. doi: 10.1038/355279a0

Lasic, D. D., Macleod, K., Huang, A., Abra, R. M., Newman, M. S., Martin, F. J., Mayhew, E. 1992. Grafted Polymer (Stealth) Liposomes. *Abstracts of Papers of the American Chemical Society, 203*, 51-.

Li, S.-D., & Huang, L. 2008. Pharmacokinetics and biodistribution of nanoparticles. *Molecular Pharmaceutics, 5*(4), 496-504.

Liu, B., Yang, M., Li, R., Ding, Y., Qian, X., Yu, L., & Jiang, X. (2008). The antitumor effect of novel docetaxel-loaded thermosensitive micelles. *European Journal of Pharmaceutics and Biopharmaceutics, 69*(2), 527-534.

Liu, D., Mori, A., & Huang, L. 1992. Role of liposome size and RES blockade in controlling biodistribution and tumor uptake of GM1-containing liposomes. *Biochimica et Biophysica Acta (BBA) - Biomembranes, 1104*(1), 95-101.

Liu, X. M., Wang, L. G., Kreis, W., Budman, D. R., & Adams, L. M. . 2001. Differential effect of vinorelbine versus paclitaxel on ERK2 kinase activity during apoptosis in MCF-7 cells. *British Journal of Cancer, 85*, 1403-1411.

Liu, Y., Lu, W.-L., Guo, J., Du, J., Li, T., Wu, J.-W., Wang, G.-L.,. 2008. A potential target associated with both cancer and cancer stem cells: a combination therapy for eradication of breast cancer using vinorelbine stealthy liposomes plus parthenolide stealthy liposomes. *Journal of Controlled Release, 129*, 18-25.

Lizano, C., Weissig, V., Torchilin, V. P., Sancho, P., Garcia-Perez, A. I., & Pinilla, M. 2003. In vivo biodistribution of erythrocytes and polyethyleneglycol-phosphatidylethanolamine micelles carrying the antitumour agent dequalinium. [Article]. *European Journal of Pharmaceutics and Biopharmaceutics, 56*(2), 153-157.

Lukyanov, A. N. G., Z. G.; Mazzola, L.; Torchilin, V. P. 2002. Polyethylene glycol-diacyllipid micelles demonstrate increased acculumation in subcutaneous tumors in mice. *Pharmaceutical Research, 19*(10), 1424-1429.

Lv, Q., Yu, A., Xi, Y., Li, H., Song, Z., Cui, J., Zhai, G. 2009. Development and evaluation of penciclovir-loaded solid lipid nanoparticles for topical delivery. *International Journal of Pharmaceutics, 372*(1-2), 191-198.

Marinibettolo, G. B. G., C.; Nicoletti, M.; Messana, I. 1980. On the alkaloids of strychnos .33. Alkaloids of *strychnos-rubigınosa*. *Phytochemistry, 19*(5), 992-994.

Maswadeh, H., Demetzos, C., Daliani, I., Kyrikou, I., Mavromoustakos, T., Tsortos, A., & Nounesis, G. 2002. A molecular basis explanation of the dynamic and thermal effects of vinblastine sulfate upon dipalmitoylphosphatidylcholine bilayer membranes. *Biochimica et Biophysica Acta (BBA) - Biomembranes, 1567*, 49-55.

Matsumura, Y., and Maeda, H.,. 1986. A New Concept for Macromolecular Therapeutics in Cancer Chemotherapy: Mechanism of Tumoritropic Accumulation of Proteins and the Antitumor Agent Smancs *Cancer Res 46*.

Medicago. 2010. Phosphate bufered saline specification sheet. In M. AB (Ed.).

Mergott, D. J., & Jacobsen, E. N. 2005. Total synthesis of (+)-yohimbine. *Abstracts of Papers of the American Chemical Society, 230*,

Mergott, D. J. Z., S. J.; Jacobsen, E. N. 2008. Catalytic asymmetric total synthesis of (+)-yohimbine. *Organic Letters, 10*(5), 745-748.

Michalowski, C. B. G., S. S.; Dalla Costa, T. 2004. Microdialysis for evaluating the entrapment and release of a lipophilic drug from nanoparticles. *Journal of Pharmaceutical and Biomedical Analysis, 35*(5), 1093-1100.

Moghimi, S. M. P., C. J. H.; Muir, I. S.; Illum, L.; Davis, S. S. 1991. Non-phagocytıc uptake of intravenously ınjected microspheres in rat spleen - influence of particle-size and hydrophilic coatıng. *Biochemical and Biophysical Research Communications, 177*(2), 861-866.

Moreira, J. N. G., R.; Allen, T. M. 2001. Targeting Stealth liposomes in a murine model of human small cell lung cancer. *Biochimica Et Biophysica Acta-Biomembranes, 1515*(2), 167-176.

Morris, P. G. F., M. N. 2008. Microtubule Active Agents: Beyond the Taxane Frontier. *Clinical Cancer Research, 14*(22), 7167-7172.

Mosmann, T. 1983. Rapid colorimetric assay for cellular growth and survival: Application to proliferation and cytotoxicity assays. *Journal of Immunological Methods, 65*(1-2), 55-63.

Muir, I. S. M., S. M.; Illum, L.; Davis, S. S.; Davies, M. C. 1991. The effect of block copolymers on the uptake of model polystyrene microspheres by kupffer cells - invıtro and invivo studıes. *Biochemical Society Transactions, 19*(3),

Mukhopadhyay, S., Handy, G.A., Funayama, S., Cordell, G.A.,. 1981. Anticancer Indole Alkaloids of Rhazya strictica *Journal of Natural Products,, 44,*, 696-701

Mustafa, S. M. B., S. A.; Ma, G. Y.; Moore, B. M.; Feller, D. R.; Miller, D. D. 2005. Synthesis and biological studies of yohimbine derivatives on human alpha(2C)-adrenergic receptors. *Bioorganic & Medicinal Chemistry Letters, 15*(11), 2758-2760.

Nakayama, M. O., T.; Miyazaki, T.; Kohori, F.; Sakai, K.; Yokoyama, M. . 2006. Molecular design of biodegradable polymeric micelles for temperature-responsive drug release. *Journal of Controlled Release, 115*, 46–56.

Needham, D., McIntosh, T. J., & Lasic, D. D. 1992. Repulsıve interactıons and mechanical stabılıty of polymer-grafted lipid-membranes. *Biochimica Et Biophysica Acta, 1108*(1), 40-48.

Ngan, V. K., Bellman, K., Panda, D., Hill, B. T., Jordan, M. A., & Wilson, L. 2000. Novel Actions of the Antitumor Drugs Vinflunine and Vinorelbine on Microtubules. *Cancer Research, 60*(18), 5045-5051.

Okouneva, T. H., B. T.; Wilson, L.; Jordan, M. A. 2003. The Effects of Vinflunine, Vinorelbine, and Vinblastine on Centromere Dynamics1. *Molecular Cancer Therapeutics, 2*(5), 427-436.

Onyueksel, H. M., P. S.; Rubinstein, I. 2009. VIP-grafted sterically stabilized phospholipid nanomicellar 17-allylamino-17-demethoxy geldanamycin: A novel targeted nanomedicine for breast cancer. *International Journal of Pharmaceutics, 365*(1-2), 157-161.

Onyuksel, H. J., E.; Rubinstein, I. 2009. Nanomicellar paclitaxel increases cytotoxicity of multidrug resistant breast cancer cells. *Cancer Letters, 274*(2), 327-330.

Park, K.. 2008. A new hydrotropic block copolymer micelle system for aqueous solubilization of paclitaxel. *Journal of Controlled Release, 126*, 122–129.

Pelletier, S. W. 1999. *Alkaloids, chemical and Biological Perspectives*. New York: Wiley Interscience Publication.

Puozzo, C., Ung, H. L., & Zorza, G. 2007. A high performance liquid chromatography method for vinorelbine and 4-O-deacetyl vinorelbine: A decade of routine analysis in human blood. *Journal of Pharmaceutical and Biomedical Analysis, 44*(1), 144-149.

Raaman, N.2006. *Phytochemical Techniques*. Delhi: Jai Baharat Printing Press.

Raymond, H. 1937. Über die Wirkung von Corynanthin auf die männliche Genitalfunktion. *Naunyn-Schmiedeberg's Archives of Pharmacology, 184*(6), 680-685.

Ribet, J. P. Z., P.; Fahy, J.; Duflos, A.; Beltran, T. 2001. Complete assignment of H-1 and C-13 NMR spectra of vinflunine. *Magnetic Resonance in Chemistry, 39*(1), 43-48.

Robert, G. M. T., Ahond, A., Poupat, C., Potier, P., Jacquemin, H., & Kan, S. K. 1983. ASPIDOSPERMA FROM GUYANA - ALKALOIDS DERIVED FROM THE SEEDS OF ASPIDOSPERMA-OBLONGUM. *Journal of Natural Products, 46*(5), 708-722.

Robieux, I. V., V.; Aita, P.; Freschi, A.; Lazzarini, R.; Sorio, R. 1996. Sensitive high-performance liquid chromatographic method with fluorescence detection for measurement of vinorelbine plasma concentrations. *Journal of Chromatography B-Biomedical Applications, 675*(1), 183-187.

Sejourne, F., Rubinstein, I., Suzuki, H., & AlkanOnyuksel, H. 1997. Development of a novel bioactive formulation of vasoactive intestinal peptide in sterically stabilized liposomes. [Article]. *Pharmaceutical Research, 14*(3), 362-365.

Sejourne, F., Suzuki, H., AlkanOnyuksel, H., Gao, X. P., Ikezaki, H., & Rubinstein, I. 1997. Mechanisms of vasodilation elicited by VIP in sterically stabilized liposomes in vivo. [Article]. *American Journal of Physiology-Regulatory Integrative and Comparative Physiology, 273*(1),

Semple, S. C., Leone, R., Wang, J., Leng, E. C., Klimuk, S. K., Eisenhardt, M. L., Ahkong, Q.-F.2005. Optimization and characterization of a sphingomyelin/cholesterol liposome formulation of vinorelbine with promising antitumor activity. *Journal of Pharmaceutical Sciences, 94*(5), 1024-1038.

Shan, X., Yuan, Y., Liu, C., Tao, X., Sheng, Y., & Xu, F. 2009. Influence of PEG chain on the complement activation suppression and longevity in vivo prolongation of the PCL biomedical nanoparticles. *Biomedical Microdevices, 11*(6), 1187-1194.

Sigerist, H. 1934. Notes and cominents on Hippocrates. *Bul. Hist. Med., 2*

Spiegel, L. 1915. Weitere Mitteilungen über das Yohimbin. III. Die Zusammensetzung des Yohimbins und seine Beziehungen zur Yohimboasäure. Meso-yohimbin, ein neues Yohimbehe-Alkaloid. *Berichte der deutschen chemischen Gesellschaft, 48*(2), 2077-2083. **Spiegel, L.** (1926). Über Yohimbehe-Alkaloide. *Berichte der deutschen chemischen Gesellschaft (A and B Series), 59*(11), 2706-2707.

Stearn, W. T. 1973. A synopsis of the genus Vinca including its taxonomic and nomenclatural history. In: Taylor WI & Farnsworth N (ed.) The Vinca alkaloids. Retrieved from

Stearn, W. T. 1978. *Vinca L. In: Davis PH (ed.) Flora of Turkey and the East Aegean islands,* (Vol. vol. 6). Edinburgh: Edinburgh University Press.

Sullivan, C. O. 2004. In vitro degradation of insulin-loaded poly (n-butylcyanoacrylate) nanoparticles. *Biomaterials*, 4375–4382.

Sultana. 1992. *Studies on the Isolationof New Potentially Bioactive Agents from Rhazya strictica, Fritillaria persica and Related Plants.* Ph.D., University of Karachi, Karachi.

Taylor, R. L. W., D. M.; Craven, P. C.; Graybill, J. R.; Drutz, D. J.; Magee, W. E. 1982. Amphotericin-B in liposomes - a novel therapy for histoplasmosis. *American Review of Respiratory Disease, 125*(5), 610-611.

Theophrastus and Galen Walsh, J. 1937. Galens writings and influences inspiring them. *Ann. Med. Hist, 6*, 1.

Torchilin, V. 2009. Multifunctional and stimuli-sensitive pharmaceutical nanocarriers. *European Journal of Pharmaceutics and Biopharmaceutics, 71*, 431–444.

Url-1 <*www.wikipedia.org*> accessed at 09.08.2011.

Url- 2 <*www.piercent.com*>**.**. accessed at 09.08.2011

Vendrig, D. T., J.; Holthuis, J. J. M. 1988. Determinatıon of *vinca* alkaloıds in plasma and urine using ion-exchange chromatography on silica-gel and fluorescence detectıon. *Journal of Chromatography-Biomedical Applications, 434*(1), 145-155.

Vorman, L., and Adams, A.,1969. Identification of rapid changes at plasma solid interfaces *J Biomed. Mater. Res., 3*.

Waksmundzka-Hajnos, M. S., J.; Kowalska, T. 2008. *Thin Layer Chromatography in Phytochemistry,* : CRC Press,.

Walser, A. a. D., C. 1965. Alkaloid Studies LII. The Alkaloids cf Vallesia Dichotoma. *Helv. Chim. Acta,, 48*, 391.

Wang, F., Bronich, T. K., Kabanov, A. V., Rauh, R. D., & Roovers, J. 2005. Synthesis and Evaluation of a Star Amphiphilic Block Copolymer from Poly(ε-caprolactone) and Poly(ethylene glycol) as a Potential Drug Delivery Carrier. *Bioconjugate Chemistry, 16*(2), 397-405.

Wang, Y., Wang, R., Lu, X., Lu, W., Zhang, C., & Liang, W. 2010. Pegylated Phospholipids-Based Self-Assembly with Water-Soluble Drugs. *Pharmaceutical Research, 27*(2), 361-370.

Ward, G. A. 2005. Measurements of binding thermodynamics in drug discovery. *Drug Discovery Today, 1543-1551*.

Weili Qiao, B. W., Yazhou Wang, Lichun Yang, Yiqiong Zhang, and Pengyu Shao. 2010. Cancer Therapy Based on Nanomaterials and Nanocarrier Systems. *Journal of Nanomaterials, 2010,* 1-9.

Weissig, V., Whiteman, K. R., & Torchilin, V. P. 1998. Accumulation of protein-loaded long-circulating micelles and liposomes in subcutaneous Lewis lung carcinoma in mice. *Pharmaceutical Research, 15*(10), 1552-1556.

Whypych, G. 2010 *Hand Book of Plasticizers,* . USA,: Chem tech Publishing. Wiley-Blackwell.. Leung's Encyclopedia of Natural Ingredients. *Leung's Encyclopedia of Common Natural Ingredients Used in Food, Drugs, and Cosmetics* Wiley-Blackwell

Working, P. K., & Dayan, A. D. 1996. Pharmacological-toxicological expert report - Caelyx(TM) - (Stealth(R) liposomal doxorubicin HCl) - Foreword. *Human & Experimental Toxicology, 15*(9), 751-785.

Yang, X. C., Y. H.; Yuan, R. 2008. Folate-encoded and Fe3O4-loaded polymeric micelles for dual targeting of cancer cells,. *Polymer, 49,* 3477–3485.

Yoshino, K. Y., Fumio; Somei, Masanori. 2008. Nucleophilic substitution reaction in indole chemistry: a synthesıs of novel 7 beta-substıtuted yohimbıne and 4a alpha-substıtuted 1,2,3,4-tetrahydro-beta-carbolıne derivatives. *Heterocycles, 76*(2), 989-994.

Zheng, C., Qiu, L., Yao, X., & Zhu, K. 2009. Novel micelles from graft polyphosphazenes as potential anti-cancer drug delivery systems: Drug encapsulation and in vitro evaluation. *International Journal of Pharmaceutics, 373*(1-2), 133-140.

APPENDICES

APPENDIX A: NMR Spectra of Vallesiachotamine
APPENDIX B: NMR Spectra of α-Yohimbine
APPENDIX C: NMR Spectra of β –Yohimbine
APPENDIX D: Spectral Data of Picrinine
APPENDIX E: NMR Spactra of 11-Hydroxypolyneuridine
APPENDIX F: Indole Alkaloids Isol. from *Vinca minor, major & herbacea*

APPENDIX A: NMR Spectra of Vallesiachotamine

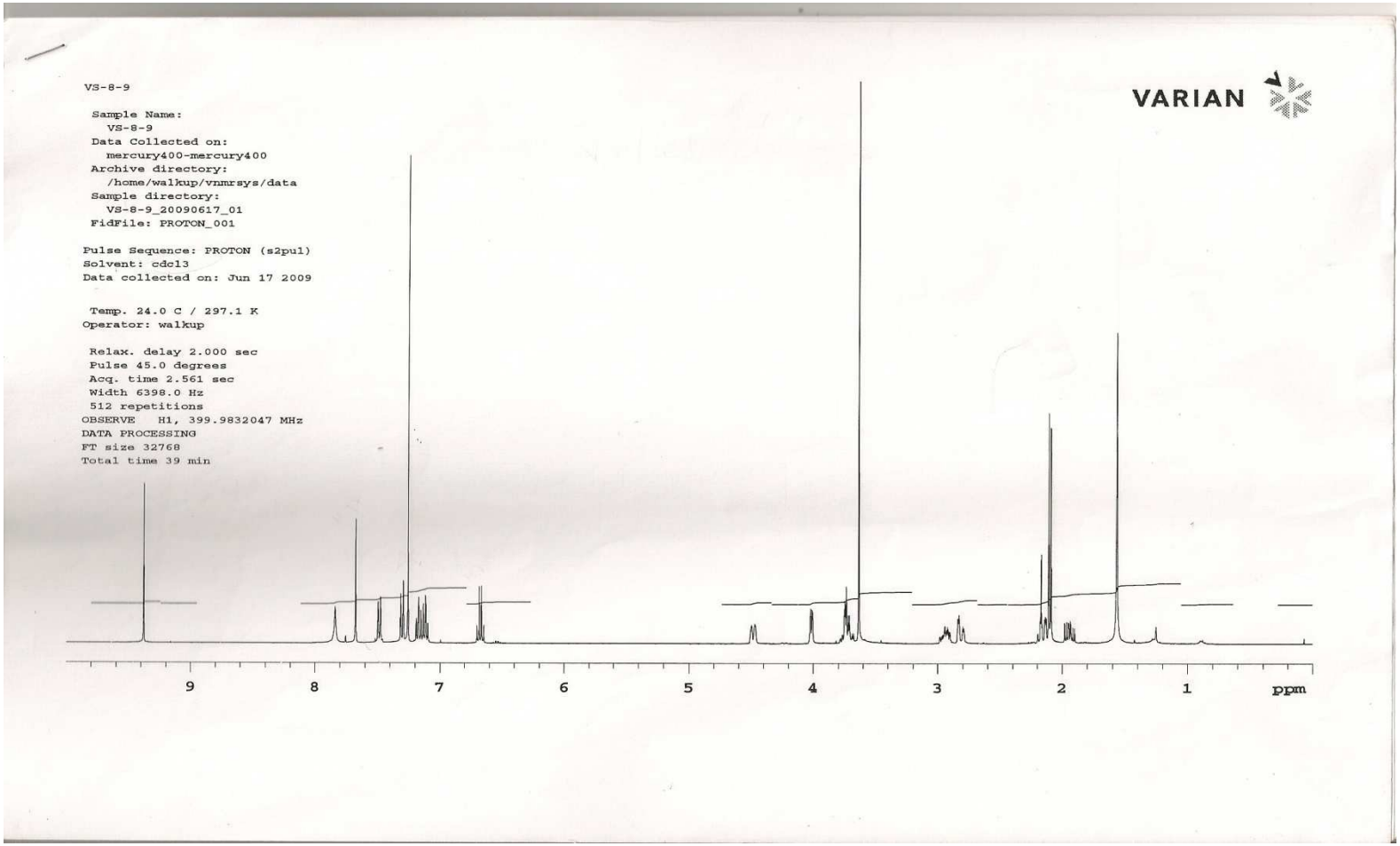

Figure A. 1: Vallesiachotamine ^{1}H NMR.

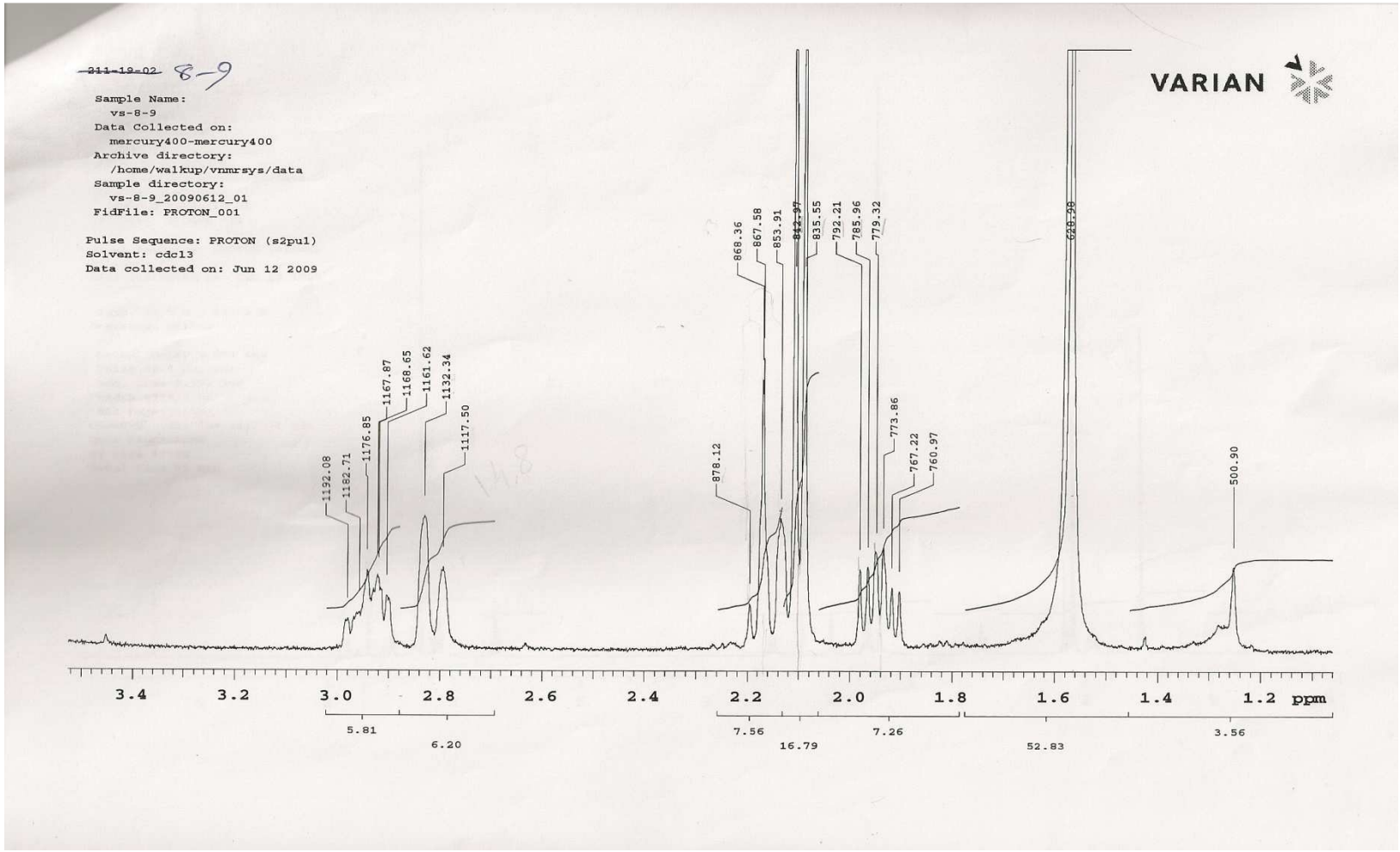

Figure A. 2: Vallesiachotamine ^{1}H NMR (1.1-3.5 ppm).

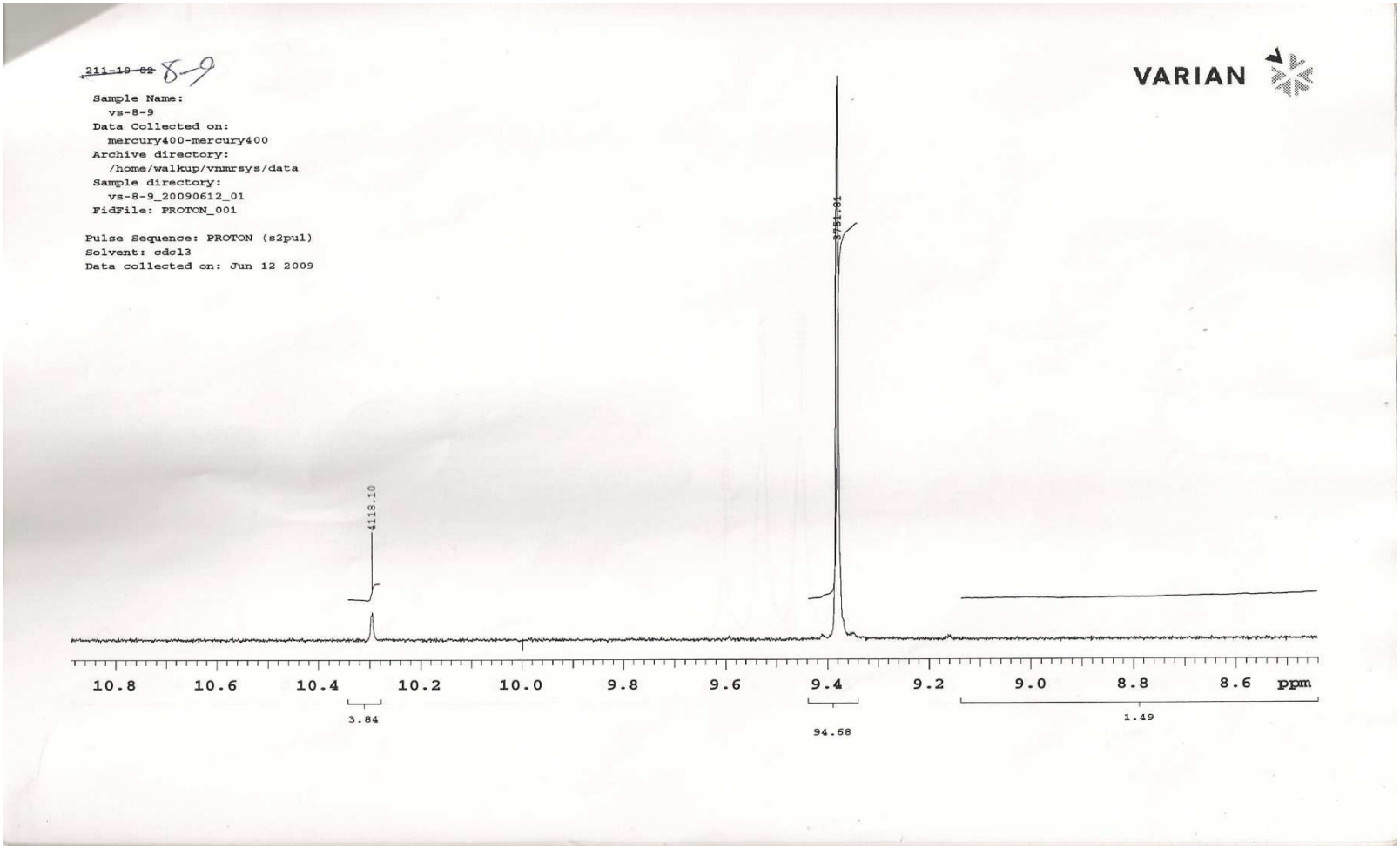

Figure A. 3: Vallesiachotamine ^{1}H NMR (8.5-10.8 ppm).

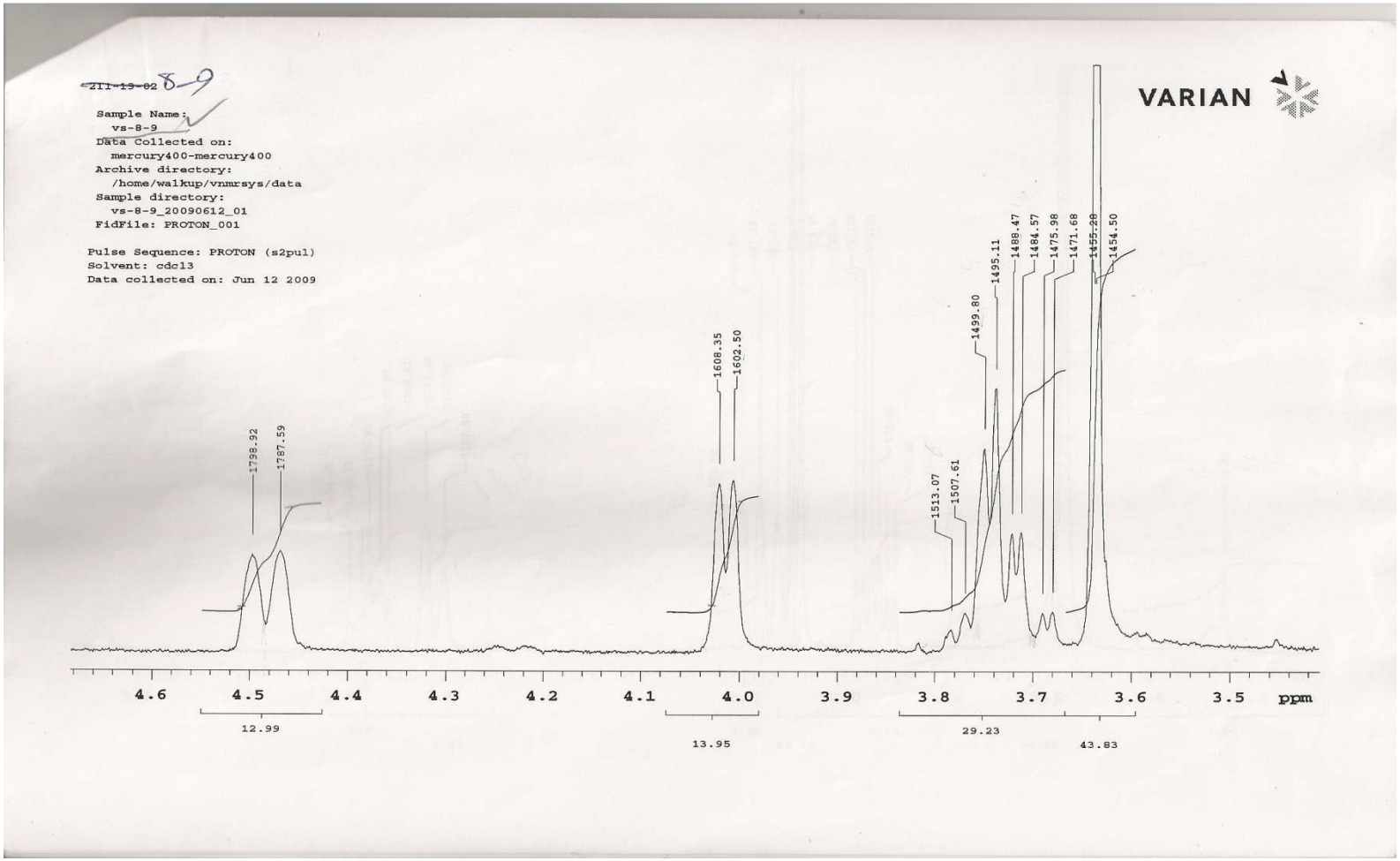

Figure A. 4: Vallesiachotamine 1H NMR (3.4-4.7 ppm).

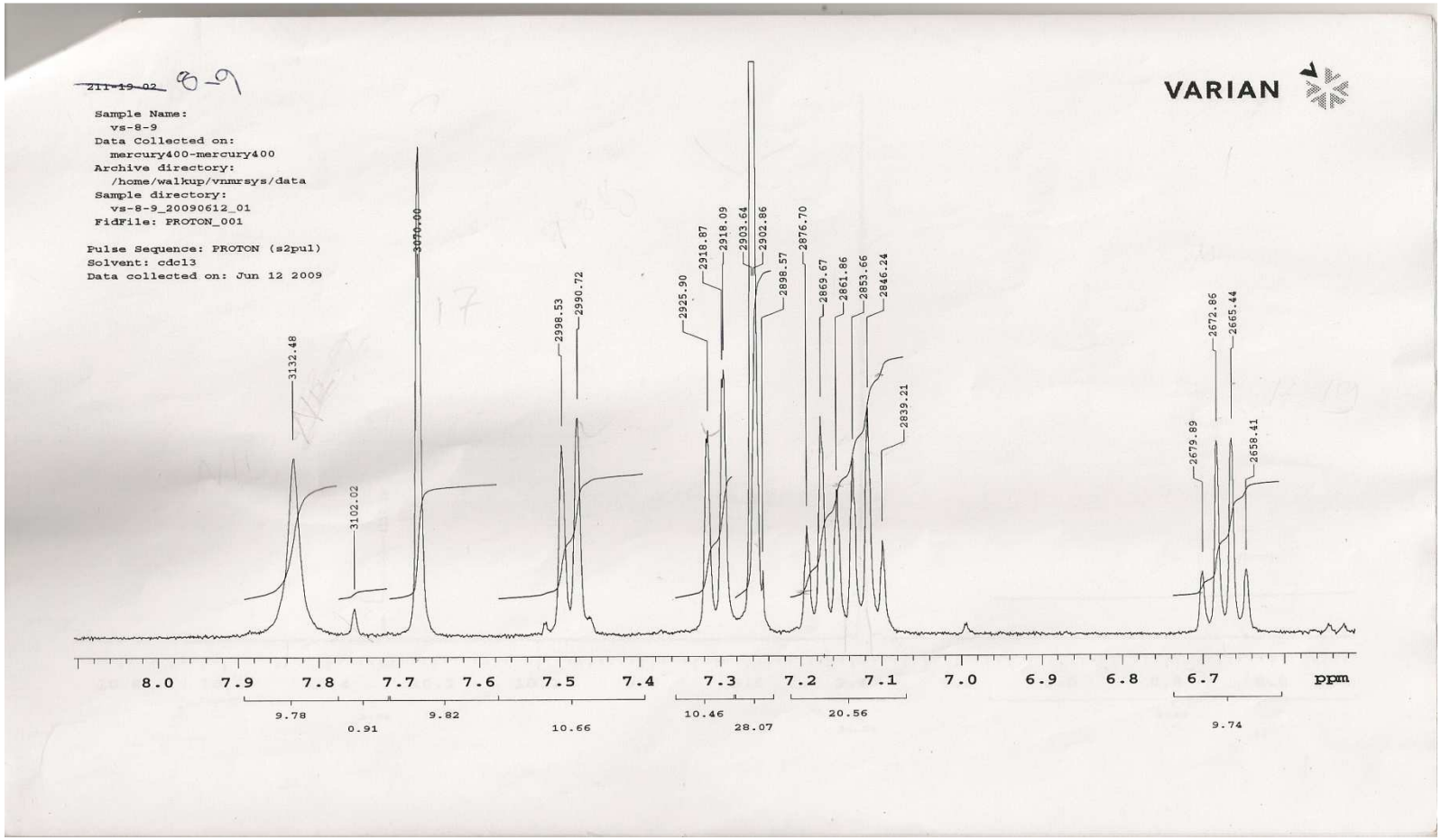

Figure A. 5: Vallesiachotamine 1H NMR aromatic area.

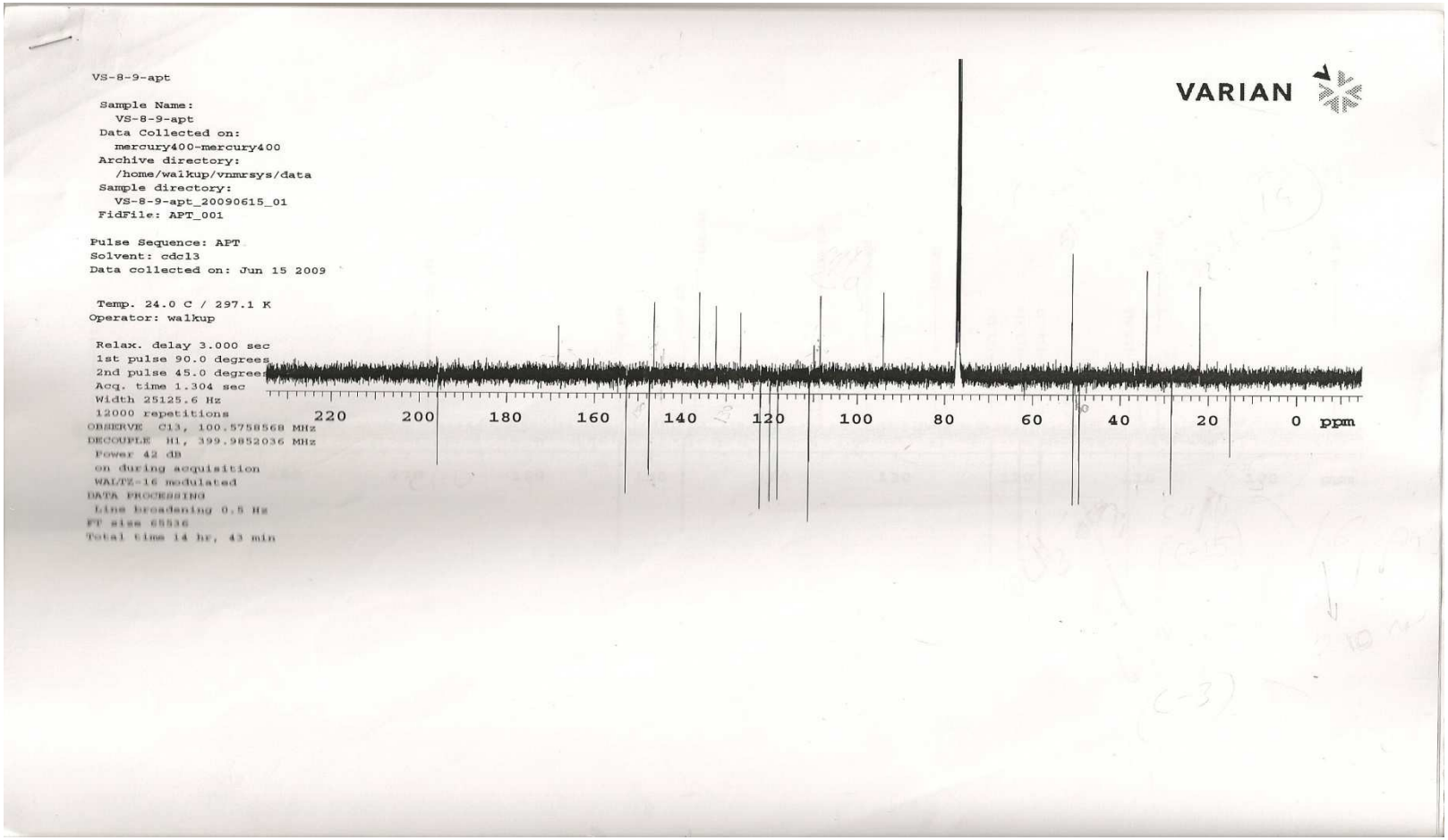

Figure A. 6: Vallesiachotamine APT spectrum.

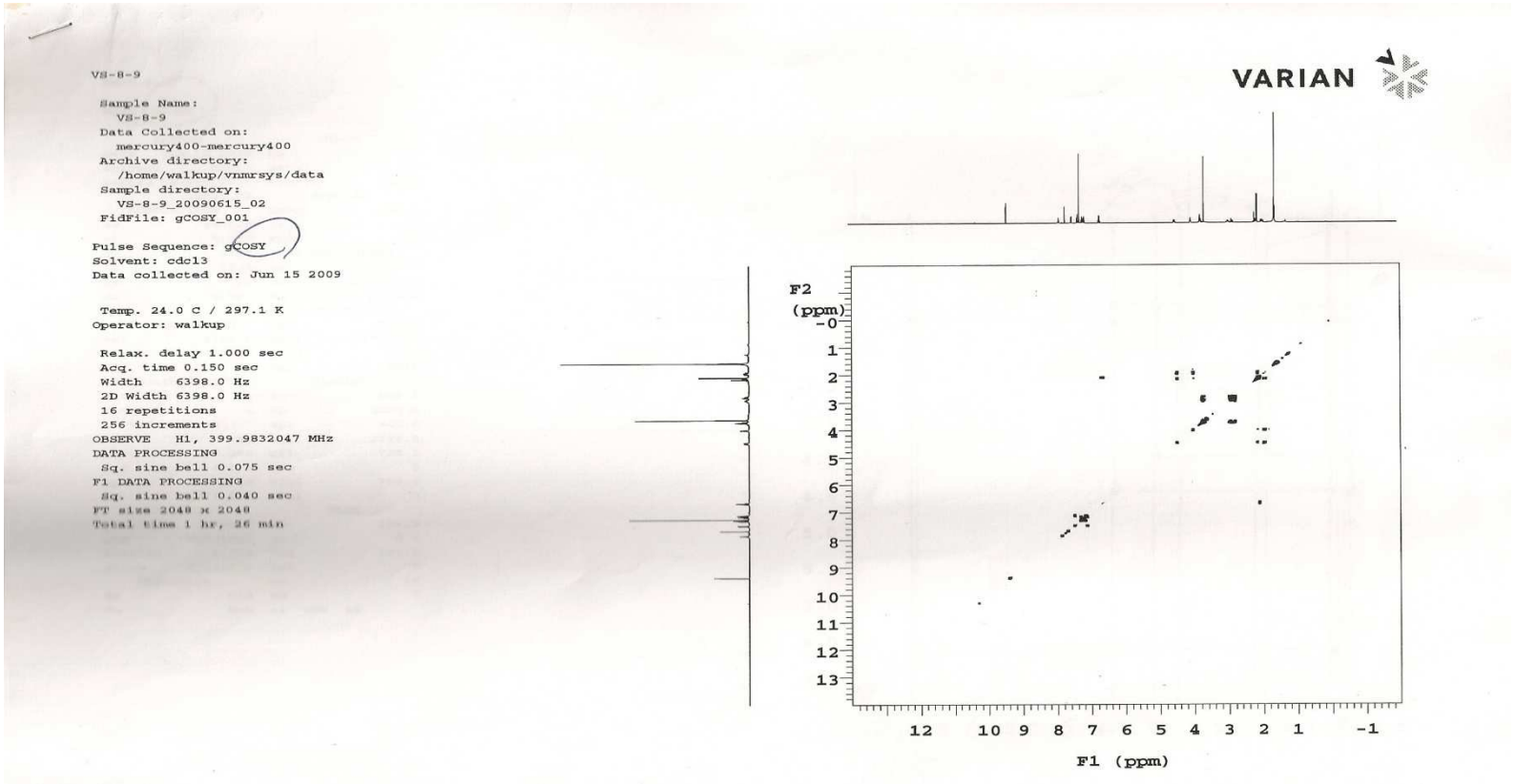

Figure A. 7: Vallesiachotamine COSY spectrum.

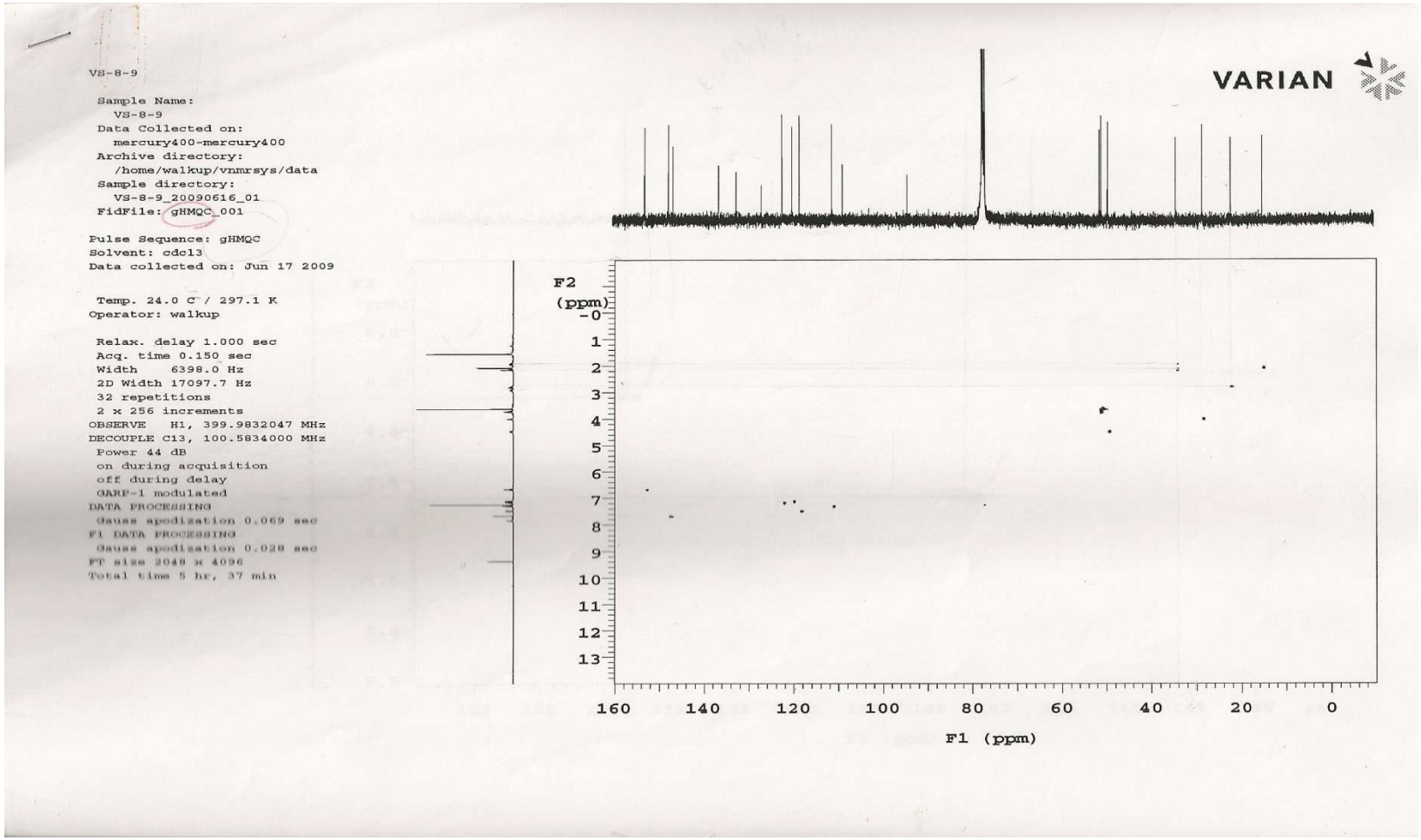

Figure A. 8: Vallesiachotamine HMQC spectrum.

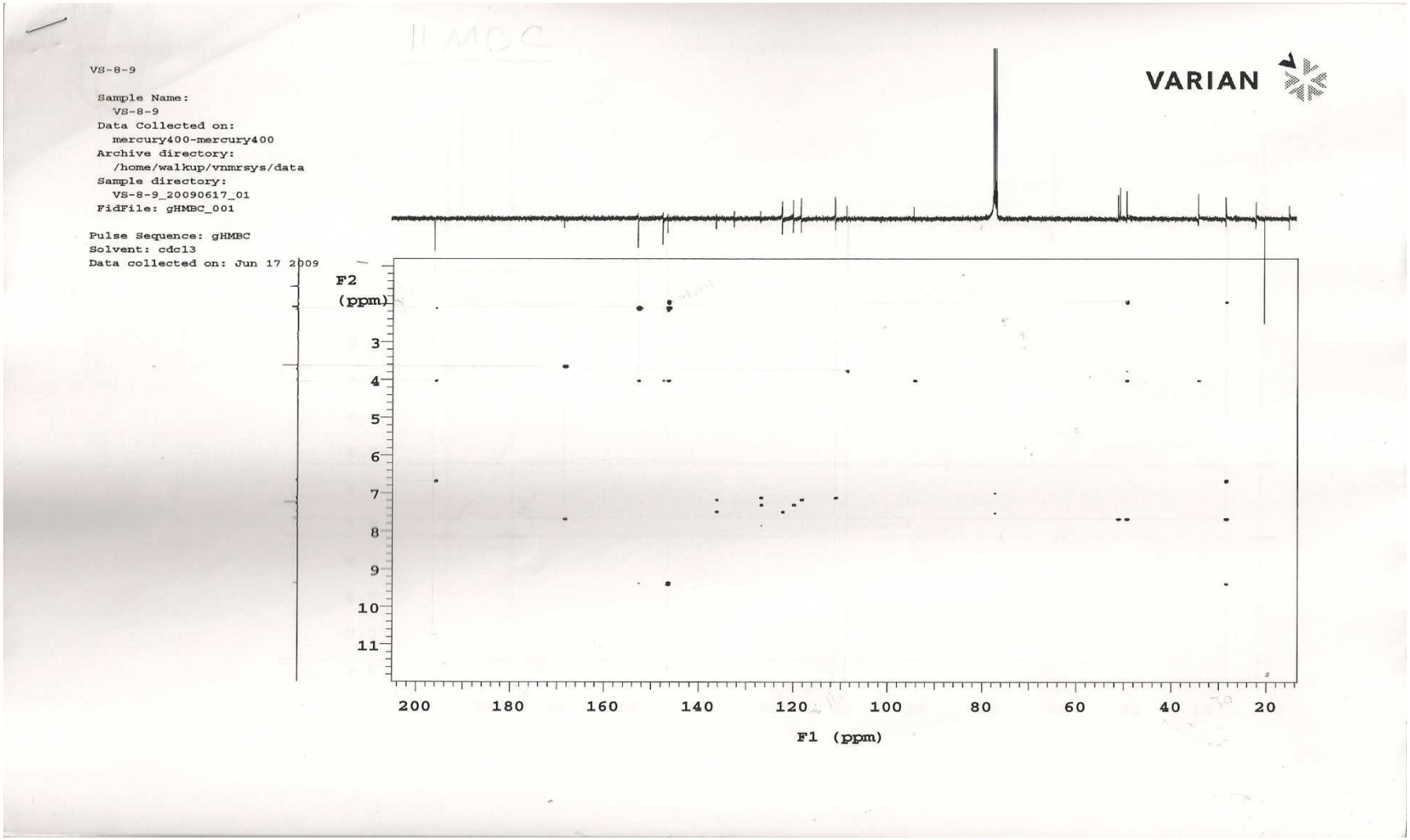

Figure A. 9: Vallesiachotamine HMBC spectrum.

APPENDIX B: NMR Spectra of α-Yohimbine

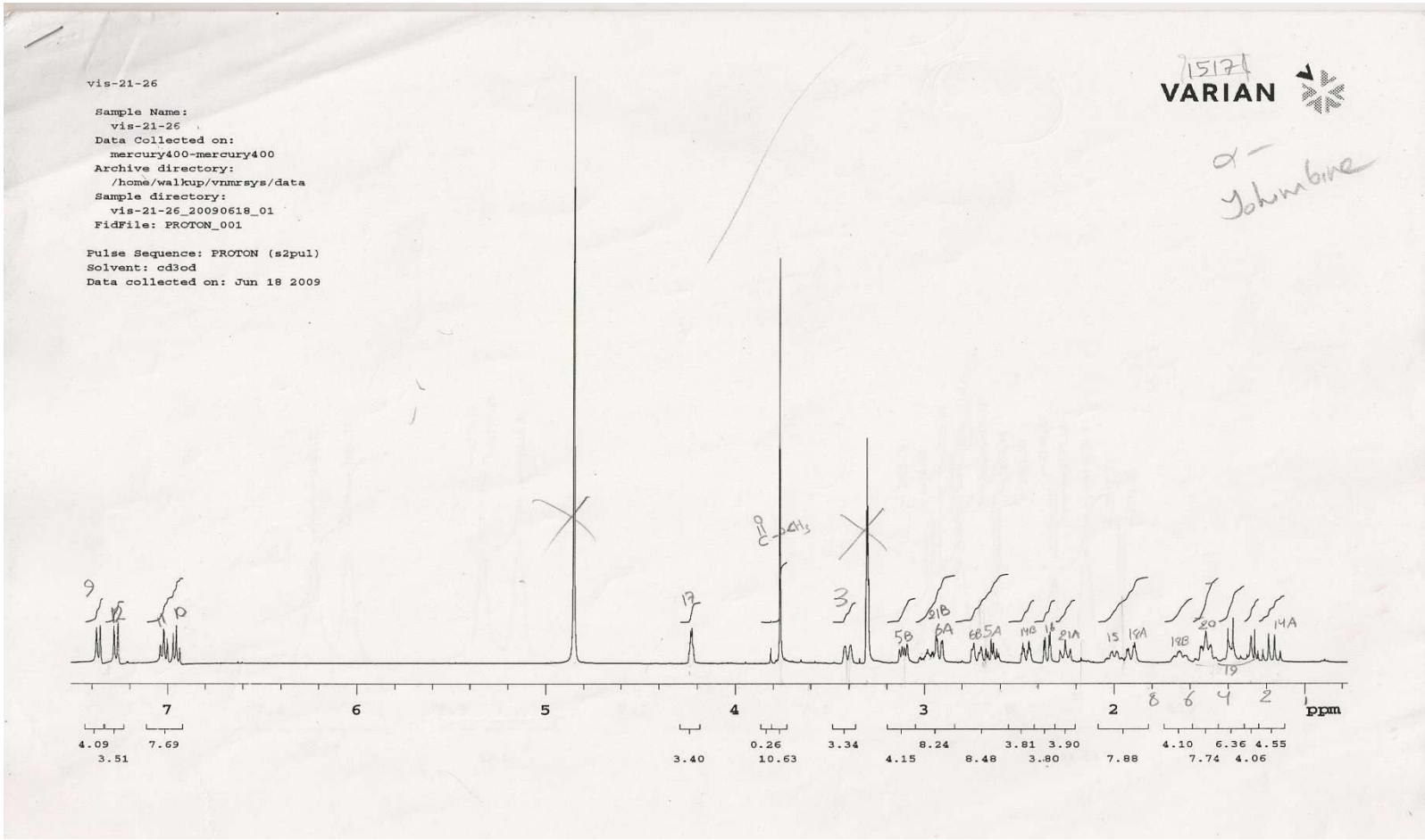

Figure B. 1: α-Yohimbine ^{1}H-NMR Spectrum.

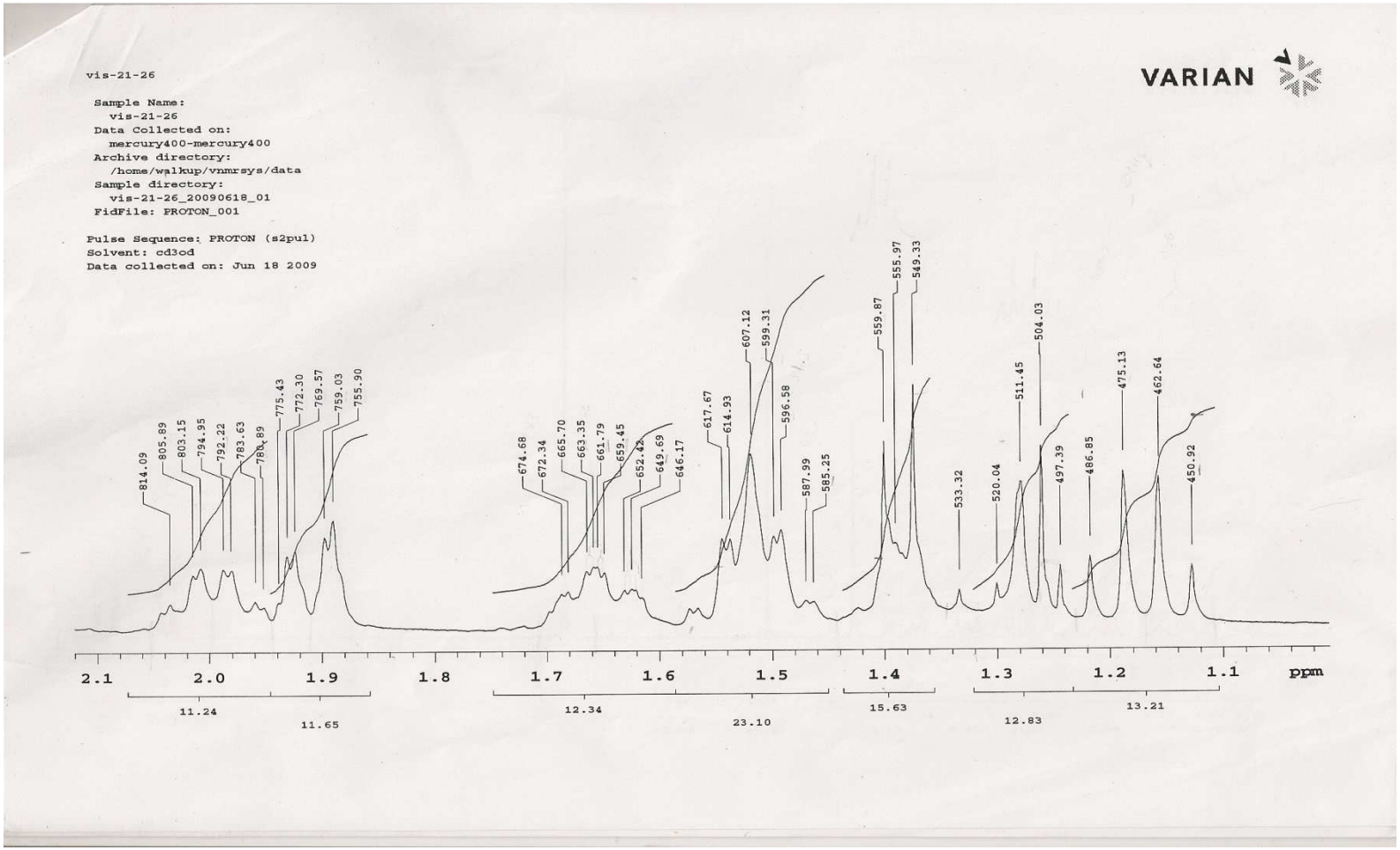

Figure B. 2: α-Yohimbine ^{1}H-NMR (1.0-2.1 ppm).

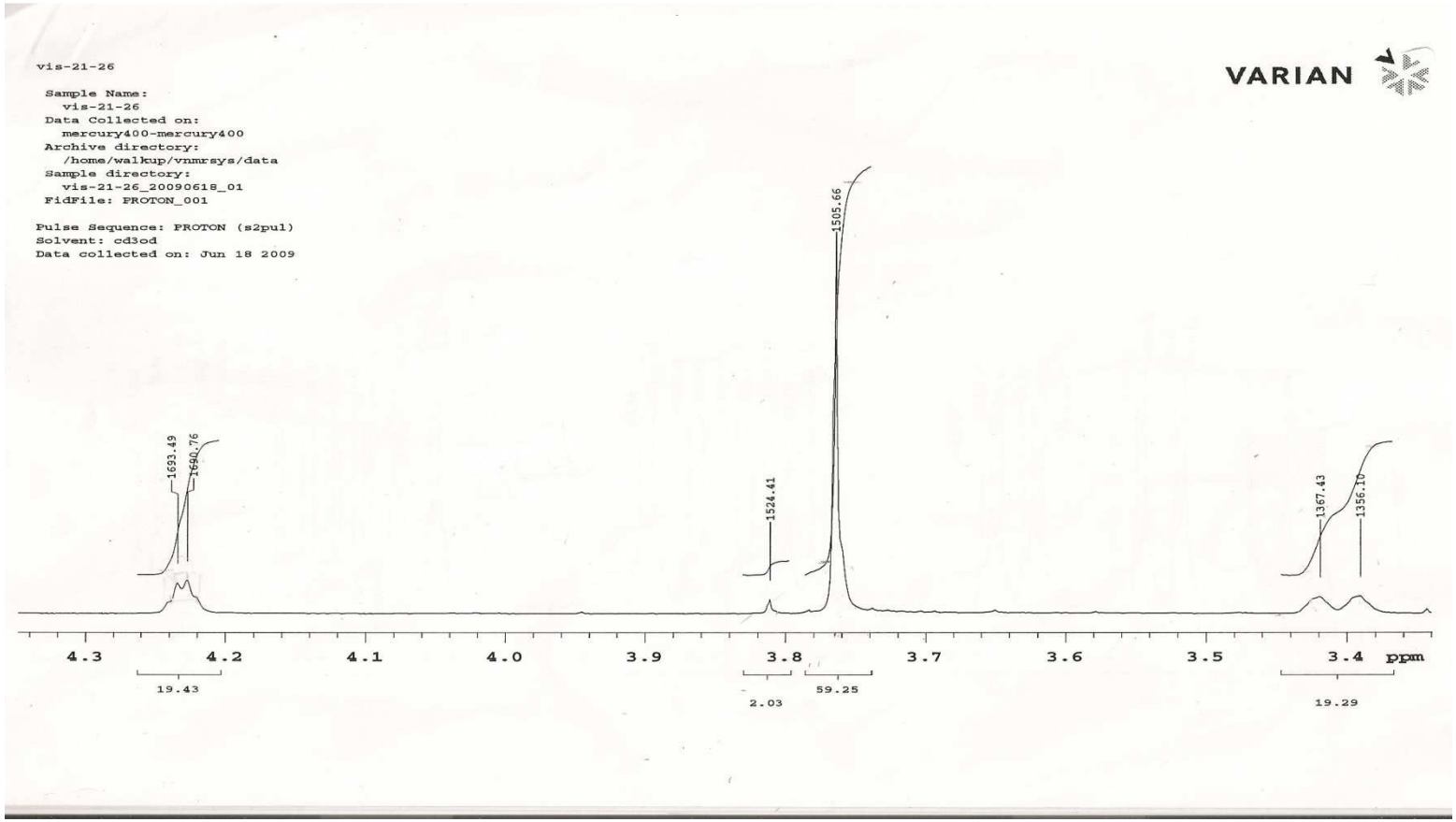

Figure B. 3: α-Yohimbine ^{1}H-NMR (3.3-4.3 ppm).

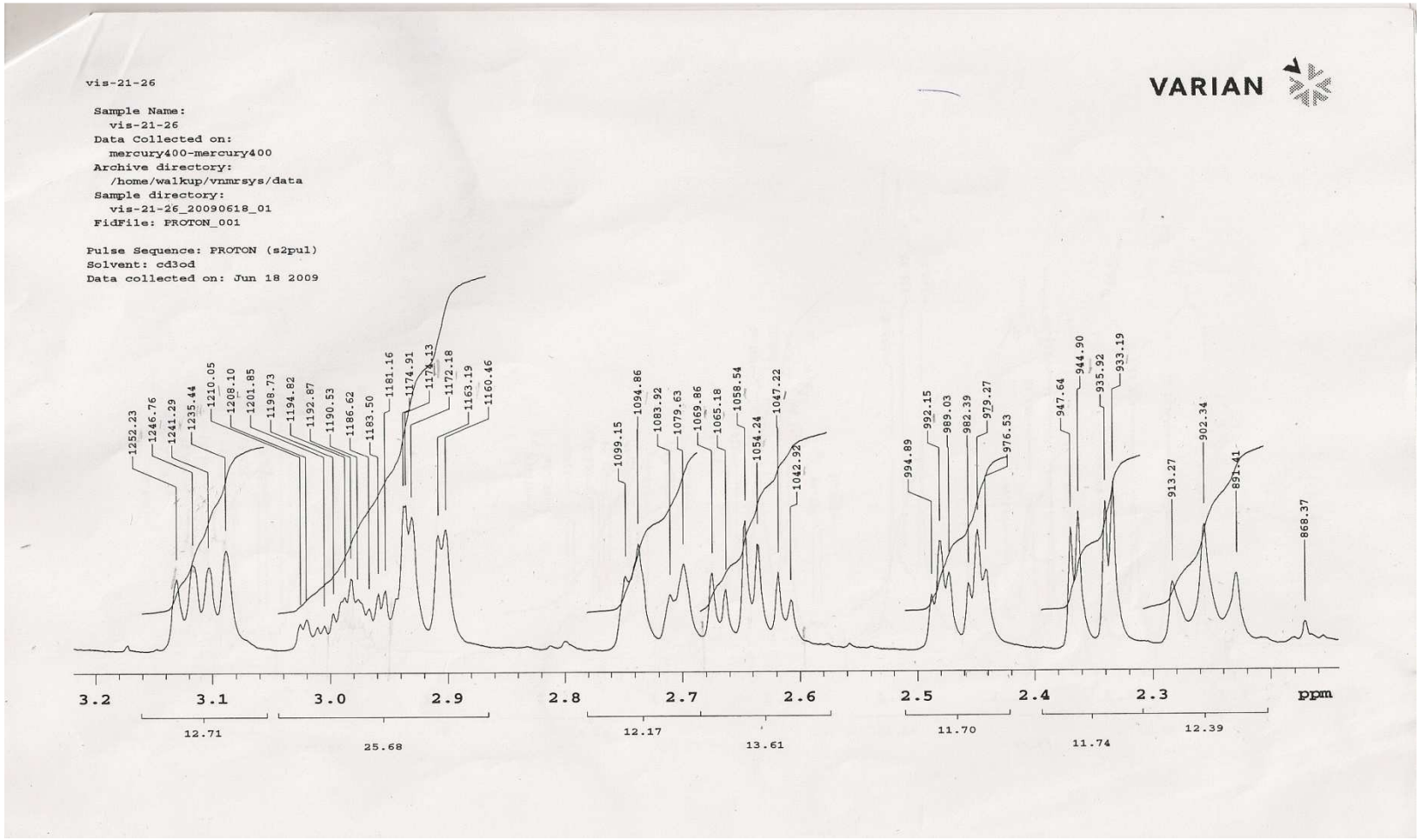

Figure B. 4: : α-Yohimbine ^{1}H-NMR (2.2-3.2 ppm).

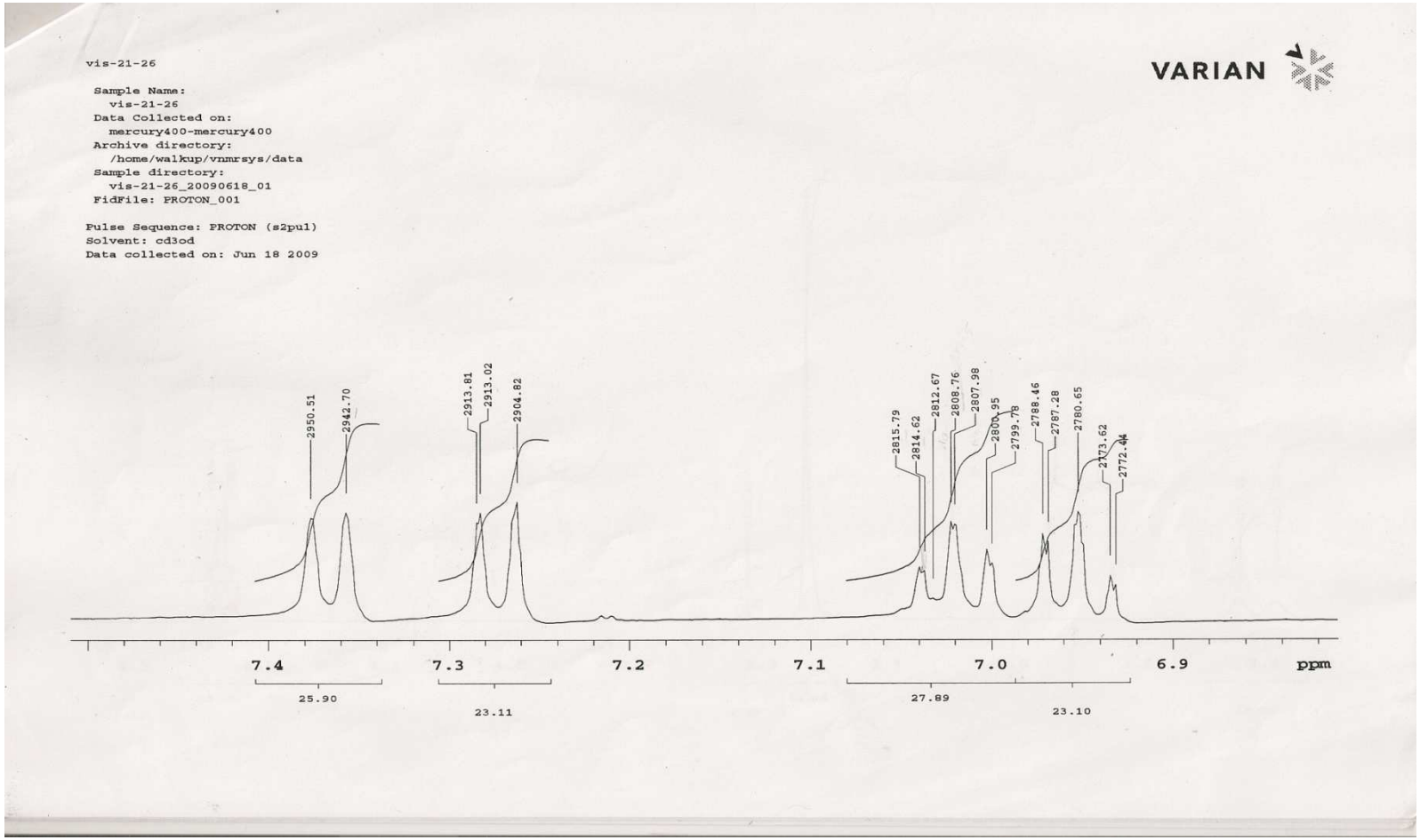

Figure B. 5: α-Yohimbine ^{1}H-NMR aromatic area.

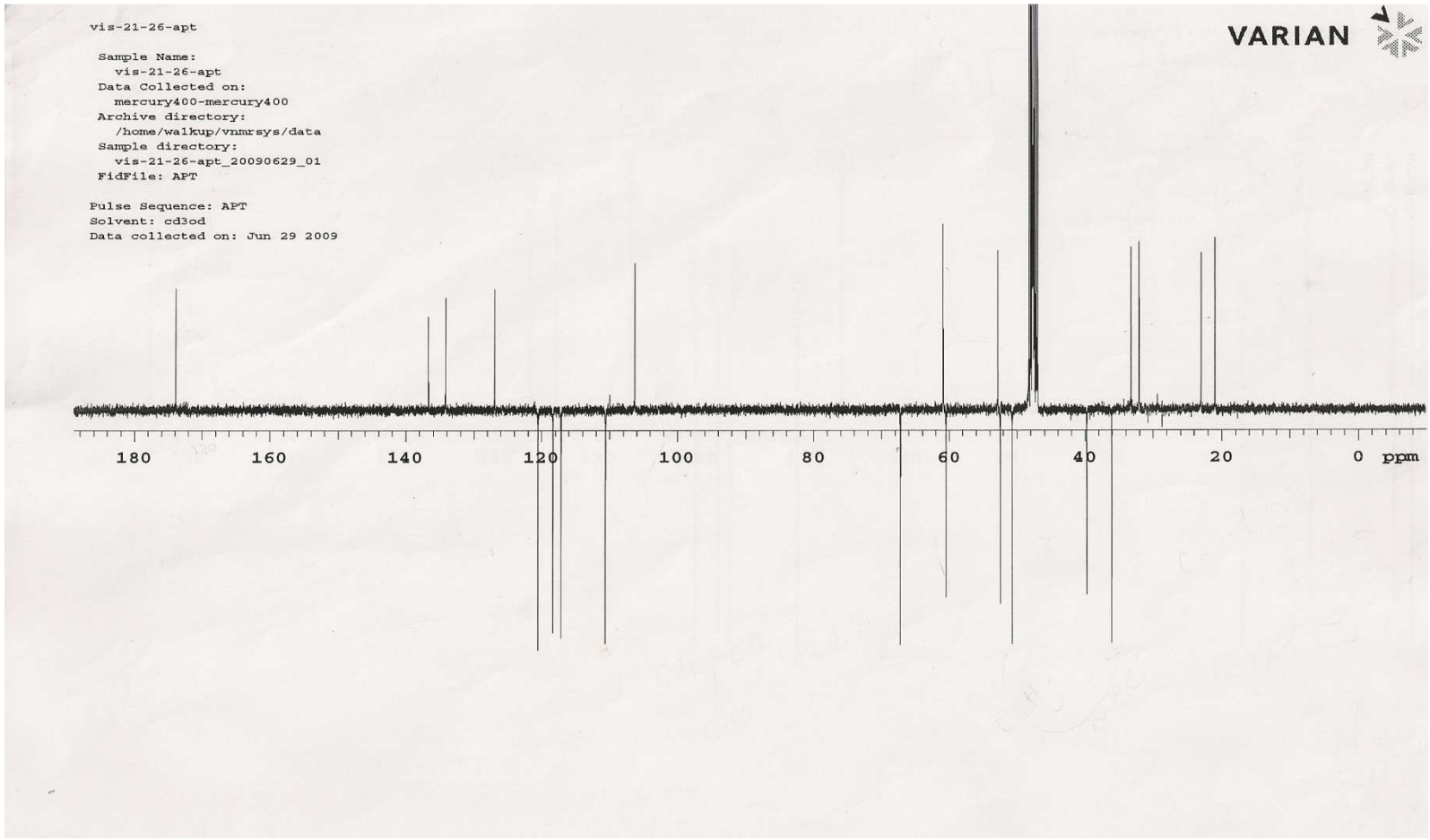

Figure B. 6: α-Yohimbine APT Spectrum.

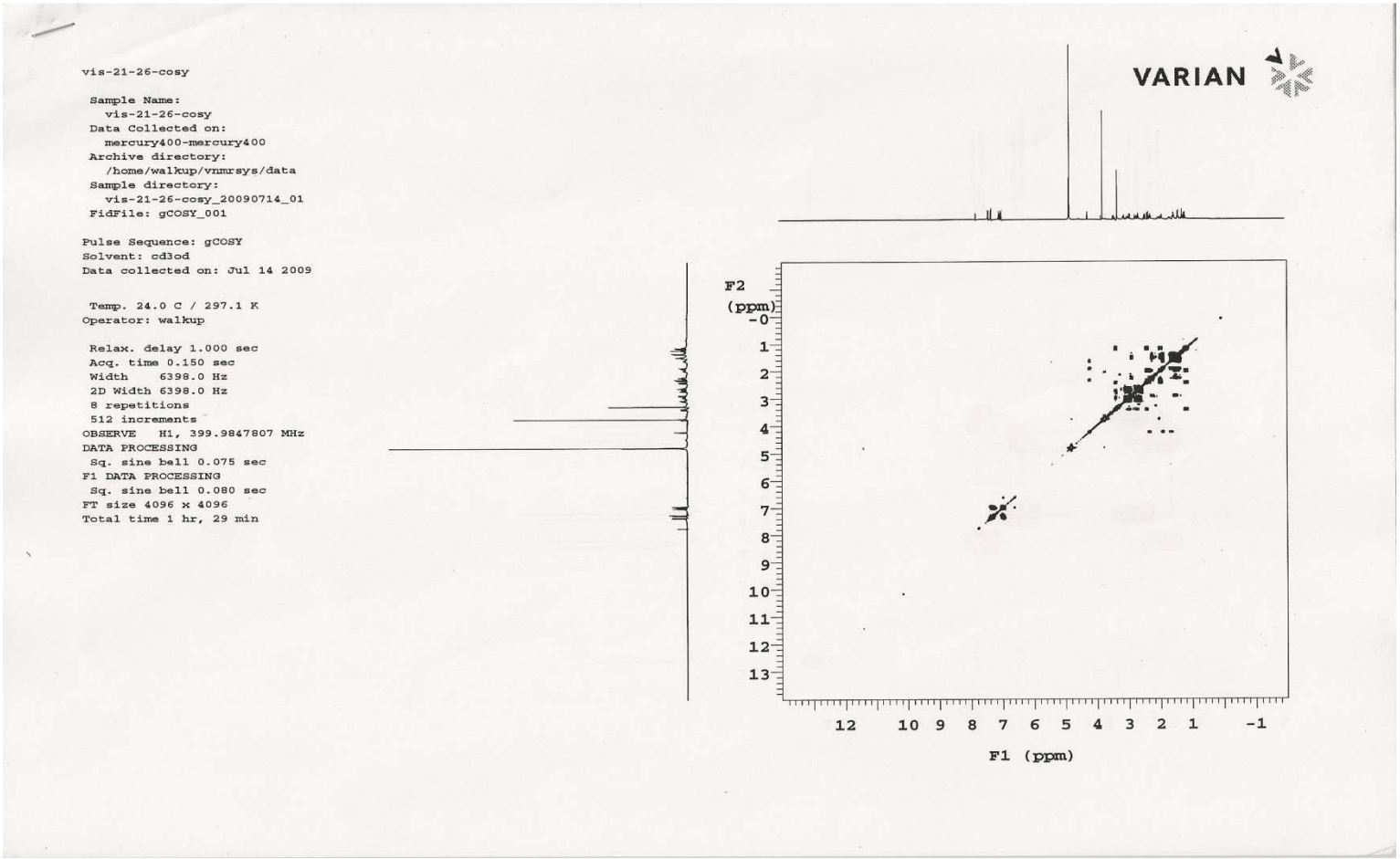

Figure B. 7: α-Yohimbine COSY Spectrum.

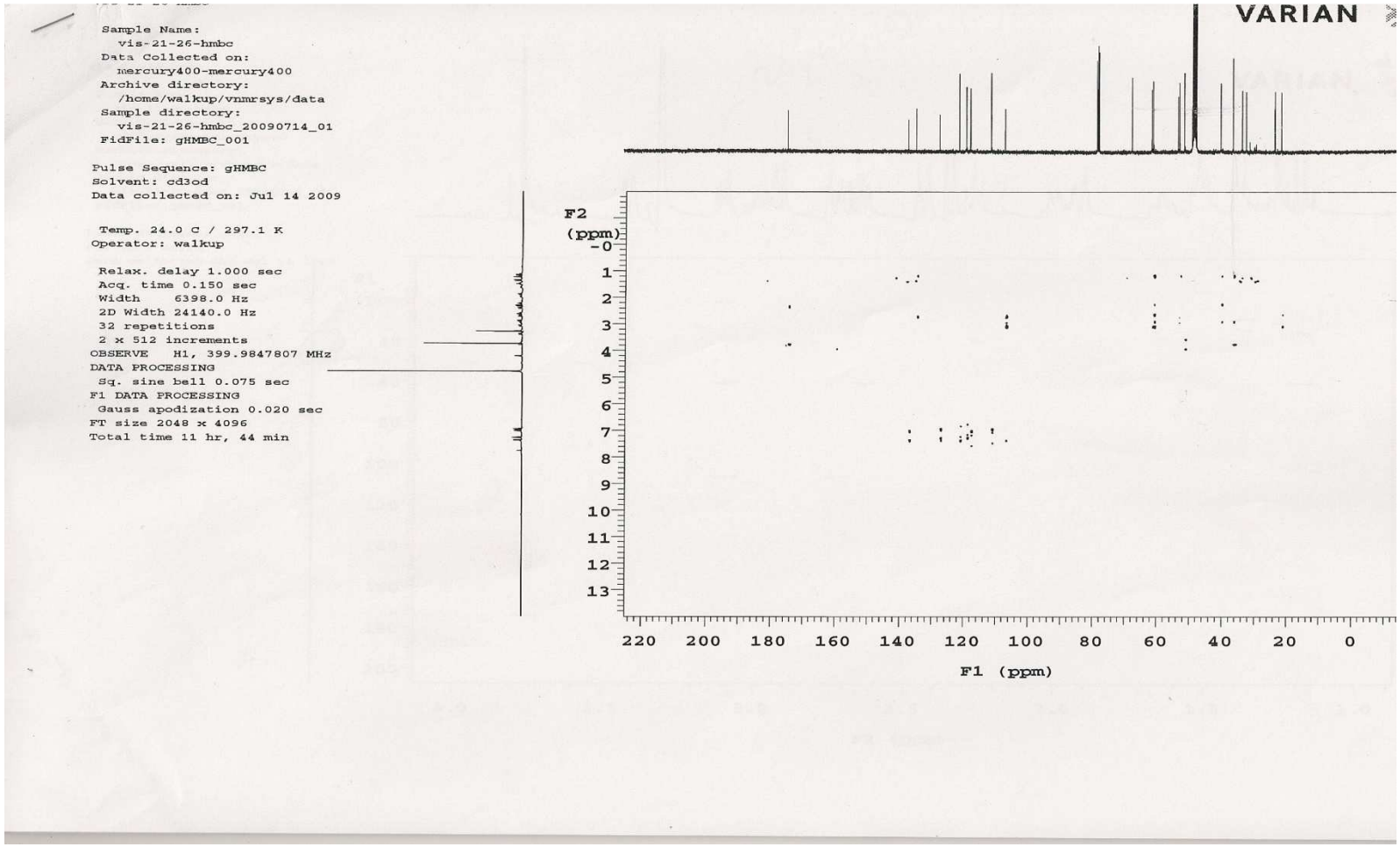

Figure B. 8: : α-Yohimbine HMBC Spectrum.

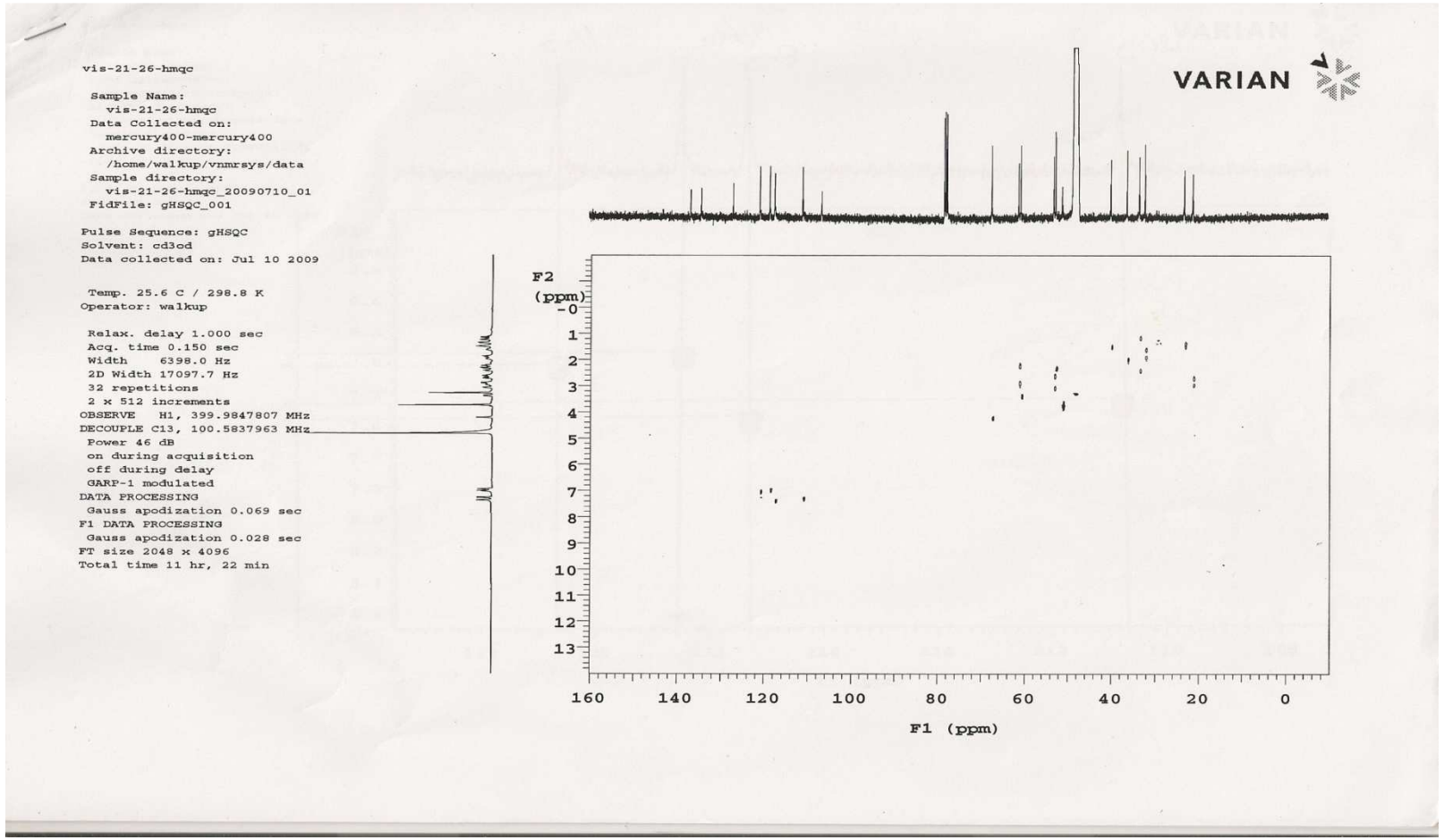

Figure B. 9: α-Yohimbine HMQC Spectrum.

APPENDIX C: NMR Spectra of β –Yohimbine

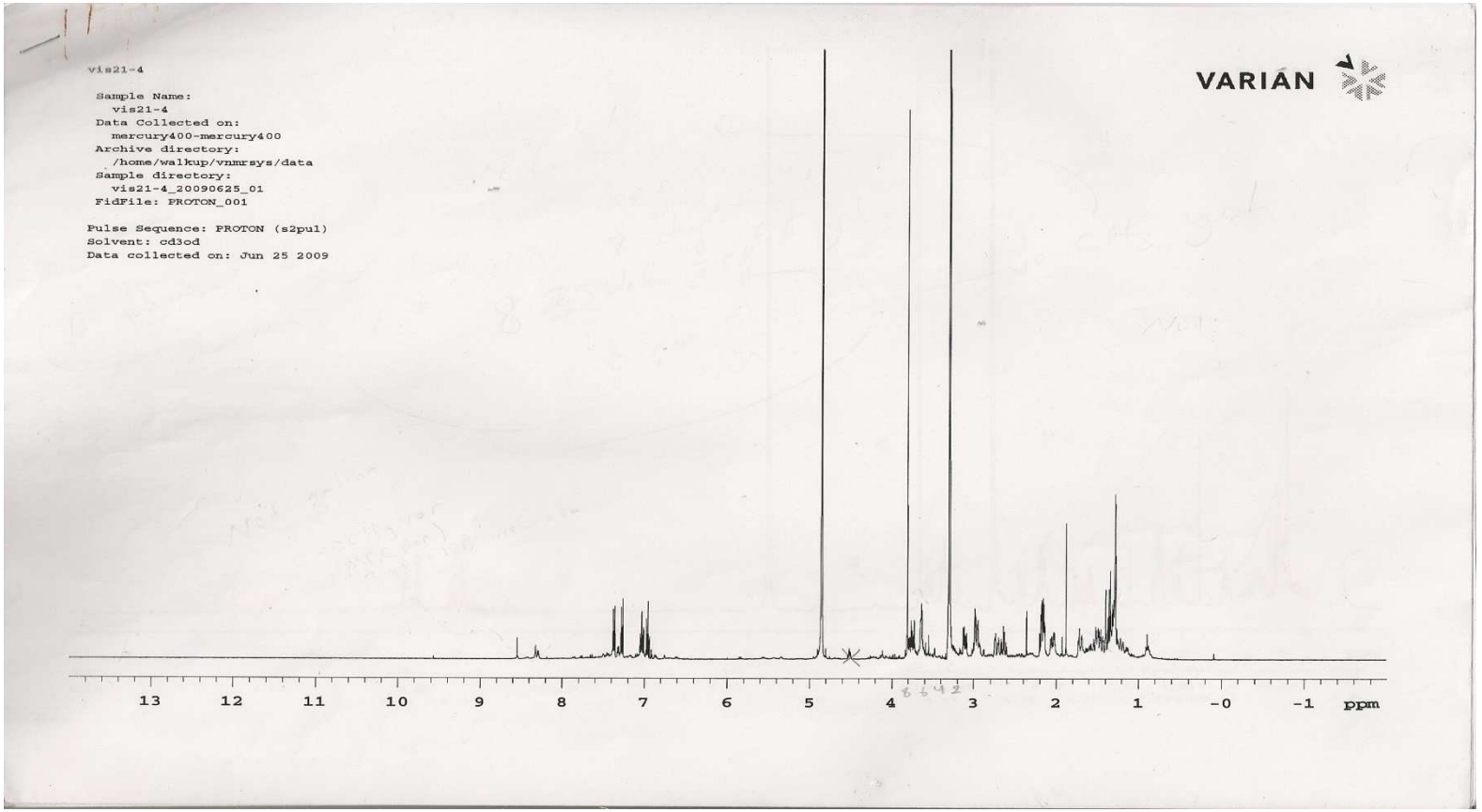

Figure C. 1: β- Yohimbine, ^{1}H-NMR.

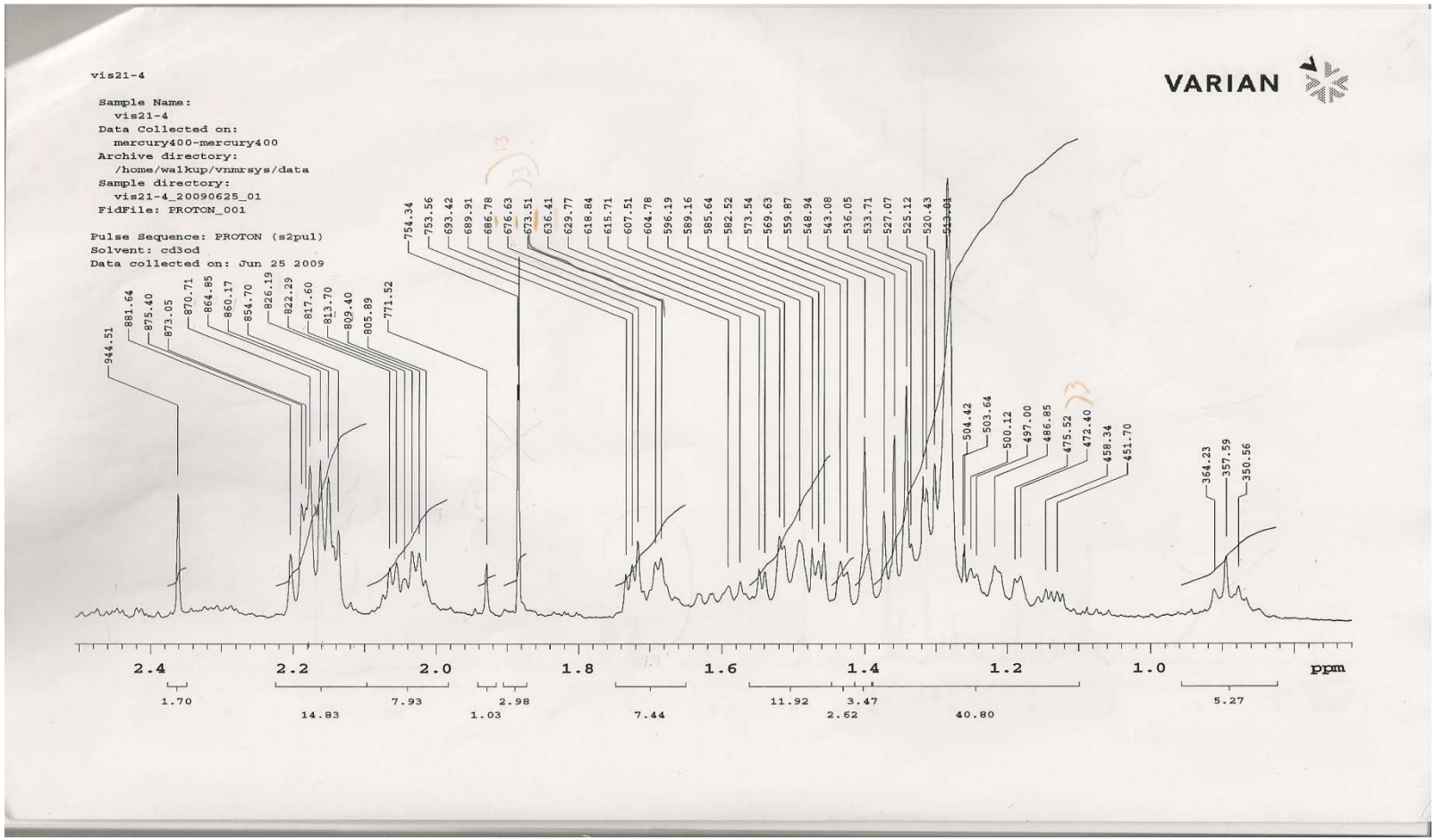

Figure C. 2: β –Yohimbine ^{1}H-NMR (1.0-2.5 ppm**).**

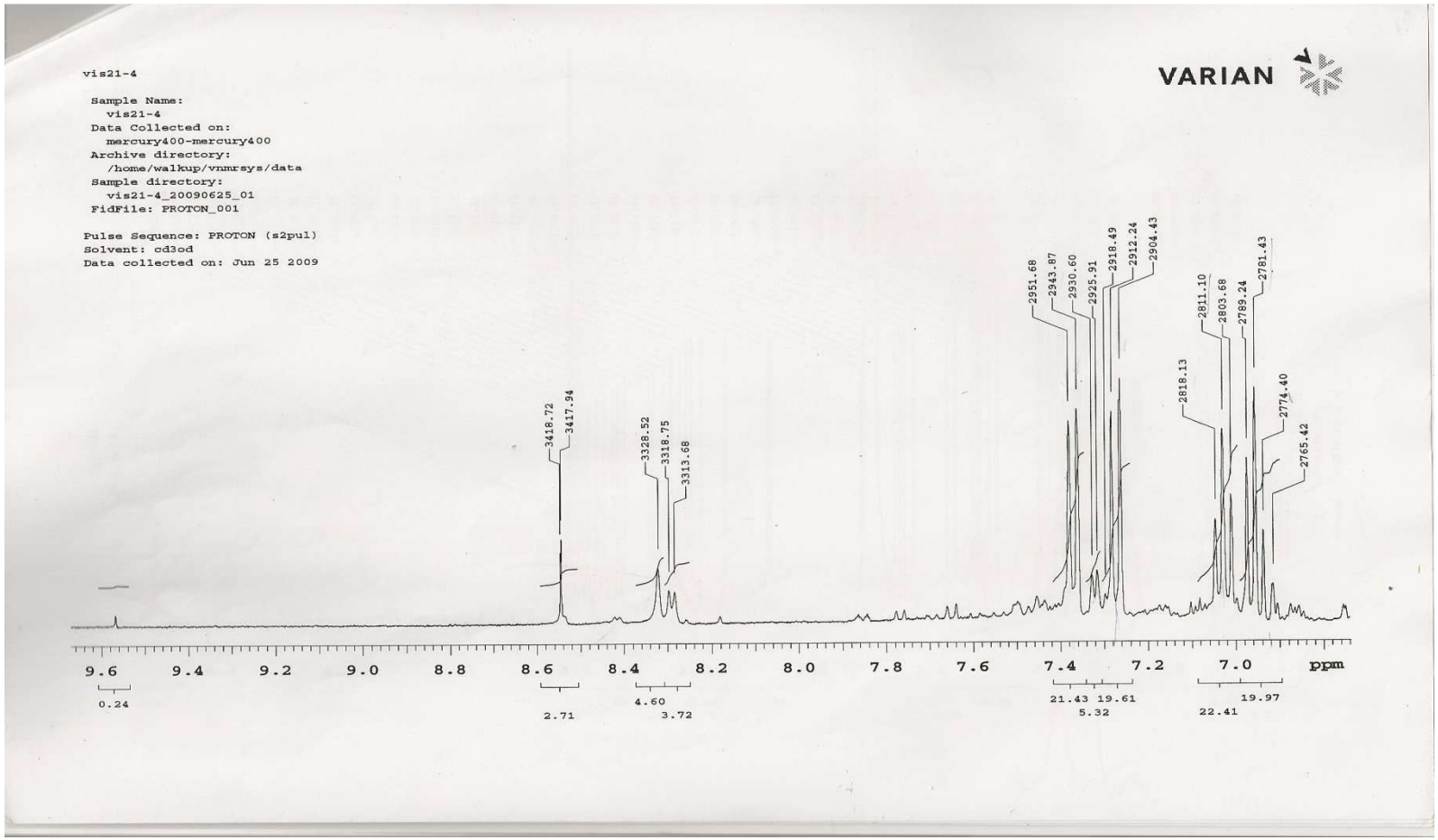

Figure C. 3: β –Yohimbine ^{1}H-NMR aromatic area.

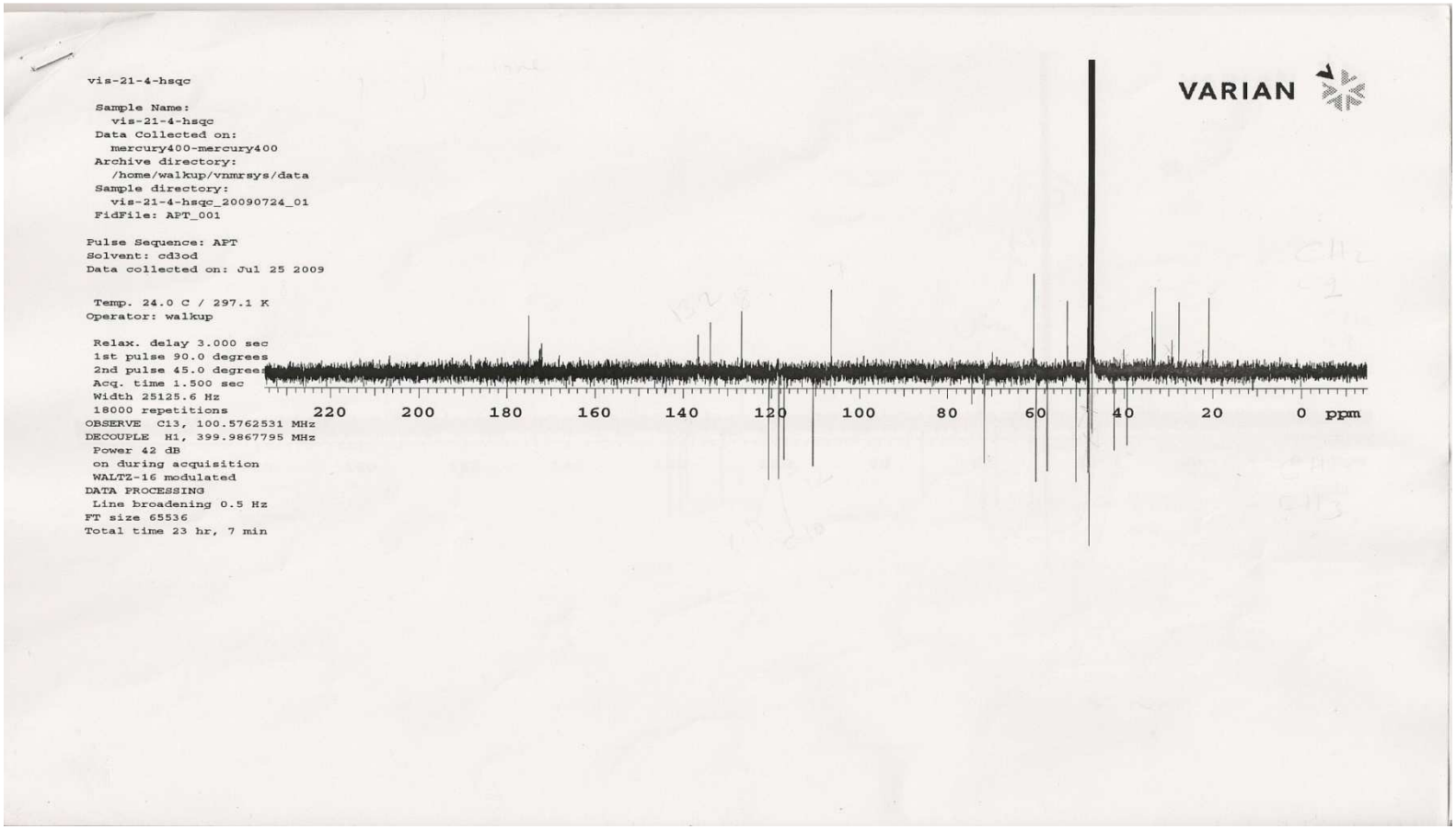

Figure C. 4: β –Yohimbine APT Spectrum.

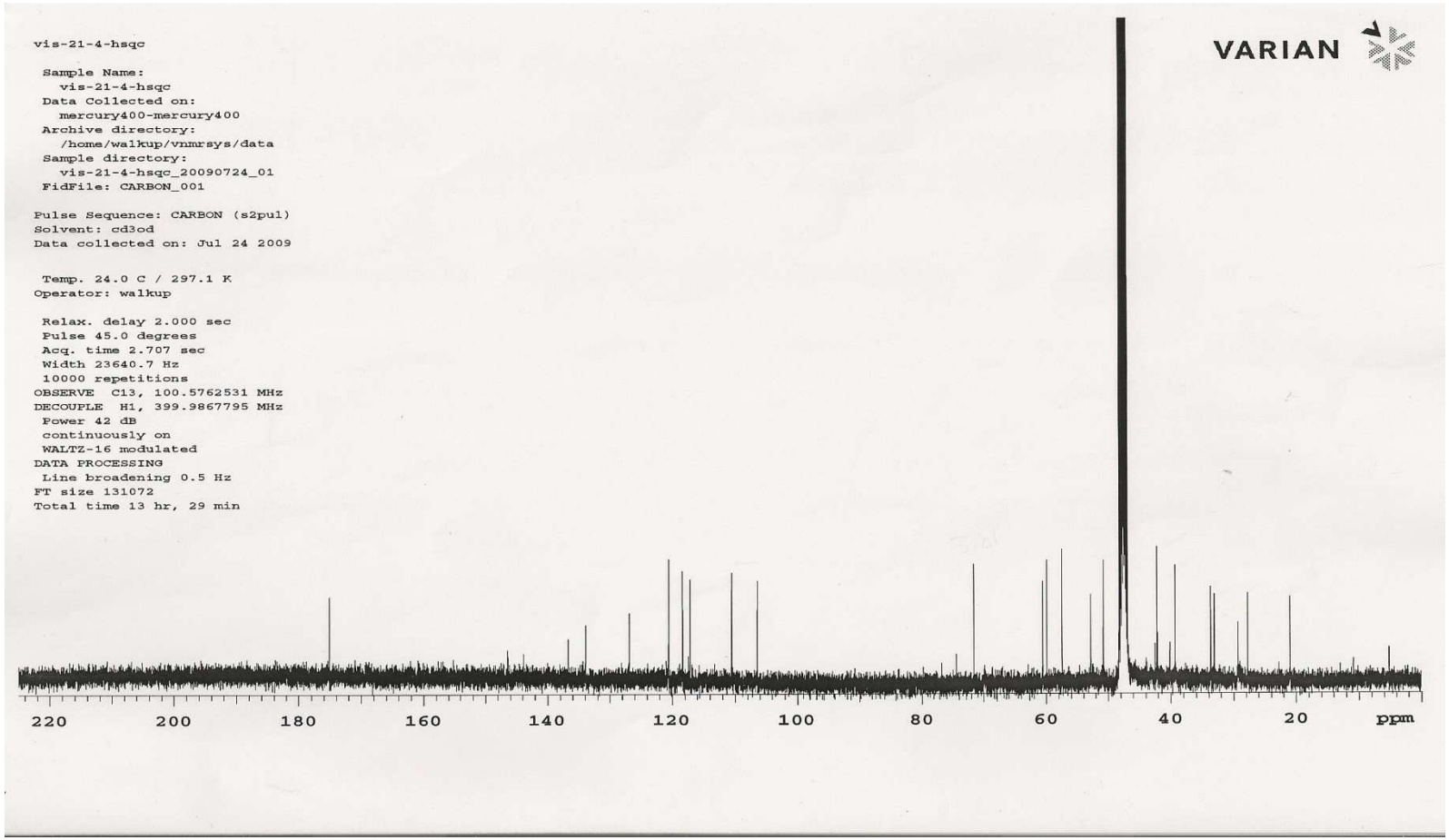

Figure C. 5: β –Yohimbine BB Spectrum.

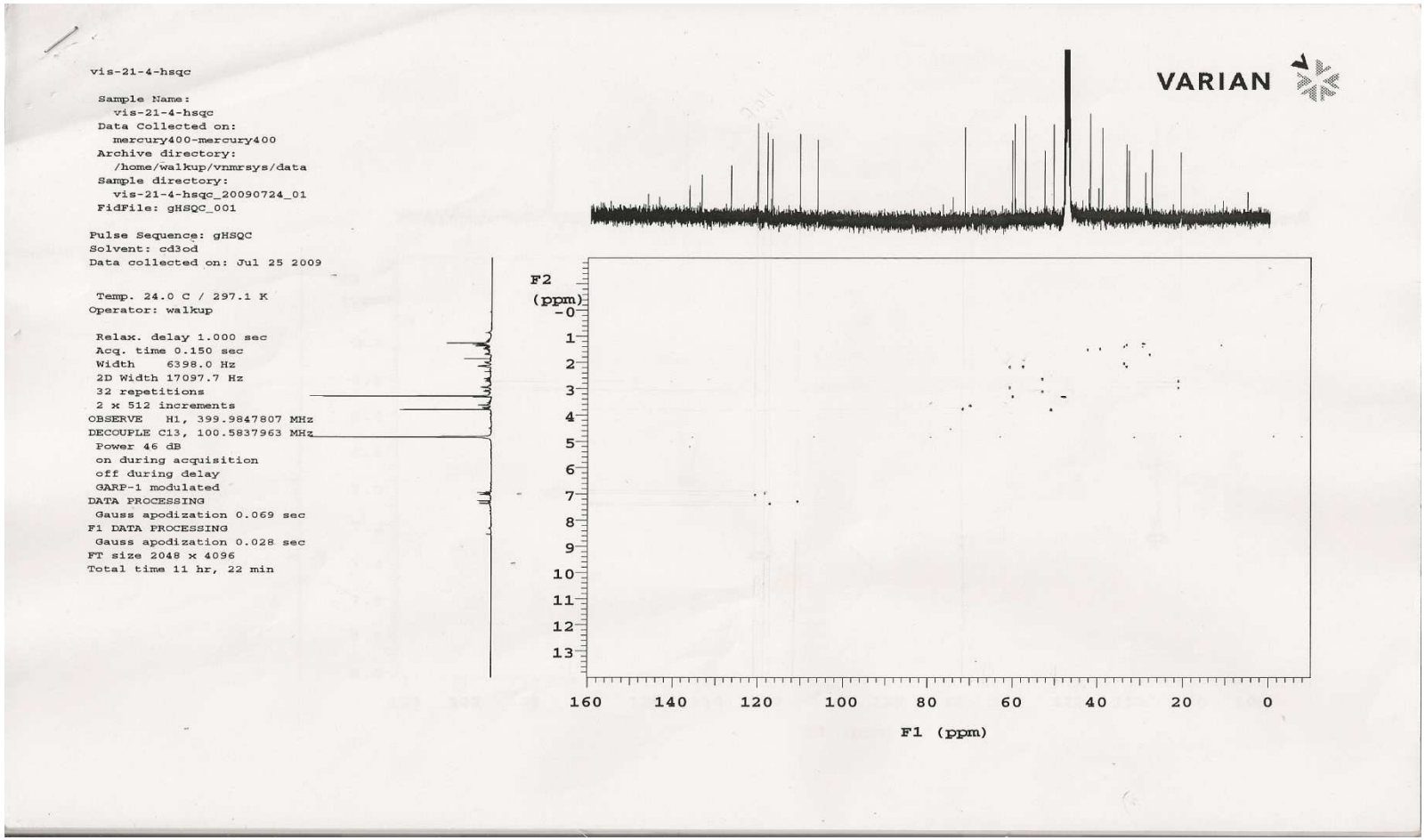

Figure C. 6: β –Yohimbine HSQC Spectrum.

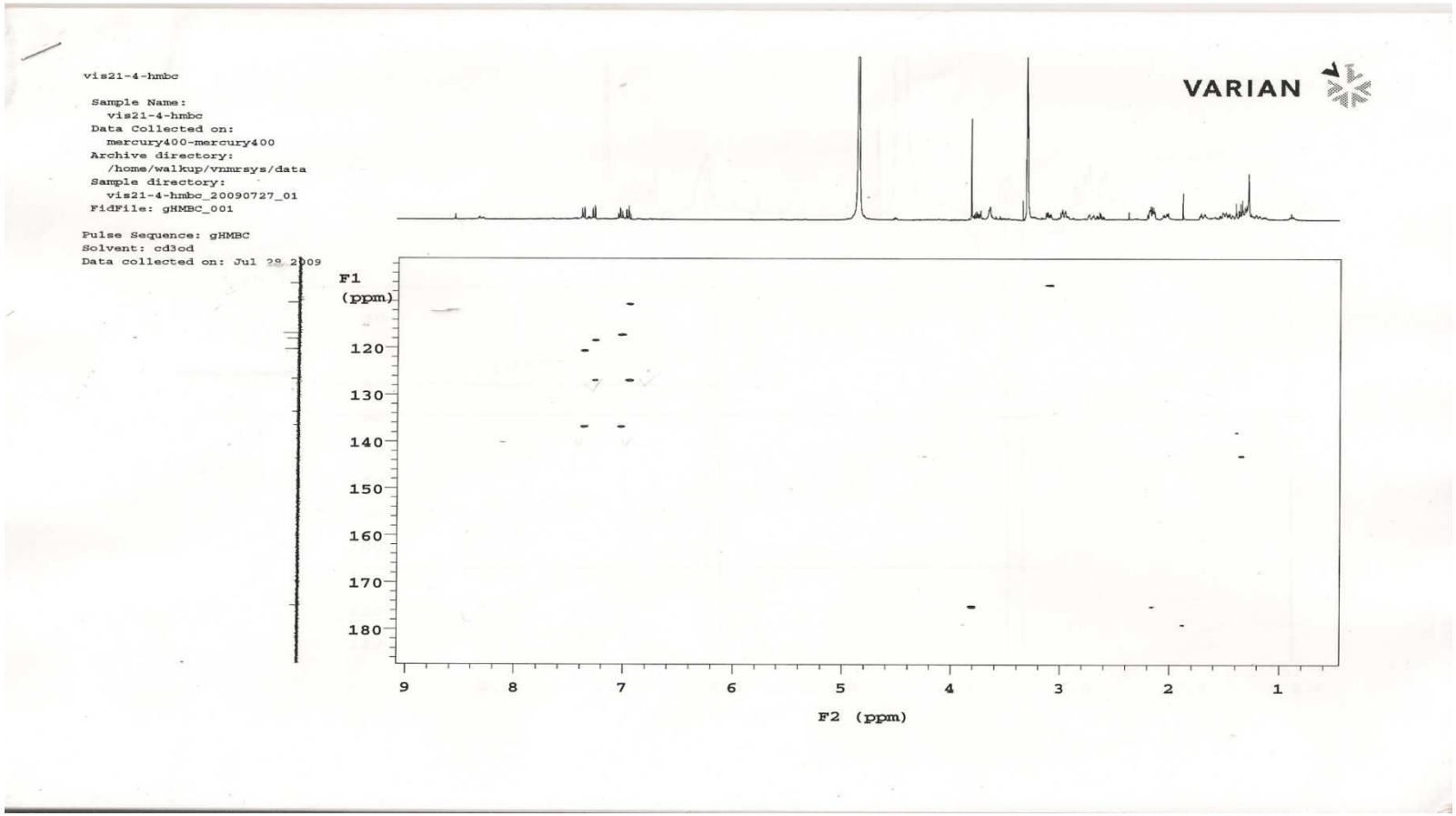

Figure C. 7: : β –Yohimbine HMBC Spectrum.

APPENDIX D: Spectral Data of Picrinine

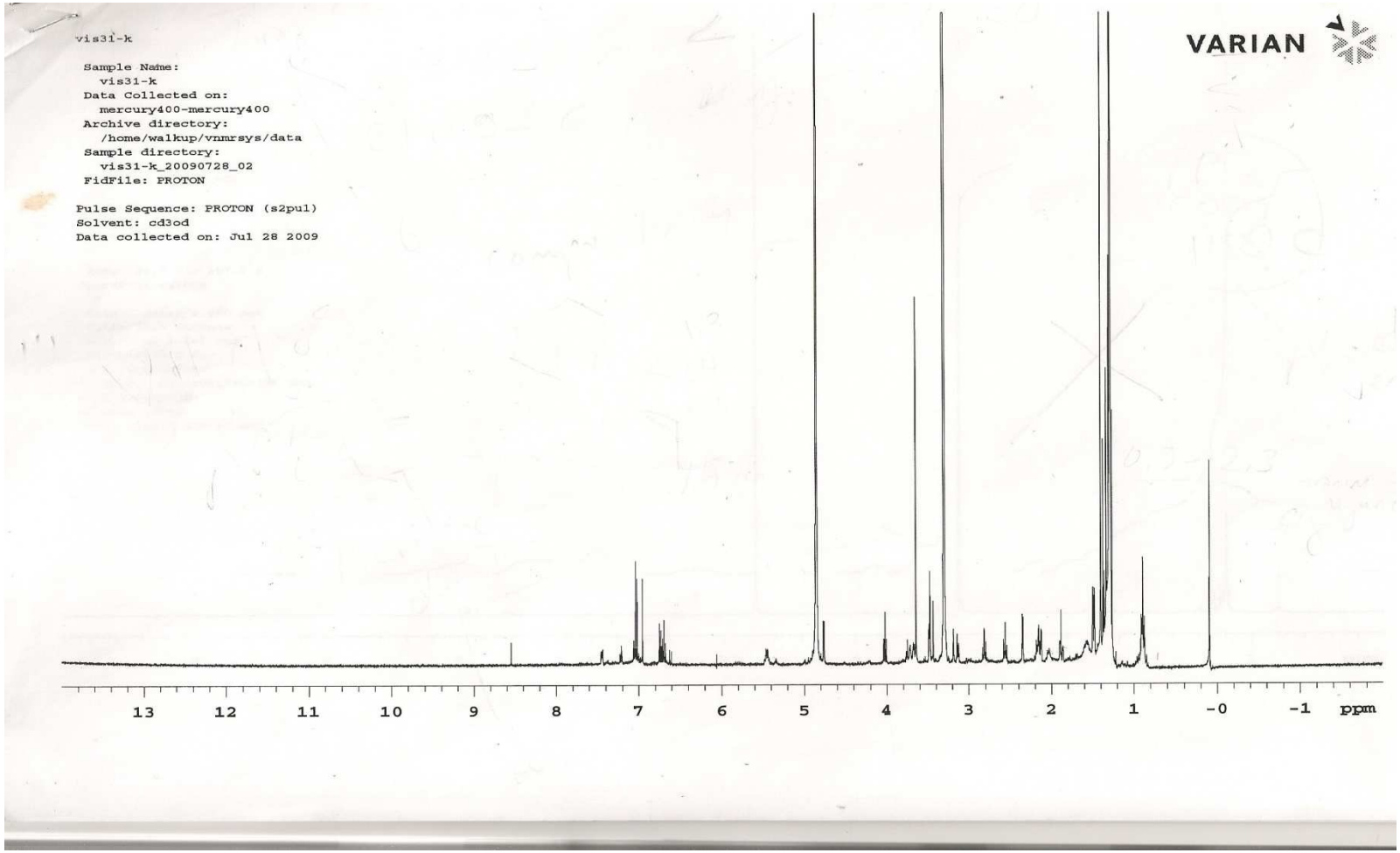

Figure D. 1: ^{1}H-NMR spectrum of Picrinine.

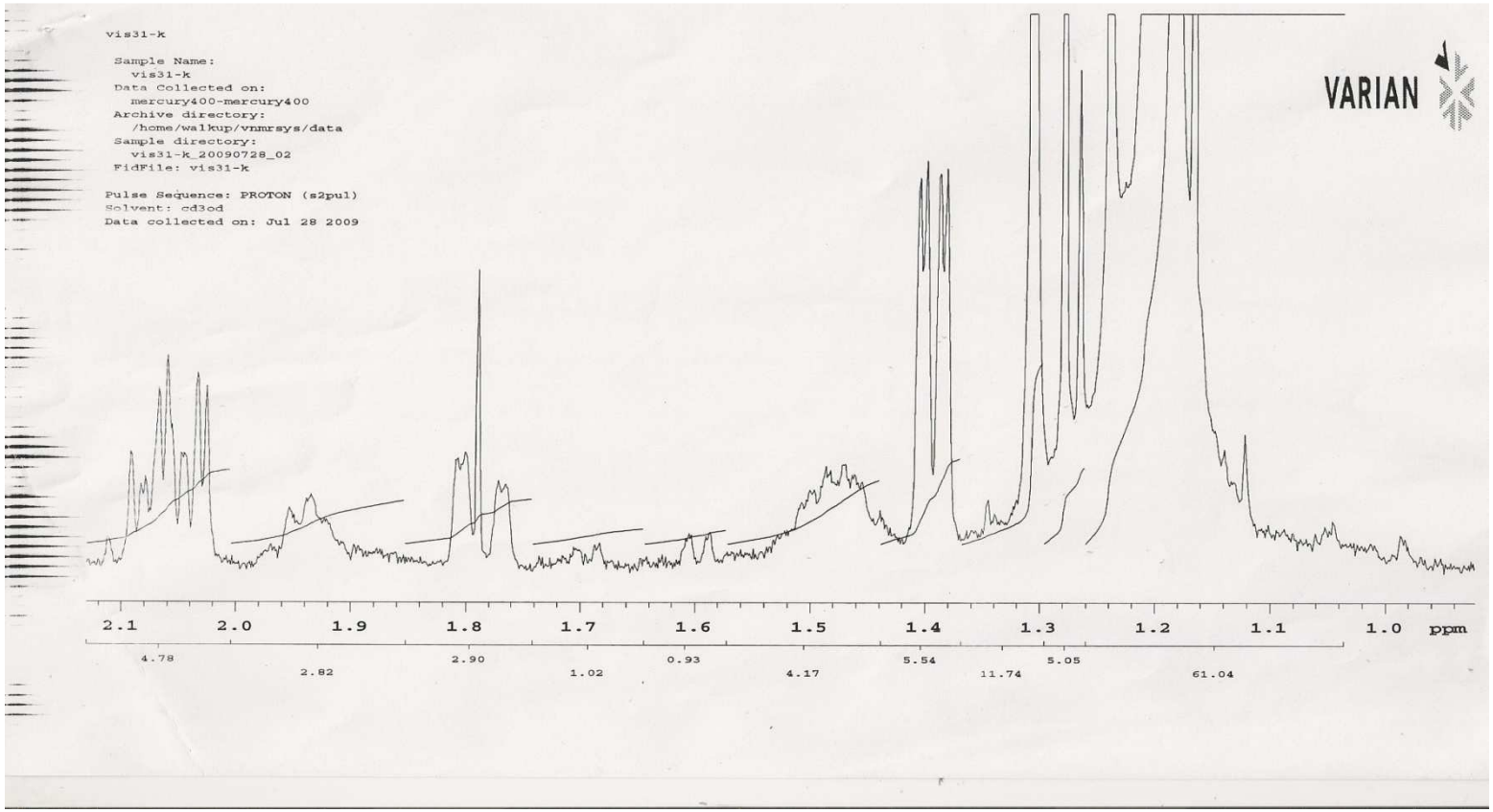

Figure D. 2: Picrinine ^{1}H-NMR (1.0-2.1 ppm).

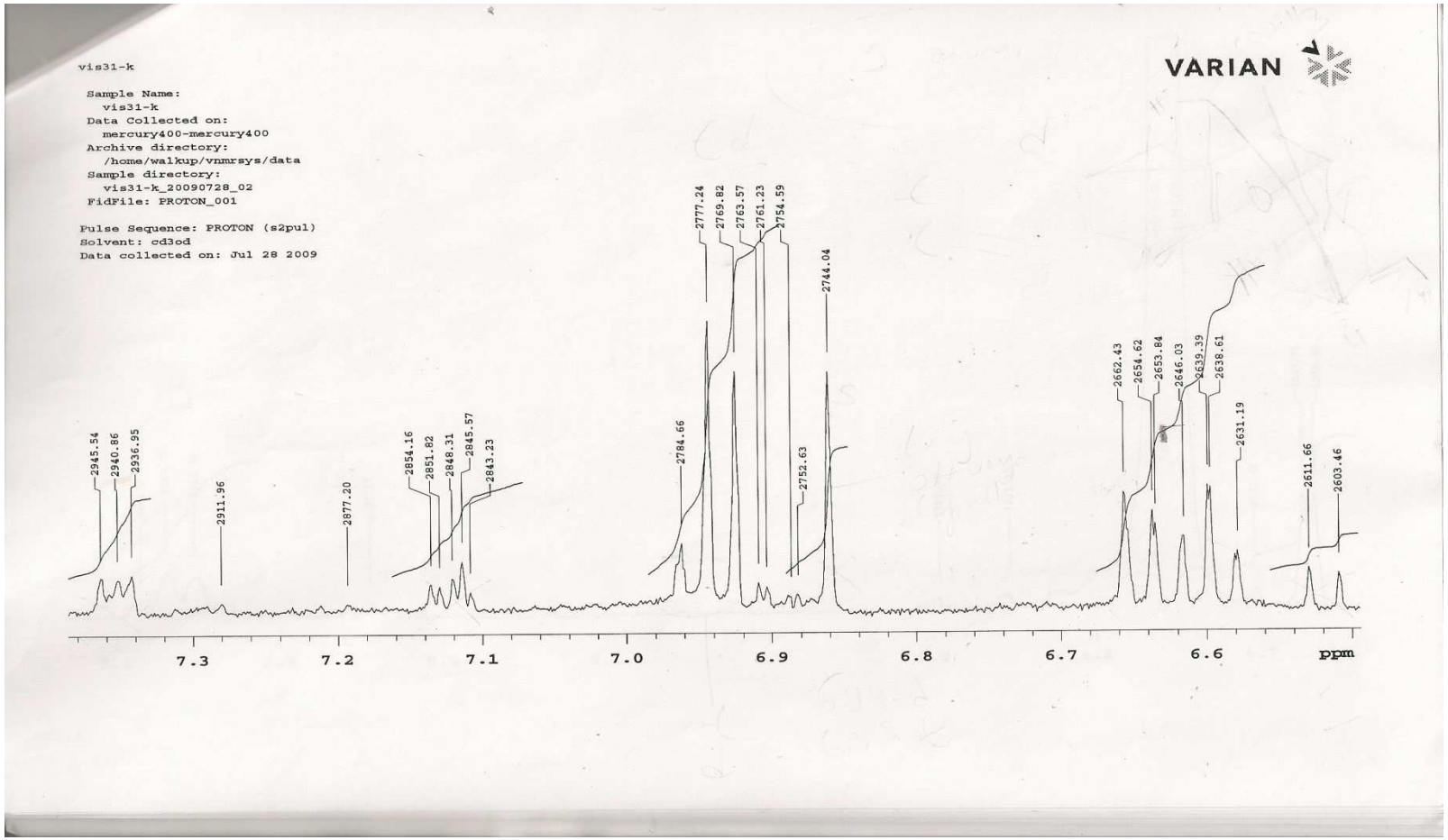

Figure D. 3: Picrinine ^{1}H-NMR Aromatic Area.

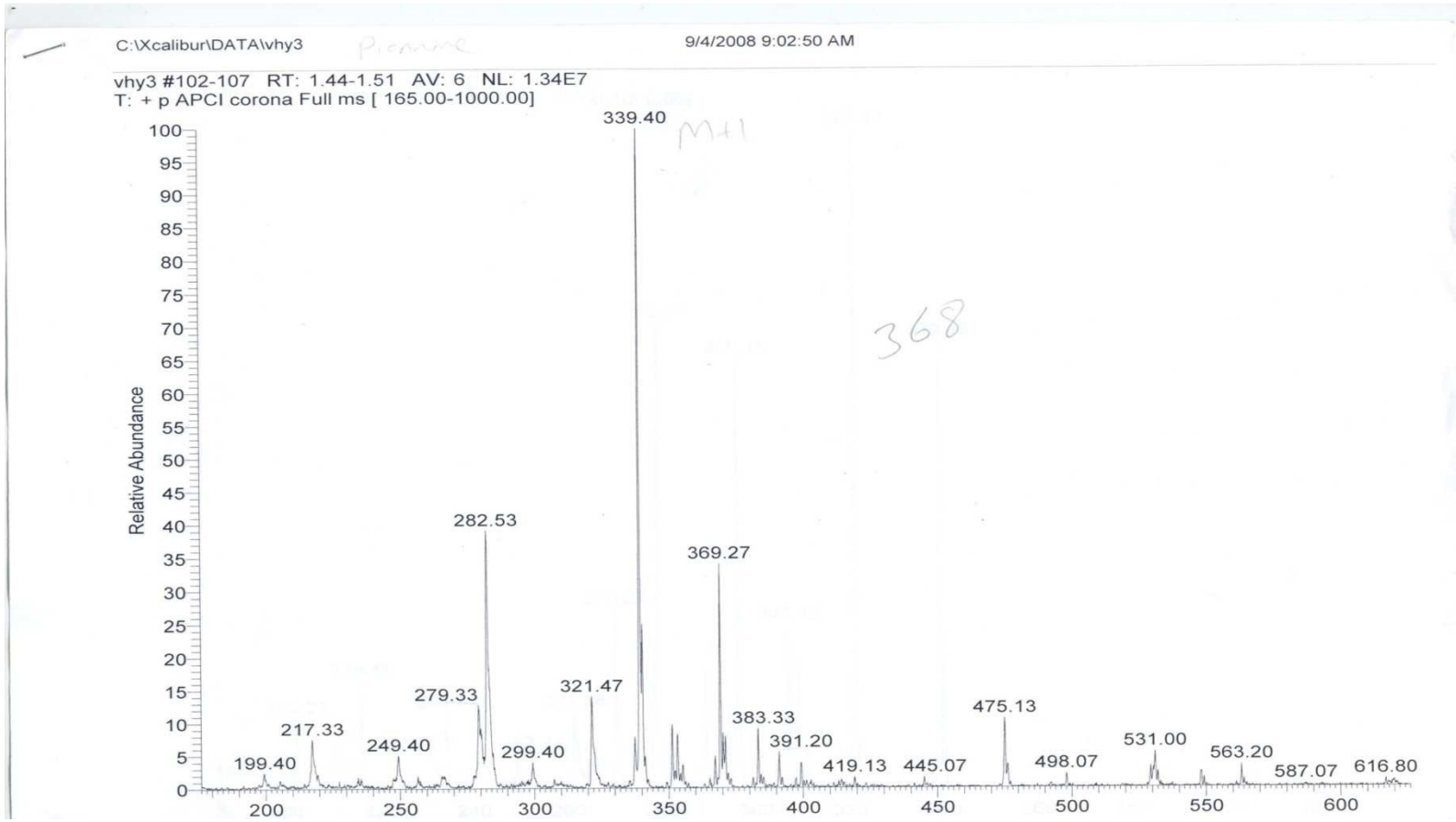

Figure D. 4: Picrinine MASS Spectrum.

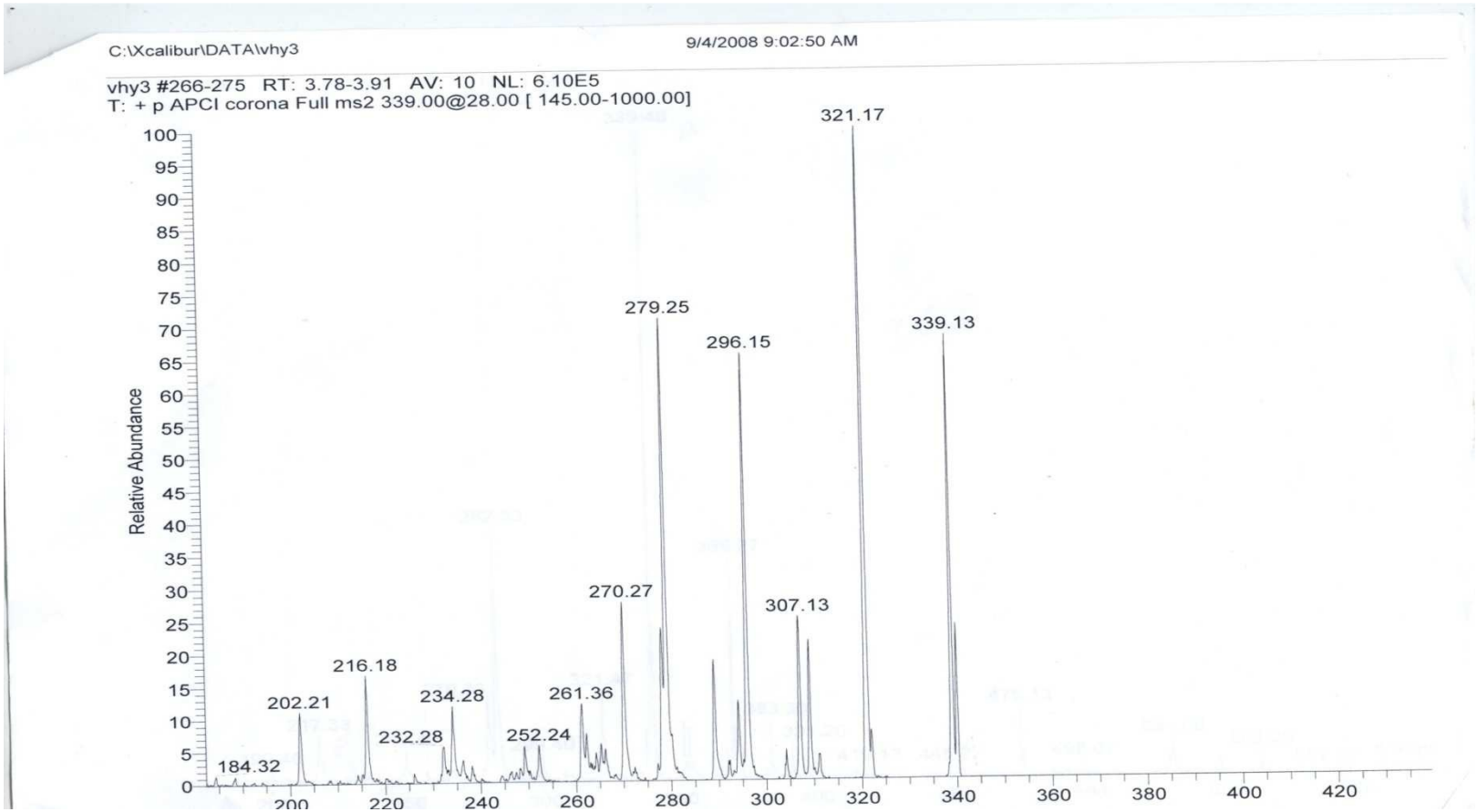

Figure D. 5: Picrinine MASS Spectrum 2.

APPENDIX E: NMR Spactra of 11-Hydroxypolyneuridine

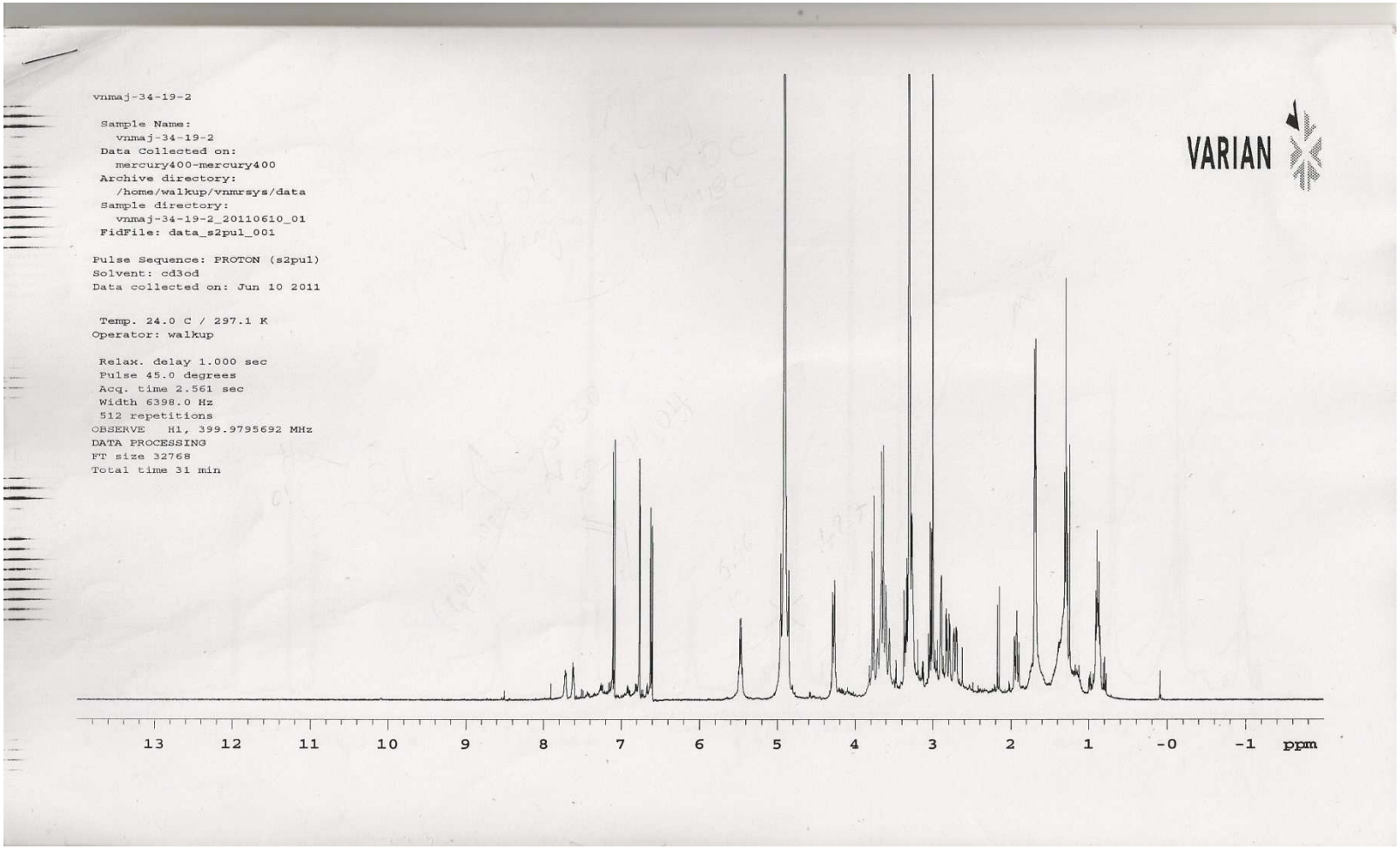

Figure E. 1: ^{1}H-NMR Spactrum of 11-Hydroxypolyneurid.

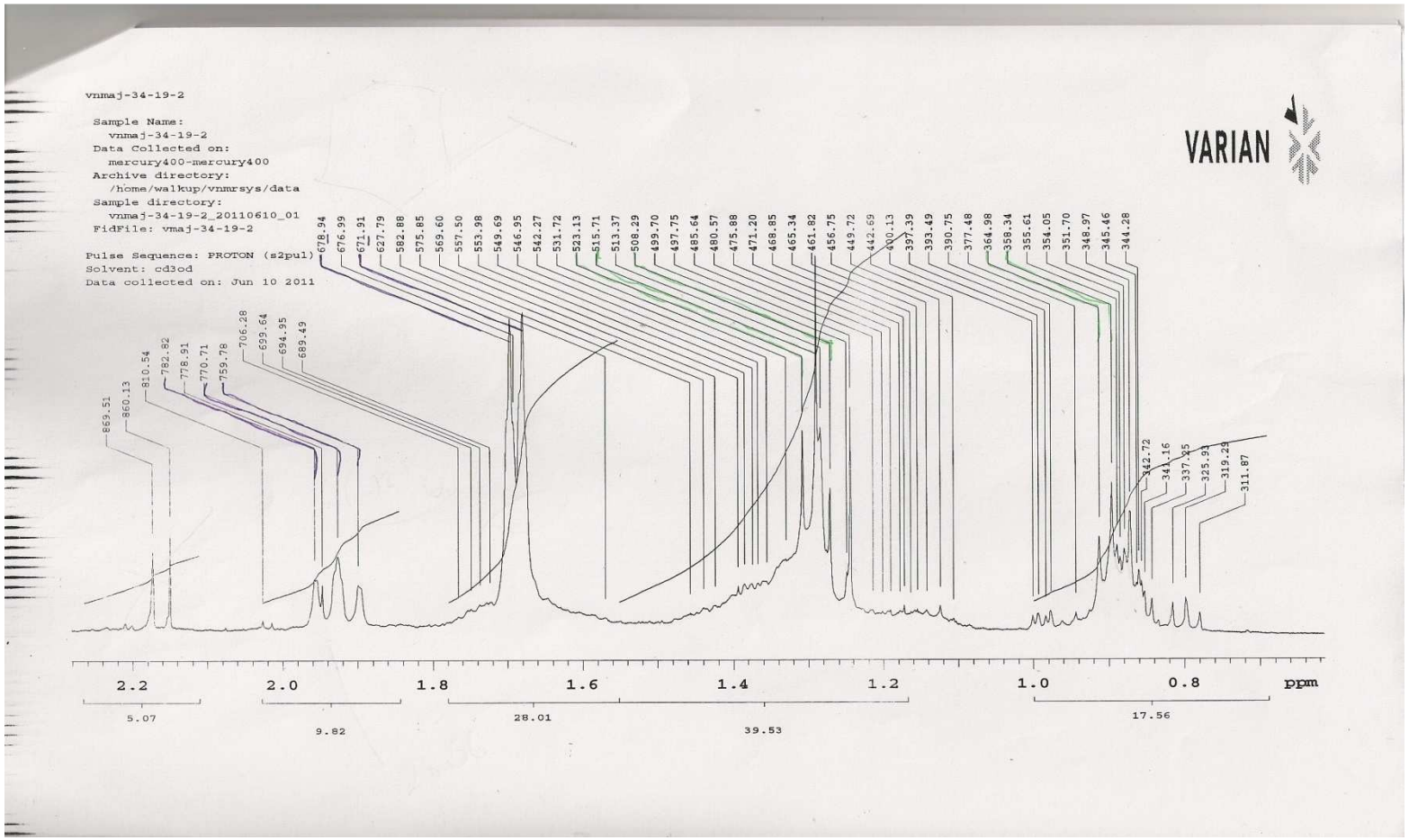

Figure E. 2: 11-Hydroxypolyneuridine ^{1}H-NMR (0.7-2.2 ppm).

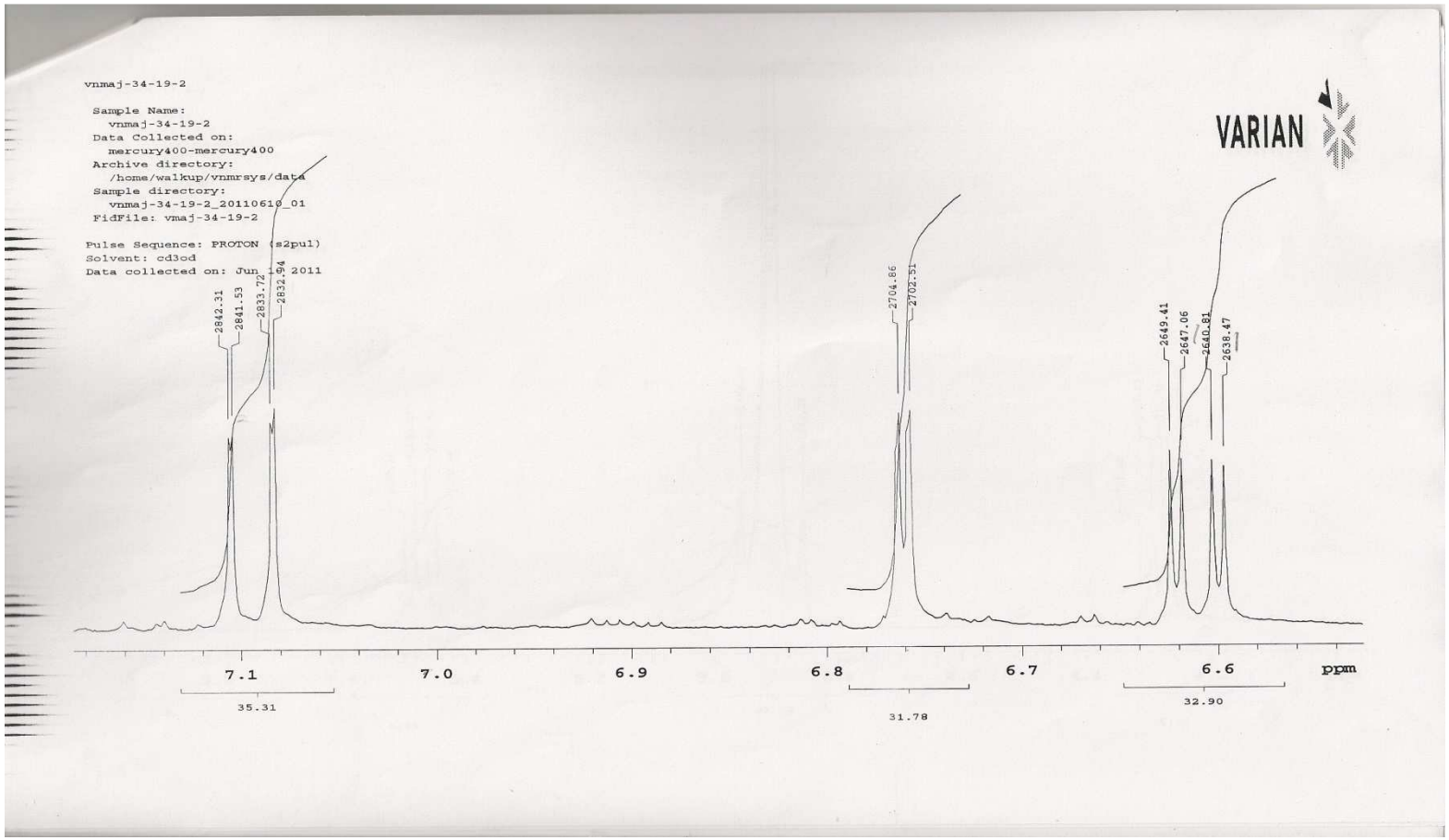

Figure E. 3: 11-Hydroxypolyneuridine ^{1}H-NMR aromatic area.

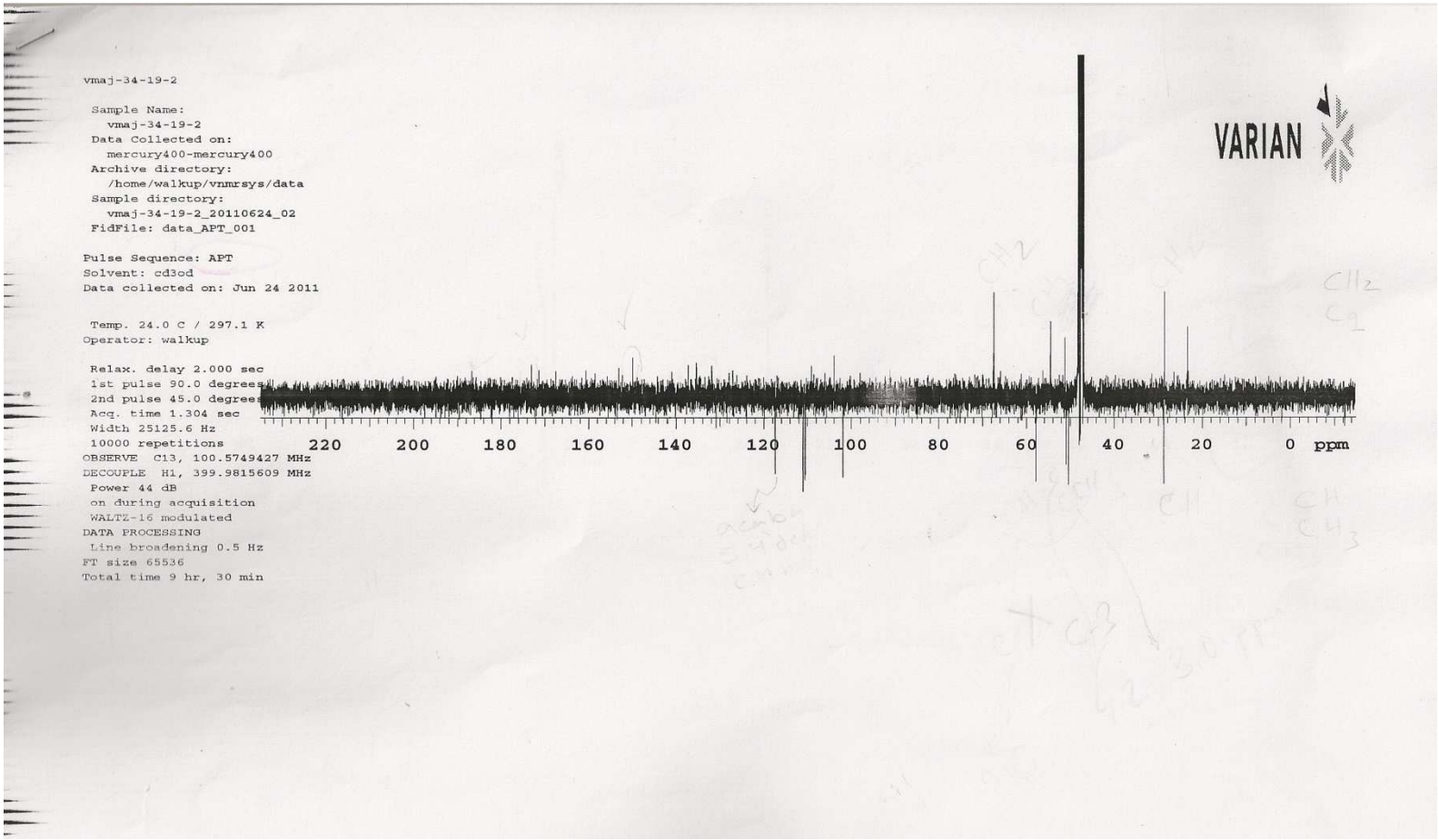

Figure E. 4: 11-Hydroxypolyneuridine APT Spectrum.

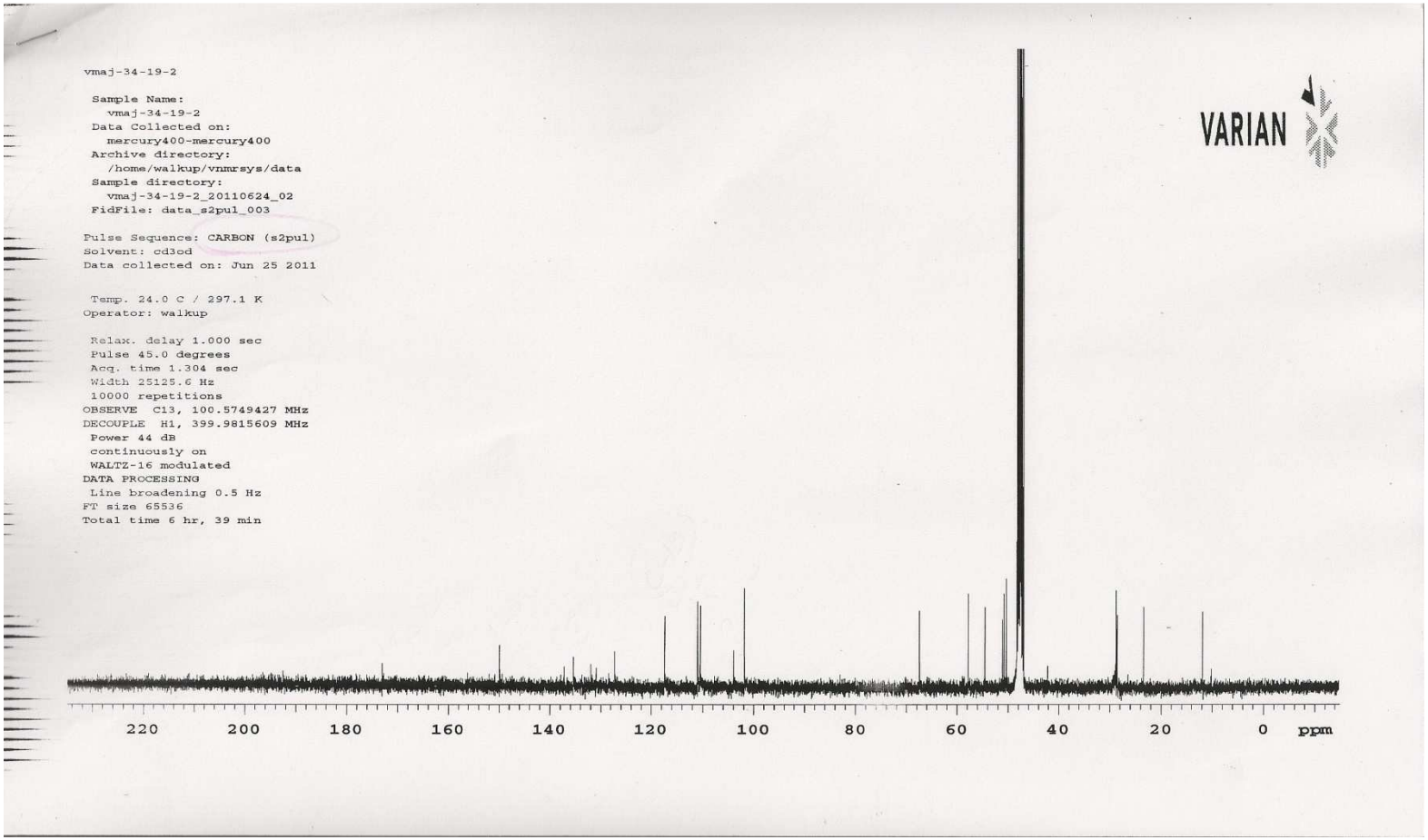

Figure E. 5: 11-Hydroxypolyneuridine BB Spectrum.

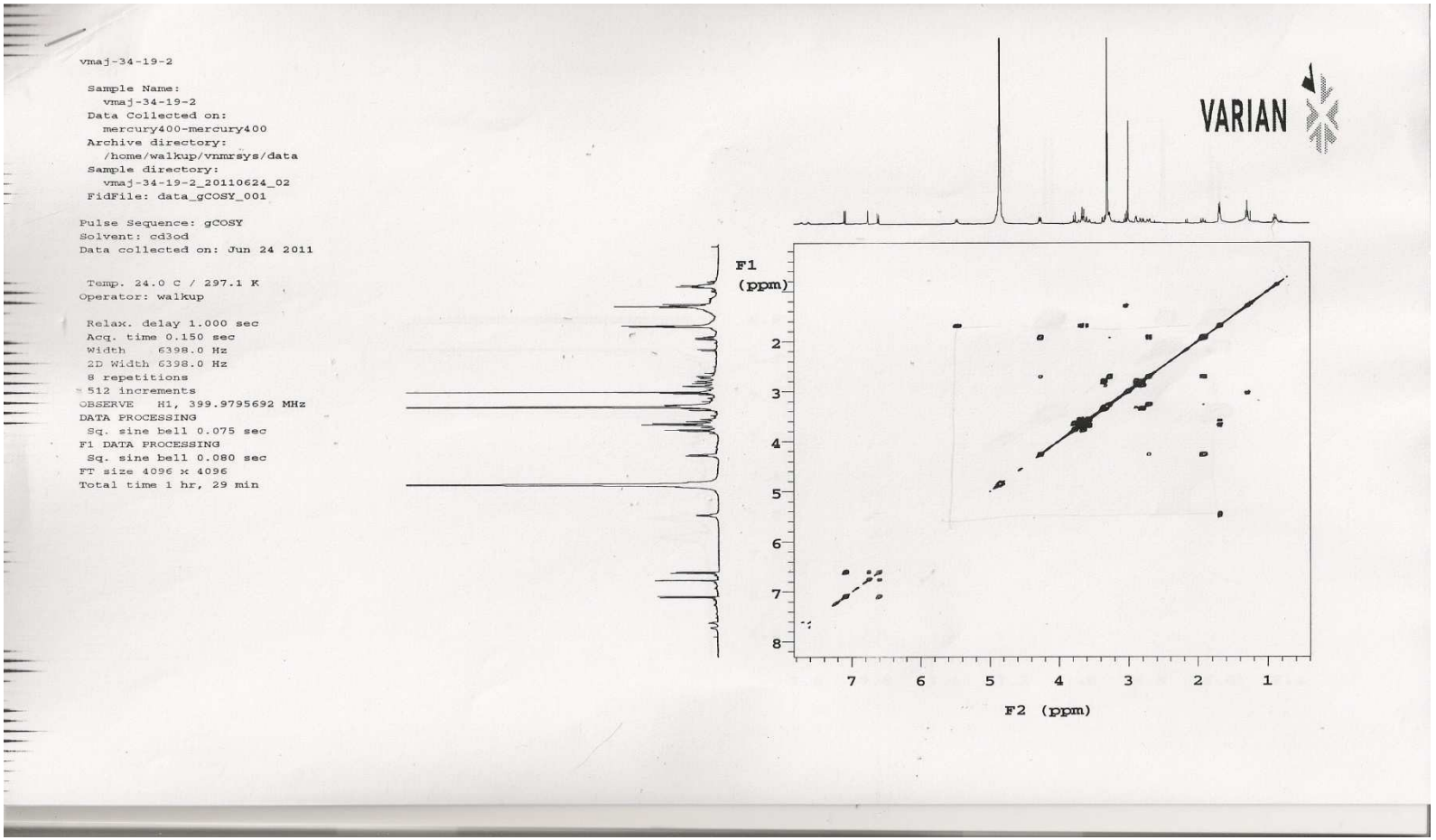

Figure E. 6: 11-Hydroxypolyneuridine COSY Spectrum.

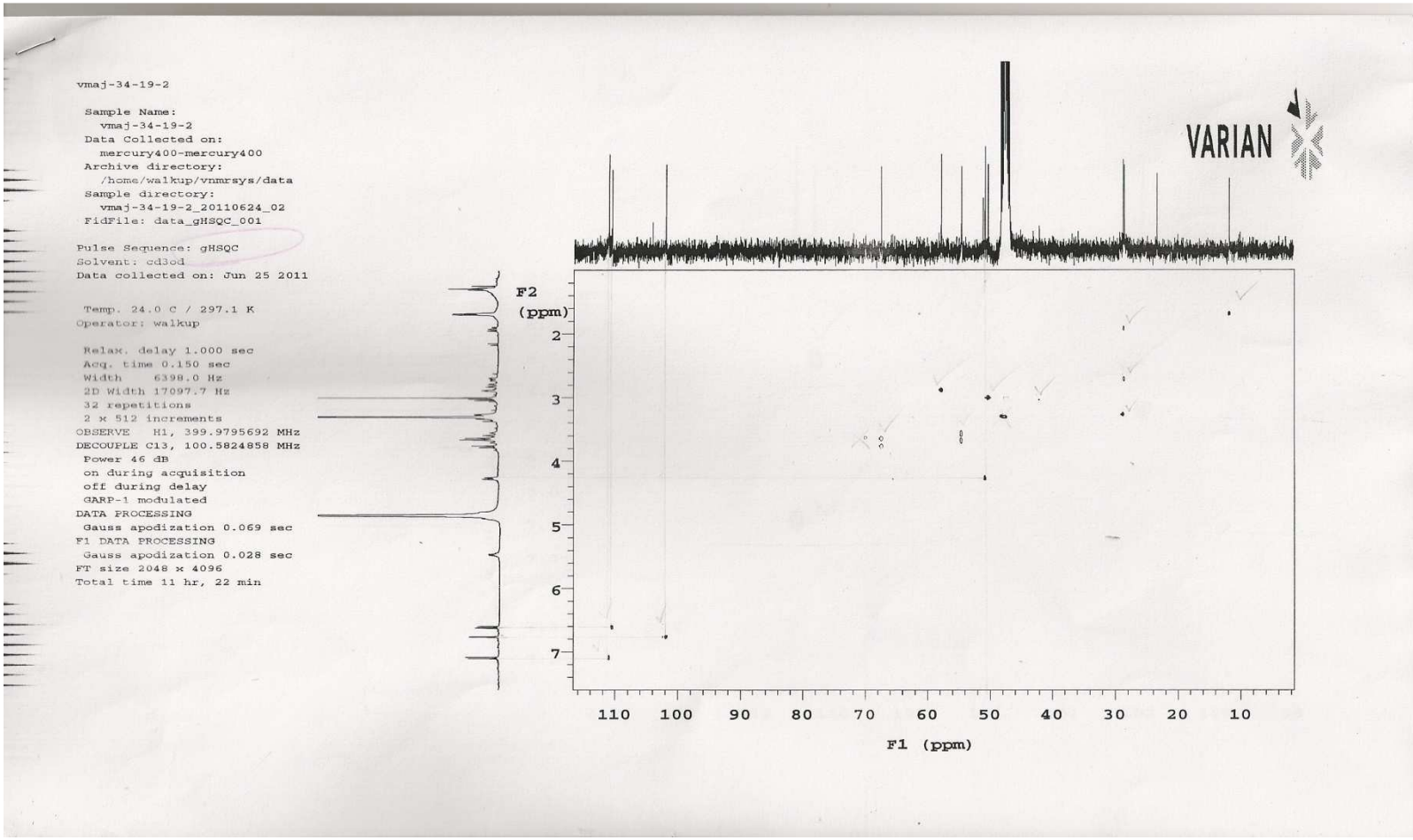

Figure E. 7: 11-Hydroxypolyneuridine HSQC Spectrum.

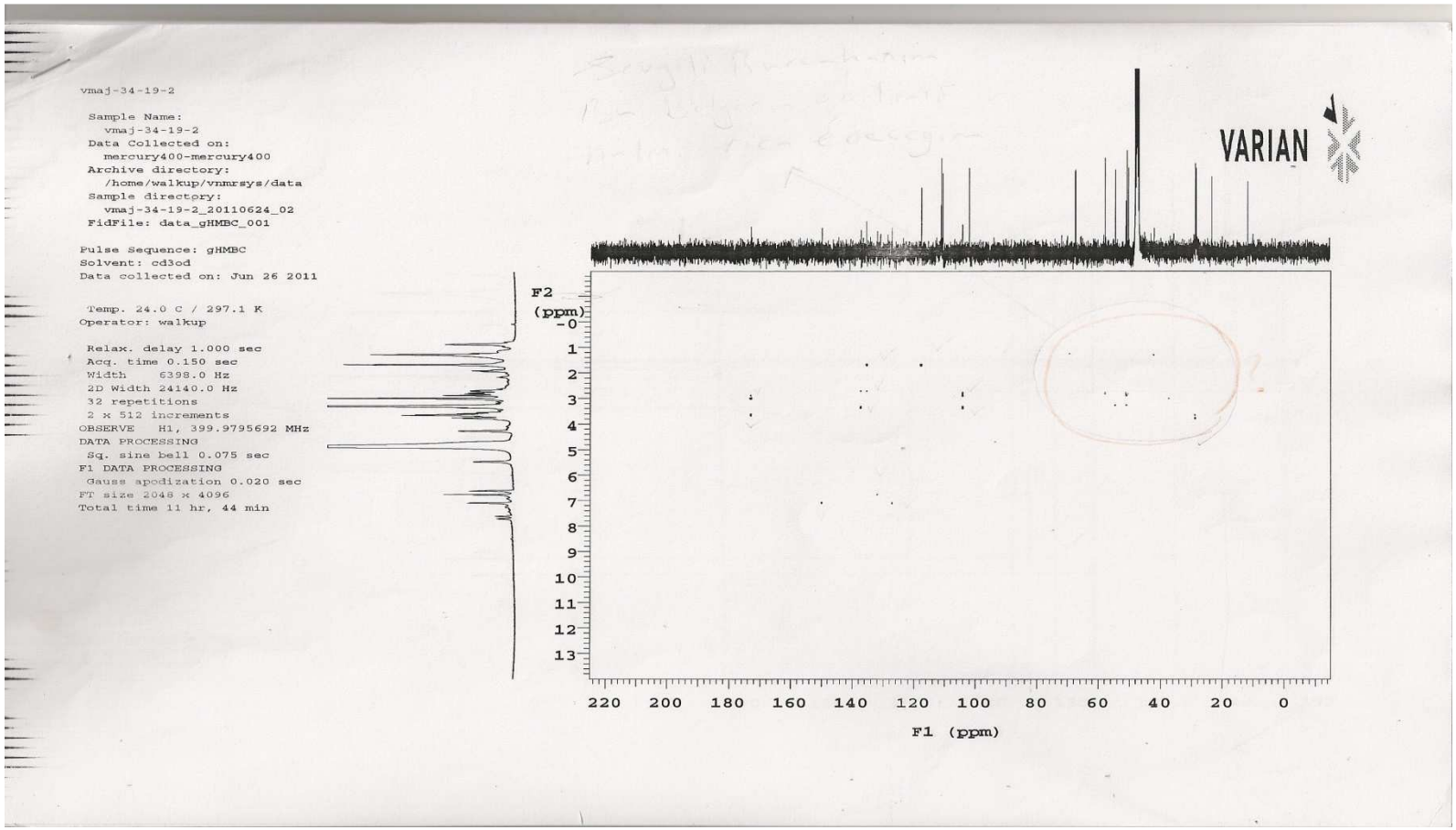

Figure E. 8: 11-Hydroxypolyneuridine HMBC Spectrum.

APPENDIX F: Indole Alkaloids Isolated from *Vinca minor, major* & *herbacea*

Table F. 1: Indole alkaloids isolated from *Vinca minor, major* and *herbacea.*

Compound	**Structure**	**Source**	**Year Published**	**Literature**
Vinoxine	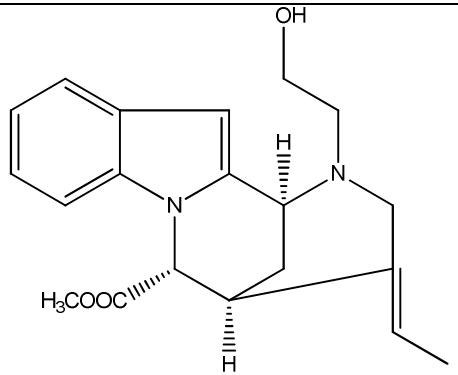	*Vinca minor*	1977	Vinoxine, A Novel Type of Indole Alkaloid, Voticky, Z. Et al. Collection Czechoslov. Chem. Commun., 42, 548-552, 1977
O-Acetylvinoxine	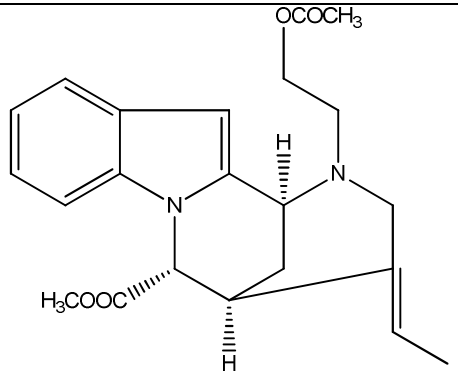	*Vinca minor*	1977	Vinoxine, A Novel Type of Indole Alkaloid, Voticky, Z. Et al. Collection Czechoslov. Chem. Commun., 42, 548-552, 1977

Table F. 1 (Contd): Indole alkaloids isolated from *Vinca minor, major* and *herbacea.*

16-epipleiocarpamine	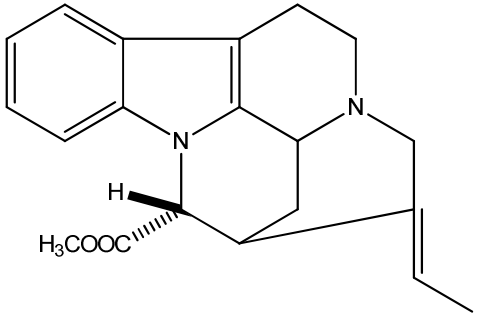	*Vinca minor*	1977	Vinoxine, A Novel Type of Indole Alkaloid, Voticky, Z. Et al. Collection Czechoslov. Chem. Commun., 42, 548-552, 1977
Pleiocarpamine	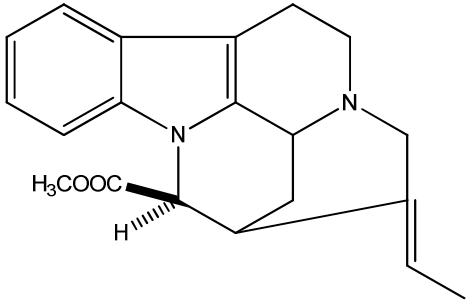	*Vinca minor*	1977	Vinoxine, A Novel Type of Indole Alkaloid, Voticky, Z. Et al. Collection Czechoslov. Chem. Commun., 42, 548-552, 1977
19-Dihydrovinoxine	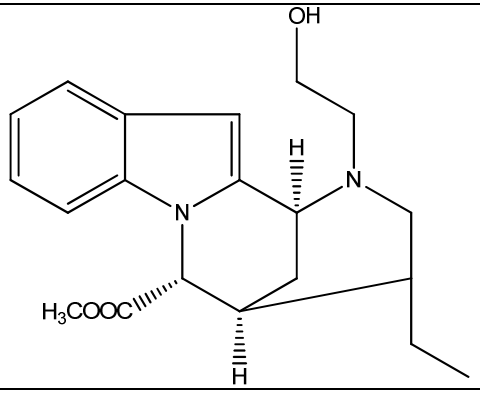	*Vinca minor*	1977	Vinoxine, A Novel Type of Indole Alkaloid, Voticky, Z. Et al. Collection Czechoslov. Chem. Commun., 42, 548-552, 1977

Table F. 1(Contd): Indole alkaloids isolated from *Vinca minor, major* and *herbacea.*

Vincarubine	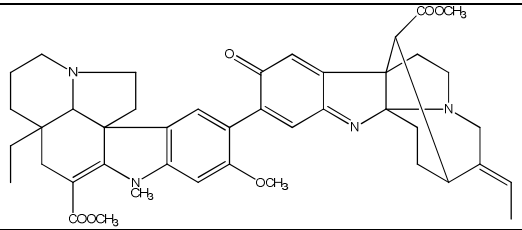	*Vinca minor*	1986	Vincarubine, A Novel Bisindole Alkaloid from Vinca minor, Proksa, B. et al. Tetrahedron Letters, 27, 5413-5416, 1986
(-)-Vincorine	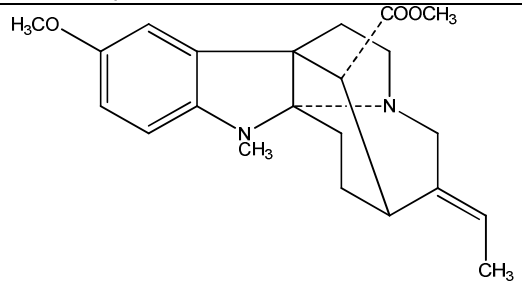	*Vinca minor*	1962	Alkaloids from Vinca minor L. Vincadine, minovine and vincorine, MOKRY J, DUBRAVKOVA L, SEFCOVIC P. Experientia. 1962 15;18:564-5.
Vincadine	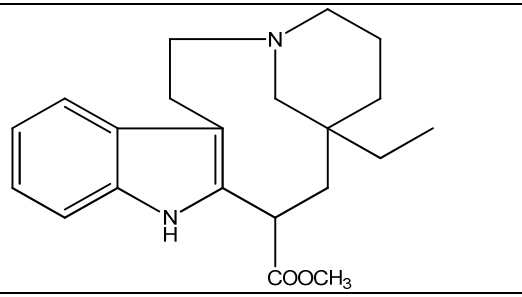	*Vinca minor*	1962	Alkaloids from Vinca minor L. Vincadine, minovine and vincorine, MOKRY J, DUBRAVKOVA L, SEFCOVIC P. Experientia. 1962 15;18:564-5.

Table F. 1(Contd): Indole alkaloids isolated from *Vinca minor*, *major* and *herbacea*.

Minovine	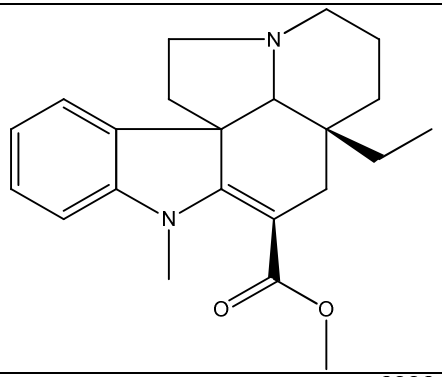	*Vinca minor*	1962	Alkaloids from Vinca minor L. Vincadine, minovine and vincorine, MOKRY J, DUBRAVKOVA L, SEFCOVIC P. Experientia. 1962 15;18:564-5.
(-)-1-Norvincorine	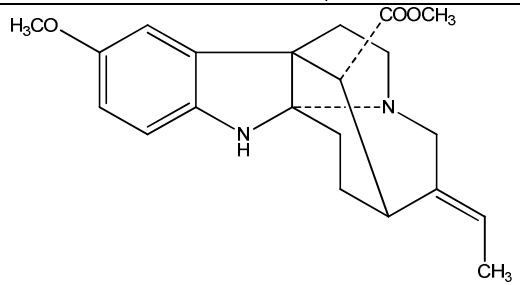	*Vinca minor*	1987	Proksa, B., Uhrín, D., Grossmann, E., & Votický, Z. (1987). (-)-1-Norvincorine, a New Alkaloid from Vinca minor. *Planta Medica*, *53*(1), 120.
Minovincine	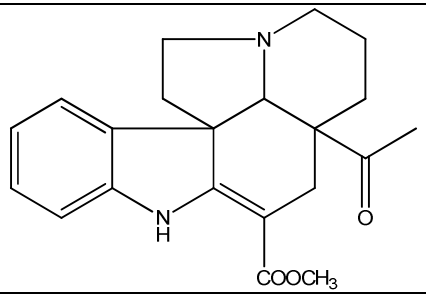	*Vinca minor*	1974	Dopke, W., Meisel,H., Structure and Stereochemistry of Alkaloid from *Vinca minor*, Die Pharmazie, 29, 68, 1974

Table F. 1(Contd): Indole alkaloids isolated from *Vinca minor*, *major* and *herbacea*.

Minovincinine	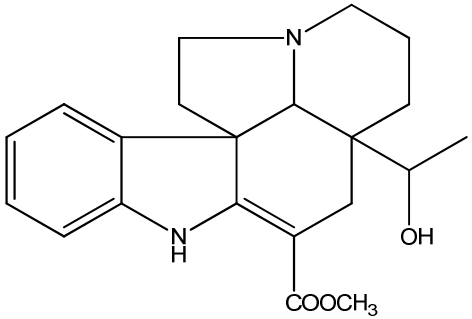	*Vinca minor*	1973	Malikov, V.M., Yunusov, S.Y., Vinca Alkaloids, Chemistry of Natural Compounds, 5, 597-617, 1977
Ervinidinine	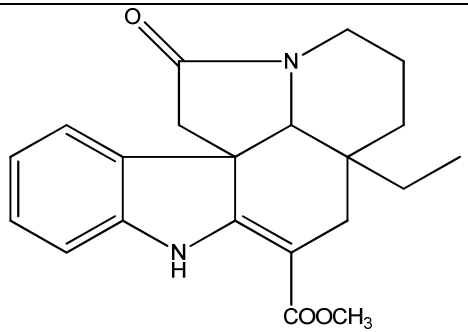	*Vinca minor*	1973	Malikov, V.M., Yunusov, S.Y., Vinca Alkaloids, Chemistry of Natural Compounds, 5, 597-617, 1977
11-Methoxyvincadiformine	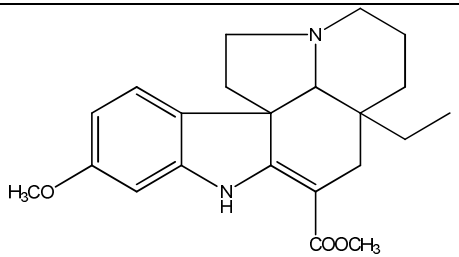	*Vinca minor*	1964	Malikov, V.M., Yunusov, S.Y., Vinca Alkaloids, Chemistry of Natural Compounds, 5, 597-617, 1977

Table F. 1(Contd): Indole alkaloids isolated from *Vinca minor*, *major* and *herbacea*.

±Vincadiformine	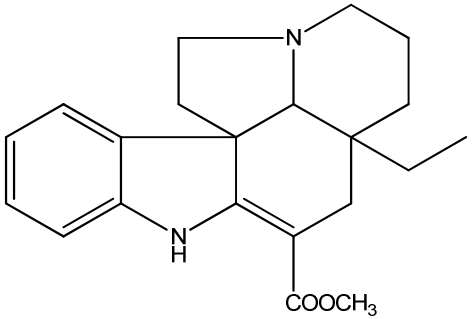	*Vinca minor*	1973	Malikov, V.M., Yunusov, S.Y., Vinca Alkaloids, Chemistry of Natural Compounds, 5, 597-617, 1977
11-Methoxyminovincine	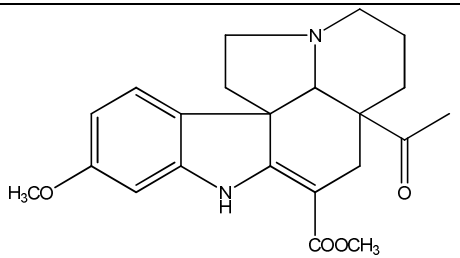	*Vinca minor*	1973	Malikov, V.M., Yunusov, S.Y., Vinca Alkaloids, Chemistry of Natural Compounds, 5, 597-617, 1977
N-Methylvincadiformine	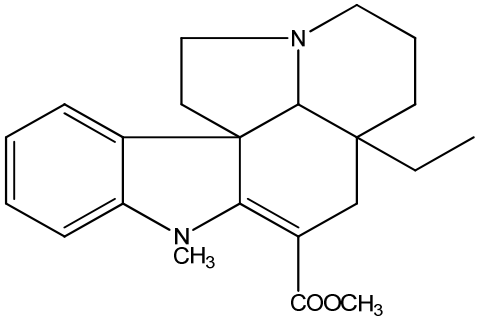	*Vinca minor*	1973	Malikov, V.M., Yunusov, S.Y., Vinca Alkaloids, Chemistry of Natural Compounds, 5, 597-617, 1977

Table F. 1(Contd): Indole alkaloids isolated from *Vinca minor*, *major* and *herbacea*.

11-Methoxyminovincinine	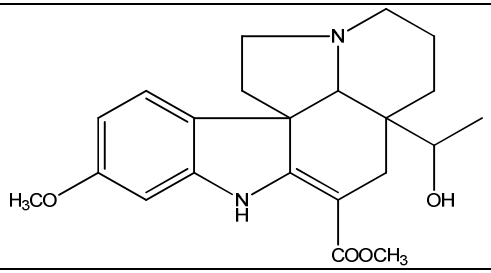	*Vinca minor*	1973	Malikov, V.M., Yunusov, S.Y., Vinca Alkaloids, Chemistry of Natural Compounds, 5, 597-617, 1977
5-Oxominovincine	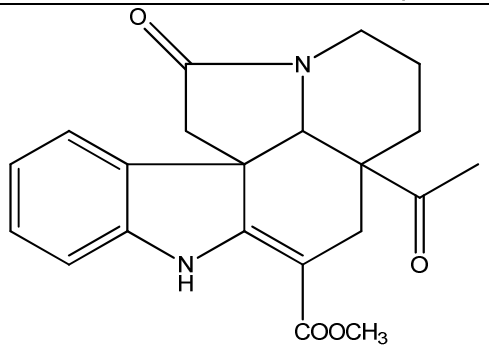	*Vinca minor*	1973	Malikov, V.M., Yunusov, S.Y., Vinca Alkaloids, Chemistry of Natural Compounds, 5, 597-617, 1977
N-Methylaspidospermidine	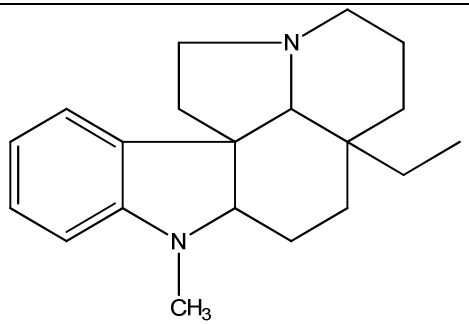	*Vinca minor*	1973	Malikov, V.M., Yunusov, S.Y., Vinca Alkaloids, Chemistry of Natural Compounds, 5, 597-617, 1977

Table F. 1(Contd): Indole alkaloids isolated from *Vinca minor*, *major* and *herbacea*.

Picrinine	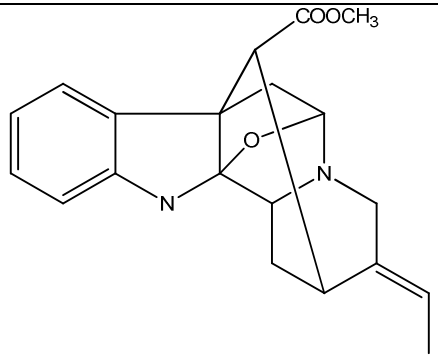	*Vinca minor*	1973	Malikov, V.M., Yunusov, S.Y., Vinca Alkaloids, Chemistry of Natural Compounds, 5, 597-617, 1977
Vincoridine	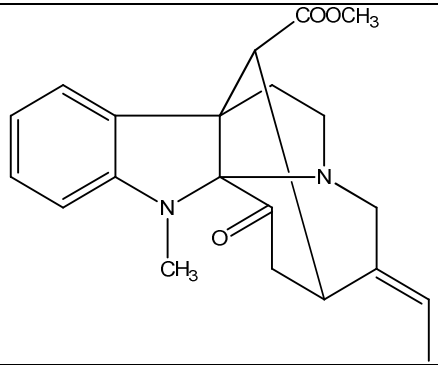	*Vinca minor*	1973	Malikov, V.M., Yunusov, S.Y., Vinca Alkaloids, Chemistry of Natural Compounds, 5, 597-617, 1977
Vincovine	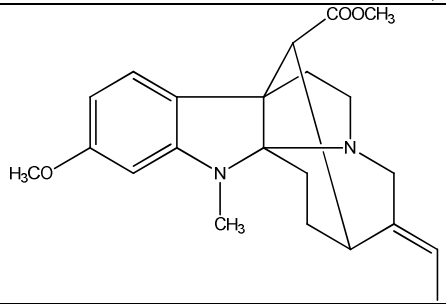	*Vinca minor*	1971	Malikov, V.M., Yunusov, S.Y., Vinca Alkaloids, Chemistry of Natural Compounds, 5, 597-617, 1977

Table F. 1(Contd): Indole alkaloids isolated from *Vinca minor*, *major* and *herbacea.*

N-Methylquebrachamine	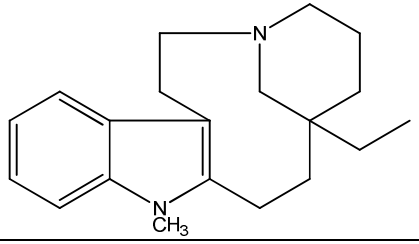	*Vinca minor*	1973	Malikov, V.M., Yunusov, S.Y., Vinca Alkaloids, Chemistry of Natural Compounds, 5, 597-617, 1977
Vincaminorine	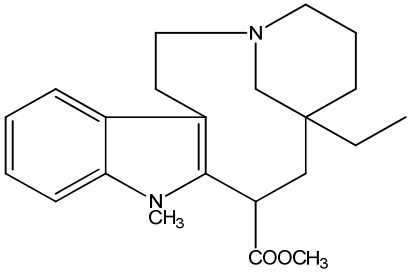	*Vinca minor*	1973	Malikov, V.M., Yunusov, S.Y., Vinca Alkaloids, Chemistry of Natural Compounds, 5, 597-617, 1977
Vincaminoridine	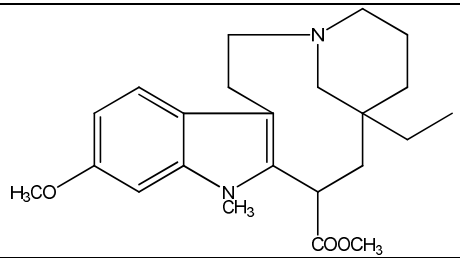	*Vinca minor*	1973	Malikov, V.M., Yunusov, S.Y., Vinca Alkaloids, Chemistry of Natural Compounds, 5, 597-617, 1977
10-Methoxyvellosimine	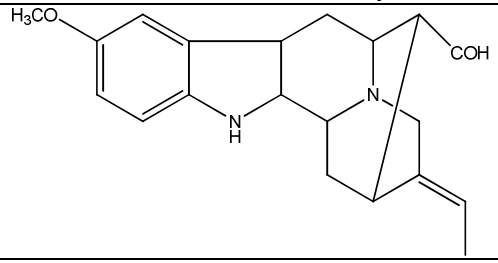	*Vinca minor*	1973	Malikov, V.M., Yunusov, S.Y., Vinca Alkaloids, Chemistry of Natural Compounds, 5, 597-617, 1977

Table F. 1(Contd): Indole alkaloids isolated from *Vinca minor*, *major* and *herbacea*.

$R=R_3=OH$; $R_1=OH$; $R_2=COOCH_3$ Vincamine	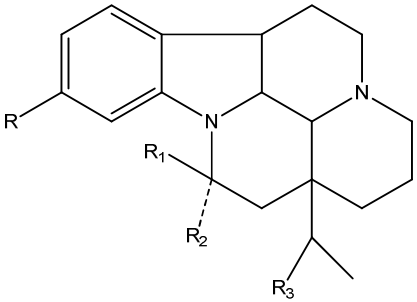	*Vinca minor*	1973	Malikov, V.M., Yunusov, S.Y., Vinca Alkaloids, Chemistry of Natural Compounds, 5, 597-617, 1977
$R=R_3=H$; $R_1=COOCH_3$; $R_2=OH$ 16-Epivincamine				
$R=R_3=H$; $R_1=R_2=O$ (±)-Eburnamonine				
$R=OCH_3$, $R_1=OH$; $R_2=COOCH_3$, $R_3=H$ Vincine				
$R=R_1=R_3=H$; $R_2=OH$, (-)Eburnamine				
$R=R_3=H$; $R_1=H;\Delta^{16,17}$ Eburnamerine				
$R=R_3=H$; $R_1=R_2=O$, (-)-Eburnamerine				
$R=R_2=R_3=H$, $R_1=OH$ (+)-Isoeburnamine				
$R=OCH_3$; $R_1=R_2=O$; $R_3=H$, 11-Methoxyburnamonine				
$R=OCH_3$; $R_1=R_2=O$; $R_3=H$, 11,12Dimethoxyeburnamonine				
$R=H$, $R_1=OH$; $R_2=COOCH_3$; $R_3=O$ Vincaminine				
$R=OCH_3$, $R_1=OH$; $R_2=COOCH_3$, $R_3=O$, Vincinine				
$R=H$, $R_1=R_3=OH$, $R_2=COOCH_3$, Hydroxyvincamine				

Table F. 1(Contd): Indole alkaloids isolated from *Vinca minor*, *major* and *herbacea.*

Reserpine	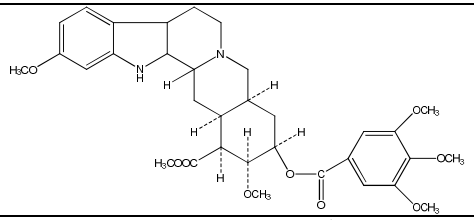	*Vinca minor*	1961	Malikov, V.M., Yunusov, S.Y., Vinca Alkaloids, Chemistry of Natural Compounds, 5, 597-617, 1977
Dehydroaspidospermide	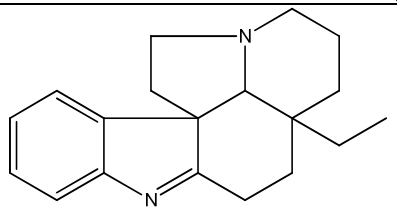	*Vinca minor*	1973	Malikov, V.M., Yunusov, S.Y., Vinca Alkaloids, Chemistry of Natural Compounds, 5, 597-617, 1977
Vinorine	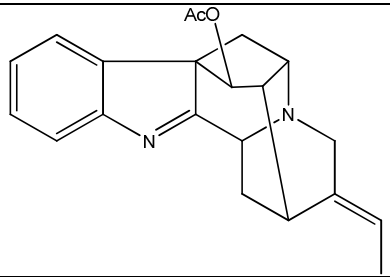	*Vinca minor*	1971	Malikov, V.M., Yunusov, S.Y., Vinca Alkaloids, Chemistry of Natural Compounds, 5, 597-617, 1977
$R=OCH_3$; $R_1=CH_2OH$, 10-Methoxydeacetylakyammiline	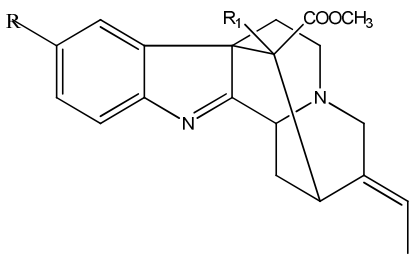	*Vinca minor*	1972	Malikov, V.M., Yunusov, S.Y., Vinca Alkaloids, Chemistry of Natural Compounds, 5, 597-617, 1977
R=H, $R_1=CH_2OH$, Deacetylakyammiline				
$R=R_2=H$, Vincamidine				

Table F. 1(Contd): Indole alkaloids isolated from *Vinca minor*, *major* and *herbacea*.

11-Methoxytetrahydroalstonine	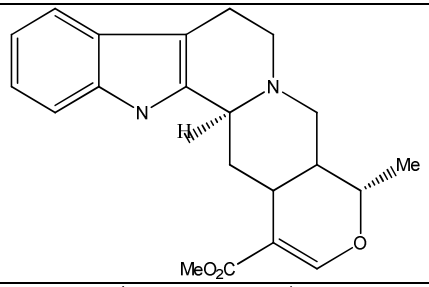	*Vinca major*	1991	Mukhopadhyay, G., Mukherjee, B., Patra, A., Chatterjee, A., Ghosh, R., Roychowdhury, P., & Kawazura, H. (1991). 11-Methoxytetrahydroalstonine, a heteroyohimbinoid alkaloid from Vinca major. *Phytochemistry*, *30*(7), 2447-2449
Reserpinine	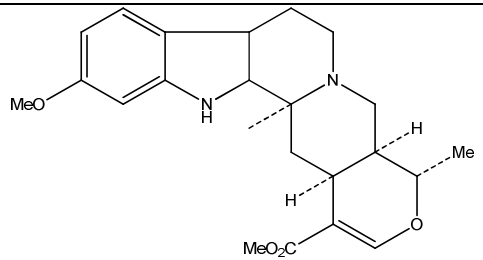	*Vinca major*	1974	A.Banerji and M. Chakrabarty, Lochaverine, A New Indole Alkaloid of *Vinca major*, Phytochemistry, 13, 2309-2312, 1974
R=H,Vincamajoreine R=COMe, O-Acetyl vincamajoreine	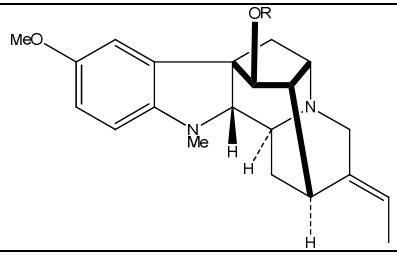	*Vinca major*	1974	A.Banerji and M. Chakrabarty, Lochvinerine, A New Indole Alkaloid of *Vinca major*, Phytochemistry, 13, 2309-2312, 1974

Table F. 1 (Contd): Indole alkaloids isolated from *Vinca minor, major* and *herbacea.*

R=OMe,R_1=H, R_2=CHO, 10-Methoxyvellosimine R=OMe,R_1=CH_2OH, R_2=H, Lochvinerine	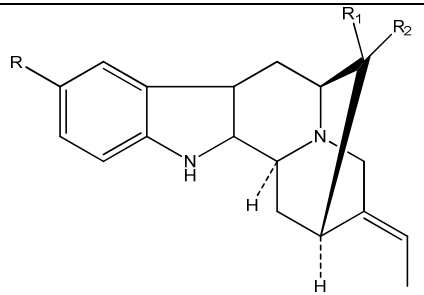	*Vinca major*	1974	A.Banerji and M. Chakrabarty, Lochvinerine, A New Indole Alkaloid of *Vinca major*, Phytochemistry, 13, 2309-2312, 1974
R_1=βCHO, R_2=Me, 10-Methoxyperakine R_1=βCH_2-OCOMe, R_2=Me, Vincawajine	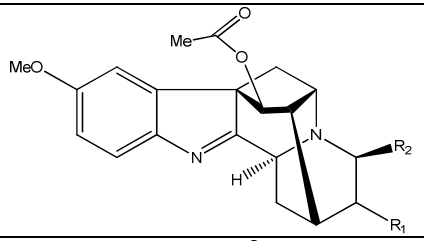	*Vinca major*	1995	Atta-Ur-Rahman, Sultana A., Nighat, F., Bhatti,M. K., Kurucu, S., Kartal, M., Alkaloids from *Vinca major*, Phytochemistry, 38, 1057-1061, 1995.
10-Methoxyvinorine	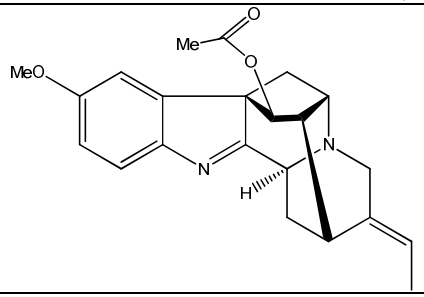	*Vinca major*	1995	Atta-Ur-Rahman, Sultana A., Nighat, F., Bhatti,M. K., Kurucu, S., Kartal, M., Alkaloids from *Vinca major*, Phytochemistry, 38, 1057-1061, 1995.

Table F. 1(Contd): Indole alkaloids isolated from *Vinca minor, major* and *herbacea.*

Akuammicine	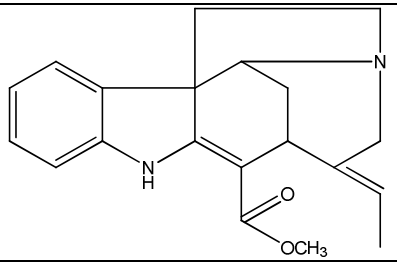	*Vinca major*	1964	Malikov, V.M., Yunusov, S.Y., Vinca Alkaloids, Chemistry of Natural Compounds, 5, 597-617, 1977
R=OCH_3, R_1=Ac; R_2=R_3=H; R_4=CH_3 Majoridine R= OCH_3, R_1= R_2= R_3=H; R_4= CH_3, Vincamajoreine R= R_1= R_3=H, R_2=$COOCH_3$, R_4= CH_3, Vincamajine R= R_3=H, R_1= Ac, R_2=$COOCH_3$, R_4= CH_3, Vincamedine	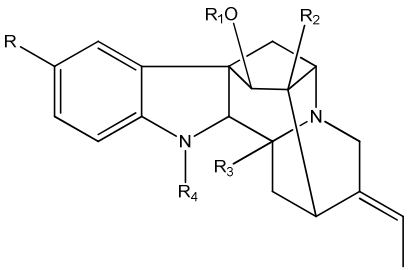	*Vinca major*	1977	Malikov, V.M., Yunusov, S.Y., Vinca Alkaloids, Chemistry of Natural Compounds, 5, 597-617, 1977
Akuammine	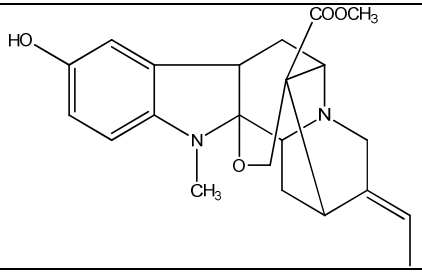	*Vinca major*	1964	Malikov, V.M., Yunusov, S.Y., Vinca Alkaloids, Chemistry of Natural Compounds, 5, 597-617, 1977

Table F. 1(Contd): Indole alkaloids isolated from *Vinca minor, major* and *herbacea.*

Vincamine	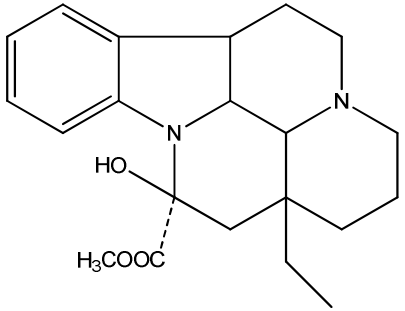	*Vinca major*	1973	Malikov, V.M., Yunusov, S.Y., Vinca Alkaloids, Chemistry of Natural Compounds, 5, 597-617, 1977
Ervine (rauniticine)	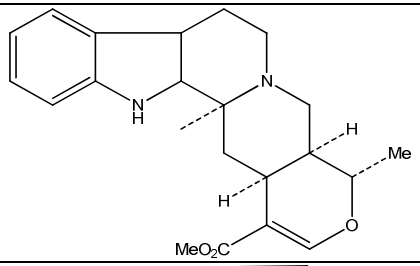	*Vinca major*	1977	Malikov, V.M., Yunusov, S.Y., Vinca Alkaloids, Chemistry of Natural Compounds, 5, 597-617, 1977
Majidine	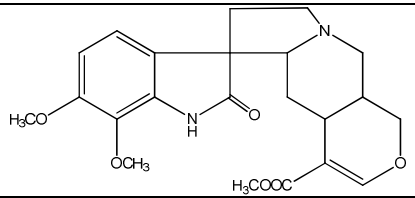	*Vinca major*	1964	Malikov, V.M., Yunusov, S.Y., Vinca Alkaloids, Chemistry of Natural Compounds, 5, 597-617, 1977
Majorinine	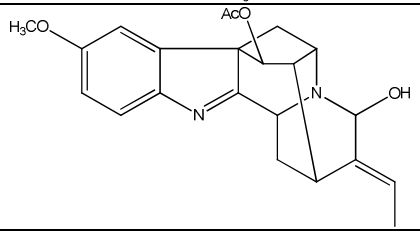	*Vinca major*	1977	Malikov, V.M., Yunusov, S.Y., Vinca Alkaloids, Chemistry of Natural Compounds, 5, 597-617, 1977

Table F. 1(Contd): Indole alkaloids isolated from *Vinca minor*, *major* and *herbacea*.

Majidine	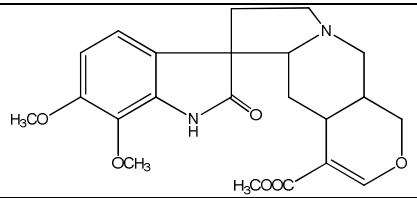	*Vinca herbaceae*	1968	I. Ognyanov, B. Pyuskyulev, I. Kompiš, T. Sticzay, G. Spiteller, M. Shamma and R.J. Shine, Alkaloids from *vinca herbacea* The structures and stereochemistry of majdine and isomajdine,TetrahedronVolume 24, 1968, 4641-4648
Isomajidine	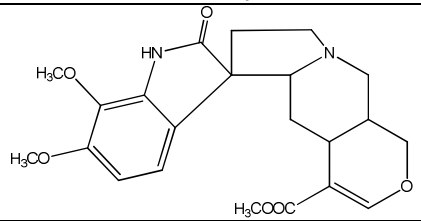	*Vinca herbacea*	1968	I. Ognyanov, B. Pyuskyulev, I. Kompiš, T. Sticzay, G. Spiteller, M. Shamma and R.J. Shine, Alkaloids from *vinca herbacea* The structures and stereochemistry of majdine and isomajdine, Tetrahedron Volume 24, 1968, 4641-4648
Akuammicine	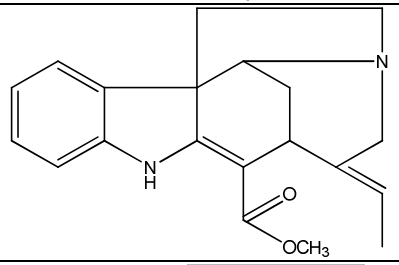	*Vinca herbacea*	1964	Malikov, V.M., Yunusov, S.Y., Vinca Alkaloids, Chemistry of Natural Compounds, 5, 597-617, 1977
Vincanine	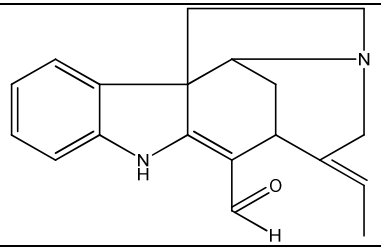	*Vinca herbacea*	1973	Malikov, V.M., Yunusov, S.Y., Vinca Alkaloids, Chemistry of Natural Compounds, 5, 597-617, 1977

Table F. 1(Contd): Indole alkaloids isolated from *Vinca minor*, *major* and *herbacea*.

R=OH, Tabersonine R=OCH_3, Methoxytabersonine	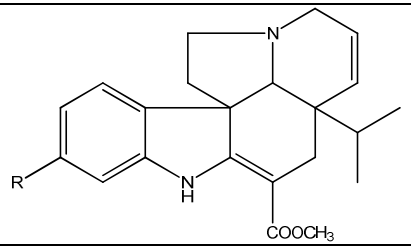	*Vinca herbacea*	1973	Malikov, V.M., Yunusov, S.Y., Vinca Alkaloids, Chemistry of Natural Compounds, 5, 597-617, 1977
N-Methyl-$\Delta^{14,15}$-dehydroaspidospermidine	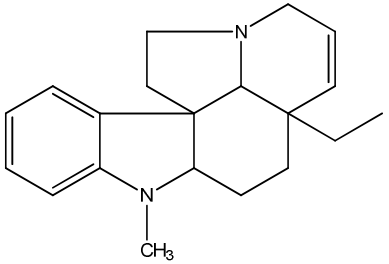	*Vinca herbacea*	1975	Malikov, V.M., Yunusov, S.Y., Vinca Alkaloids, Chemistry of Natural Compounds, 5, 597-617, 1977
Venalstonine	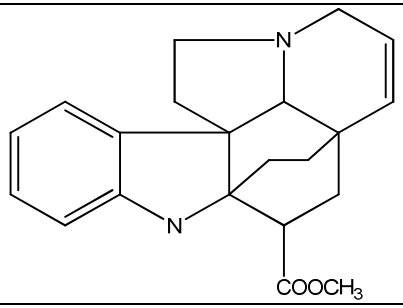	*Vinca herbacea*	1969	Malikov, V.M., Yunusov, S.Y., Vinca Alkaloids, Chemistry of Natural Compounds, 5, 597-617, 1977

Table F. 1(Contd): Indole alkaloids isolated from *Vinca minor*, *major* and *herbacea.*

R= R_1=R_3=R_4=H, R_2=$COOCH_3$, Vincarine R= R_1= R_4=H, R_2=$COOCH_3$, R_3=OH, Herbaline, R= R_1=H, R_2=$COOCH_3$, R_3=OH, R_4=CH_3, Herbamine	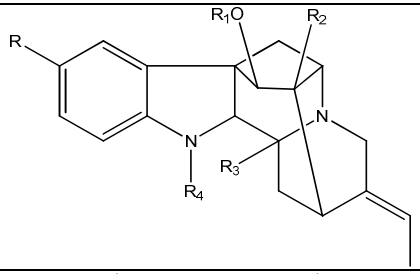	*Vinca herbacea*	1972	Malikov, V.M., Yunusov, S.Y., Vinca Alkaloids, Chemistry of Natural Compounds, 5, 597-617, 1977
R=R_3=OH; R_1=OH; R_2=$COOCH_3$ Vincamine	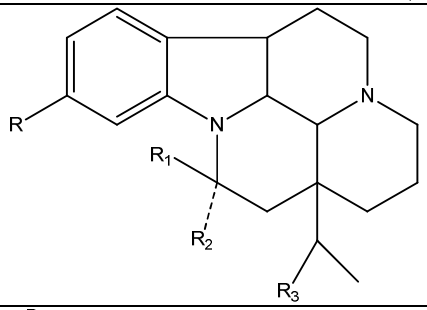	*Vinca herbacea*	1968	Malikov, V.M., Yunusov, S.Y., Vinca Alkaloids, Chemistry of Natural Compounds, 5, 597-617, 1977
R=H, Herbaine R=OMe, Herbaceine	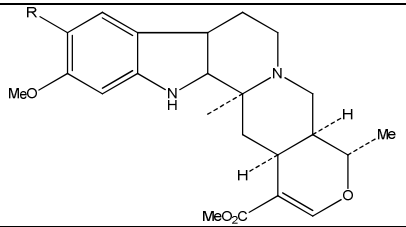	*Vinca herbacea*	1963	Malikov, V.M., Yunusov, S.Y., Vinca Alkaloids, Chemistry of Natural Compounds, 5, 597-617, 1977
Reserpinine	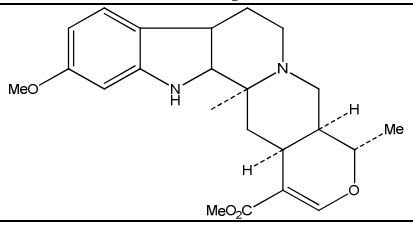	*Vinca major*	1974	A.Banerji and M. Chakrabarty, Lochaverine, A New Indole Alkaloid of *Vinca major*, Phytochemistry, 13, 2309-2312, 1974

Table F. 1(Contd): Indole alkaloids isolated from *Vinca minor*, *major* and *herbacea.*

Majidine	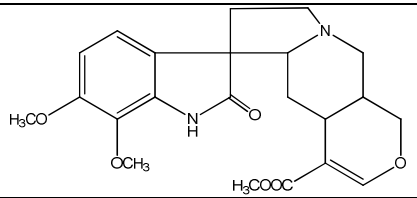	*Vinca herbacea*	1964	Malikov, V.M., Yunusov, S.Y., Vinca Alkaloids, Chemistry of Natural Compounds, 5, 597-617, 1977
R=OCH_3, 16-carboxyherbavine R=H, Herbaline	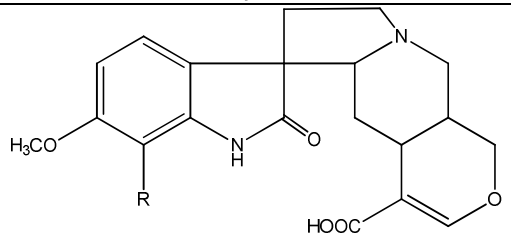	*Vinca herbacea*	1975 1973	Malikov, V.M., Yunusov, S.Y., Vinca Alkaloids, Chemistry of Natural Compounds, 5, 597-617, 1977
Skimmianine	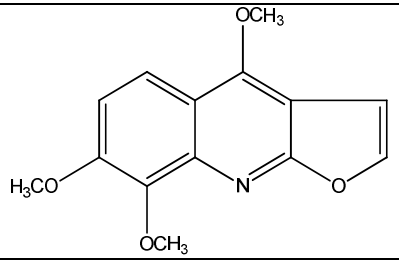	*Vinca herbacea*	1971	Malikov, V.M., Yunusov, S.Y., Vinca Alkaloids, Chemistry of Natural Compounds, 5, 597-617, 1977

CURRICULUM VITAE

CURRICULUM VITAE

Candidate's full name: Fatemeh BAHADORI

Place and date of birth: Tabriz/ IRAN, 03.07.1974

Permanent Address:

Universities and Colleges attended:

Tabriz Azad Islamic University 1994-1996 (Laboratory Technician)

Ankara University- Faculty of Sciences, 1996-1998 (Chemistry)

Çanakkale 18 Mart University, Faculty of Science and Letters, Department of Chemistry 1998-2000 (Bachelor of Science in Chemistry)

Çanakkale 18 Mart University, Faculty of Science and Letters, Department of Chemistry 2000-2004 (Master of Science in Chemistry)

Istanbul Technical University, Institute of Science and Technology 2007-2011 (PhD, Chemistry)

University of Illinois at Chicago, Faculty of Pharmacy, Department of Biopharmaceutical Sciences, Reasearch Schooler, January- September 2010

Publications:

- Mehmet Boga, Ufuk Kolak **, Gulactı Topcu** , Fatemeh Bahadori , Murat Kartal, Norman R. Farnsworth "Two New İndole Alkaloids from *Vinca herbacea*",4/4, Phytochemistry Letters, 2011

- Demirkiran,O., **Topcu G**., Bahadori F., Ay M., Nazemiyeh H., Choudhary I., "Two New Phenylpropanoid Glycosides from the Leaves and Flowers of Erica arborea", Helvetica Chimica Acta, 93 (1), 77-83,2010.

- **Nazemiyeh, H**., Bahadori, F., Delazar, A., Ay, M., Topcu, G., Nahar, L., Majinda, R.R. T., Sarker, S.D "Antioxidant phenolic compounds from the leaves of *Erica arborea* (Ericaceae)", *Nat. Prod. Res. 22*, 1385-1392, 2008.

- **Nazemiyeh, H**., Bahadori, F., Delazar, A., Ay, M., Topcu, G., Kolak, U.,Nahar, L., Auzie, A.A., Sarker, S.D. "Tricetin 4'-O-alpha-L-rhamnopyranoside: A new flavonoid from the aerial Antioxidant phenolic compounds from the leaves of*Erica arborea* (Ericaceae)"*Chem. Nat. Compds.* , 2008, *44*, 174-178.

- Ay, M., Bahadori, F., Öztürk,M., Kolak, U. and **G. Topçu,**. "Antioxidant Activity of Erica arborea" *Fitoterapia***,** *78* , 571-573, 2007. .